Principles of organisation within the pathways in the brainstem and thalamus

Christodoulos Skliros

Main supervisor: Associate Professor Andrew J. Moorhouse

Co-supervisors: Professor Emeritus Ken W. S. Ashwell, Associate Professor Wei Wen

A thesis submitted in fulfilment of the requirements for the degree of

Doctor of Philosophy

UNSW SYDNEY

School of Medical Sciences
Faculty of Medicine
The University of New South Wales

2022

The term “magnetic resonance histology” (MRH) was coined by Dr. G. Allan Johnson et al. (1993) and refers to the use of ultra-high-magnetic field strengths to characterise tissue structures in ex vivo specimens.

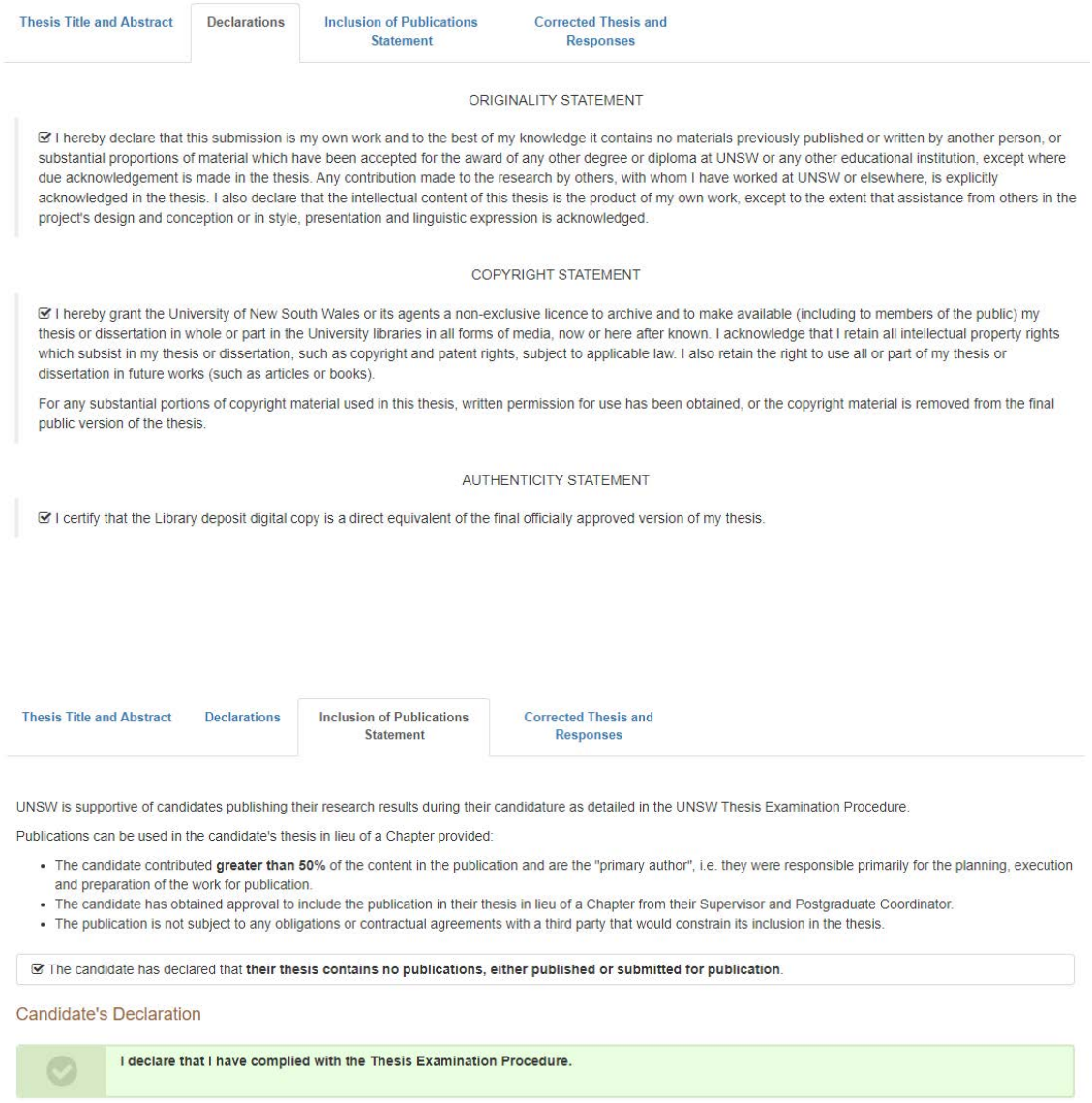

Thesis Title and Abstract | Declarations | Inclusion of Publications Statement | Corrected Thesis and Responses

ORIGINALITY STATEMENT

☑ I hereby declare that this submission is my own work and to the best of my knowledge it contains no materials previously published or written by another person, or substantial proportions of material which have been accepted for the award of any other degree or diploma at UNSW or any other educational institution, except where due acknowledgement is made in the thesis. Any contribution made to the research by others, with whom I have worked at UNSW or elsewhere, is explicitly acknowledged in the thesis. I also declare that the intellectual content of this thesis is the product of my own work, except to the extent that assistance from others in the project's design and conception or in style, presentation and linguistic expression is acknowledged.

COPYRIGHT STATEMENT

☑ I hereby grant the University of New South Wales or its agents a non-exclusive licence to archive and to make available (including to members of the public) my thesis or dissertation in whole or part in the University libraries in all forms of media, now or here after known. I acknowledge that I retain all intellectual property rights which subsist in my thesis or dissertation, such as copyright and patent rights, subject to applicable law. I also retain the right to use all or part of my thesis or dissertation in future works (such as articles or books).

For any substantial portions of copyright material used in this thesis, written permission for use has been obtained, or the copyright material is removed from the final public version of the thesis.

AUTHENTICITY STATEMENT

☑ I certify that the Library deposit digital copy is a direct equivalent of the final officially approved version of my thesis.

Thesis Title and Abstract | Declarations | Inclusion of Publications Statement | Corrected Thesis and Responses

UNSW is supportive of candidates publishing their research results during their candidature as detailed in the UNSW Thesis Examination Procedure.

Publications can be used in the candidate's thesis in lieu of a Chapter provided:

- The candidate contributed **greater than 50%** of the content in the publication and are the "primary author", i.e. they were responsible primarily for the planning, execution and preparation of the work for publication.
- The candidate has obtained approval to include the publication in their thesis in lieu of a Chapter from their Supervisor and Postgraduate Coordinator.
- The publication is not subject to any obligations or contractual agreements with a third party that would constrain its inclusion in the thesis.

☑ The candidate has declared that **their thesis contains no publications, either published or submitted for publication**.

Candidate's Declaration

I declare that I have complied with the Thesis Examination Procedure.

Thesis abstract

There are few detailed studies on the pathways through the human brainstem and even fewer on those through the pons. This thesis aims to address this lack of fine detail, and used ultra-high-field magnetic resonance imaging (MRI) of human and macaque brains to identify and characterise fibre tracts connecting cortical and spinal areas as they traverse through brainstem and thalamic structures. The material in this thesis is based on a unique dataset of ultra-high-field (7 Tesla – Duke and 11, 7 Tesla – Johns Hopkins) MRI scans on postmortem specimens, on which deterministic tractography has been applied based on high-angular-resolution diffusion imaging (HARDI) and subsequently higher order tensor glyph models.

The first results section of the thesis (Chapter 3) maps the descending fibre bundles associated with movement. From the motor cortical areas, the fibres of the internal capsule are traced through the crus cerebri, basilar pons and pyramids in three dimensions to reveal their organisation into functional and topographic subdivisions. While human cortico-pontine, -bulbar and -spinal tracts were traditionally considered to be dispersed, or a "melange", I show here a much more discrete and defined organisation of these descending fibre bundles.

Nine descending fibre bundles are identified and their anatomical location and terminations are described. A hitherto unknown pathway at the midline of the pons has been discovered and named herein as the *Stria Pontis* which connects the neocortex to the pontine tegmentum. Ten transverse fibre bundles connecting the pontine nuclei to the cerebellum are also identified. These newly identified tracts suggest possible functional subdivisions (cervical, thoracic, lumbar and sacral) and may aid in surgical treatment of tumours in the basilar pons.

The second results section (Chapter 4) analyses the sensory pathways through the brainstem and thalamus; the dorsal column - medial lemniscus pathway, the spinothalamic tract, the spinal trigeminal tract and the trigeminothalamic tracts. These are mapped from the medulla oblongata to their respective nuclei of termination in the thalamus. Most particularly, the novelty of this Chapter is the fact that this is the first time that we have succeeded in precisely mapping the spinothalamic pathway through the brainstem and thalamus. This reveals the anatomical relationship between these sensory tracts at a resolution (50 μm) that approaches that of histology, thus exploiting the advantages that diffusion tensor imaging (DTI) and deterministic tractography can offer as investigative tools.

The third results section (Chapter 5) analyses the dentato-rubro-thalamic tract, which is the afferent projection from the cerebellum to the thalamus, part of the cerebrocerebellar motor circuits, and which provides feedback on fine adjustments and control of motor acts. The mapping identifies the superior cerebellar peduncle, the patterning of the fibres within the superior cerebellar decussation, the patterning of the fibres within the red nucleus and finally the projection of the dentato-rubro-thalamic tract from the red nucleus to the ventral lateral nucleus of the thalamus. This

Chapter identifies the afferent component of the cerebrocerebellar circuit, that complements the efferent projections described above. Finally, I characterised 117 already known anatomical parts, areas and structures of the brainstem and thalamus in 3D, using magnetic resonance (MR) histology.

The ultra-high resolution mapping of the descending motor circuits and their cerebellar feedback loops, alongside the sensory tracts provides an improved diagnostic, therapeutic, and investigative tool. Clinically, these anatomical maps may be of value in conditions such as neurological upper or lower limb impairments associated with a tumour in the ventral or dorsal basilar pons respectively. Keyhole neurosurgery, edema drainage, pharmacological antiedema treatment and stereotactic radiotherapy, for example, can be more efficiently applied, thus reducing damage of adjacent bundles and structures. Similarly, mapping the sensory pathways may offer neurosurgical targets for pathologies such as mass lesions, ectatic vessels and trigeminal neuralgia. Finally, more accurate identification of the dentato-rubro-thalamic tract may improve surgical treatment of pathologies such as essential tremor, or assist pathway mapping for deep brain stimulation. As technologies develop, we can learn more about the structures and pathways connecting our brain to our muscles and sensory systems, and this thesis takes a further step in this direction, complementing and enhancing the insights provided by more traditional techniques such as histology, viral tracing, electrophysiology and brain ablation.

Acknowledgements

The experiments of the present study were carried out between 2018 and 2020 in the Paxinos lab, NeuRA Foundation, Department of Anatomy, Faculty of Medicine, School of Medical Sciences, UNSW, Sydney, Australia. The Paxinos lab and the Foundation provided me with computing resources, my private office, books, information technology support, as well as a salary and an additional secondary scholarship for my scientific endeavours. Moreover, the present study was further developed in the Moorhouse lab (Neurobiology Research Laboratory) where the final form of my research was accomplished. The material I used for this investigative study derived exclusively from Duke and Johns Hopkins Universities.

First of all, I would like to thank from the bottom of my heart my mentor and friend Scientia Professor George Paxinos AO. The Professor has been my mentor in neuroanatomy over many years and we have developed a unique friendship with mutual respect. Thanks to him I have acquired an extensive knowledge in microscopic anatomy of the central nervous system. I have studied his atlases and he offered me a unique opportunity to delineate together for an extensive period of time which rendered me capable of successfully carrying out the present study. Professor Paxinos has been extremely generous for hosting me in his house for 2.5 years and has helped me immensely in my professional and personal life. He assisted me in learning a variety of skills which are important in academia such as editing my curriculum vitae, and preparing all the documentation for a successful admission into a Ph.D. degree. In addition, he provided me with significant academic training in a variety of fields. Moreover, the Professor taught me and guided me through theoretical neuroscience on a daily basis at his house and in his laboratory. Therefore, I successfully acquired two international scholarships (Tuition fee scholarship and NeuRA scholarship) and a salary (NHMRC: APP1140295) which permitted me to live and work decently during my doctoral degree in Australia. The Professor and I worked together on this project, he supervised me and corrected any possible mistakes and pitfalls which are very common in this type of brain mapping. I will always think of him with fond memories, and look back on those years with respect and affection.

I would like to express my sincere gratitude to my primary supervisor Professor Andrew Moorhouse without whom this Ph.D. project would have never been completed. I would like to thank him for having been beside me through highs and lows in the final year of my doctorate. I am grateful to him for many interesting discussions on neuroanatomy and brain connectomics. I have also acquired a considerable amount of skills from his experience on how to create a thesis, figures and Chapters. My doctorate took on a new dimension with Professor Moorhouse's contributions. Professor Moorhouse is an extremely talented lecturer and author, I am particularly indebted to him for having taught me how to optimise my academic writing and give high level lectures. Professor Moorhouse has validated and supervised my research, he scientifically contributed to my work and taught me how to conduct my research in relation to other techniques and experimental findings from previous authors, and how to avoid pitfalls which are very common in basic research. I appreciate his ethical values, scientific approach in medicine, critical thinking and has been an inspirational academic who I consider a friend and a true mentor.

Special thanks to my secondary supervisor Professor Wei Wen and his collaborator Forrest Koch who guided me through the world of biomedical engineering and showed me how to optimise tractography at this deep level at which I was operating. Professor Wen was the only one to help me from the very beginning. Moreover, when my computer at NeuRA could not process my data due to their large size, Professor Wen completed the post-processing using a higher performance computer at UNSW. In this way I later managed to create the algorithms for my tensor glyphs. I also acknowledge Forrest Koch for having assisted me to create the GRE file which I used as anatomical background for tractography in order to produce images with accurate anatomical delineations and annotations.

I greatly appreciate my secondary supervisor Professor Ken W. S. Ashwell for having provided me with his vision for my research. He guided me step by step through my journey as a neuroanatomist and gave me his know how regarding

comparative and descriptive anatomy. He also taught me how to delineate during our meetings for brain mapping. We had very passionate and interesting scientific conversations throughout the years I have been at UNSW almost on a daily basis. He also gave me very constructive feedback concerning my writing.

I also express my gratitude to Dr Steve Kassem for all his support, assistance, and supervision during the period that I worked in the Paxinos lab. Dr Kassem is an expert in neuroanatomy of the central nervous system and he investigates brain structures using modified Golgi staining and other histology techniques. Dr Kassem supported me regarding IT issues, taught me how to be adept in programs such as Adobe illustrator, endnote, and how to acquire a variety of skills which were pivotal for continuing my doctoral studies. In addition, he validated my work and showed me a variety of histology techniques which I should use to assess my findings. Dr Kassem and I had very interesting scientific conversations during my period in the Paxinos lab and I am looking forward to working with him on future projects.

I would kindly like to thank my colleague and friend Dr Kevin R. Sitek from the Massachusetts Institute of Technology (MIT) for his comments and feedback regarding my anatomical descriptions, tractography, tensor glyphs and manuscript. His work on the human subcortical auditory system inspired me to follow my quest for the motor and sensory projections. His consistent support has been pivotal for the completion of my research.

I am extremely grateful to my collaborator Professor Manisha Aggarwal at Johns Hopkins University who provided me with the highest quality postmortem human specimens 3 and 4, material only found in specific research centres around the world, in order to complete my research on the brainstem pathways. Professor Aggarwal has always been beside me and supported my work in this highly specialised field of research. She shared her knowledge with me on Diffusion Tensor Imaging and I have constantly followed up with her so that I would excel in connectomics. Professor Aggarwal and her collaborator Professor Susumu Mori who is considered a pioneer in connectomics, both are a true inspiration to me. Through

the present study we created the fundamentals for a long term collaboration and friendship.

I am also extremely grateful to my collaborator Dr Evan Calabrese from the University of California, Berkeley for his support and friendship. He repeatedly gave feedback on my work. I greatly appreciate his detailed comments on my manuscript and his scientific opinion on my subdivisions of the descending and transverse fibre bundles as well as the novel pathway I discovered the *Stria Pontis*. He significantly contributed to creating the data I used from the Duke Center for In Vivo Microscopy, which achieved an unprecedented resolution (50 μm) for an MRI-project in biomedical engineering. Due to his expertise as a researcher and a medical doctor I foresee a long term collaboration. I respect him and I consider him a true friend.

Finally, I explicitly express my gratitude and I am full of praise for the director of the Duke Center for In Vivo Microscopy Professor G. Allan Johnson for having provided me with the highest resolution and quality of volumetric set of data ever achieved for my research. The material I used from Duke was created by a unique especially modified 7T small animal MRI scanner (US patent # 6,023,162- Three Dimensional Morphology by Magnetic Resonance Imaging) which is the only one of its kind and for this I will always be grateful to Professor Johnson. I have always had a deep admiration and respect for his work and I have also been inspired by his unique and unprecedented contribution to science. This work would have never been accomplished without his invaluable contribution. Professor Johnson is the scientist who created the data that I studied and most particularly the human specimen 1. In addition, the high quality and sophisticated post-processing performed at Duke, specifically for human specimen 1 was such that it later laid the foundations for me to conceptualise the present study, optimise my techniques and create the detailed deterministic tractography and tensor glyphs presented herein.

I hereby dedicate this investigative study to the scientists for whom I have the utmost respect:

Scientia Professor George Paxinos AO and Professor G. Allan Johnson.

In addition, I dedicate this research and its applications to people with quadriplegia.

This is the work in which the pyramidal tract has been subdivided in its entirety from the internal capsule to the spinal cord.

This is my original work.

Sydney, January 2022

Christodoulos K. Skliros M.D.

Overview

This thesis is composed of six Chapters. In the first Chapter I deliver an introduction to the anatomy of the brainstem and I analyse the brainstem pathways according to the orientation of the information through which it is conveyed. I described in total 26 pathways with particular emphasis on the corticospinal and spinothalamic tracts. In the last section of the first Chapter I report my final considerations and the aims of the present study. The scope of the literature reviewed in Chapter 1 is to describe the major white matter tracts through the brainstem and spinal cord. Given my thesis investigates the cerebrocerebellar circuit, there is particular emphasis on the corticospinal tract which is part of the pyramidal descending motor pathway; and the sensory projections that convey sensory information from the periphery to the neocortex and include the cuneate and gracile fasciculi (which are part of the dorsal column – medial lemniscus pathway), and the spinothalamic tract. In addition, I review the rubrospinal, vestibulospinal, medial and lateral reticulospinal, and tectospinal tracts, which are all part of the extrapyramidal system that integrates and modulates motor commands. I also review projections which course through the brainstem that are not specifically investigated in the results chapters but provide completeness and are important landmarks through the brainstem and thalamus. White matter tracts such as the spinoparabrachial, spinomesencephalic, spinohypothalamic, spino-olivary and interstitiospinal are not investigated in this thesis and not reviewed in Chapter 1. Therefore, the projections through the brainstem and thalamus have been subdivided into three major categories: 1) the descending spinal projections which include the corticospinal, the hypothalamospinal and cerebellospinal tracts; 2) the projections from the brainstem

to the spinal cord which comprise the vestibulospinal, tectospinal, interstitiospinal and medial reticulospinal tracts (Group A), as well as the rubrospinal, lateral reticulospinal, solitariospinal, coeruleospinal, raphespinal, spinal and principal trigeminospinal, gracilospinal, cuneospinal tracts, and finally the projections from the retroambiguus nucleus to the spinal cord (Group B); 3) the ascending spinal projections which comprise the dorsal column pathways such as the cuneate and gracile fasciculi, the postsynaptic dorsal column pathway, the projections through the ventrolateral funiculus such as the spinocerebellar, spinocervico thalamic, spinoreticular, and spinothalamic tracts. In the final sections of the introduction I integrate the pyramidal and extrapyramidal systems, reporting the cerebrocerebellar circuit as feedback loop which is crucial for motor control. Subsequently, I describe the functional aspects of DTI and tractography with which this research has been conducted. In addition, I review prior literature in DTI and tractography of the human brainstem, and the relationship between DTI / Tractography and Classical Tracing Techniques. Finally, I conclude with the research statements, overall aim and hypothesis of the present study.

In the second Chapter, this thesis reports the general methods and additional methodological approaches by which this research has been conducted. In addition, I summarise the steps involved in this ultra-high-field 3D brain mapping, anatomical delineations and fibre tracking in 3D.

In the third Chapter, this thesis maps the descending bundles within the internal capsule, crus cerebri, basilar pons and pyramids. The internal capsule has been subdivided into four longitudinal bundles. The three external bundles of the

internal capsule continue into the crus cerebri as cortico-pontine, -bulbar, -spinal projections whereas the fourth most internal fibre bundle terminates into the substantia nigra, pars reticulata (SNR). In addition, the crus cerebri has been subdivided into three groups of bundles that appear as curved lamellae (primary subdivisions) which contain 9 fibre bundles (secondary subdivisions). These fibre bundles descend into the basilar pons and finally converge into the pyramids. The transverse fibres of the pons have been subdivided into three main groups of bundles which are anatomically and functionally connected to the respective groups of the descending fibre bundles. Thus, this thesis presents the first study that maps the basilar pons and its constituent descending and transverse fibre bundles in 3D. In addition, I discovered a ventrodorsally elongated fibre bundle at the midline of the basilar pons and tegmentum which transpires from each of the transverse fibres of the pons, veers laterally into the tegmentum and projects in the vicinity of the cranial nerve nuclei. I named and anatomically described, herein, this novel pathway as the *Stria Pontis*. I suggested an architectural model that consists of 9 descending fibre bundles which alternate with 10 transverse fibres of the pons, although there is a degree of variability between the specimens and between the left and right hemispheres. At the midline of the pons the *Stria Pontis*, which is always stable, courses into the tegmentum vertically in respect of the other bundles in the basilar pons. This variability and interdigitations may provide some degree of overlap at the precise site of branching.

In the fourth Chapter of my thesis, I analyse the sensory pathways such as the dorsal column-medial lemniscus pathway (dcml), the spinothalamic (spth), the ventral and dorsal trigeminothalamic tracts (vtt & dtt). In addition, the trajectories of

the sensory root of the trigeminal nerve (s5) and the spinal trigeminal tract (sp5) are also identified. This new information reveals the anatomical relationship of the above pain pathways and furthermore provides a detailed anatomical description of the trajectories of the pain pathways in three dimensions. Finally, I precisely map the spth from the spinal cord to ventral posterolateral nucleus (VPL) of the thalamus. Again, such information provides a valuable tool for surgery or other interventions, and for better diagnosing neuropathic symptoms.

In the fifth Chapter of this work I report a novel approach towards descriptive anatomy based on the unique ultra-high-resolution magnetic resonance imaging/diffusion tensor imaging (MRI/DTI) data. The ultra-high-field scanner and advanced post-processing enabled me to use deterministic tractography and to create tensor glyphs to anatomically investigate the superior cerebellar peduncle (scp). In addition, I identified the pattern of the fibres within the superior cerebellar decussation (xscp), and I described how the dentato-rubral and dentato-thalamic tracts project within the red nucleus. Finally, I demonstrated the projection of the cerebellothalamic tract as far as the ventral tier of the thalamus. This work provides an ultra-high-resolution tool that may assist in pathologies such as essential tremor.

Finally, in the sixth Chapter, I provide some overall conclusions of the major findings and the clinical applications that may benefit from these ultra-high-resolution delineations due to the fact that there is a lack of precise anatomical information in the literature about the brainstem pathways analysed herein, and most particularly referring to the pattern of the fibres within the same pathways.

List of abbreviations

117 anatomical parts, areas, structures:

10n: vagus nerve

12N: hypoglossal nucleus

3n: oculomotor nerve

3V: third ventricle

4n: trochlear nerve

4N: trochlear nucleus

4V: fourth ventricle

5n: trigeminal nerve

6n: abducens nerve

7n: facial nerve

8n: vestibulocochlear nerve

ac: anterior commissure

AD: axial diffusivity

ami: amiculum

Aq: cerebral aqueduct

Ar: arcuate nucleus

AV: anteroventral nucleus of the thalamus

bic: brachium of the inferior colliculus

CC: central canal

CIC: central nucleus of the inferior colliculus

cp: cerebral peduncle

csc: commissure of the superior colliculus

ct: cerebellothalamic tract

ctg: central tegmental tract

cu: cuneate fasciculus

Cu: cuneate nucleus

DH: dorsal horn of the spinal cord

drt: dentato-rubro-thalamic tract

dsc: dorsal spinocerebellar tract

DTI: diffusion tensor imaging

dtt: dorsal trigeminothalamic tract

DWI: diffusion weighted imaging

E: ependyma

ECu: external cuneate nucleus

f: fornix

FA: fractional anisotropy

FAC: fractional anisotropy colour

fr: fasciculus retroflexus

gr: gracile fasciculus

Gr: gracile nucleus

GRE: gradient recalled echo

H1: field H1 of Forel

H2: field H2 of Forel (lenticular fasciculus)

Hb: habenula

Hy: hypothalamus

ia: internal arcuate fibres

IC: inferior colliculus

ic: internal capsule

icp: inferior cerebellar peduncle

IOPr: inferior olive, principal nucleus

IRt: intermediate reticular nucleus

isRt: isthmic reticular formation

lcs: lateral corticospinal tract

lfp: longitudinal fibres of the pons (which are the descending fibre bundles through the basilar pons)

ll: lateral lemniscus

LPCu: lateral pericuneate nucleus

LPGi: lateral paragigantocellular nucleus

LRt: lateral reticular nucleus

MB: mammillary body

mcp: middle cerebellar peduncle

MD: mean diffusivity

MdD: medullary reticular nucleus, dorsal part

MdV: medullary reticular nucleus, ventral part

MG: medial geniculate nucleus

ml: medial lemniscus

mlf: medial longitudinal fasciculus

MRI: magnetic resonance imaging

mRt: mesencephalic reticular formation

mt: mammillothalamic tract

mtg: mammillotegmental tract

MVe: medial vestibular nucleus

oc: olivocerebellar tract

opt: optic tract

p1Rt: prosomere 1 reticular formation

PBP: parabrachial pigmented nucleus

pc: posterior commissure

PCRt: parvicellular reticular nucleus

Pi: pineal gland

Pn: pontine nuclei

PnC: pontine reticular nucleus, caudal part

PnO: pontine reticular nucleus, oral part

Pr5: principal sensory trigeminal nucleus

Pul: pulvinar

py: pyramidal tract

pyx: pyramidal decussation

R: red nucleus

RD: radial diffusivity

RLi: rostral linear nucleus

RMC: red nucleus, magnocellular part

RPC: red nucleus, parvicellular part

rs: rubrospinal tract

Rt: reticular nucleus

SC: superior colliculus

scp: superior cerebellar peduncle

smv: superior medullary velum

SN: substantia nigra

SNCD: substantia nigra, pars compacta dorsalis

SNR: substantia nigra, pars reticulata

sol: solitary tract

SolI: solitary nucleus, interstitial part

sp5: spinal trigeminal tract

Sp5C,1,2,3/4: spinal trigeminal nucleus, caudal part, laminae one to four

Sp5C: spinal trigeminal nucleus, caudal part

Sp5I: spinal trigeminal nucleus, interpolar part

Sp5O: spinal trigeminal nucleus, oral part

spth: spinothalamic tract

SpVe: spinal vestibular nucleus

STh: subthalamic nucleus of Luys

tfp: transverse fibres of the pons

tfp1: most ventral transverse fibre of the pons (ventral arcuate)

tfp10: most dorsal transverse fibre of the pons (dorsal arcuate)

Thal: thalamus

ts: tectospinal tract

tth: trigeminothalamic tract

tz: trapezoid body

vfu: ventral funiculus

VH: ventral horn of the spinal cord

VLTg: ventrolateral tegmental area

VPL: ventral posterolateral nucleus

VPM: ventral posteromedial nucleus

vsc: ventral spinocerebellar tract

VTA: ventral tegmental area

vtt: ventral trigeminothalamic tract

x4n: decussation of the trochlear nerve

xml: sensory decussation

xscp: decussation of the superior cerebellar peduncle

ZI: zona incerta

The abbreviations reported in this research are consistent with what was established by Paxinos et al. (2020).

Table of contents

Thesis abstract …….. i

Acknowledgements ……...……. iii

Overview ……...… viii

List of abbreviations..... xii

Table of contents..... xx

CHAPTER 1: General introduction 1

1.1 Historical approaches to neuroanatomy are defined by available experimental techniques ……...…… 2

1.2 Synopsis of the nervous system …….. 3

1.3 The brainstem pathways ……. 7

1.4 Descending spinal projections 7

Corticospinal Tract: Overview in Rodents and Humans 8

Hypothalamospinal Tract ……..... 20

Cerebellospinal Tract ……..... 20

1.5 Projections from the brainstem to the spinal cord …….. 21

Group A ……. 22

Vestibulospinal Tract 22

Tectospinal Tract ……... 23

Medial reticulospinal Tract …… 24

Group B ……. 25

Rubrospinal Tract …….. 25

Lateral reticulospinal Tract …… 26

Solitariospinal Tract …….. 27

Coeruleospinal Tract ……. 27

Raphespinal Tract …….. 27

Spinal and Principal Trigeminospinal Tracts …… 28

Gracilospinal and Cuneospinal Tracts ……... 28

Retroambiguus Nucleus to the Spinal Cord …….. 28

1.6 Ascending spinal projections …….. 29

Dorsal Column Pathways …….. 29

Cuneate and Gracile Fasciculi ……... 30

The Postsynaptic Dorsal Column Pathway …… 31

Ventrolateral Funiculus …… 32

Spinocerebellar Tracts ……... 33

Spinocervico thalamic Pathway …… 35

Spinoreticular Tract ……... 37

Spinothalamic Tract …….. 37

1.7 Integration of pyramidal and extrapyramidal systems to control posture and movement …… 42

The cerebrocerebellar circuit…….. 47

1.8 Impact of DTI on clinical research and applied science ……. 59

Technical aspects of DTI …….…..... 60

Calculating DTI measurements ……..... 61

DTI scalars ……..…….. 62

Fractional Anisotropy Colour (FAC) maps ……..…..... 64

Tensor Glyphs derived from diffusion tensor imaging ……..……... 65

Step-by-step approach in Deterministic vs Probabilistic Tractography 66

The potential of Postmortem Tractography …….…..…… 70

Optimisation and Limitations of DTI and Tractography ……..…… 72

Interpretation of DTI ……..… 75

High Angular Resolution Diffusion Imaging (HARDI) ……...…… 76

1.9 Development of DTI to map the human brainstem ……..…… 77

1.10 Relationship between DTI / Tractography and Classical Tracing Techniques

….……...…….. 87

1.11 Concluding statements …… 90

Overall aim of the present study …… 92

CHAPTER 2: General methods …… 94

2.1 Johns Hopkins University human specimens ……. 96

Specimen preparation …… 96

Image acquisition …….. 97

Image processing ……... 98

2.2 Duke University human specimens …… 98

Specimen preparation …… 98

Image acquisition …….. 99

Image processing ……. 100

Diffusion tractography …….……..... 101

2.3 Duke University macaque specimen..... 105

Specimen preparation …….. 105

Image acquisition 106

Image processing ……. 107

2.4 Comments regarding the different specimens ……... 107

2.5 Methodological analysis of brain mapping, anatomical delineations and fibre tracking..... 109

2.5.1 Methodology 109

2.5.2 Deterministic Tractography 109

2.5.3 GRE intensity differences between nuclei and tracts 110

2.5.4 Tract annotations and delineations 118

2.5.5 Using the tensor glyphs to obtain accurate anatomical information on the FAC orientation 120

CHAPTER 3: Redefining the pathways in the basilar pons through ultra-high-field MRI, tractography and tensor glyphs 122

3.1 Introduction 123

3.2 Specific methods 127

3.3 Results 128

3.3.1 Orientation of the images and specimens 128

3.3.2 Overall anatomical descriptions of the subdivisions of the descending fibre bundles (corticopontine, -bulbar, -spinal tracts) traced from the internal capsule through to the medullary pyramids, including the projections to the SNR 129

3.3.3 Subdivisions of the crus cerebri and of the descending fibre bundles in the basilar pons (longitudinal fibres of the pons); (Pontine Homunculus) 149

3.3.4 Subdivisions of the transverse fibres of the pons 159

3.3.5 Subdivisions of the descending fibre bundles/subdivisions of the transverse fibres of the pons in the macaque 162

3.3.6 Subdivisions of the pyramidal tract 163

3.3.7 The corticopontine tract 163

3.3.8 The principle of topology ……..…….…. 167

3.3.9 The *Stria Pontis* ……..…….. 174

3.4 Discussion …… 177

3.4.1 The Corticopontine tract is formed collectively by fibres peeling off from all the descending bundles ……... 178

3.4.2 The topography of the fibre bundles in the crus cerebri and basilar pons ……..…….. 181

3.4.3 The *Stria Pontis* ……..…….. 182

3.4.4 Possible Functional Consequences of the Inter-relationship Between the Longitudinal and Transverse fibres of the Pons …….….. 185

3.4.5 Comparative Anatomy ……..……... 186

3.4.6 The striatonigral and corticonigral projections ……..…….. 187

3.4.7 Clinical relevance ……..……... 188

3.4.8 Implications for Specific Surgical Procedures ……. 190

CHAPTER 4: Sensory pathways in the human and macaque brainstem and thalamus……...…. 193

4.1 Introduction ……..….. 194

4.2 Specific tractography methods …….……..... 199

4.3 Results …….…..... 201

4.3.1 Anatomical details of the dorsal column - medial lemniscus pathway in the medulla oblongata ……...……..... 201

4.3.2 Anatomical details of the spth in the medulla oblongata ……..... 206

4.3.3 Topography of the spinal trigeminal tract (sp5) from the pons to the caudal medulla oblongata ……..……..... 209

4.3.4 Anatomical details of the ml, spth, 5n, vtt and dtt in the pons …..…..... 210

4.3.5 Topography of the ml, spth and tth in the isthmus, midbrain and thalamus ……..…….. 216

4.4 Discussion …… 220

4.4.1 Implications for surgical treatment of pain and brain trauma …..…… 220

4.4.2 Advances in knowledge of the sensory tracts …….…..…… 222

4.4.3 Advanced resolution of the trigeminal pathways ……..……... 224

4.4.4 Comparing macaque and human brainstem structures ……. 227

CHAPTER 5: The dentato-rubro-thalamic tract in the human and macaque ……..……. 229

5.1 Introduction …….. 230

5.2 Specific methods …….…. 233

5.3 Results …….. 235

5.3.1 Topography of the scp and analysis of the fibre arrangement from caudal pontine levels to the isthmus ……...……. 235

5.3.2 Analysis of the fibre arrangement of the drt into the xscp ……..…. 240

5.3.3 Topography of the drt from the xscp to the red nucleus ……..…. 243

5.3.4 Arrangement of the drt at the level of the red nucleus ……..……...… 247

5.3.5 Topography of the cerebellothalamic tract through the diencephalon ……..... 252

5.4 Discussion …… 256

5.4.1 Decussating vs non-decussating pathway ……..…….. 257

5.4.2 Terminations of the drt ……..……... 258

5.4.3 Implications for DBS treatment of tremor ……...……. 259

5.4.4 The complexity of the drt ……..……... 261

5.4.5 Clinical Implications ……..…….. 263

CHAPTER 6: Conclusions 265

6.1 Synopsis of Discoveries ……... 267

6.2 Complex mathematical algorithms and sophisticated higher order techniques promote modernised fibre tracking ……..…. 269

6.3 Implications of the work …….. 271

6.4 Future Perspectives …….. 272

6.5 Final Comment ……. 273

References 275

Appendix 310

CHAPTER 1:
General introduction

1.1 Historical approaches to neuroanatomy are defined by available experimental techniques

Since the origins of neuroanatomy, the development of increasingly sophisticated techniques for neural network visualisation such as Golgi, Nissl and myelin staining has contributed to unravel the enigma of the central nervous system. The first known written document of neuroanatomy is an ancient Egyptian manuscript (circa 1600 BCE), which describes 48 case histories of tumours, head injuries and therapeutic procedures, called the Edwin Smith Papyrus (Atta, 1999). The next ground-breaking discovery in neuroanatomy was made from the Greek pre-Hippocratic writer and thinker Alcmaeon of Croton, who understood that the brain and not the heart controlled the body functions, and that the various senses were connected to the brain (Rose, 2009). Throughout the centuries considerable contributions in the field of neuroanatomy were made (Galen, Herophilus, and Erasistratus of Alexandria). However, it was not until Pope Sixtus IV that neuroanatomy was reanimated by changing the papal policy to allow human dissection. This successively led to an explosion of cadaver-centric studies during the Renaissance in Italian cities such as Bologna, Florence, Padua and Messina (Giovanni Alfonso Borrelli, Marcello Malpighi); (Nanda et al., 2016).

More recently, the use of scientific methods such as Wallerian degeneration, silver staining (Golgi), aniline dyes (Nissl), Luxol fast blue stain (myelin); (Pearce, 2000) significantly contributed to brain mapping but it was not until pioneers such as Alf Brodal (1910-88) who generated extensive academic work using biological

tracers in experimental animals such as monkeys, cats and dogs, that brain mapping took on a new dimension (Holck, 2001).

However, there was a lack of studies in humans due to the fact that viral tracing is permitted only in non-human primates and most significantly all the above methods do not permit the study of brain structures in its natural 3D space. Over the last decades, major advances in neuroimaging shed light into brain anatomy and provided sophisticated techniques such as diffusion tensor imaging (DTI), tractography and higher order techniques based on mathematical principles (tensor glyphs); (Basser et al., 1994b).

Only the advent of ultra-high-field magnetic resonance imaging (MRI) made it possible for the application of the aforementioned fledgling techniques to investigate the brain pathways in an unprecedented level of spatial isotropic resolution that approaches that of histology. Note that current ultra-high-field MRI has a resolution almost ten-fold higher than that obtained from clinical MRI (Calabrese et al. (2015b); see Chapter 5.1).

This thesis exploits the opportunities given by this powerful tool to shed light into the brainstem pathways and most importantly to reveal the pattern of fibres within the various bundles and components of these pathways.

1.2 Synopsis of the nervous system

The nervous system is a highly specialised network in animals, which coordinates movement and sensory information by transmitting nerve impulses

between parts of the body. In vertebrates, the nervous system consists of two parts. The central nervous system which contains the brain and spinal cord and the peripheral nervous system which is made of nerves connecting the central nervous system to every other part of the body (Catala and Kubis, 2013). The brain is the central organ (of approximately 1.3 kilograms in weight) of the nervous system, which controls all functions of the body, the brain enclosed and protected within the skull consists of the cerebrum, cerebellum and brainstem (Hartmann et al., 1994). During the early development of the nervous system, three primary brain vesicles begin to form which are, from rostral to caudal, 1) the forebrain (prosencephalon), 2) the midbrain (mesencephalon) and 3) the hindbrain (rhombencephalon). Subsequently, these develop into five secondary brain vesicles. At this five-vesicle stage, the forebrain separates into the telencephalon and diencephalon. The telencephalon develops into the cerebrum. The cerebrum is the largest part of the brain which contains the two cerebral hemispheres, and subcortical structures such as the hippocampus, basal ganglia and olfactory bulb (De Lahunta et al., 2016, Hébert and Fishell, 2008). According to traditional subdivisions the diencephalon consists of the thalamus, hypothalamus, subthalamus and epithalamus. However, modern gene-marker based conceptions by Martinez-de-la-Torre et al. (2018) exclude the hypothalamus from the diencephalon. The hypothalamus is more properly considered part of the telencephalon. The midbrain is the most rostral part of the brainstem (see below) and consists of the tectum, the cerebral aqueduct, tegmentum and the cerebral peduncles. The hindbrain is the last developmental categorisation of the central nervous system, in vertebrates, and includes the medulla oblongata, pons Varolii, and cerebellum (Stiles and Jernigan, 2010).

The brainstem is of significance because it regulates cardiac and respiratory function, movement and arousal, as well as cognition and emotion through its numerous groups of neurons, or nuclei, that integrate afferent and efferent information. It also controls the activation or inhibition of the neocortex via the reticular formation, thus playing an important role in maintaining arousal and consciousness. The brainstem is the caudal part of the brain which connects to the diencephalon rostrally, and to the spinal cord caudally. Hence, it is both a key relay structure and an important homeostatic control centre. Traditionally the brainstem is subdivided into three parts: the midbrain, the pons and the medulla oblongata (Fig. 1.1). The brainstem has specific motor and sensory functions associated with the head and neck, innervating important facial and throat muscles and receiving important sensory input from these same regions. Moreover, a vast number of pathways pass through the brainstem en route to the neocortex on one hand, and to the spinal cord on the other (Angeles Fernández-Gil et al., 2010). In this literature review, the major pathways of the brainstem and their connections to autonomic regulatory centres will be described.

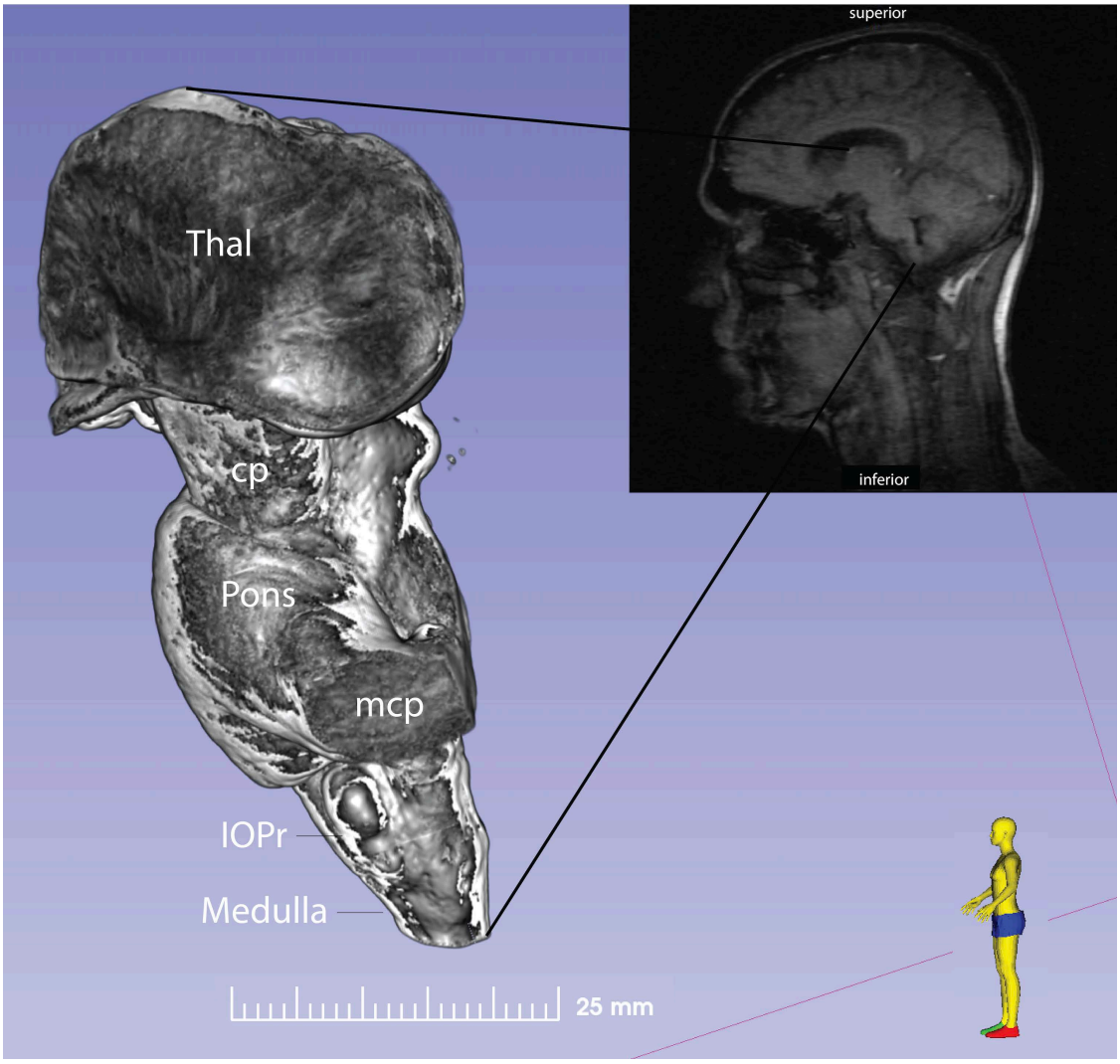

Fig. 1.1. A sagittal section of the head and neck obtained from a mainstream MRI (courtesy by C. Skliros, top, right) showing the main parts of the central nervous system such as the neocortex, cerebellum, thalamus, brainstem and spinal cord. *The magnified inset shows the 3D morphology of the brainstem and thalamus (courtesy by the Duke Center for In Vivo Microscopy). Abbreviations: Thal: thalamus, cp: cerebral peduncle, Pons: pons Varolii, mcp: middle cerebellar peduncle, IOPr: inferior principal olivary nucleus, Medulla: medulla oblongata.*

1.3 The brainstem pathways

The brainstem pathways can be classified based on the direction of transmission of the information which is conveyed in relation to other structures of the central nervous system. In this review I provide three broad categories: 1) the descending spinal projections which originate from supraspinal centres and terminate in the spinal cord, 2) the projections from the brainstem to the spinal cord which originate from nuclei in the brainstem and project to the spinal cord, and 3) the ascending spinal projections which carry somatic and visceral information to supraspinal centres (brainstem, thalamus and neocortex). This review Chapter is subdivided so each of these categories is described separately. I emphasise particularly the corticospinal and spinothalamic tracts.

1.4 Descending spinal projections

The 1st category of fibre tracts through the brainstem are the descending spinal projections. These projections originate in the cerebral cortex and the cerebellum. In this section I will briefly describe: the corticospinal tract, the hypothalamospinal and cerebellospinal tracts.

These descending spinal projections are responsible for eliciting voluntary motor functions and for control of muscle tone, reflexes, balance and for autonomic responses (Aravamuthan et al., 2007).

Corticospinal Tract: Overview in Rodents and Humans

The corticospinal tract, as the name suggests, is composed of fibres with origins in the neocortex and with terminal projections towards the spinal cord. The corticospinal tract is formed by axons of the pyramidal cells located in the cerebral cortex, and principally in the primary motor cortex. These axons originate from across the full lateral to medial extent of the cortex and hence fibres of the corticospinal tract descend from multiple directions as they converge into the internal capsule and then towards the brainstem. The fibres converge and travel on the anterior surface of the medulla, giving the impression of an inverted pyramid protruding from the surface (the "medullary pyramids"). This feature and the fact that its fibres arise from the pyramidal cells gives rise to the alternate name for the corticospinal tract, as the pyramidal tract (Davidoff, 1990). The pyramidal tract also contains the corticobulbar tract which carries information to the medulla oblongata (Canedo, 2003).

Marked differences in the pyramidal tract exist between primates and rodents. For example, the pyramidal tract may be relatively small in the rodents compared to the pyramidal tract observed in the primates (Paxinos, 2015). Furthermore, there is a major difference in the course of the corticospinal tract (Heffner and Masterton, 1983). In the spinal cord white matter, the corticospinal tract can be subdivided into two parts: the ventral or anterior; and the dorsal (rat) or lateral (human) corticospinal tracts. For the rat, the dorsal pathway is located in the dorsal column of the spinal cord and is the largest subdivision in rodents. In contrast, in primates it is a major fibre bundle in the lateral column.

Function of the corticospinal tract

The ventral corticospinal tract is primarily responsible for postural movement of the trunk and axial muscles. The cortical control is both ipsilateral and contralateral.

The lateral corticospinal tract sends fibres to innervate motoneurons which are responsible for the extremity muscles of the contralateral upper and lower limbs (contralateral cortical innervation); (Nathan et al., 1990). On the other hand, there is currently compelling evidence from studies using transcranial magnetic stimulation that both hemispheres are involved in control of each limb, suggesting the possibility of compensatory recovery of function after lesions such as strokes (Jankowska and Edgley, 2006, Wassermann et al., 1991).

Finally, the corticospinal tract is responsible for modulating sensory information from the body due to the fact that also the somatosensory cortex (postcentral gyrus) participates in the formation of its fibres (Mollet, 2008).

Origin of the corticospinal tract

Brodmann (1909) used a staining method (Nissl) to classify different cell morphologies within the cortex and thereby subdivide the cortex into different areas. The Primary motor cortex was labelled as area 4, and the Premotor cortex as area 6. Kuypers (1981) showed that area 4 and 6 gave rise to 60% of the corticospinal tract fibres in non-human primates whereas the other 40% had their cell bodies in the postcentral gyrus and parietal areas. In humans, about 80% of the corticospinal tract originates in areas 4 and 6. The laminar origin of the corticospinal tract is cortical

layer 5, where the pyramidal cells are clustered in groups of varied size - the largest neurons (giant pyramidal or Betz cells) are found in the precentral cortex. The human corticospinal tract is composed of over one million axons, three quarters of which are myelinated. The dimensions of the axons vary, with 80 % less than 2 microns in diameter and the rest ranging from 5 to about 22 microns (Lassek and Evans, 1946, Lassek, 1940).

Passage through the internal capsule and brainstem

In the internal capsule, the fibres of the corticospinal tract condense to form the major part of its posterior limb. At the level of the midbrain they pass through what was originally labelled as the basis pedunculi, but what is now more commonly called the cerebral peduncle, to enter into the basilar pons. The fibre tracts maintain some relationship to the topography observed at the motor cortex (the motor homunculus), with fibres related to muscles of the hand found in the antero-medial part of the longitudinal fibres of the pons (lfp), whereas fibres controlling the leg muscles are found postero-laterally (Hong et al., 2010a).

Collaterals to brainstem

It should be appreciated that the fibres of the corticospinal tract give rise to a vast number of collaterals, and these collaterals branch off at multiple levels through both brainstem and spinal cord. These collaterals branch off to innervate different nuclei within the brainstem, including those associated with ascending sensory systems; those that form the descending bulbospinal systems; and finally to the

precerebellar nuclei such as the pontine nuclei and the inferior olive, principal nucleus (Kuypers, 1981, Armand, 1982). At the level of the spinal cord, histological studies have demonstrated that fibres of the corticospinal tract can branch off to innervate the ventral horn across multiple spinal segments (Sengul and Watson, 2012). Many neurons from primary, premotor and supplementary areas of the motor cortex that form the corticospinal tract also have collaterals that terminate into the different nuclei of the reticular formation from which the reticulospinal tract originates (see below), thus exerting the pyramidal control on extrapyramidal systems.

Collaterals to the vestibulospinal neurons have also been identified; In this case the projections derive mainly from premotor and parietal cortical areas (Jankowska and Edgley, 2006). According to Keizer and Kuypers (1984), there are more projections to vestibular nuclei originating from cortical areas which control the proximal rather than distal muscle groups. These collaterals also terminate into the bulbar reticular formation and onto interneurons in the spinal cord. The same projections terminate in brainstem and spinal interneurons, thus exerting a two-way control over the extrapyramidal systems. Finally, experiments in monkeys have demonstrated a severe deficit in precision grip tasks following lesions of the corticospinal tract. This has been confirmed by other studies where collaterals have been traced from the corticospinal tract to dorsal column nuclei, suggesting that they also control distal movements in relation to somaesthetic inputs (Canedo, 1997).

Pyramidal decussation

As we follow the corticospinal fibres pass the pons to the medulla, they converge ventrally to form discrete bundles known as the medullary pyramids.

At the most caudal part of the medullary pyramids some fibres cross, or decussate to the other side forming the lateral corticospinal tract. The lateral corticospinal tract in primates is formed after the pyramidal decussation which was considered to be in the caudal medulla. However, more recent rhombomeric analyses examined the distribution of AZIN2 (antizyme inhibitor 2) expression in adult mouse hindbrain (rhombomeric segmentation of the hindbrain) and concluded that the decussation occurs more caudally, within a zone defined as part of the spinal cord (Martinez-de-la-Torre et al., 2018). It is worth noting that, on the other hand, this study was conducted in mice. Therefore, this topography may not be applicable in humans. The extent of fibres which decussate and which remain in the ipsilateral side is also debated. Up to 30% of the corticospinal fibres in humans have been reported to descend ipsilaterally, as demonstrated from cases with lesions above the spinal cord, following anterolateral cordotomies where the cord was sectioned in the anterolateral quadrant, and from causes of motor neuron disease (Nathan et al., 1990, Armand et al., 1997). The fibres that do cross over form the lateral corticospinal tract that continues to its termination in the spinal ventral horn. The lateral corticospinal tract is located in the lateral funiculus of the spinal cord (Fig. 1.2a, 1.2b). Topographically, this tract is placed medial to the dorsal spinocerebellar tract until the end of its route in the lumbar and sacral segments (Nakanishi et al., 2004, Souma et al., 2009). The ipsilateral fibres form the ventral corticospinal tract and these instead descend in the ventral funiculus which is the white matter lying between the

ventral median fissure (Fig. 1.2a, 1.2b) and the ventral roots of the spinal nerves. These fibres are all thought to cross at the level of termination in the spinal cord, in a transverse bundle termed the ventral white commissure.

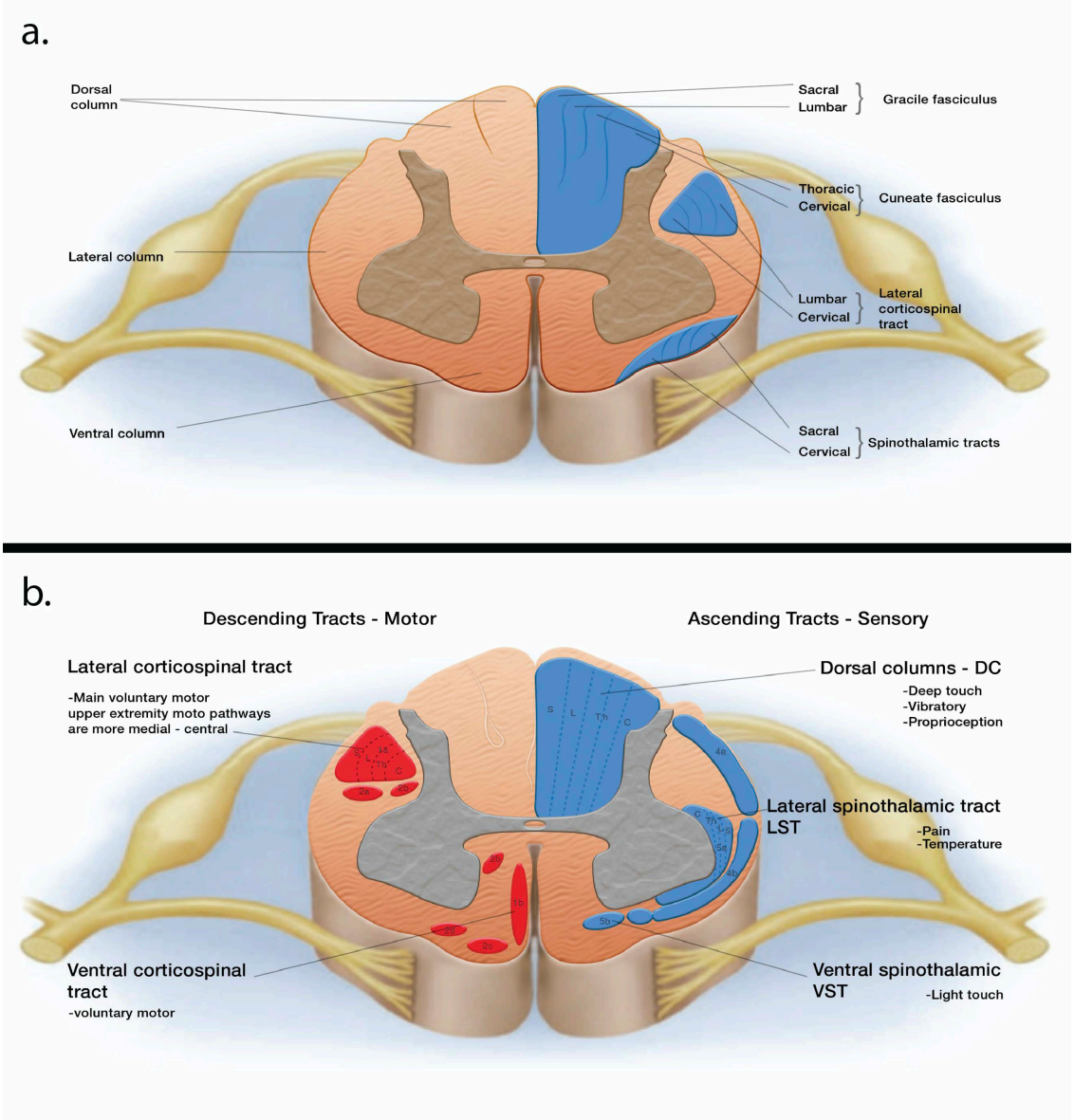

Fig. 1.2. Schematic representation of a cross section of the spinal cord showing the longitudinal subdivisions of white matter. *In (a) are reported the ventral, lateral and dorsal columns or funiculi which subdivide the spinal cord into longitudinal areas of white matter. Note the somatotopic organisation of the spinothalamic and lateral corticospinal tracts as well as that of the gracile and cuneate fasciculi (picture in (a) extensively modified by original taken from: http://kypho.com/dorsal-column.html). In (b) are reported the descending (motor system) and ascending (sensory system) tracts, in relation to their somatotopy. Note the somatotopy of the lateral corticospinal tract in relation to the dorsal column pathway. Abbreviations: C: cervical, Th: thoracic, L: lumbar, S: sacral (picture in (b) extensively modified by original taken from: https://www.orthobullets.com/spine/2004/spinal-cord-anatomy).*

Again, this is based on isolated lesions in the corticospinal tract fibres as well as from studies of Wallerian degeneration in living (MRI) and postmortem human specimens (Szymanski et al., 2020, Becerra et al., 1995). As more fibres decussate moving caudally through the medulla and spinal cord, the ventral corticospinal tract diminishes in size as it travels down to the levels of the lower thoracic cord (Brösamle and Schwab, 1997). The areas of termination of this ventral corticospinal pathway interestingly overlap with the areas of termination of the crossed (lateral corticospinal) pathway. Indeed, a number of fibres that form the ventral corticospinal tract overlap with the contralateral lateral corticospinal fibre projections (Nathan et al., 1990, Galea and Darian-Smith, 1994).

Termination in spinal cord

The recognised sites of termination of the corticospinal tract in humans are: a) the lateral parts of laminae 5-7, b) the dorsolateral motor neuron column (lamina 9), and c) the lateral parts of the central and ventrolateral motor neurons (lamina 9) (Fig. 1.3c). A minority (but up to 20%) of the fibres that form the human corticospinal tract terminate directly on motor neuron dendrites in lamina 9. Similarly, in non-human primates, lamina 8 (interneurons) and the medial part of lamina 7 (the intermediate region) receive the bulk of terminal projections of the corticospinal tract (Kuypers, 1981, Li and Martin, 2000, Sengul and Watson, 2012).

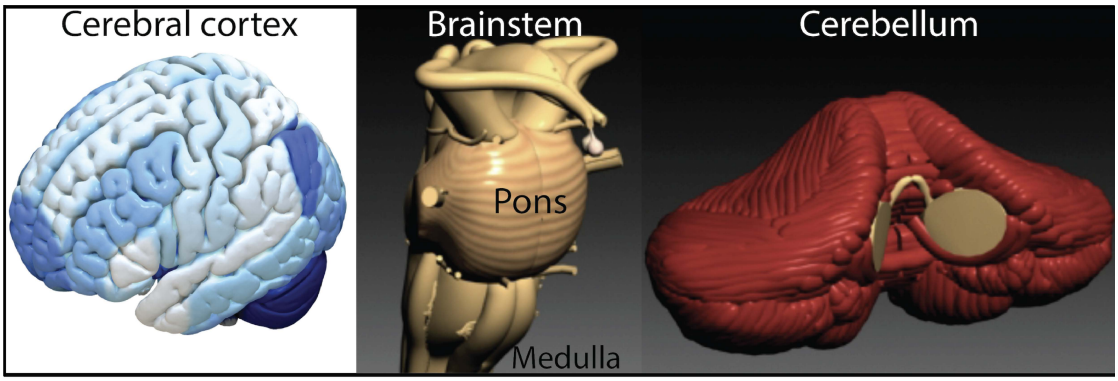

a.

Pons Varolii

Transverse section at the level of the trigeminal nerve

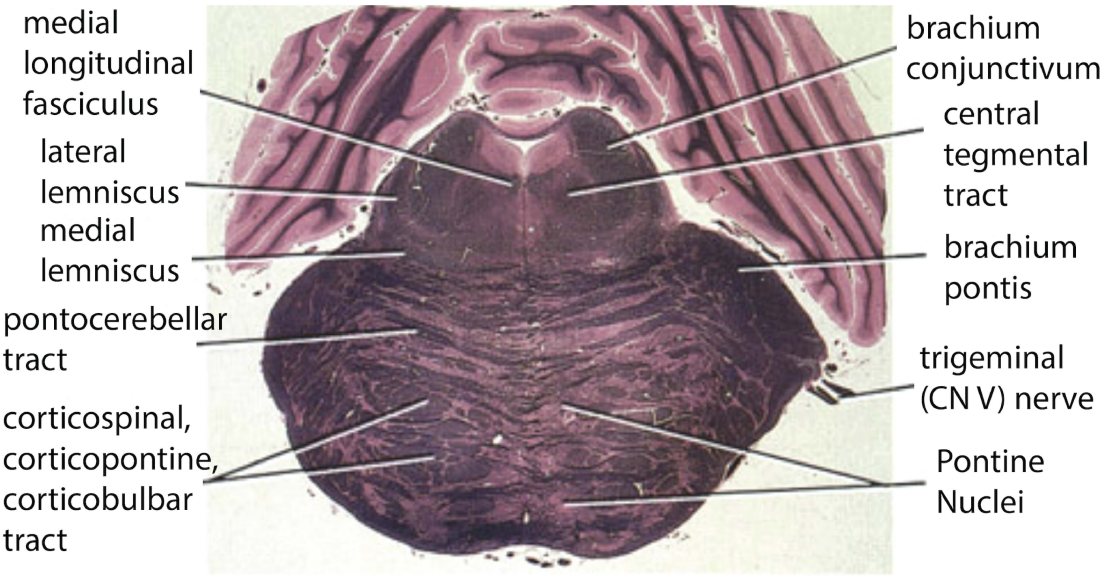

b.

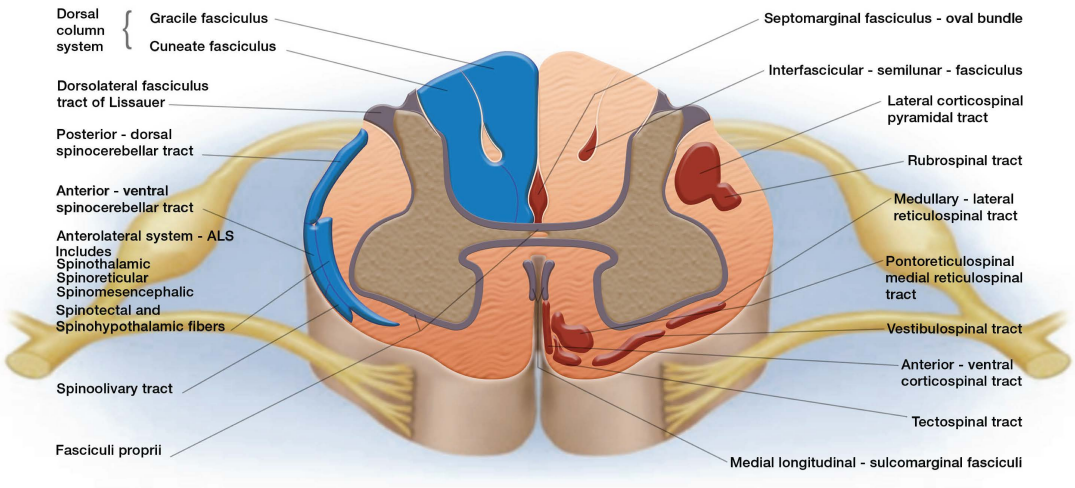

Spinal cord

C.

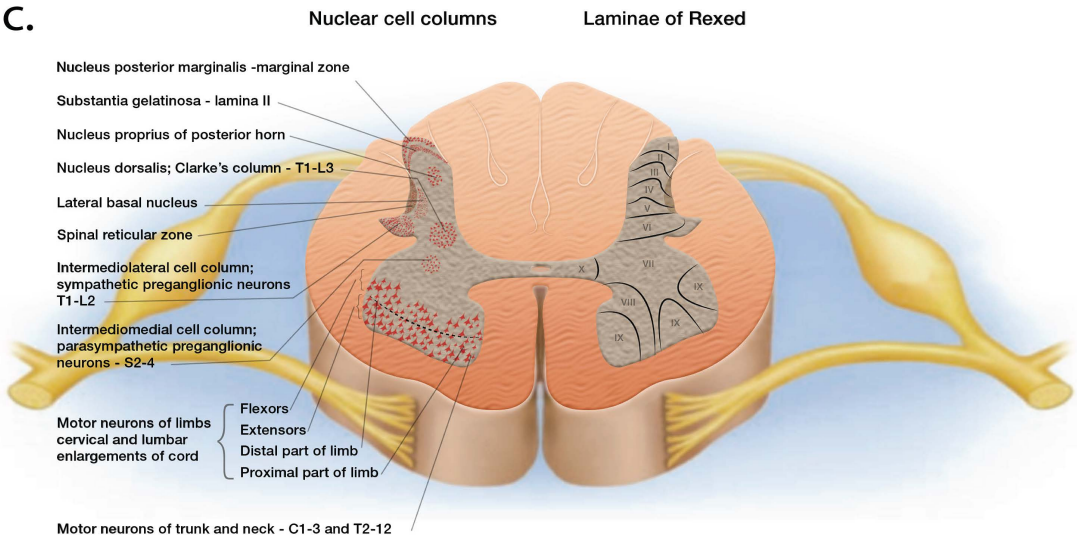

Spinal cord

Fig. 1.3. The spinal cord is a tubular part of the central nervous system which extends from the medulla oblongata to the lumbar region of the spine. *Information that travels to and from (blue and red arrows respectively) supraspinal centres such as the neocortex, diencephalon, brainstem and cerebellum traverses through the pons Varolii which is designated as a relay centre (a). The descending pathways such as the lateral corticospinal and rubrospinal, the reticulospinal and vestibulospinal are located within the various columns and convey information associated with balance and postural control (picture in (b) extensively modified by original from Carl B Spinner, 2015, Spinal Cord Medial Lemniscus Pathway). Spinal neurons are organised into laminae and nuclei (c). The laminae of Rexed consist of ten layers (I to X) of grey matter that form vertical columns through the spinal cord. The nuclear group of cell columns on the other hand, are groups of cell bodies in the spinal cord which can be subdivided from dorsal to ventral as seen in (c). Picture in (c) extensively modified from original Biswas 2015. Image at the top right taken from: Blause.com staff (2004). "Medical gallery of Blausen Medical 2014. Image at the top in the middle taken from: www.3d-brain.ki.se/atlas/medulla_oblongata.html. Image at the top left taken from: https://www.lead-dbs.org/helpsupport/knowledge-base/atlasesresources/cortical-atlas-parcellations-mni-space/. Image in (a) taken from: https://www.anatomyatlases.org/MicroscopicAnatomy/Section17/Plate17336.shtml.*

Variability of the corticospinal pathway

As indicated earlier, some marked differences exist between rodent and primate in the location of the corticospinal tract in the spinal cord, but other aspects of the course of the corticospinal tract are variable, even within the same species. Variations of the trajectory of the fibres, particularly at the pyramidal decussation such as aberrant pyramidal bundles or even absent pyramidal decussation, have been identified anatomically. Some of the variability occurs in different sides of the brainstem, which is of particular interest given that different people (and rodents) show hand dominance. For example, the fibres in the left pyramid usually decussate at a more rostral level in comparison with those of the right pyramid (Nathan and Smith, 1955, Yakovlev and Rakic, 1966). The right side of the cervical spinal cord in humans also typically receives more fibres from both cerebral hemispheres, as compared to left segments (Nathan et al., 1990). However, the same authors suggested this is not connected to handedness, but rather to the anatomical feature that in 75% of the cases the corticospinal tract decussates at a more rostral level from left to right compared to the right fibres. Half of the fibres that form the corticospinal tract are not detectible beyond the cervical spine. The remaining continues into the thoracic, lumbar and sacral spine. Consistently, a clear decrease in quantity of the axons that form the lateral corticospinal tract is observed in transverse sections throughout the spinal cord from the cervical to the sacral segments.

Development of the corticospinal tract

In humans, the corticospinal tract is relatively slow to develop in terms of reaching its targets. At 8 weeks of conception, the axons can be identified elongating

towards the pyramidal decussation and by 24 weeks post-conceptional age they reach the lower part of the cervical spina (Eyre et al., 2000). By 40 weeks post-conception, myelination can also be detected, although it does not reach adult levels until at least ages of 2-3 years. Fine gestures such as independent finger movements are evident within the first year postnatally. Finally, a decrease in the number of corticospinal axons has also been observed with age with a concomitant decrease in conduction velocity (ten Donkelaar et al., 2004, Eyre et al., 2000, Eyre, 2007).

Hypothalamospinal Tract

The fibres that originate from the ipsilateral paraventricular hypothalamic nuclear complex and from the lateral hypothalamus and the parafornical area constitute a descending central autonomic pathway known as the hypothalamospinal tract (Basbaum and Fields, 1979, ten Donkelaar et al., 1980, Holstege, 1987). These fibres descend in the dorsal part of the lateral funiculus (Saper et al., 1976) to synapse in laminae 1, 2, 9, 10 (Fig. 1.3c) of the spinal cord, as well as in the sacral parasympathetic and intermediolateral nuclei. This pathway is thought to be involved in the regulation of blood pressure and the stress response. Several neuropeptides (e.g. oxytocin, vasopressin and met-enkephalin) have been identified by Sofroniew (1985) in the spinal cord projections from the paraventricular nucleus.

Cerebellospinal Tract

The fastigial nucleus in the cerebellum gives rise to fibres that cross the midline and leave the cerebellum as part of the uncinate fasciculus (Fukushima et al., 1977). These fibres descend in the ventral part of the lateral funiculus (Fig. 1.2a) to

synapse on ventral horn neurons of the cervical spinal cord (Fig. 1.3c). These fibres are activated by somatic and labyrinthine stimuli and are thought to be involved in the coordination of balance.

In summary, there are three major descending pathways that course through the brainstem to terminate in the spinal cord. The pyramidal, the hypothalamospinal and the cerebellospinal tracts which originate in the cerebral cortex, hypothalamus and cerebellum, respectively.

1.5 Projections from the brainstem to the spinal cord

Apart from the corticospinal tract, the hypothalamic and the cerebellospinal tracts, the rest of the fibres that project to the spinal cord originate from nuclei found within the brainstem. Kuypers (1981) has subdivided the descending projections originating from the brainstem into groups A and B.

Group A comprises the vestibulospinal, tectospinal, interstitiospinal and medial reticulospinal tracts, all descending via the ventral and ventrolateral funiculi of the spinal cord. They terminate on neurons in spinal laminae 5-7 (Fig. 1.3c) ventromedially on both sides of the cord, presenting a vast degree of collateral fibres. Their projections control and adjust posture, co-ordinate limb and trunk movements, correct orientation of the head in relation to the body and play a significant role in coordinating the limb muscles synergistically (Green and Angelaki, 2010, Allen, 2008, Baker and Perez, 2017).

Group B comprises the rubrospinal and lateral reticulospinal tracts. They descend through the dorsolateral funiculus (Fig. 1.2a, 1.3b) presenting low collateralisation, and terminating on the dorsolateral parts of spinal laminae 5, 6 and 7 (Fig. 1.3c) as well as the motor neurons that innervate the distal limb muscles (Fig. 1.3c). The projections originating from group B finalise and supplement the motor control in association with group A and are responsible for flexion movements of the distal and proximal muscles of the limbs, particularly of the elbow and hand (Fig. 1.3c); (Nathan and Smith, 1982, Brownstone and Chopek, 2018, Peterson and Barnes, 1984).

Group A

Vestibulospinal Tract

The vestibular nuclei of the rhombencephalon give rise to the vestibulospinal tract. Most significantly, the lateral vestibular nucleus is the origin of the large lateral vestibulospinal tract, whereas the medial and spinal vestibular nuclei give rise to the medial vestibulospinal tract. The lumbosacral spinal segments receive afferent input from cells found in the dorsolateral part of the vestibular nuclear complex, whereas the thoracic and cervical segments receive fibres from the rostroventral parts of the nuclear group (Jang et al., 2018).

Fibres of the lateral vestibulospinal tract (lvs) descend in the ventral and lateral funiculi without any crossing throughout the spinal cord. At the level of laminae 7-8 (Fig. 1.3c) of the ventral horn, lvs fibres enter to synapse on both α- and

γ- motor neurons of lamina 9. Axons of lvs have an excitatory effect on motor neurons which innervate extensor muscles of the neck, back and extremities, whereas an inhibitory effect is applied to flexor muscles (Fig. 1.3c); (Grillner et al., 1970, Hongo et al., 1975).

Nathan et al. (1996) have identified degenerating fibres of the lateral vestibulospinal tract after spinal cord transections and cordotomies. These axons lie only on the periphery of the spinal cord at the level of the first three cervical segments, but shift laterally relative to the anterior roots before settling in the sulcomarginal angle for the rest of the cervical segments. More caudally, lvs fibres descend lateral to the ventral roots at the level of the thoracic spinal cord.

Neurons originating from the ipsilateral and contralateral medial vestibular nucleus, as well as from the spinal vestibular nucleus, give rise to the medial vestibulospinal tract (mvs). As Nyberg-Hansen (1966) pointed out the mvs occupies the ventral column adjacent to the sulcomarginal fasciculus. The mvs terminates in laminae 7-8 (Fig. 1.3c) at the level of the cervical and upper thoracic spinal cord. Its effect is inhibitory by monosynaptic and polysynaptic terminations on motor neurons that innervate muscles of the upper back and neck (Fig. 1.3c).

Tectospinal Tract

It has been demonstrated experimentally, in monkeys, cats and rats, that the tectospinal tract (ts) originates from the intermediate and deep layers of the posterolateral superior colliculus in the brainstem and projects to the upper cervical spinal segments (Castiglioni et al., 1978). It has been hypothesised by Castiglioni et al. (1978) that an ipsilateral tectospinal bundle arises from the anteromedial superior

colliculus. As Watson et al. (2008) noted, the superior colliculus receives inputs from the visual auditory and somatosensory systems. The ts fibres cross in the dorsal tegmental decussation throughout the length of the pons and medulla to reach the ventral funiculus at the level of the spinal cord (Fig. 1.2a, 1.3b). The ts projections terminate on interneurons in laminae 5-8 (Fig. 1.3c) and innervate motor neurons of the neck through polysynaptic connections, thereby inhibiting ipsilateral muscles while having an excitatory effect on the contralateral muscles. The major function of the ts is to coordinate neck movements and reflex postural control of the head in connection with visual information (Nyberg-Hansen, 1964).

Medial reticulospinal Tract

Phylogenetically, the reticulospinal tracts (medial and lateral reticulospinal; mrs, lrs) are among the oldest pathways of the vertebrate brain. The reticular formation of the pons and medulla is the site of origin of these neurons and the pathways are believed to take part in postural control, movement regulation and modulation of autonomic and sensory inputs (Peterson et al., 1975). These neurons receive multiple afferents such as vestibular, tectal, cerebellar and somatosensory inputs. They are believed to have an integrative role to coordinate whole-body movement as Drew and Rossignol (1990) have shown from experiments with microstimulation of the reticular formation.

The medial reticulospinal tract arises from the medial tegmental fields of the pons and medulla, originating from the ipsilateral rostral gigantocellular reticular nucleus and pontine caudal reticular nucleus. The mrs descends ipsilaterally in proximity to the medial longitudinal fasciculus to reach the ventral funiculus in the

spinal cord (Fig. 1.2a, 1.3b); (Baker, 2011). It synapses in laminae 6-9 (Fig. 1.3c) throughout the entire length of the spinal cord. Fibres from the pons descend more ventrally and have a more excitatory effect on axial and limb muscles compared to those arising from the medulla. The mrs is also excitatory to axial muscles (Nyberg-Hansen, 1965).

Group B

Rubrospinal Tract

The red nucleus (principally the caudal magnocellular section) gives rise to the rubrospinal tract as Massion (1967) and Murray and Gurule (1979) stated. According to ten Donkelaar (1988), the rubrospinal tract (and by extension its site of origin the magnocellular part of the red nucleus) regressed in size during primate evolution (Onodera and Hicks, 2009). In a comparative study made by Padel et al. (1981) it has been demonstrated that the number of axons that constitute the rubrospinal tract is about twice as large in the quadrupedal baboon as the bipedal gibbon. As ten Donkelaar (1988) reported this could be the consequence of the corticospinal systems taking greater control during the evolution of forelimb muscles in bipedal species.

The human rubrospinal tract (rs) originates from 150-200 giant neurons in the magnocellular part of the red nucleus, and contains fibres that are highly myelinated. They project to the brainstem and to the first three segments of the cervical spinal cord (Nathan and Smith, 1982). Axons of the rs decussate at the level of the ventral mesencephalic tegmentum and lie in proximity to the corticospinal tract as they

descend in the dorsolateral funiculus of the spinal cord (Fig. 1.2a, 1.3b). Antal et al. (1992) and Kuchler et al. (2002) found that the rodent rs terminates ipsilaterally on laminae 5-7 (Fig. 1.3c) at the level of the cervical and lumbosacral enlargements.

A topographic organisation has also been described for this pathway, whereby the axons terminating in the cervical enlargement (Fig. 1.3c) originate from the caudal part of the red nucleus and most particularly the dorsomedial region, whereas the fibres that terminate at the level of the lumbrosacral enlargement originate from the ventrolateral region of the red nucleus (rat - Strominger et al. (1987), monkey - Larsen and Yumiya (1980).

The rubrospinal tract exerts an excitatory effect on the flexor α- motor neurons and an inhibitory effect on the extensor α- motor neurons of the limbs (Fig. 1.3c), so that there is a synergistic effect between intralimb and interlimb coordination (Lavoie and Drew, 2002).

Lateral reticulospinal Tract

The medial part of the gigantocellular reticular nucleus of the pons gives rise to fibres that form the lateral reticulospinal tract (lrs). Its axons descend ipsilaterally and ventrally in the lateral funiculus in proximity to the ventral horn (Fig. 1.3b). Nyberg-Hansen (1965) demonstrated that in cats that lrs fibres end in laminae 1,5 and 6 as well as in laminae 7-9 (Fig. 1.3c) throughout the entire length of the spinal cord.

Its function is crucial in the phenomenon called ‘diffuse noxious inhibitory control’. Villanueva and Le Bars (1995) have shown with combined physiological measurements and provoked nociceptive reflexes that the reticular nuclei form

negative feedback spino-bulbo-spinal loops so that neurons in the dorsal horn of the spinal cord (Fig. 1.3c) are intensely inhibited after nociceptive pain.

Solitariospinal Tract

The ventrolateral part of the nucleus of the solitary tract in the medulla oblongata is the site of origin for the solitary tract and the solitariospinal tract. These fibres cross and descend in the contralateral ventral funiculus and ventrally in the lateral funiculus. Its role is respiratory regulation, emesis and micturition. Its fibres synapse on the phrenic nucleus at the level of C4-C6 and in laminae 9 (Fig. 1.3c) at the level of the thoracic spinal cord (Loewy and Burton, 1978).

Coeruleospinal Tract

Noradrenergic A4 and A6 cell groups in the locus coeruleus give rise to coeruleospinal projections in the spinal cord. These axons synapse on ventral horn neurons (Fig. 1.3c), the sacral parasympathetic nucleus and the deep dorsal horn as well as on intermediate grey. In addition, the nucleus subcoeruleus A7 group gives rise to descending fibres through the dorsolateral funiculus that synapse on laminae 1-3 (Fig. 1.3c). The latter is thought to be one of the centrifugal pain control systems that plays a crucial role in spinal nociceptive processing through the induction of antinociception at the level of the spinal cord (Tsuruoka et al., 2012).

Raphespinal Tract

Neurons in the raphe magnus, raphe obscurus and raphe pallidus nuclei give rise to serotoninergic fibres that run throughout the length of the dorsolateral

funiculus in proximity to the lateral corticospinal tract (Fig. 1.2b). These axons synapse in laminae 1, 2 and 5 (Fig. 1.3c) of the dorsal horn (Skagerberg and Bjorklund, 1985). According to Mason (1999), this fibre tract is crucial in controlling nociception through bulbospinal serotoninergic neurons and descending pain modulation at the level of the spinal cord and it is also involved in modulating reproductive, autonomic and excretory function.

Spinal and Principal Trigeminospinal Tracts – Gracilospinal and Cuneospinal Tracts

Leong et al. (1984) identified descending fibres from the spinal and principal trigeminal nuclei as well as from the gracile and cuneate nuclei named gracilospinal and cuneospinal tracts. These projections synapse in the dorsal horn at the level of the cervical spinal cord (Fig. 1.3c). The authors identified the above projections in adult albino rats, by injecting horseradish peroxidase into the cervical and lumbosacral segments of the spinal cord.

Retroambiguus Nucleus to the Spinal Cord

VanderHorst et al. (2001) identified spinal projections from the nucleus retroambiguus that descend in the contralateral ventral funiculus and ventrally in the lateral funiculus before innervating the laryngeal motor neurons.

In summary, a variety of different tracts descend from brainstem nuclei to the spinal cord in order to integrate motor control, nociception, autonomic, excretory function, and respiratory regulation.

1.6 Ascending spinal projections

These ascending pathways transfer somatic and visceral information such as touch and thermal sense, kinaesthesia and nociception.

Dorsal Column Pathways

The dorsal column pathways are ascending sensory spinal projections of the central nervous system that convey sensation of fine touch, proprioception, two-point discrimination and vibration (Leonard et al., 1992).

These pathways convey information from sensory mechanoreceptors in the periphery. This information travels through the first order-neuron the body of which is located in the dorsal root ganglion. The signal will travel through the axon of the neuron through the posterior root of the spinal cord, into the posterior horn, and then through the posterior column towards the medulla oblongata. Therefore, information from the lower body, below the level of the thoracic vertebra T6 will be conveyed through axons located in the medial part of the posterior column called the gracile fasciculus. Information from the upper body is conveyed by peripheral sensory axons that enter at or above T6 and are located in the lateral part of the posterior column called the cuneate fasciculus. Moreover, additional refined forms of proprioception such precision grasping is conveyed in the cuneate fasciculus (Glendinning et al., 1992).

The cuneate and gracile fasciculi ascend throughout the spinal cord until the medulla oblongata where upper body neurons (cuneate fasciculus) synapse with neurons in the cuneate nucleus and lower body neurons (gracile fasciculus) synapse with neurons in the gracile nucleus. These second order sensory neurons then project

through the brainstem and further to the thalamus and to the primary somatosensory cortex in the postcentral gyrus of the parietal lobe (Nosek, 1998, Barrett et al., 2015); (Figs 1.2 & 1.3).

Cuneate and Gracile Fasciculi

These two large ascending pathways (the direct dorsal column pathways) ascend in a region of the spinal cord known as the dorsal funiculus and is divided into two by the posterior intermediate septum. The cuneate fasciculus or tract of Burdach is situated lateral to the gracile fasciculus and conveys information from the upper truck and extremities from the sixth thoracic until the first cervical segment.

The gracile fasciculus or tract of Goll can be identified within the entire length of the spinal cord and conveys inputs from the lower trunk and extremities until the sixth thoracic segment (Figs. 1.2 & 1.3); (Luria and Laufer, 2007, Mai and Paxinos, 2012).

Hughes (1976), showed that the two fasciculi emerge as distinct fibre bundles in proximity to the midline during the ninth week of gestation. Their fibres ascend ipsilaterally to synapse on neurons in the gracile and cuneate nuclei within the medulla oblongata, respectively. The fibres are highly myelinated, with myelination complete by 36 weeks of gestation (Tanaka et al., 1995). The cuneate and gracile fasciculi originate from the central processes of dorsal root ganglion cells, which enter through the dorsal roots in the spinal cord and ascend towards the brainstem. The more caudal the fibres enter the spinal cord, the more medial are located within the dorsal funiculus and fibres from each segment are progressively shifted medially by fibres entering at more rostral levels. This topographical anatomy of the posterior

columns within the dorsal funiculus (Smith and Deacon, 1984) is also preserved in the dorsal column nuclei (gracile and cuneate nuclei) in the medulla oblongata. The internal arcuate fibres (second order neurons that project rostralwards) which originate from the cuneate and gracile nuclei, cross the midline and ascend as the medial lemniscus, which then synapses in the ventroposterolateral nucleus of the thalamus.

The entire projection can be identified as the dorsal column-medial lemniscus pathway.

The Postsynaptic Dorsal Column Pathway

A considerable number of first order neurons do not project directly to the gracile and cuneate nuclei in the medulla oblongata, instead they terminate on spinal neurons in the posterior columns whose axons then ascend and synapse into the gracile and cuneate nuclei (Tracey, 2004). This is the indirect Postsynaptic Dorsal Column Pathway whose cells are second order relay neurons in the spinal cord. The postsynaptic dorsal column pathway is the major pathway that conveys cutaneous mechanical and visceral nociceptive stimuli. Clinical studies conducted by Becker et al. (1999), Nauta et al. (1997), Hirshberg et al. (1996) on patients affected by visceral cancer showed that a midline myelotomy at the level of the thoracic spinal cord achieved considerable pain relief. Experiments in rats with chemically induced pancreatitis (Houghton et al., 1997) and colorectal distension (Palecek et al., 2002) demonstrated that dorsal column lesions significantly diminish certain behavioural responses after nociception.

Neurons of the postsynaptic dorsal column pathway lie in laminae 3-4, 5-7 (Fig. 1.3c) and primarily lamina 4 and adjacent laminae (Rustioni et al., 1979) and lamina 10 (Bennett et al., 1983). In monkeys, the postsynaptic dorsal column pathway arises from only 1000 neurons at the level of the cervical and lumbar enlargements (Fig. 1.3c). These axons synapse ipsilaterally in the gracile and cuneate nuclei. According to Rustioni et al. (1979), there is a somatotopic representation where projections from lumbar segments of the spinal cord terminate in the rostral part of the gracile nucleus, whereas afferents from the cervical enlargement (Fig. 1.3c) synapse in the cuneate and external cuneate nuclei. More rostrally, these axons form part of the medial lemniscus, transmitting inputs to the contralateral thalamus.

Ventrolateral Funiculus

Anatomically, the white matter of the spinal cord is divided into regions referred to as funiculi. Each half of the spinal cord contains a dorsal funiculus, a dorsolateral, a ventrolateral and a ventral funiculus. The ventrolateral funiculus contains multiple ascending projections. These include the spino-cerebellar, -parabrachial, -mesencephalic, -hypothalamic, -olivary, -cervicothalamic, -reticular, and finally, -thalamic tracts (Fig. 1.3b). Information such as non-discriminative touch, pressure, thermal stimuli and nociception is transmitted by axons found within the ventrolateral funiculus. The tracts which play a pivotal role in nociception are the spino-thalamic, -mesencephalic, -reticular, -cervicothalamic and the postsynaptic dorsal column pathway (see above); (Reed et al., 2006).

The most significant pathways in this region of spinal cord white matter are the spinothalamic tracts, which mediates sensory-discriminative pain (see below);

and the spinomesencephalic and spinoreticular tracts, which process motivational-affective aspects of nociception (Willis, 1985). Other tracts that form part of the ventral funiculus are often referred to as spinolimbic tracts, because they play a pivotal role in autonomic, endocrine and affective-motivational responses of nociception and contribute to affective behaviours such as arousal and attention. These pathways are the spinoreticular, spinoamygdalar and spinohypothalamic tracts (Ammons, 1987, Menétrey and De Pommery, 1991).

Spinocerebellar Tracts

Proprioceptive and cutaneous information from Golgi tendon organs and muscle spindles is conveyed through the dorsal and ventral spinocerebellar tracts (muscle afferent pathways). The cuneocerebellar and rostral spinocerebellar tracts transfer inputs from the upper limbs to the cerebellum for the coordination of movement. For muscles of the upper cervical segments (where the central cervical nucleus is located) the indirect spinoreticulocerebellar and olivocerebellar projections relay information to the cerebellum (Fig. 1.3b); (Stecina et al., 2013).

The dorsal spinocerebellar tract (dsc) is formed by neurons of the ipsilateral dorsal nucleus (Fig. 1.3c, Clarke's column) which is found from T1-L2 segments in the spinal cord (Smith (1976). The dsc occupies the dorsal part of the lateral funiculus in proximity to the lateral corticospinal tract (Fig. 1.2b, 1.3b). They originate in the intermediate and dorsal laminae at the level of the thoracic and lumbosacral segments and, in the rat and cat at least, this tract projects to the vermis and paravermal regions of the cerebellum (Matsushita et al., 1979). The dsc conveys

information for fine coordination of separate hindlimb muscles (Edgley and Gallimore, 1988, Kim et al., 1986).

The ventral spinocerebellar tract (vsc) is located more ventrally on the margin of the lateral funiculus (Fig. 1.3b), arising from laminae 5-7 of the thoracic and lumbar spinal segments (Fig. 1.3c); (Xu and Grant, 2005). Yaginuma and Matsushita (1989) demonstrated that the majority of spinal border cells (anterior horn neurons L5 to T12) give rise to axons that cross the midline, at the same spinal level, to ascend as the ventral spinocerebellar tract, although there is a small number of fibres that ascend ipsilaterally. The vsc axons pass through the medulla and pons to traverse the dorsal part of the superior cerebellar peduncle and recross to synapse in the ipsilateral lobe of the cerebellum. The vsc mediates information related to coordinated movement and posture of the lower limb (Kim et al., 1986, Yaginuma and Matsushita, 1989).

The rostral spinocerebellar tract arises from laminae 5-7 of the cervical spinal cord (Fig. 1.3c). It functionally corresponds to the ventral spinocerebellar tract, but for the upper extremities. The tract ascends ipsilaterally in the ventral part of the lateral funiculus to pass through both the superior and inferior cerebellar peduncles and terminate in the cerebellum (Kayalioglu, 2009).

Proprioception, touch and pressure from the upper trunk, neck and upper limbs are transmitted to the cerebellum through the spinocuneocerebellar or cuneocerebellar tract. This pathway is functionally similar to the dorsal spinocerebellar tract but serves these more rostral regions. The afferents travel through the cuneate fasciculus before terminating in the external or accessory cuneate

nucleus. From here the cuneocerebellar tract is formed and terminates in the ipsilateral cerebellum via the inferior cerebellar peduncle (Cooke et al., 1971).

Concerning other ascending projections towards the cerebellum, Matsushita and Yaginuma (1995) demonstrated that the central cervical nucleus located laterally to area 10 in C1-C4 segments, receives information from both the labyrinth and deep dorsal neck muscles. Its axons cross the midline at the same spinal level to ascend in the ventral funiculus, passing mainly through the superior cerebellar peduncle to terminations in the cerebellum.

Spinocervico thalamic Pathway

Light cutaneous and noxious stimuli are also transmitted by another fibre-tract which consists of two parts, the spinocervical and cervicothalamic tracts (Fig. 1.3b). The spinocervical tract arises from lamina 1-3, 4 and 5, mainly at the cervical enlargement (Fig. 1.3c) but also throughout the entire spinal cord as Bryan et al. (1974), Brown et al. (1980) and Craig and Tapper (1978) demonstrated. It ascends ipsilaterally through the dorsolateral part of the lateral funiculus and terminates in the lateral cervical nucleus, which lies in the lateral funiculus close to the dorsal horn of the C1-C4 spinal cord segments (Fig. 1.3c); (Truex et al., 1970). Craig and Burton (1979) highlighted a somatotopic organisation in the cat such that rostral parts of the body are represented in the medial part of the lateral cervical nucleus, whereas caudal parts are found in the lateral part. Subsequently neurons, originating in the lateral cervical nucleus, form the cervicothalamic tract and decussate at the level of the upper cervical segments of the spinal cord where the ventral white commissure is located before ascending to reach the contralateral thalamus. Berkley et al. (1980)

identified that these projections terminate in the medial part of posterior thalamic nucleus and the ventroposterolateral nucleus of the contralateral thalamus.

It has been hypothesised that the function of the spinocervical tract is to transmit nociceptive stimuli. Hamann et al. (1978) found that a variety of axons constituting the spinocervical tract are activated by noxious muscle stimulation. Those axons from cutaneous receptors are activated by noxious mechanical stimuli, thermal energy and light touch such as hair movement (Cervero et al., 1977). Craig (1978) identified that dorsal column nuclei project to the lateral cervical nucleus after they receive spinocervical collateral projections. Cao et al. (1993) and Djouhri and Jankowska (1998) demonstrated that spinocervical tract collaterals terminate with excitatory synaptic inputs on neurons which form the spinothalamic, spinoreticular, spinomesencephalic and postsynaptic dorsal column pathways. In turn, neurons of the periaqueductal grey, cuneiform nuclei and raphe magnus are found to exert a tonically inhibitory effect on these spinocervical tract neurons (Dostrovsky, 1984). Broman and Blomqvist (1989) showed that the lateral cervical nucleus of rat and cat is subject to serotoninergic innervation, leading them to hypothesise the existence of a descending pathway capable of modulating the transmission of somatosensory information. The same authors pointed out that although there are few GABA-immunoreactive neurons in the lateral cervical nucleus compared to other somatosensory relay nuclei, their presence in the monkey indicates that there is an extrinsic GABAergic input or that the collaterals containing GABA ramify widely in the lateral cervical nucleus.

Spinoreticular Tract

The highly myelinated spinoreticular tract arises from laminae 7-8, the lateral reticulated part of lamina 5 and more sparsely in lamina 1, and area 10 (Fig. 1.3c), and the lateral spinal nucleus. The spinoreticular tract ascends intertwined with spinothalamic fibres in the ventrolateral funiculus (Fig. 1.3b). In fact, some of its axons are collaterals of the spinothalamic tract. A vast number of nuclei such as the dorsal, gigantocellular and lateral reticular nuclei, the oral and caudal reticular nuclei in the pons, the central reticular and raphe magnus nucleus as well as the dorsal and lateral paragigantocellularis nuclei receive afferents from this spinoreticular tract (Mehler et al., 1960).

The reticular formation of the brainstem and the spinoreticular tract play a pivotal role in conditioned pain modulation. Menetrey et al. (1980) demonstrated that the nucleus raphe magnus and the reticular formation in the medulla act as a descending inhibitory control on spinoreticular tract afferents. Hence, this system controls motivational-affective aspects of nociception as well as motor and neurovegetative responses to nociceptive stimuli (Millan, 1999).

Spinothalamic Tract

The somatosensory region of the thalamus receives afferents conveying nociception and temperature as well as pressure and non-discriminative touch (crude touch). These afferents constitute the spinothalamic tract, which can be subdivided into a ventral or anterior (the paleospinothalamic) and a lateral (or neospinothalamic) tracts (Fig. 1.2a, 1.2b & 1.3b); (Kevetter and Willis, 1984). Apkarian and Hodge (1989b) and Ralston and Ralston (1992) also identified a separate pathway in

primates named the dorsolateral spinothalamic tract. At the level of the spinal cord, the ventral and lateral spinothalamic tracts are intermingled with the spinohypothalamic, spinoreticular, reticulospinal and spinomesencephalic tracts (Fig. 1.3b) and yet ascend separately to reach the brainstem where they merge to form the spinal lemniscus.

The ventral funiculus contains the ventral spinothalamic tract through which pressure sensations and crude touch are conveyed to the upper centres (Fig. 1.2b). In turn, the lateral spinothalamic tract, which transfers temperature and pain sensations, is located in the ventral part of the lateral funiculus in proximity and ventral to the spinocerebellar tract (Fig. 1.3b). Friehs et al. (1995) found clinical evidence for segregated pain and temperature conduction suggesting that two different components within the spinothalamic tract transfer temperature and pain sensation: the former is situated more ventrally and the latter more dorsally. Spiller and Martin (1912) developed the surgical partial division of the spinal cord through ventrolateral cordotomy in order to treat chronic unbearable pain from tumours of the cauda equina. Cordotomies utilise the percutaneous approach at the level of C1-C2, guided by fluoroscopy or CT. This technique is able to produce pain relief by severing the spinothalamic tract, which is located in the anterolateral quadrant of the spinal cord, demonstrating that this is the main pathway to convey nociception from the spinal cord to the cortex (Shepherd et al., 2017).

The ventral spinothalamic tract arises from laminae 1, 4-5, 7, 8 and area 10 (Fig. 1.2b, 1.3c); (Apkarian and Hodge, 1989b) although Trevino and Carstens (1975) found that there are significant differences in the location of the spinothalamic neurons between species. In the rhesus monkey, the majority of tract neurons are

situated in the contralateral lamina 1, 4-5 with the rest in laminae 6-8 (Fig. 1.3c). In humans, on the other hand, the segmental and laminar organisation is not well documented. Similarly, literature is sparse on common lab mammals to make translational comparison to, Klop et al. (2005), Burstein et al. (1990b), Apkarian and Hodge (1989b) identified 6000, 9500 and 18000 spinothalamic tract neurons in cats, rats and monkeys, respectively, with the majority contralateral. Granum (1986), Klop et al. (2005) and Apkarian and Hodge (1989a) reported that most tract neurons are ipsilateral at the level of the upper cervical segments. Of note it is interesting to see that the cat, which one would assume had more spinothalamic neurons than the rat, in fact has less, however more study is obviously required.

The dorsolateral spinothalamic tract makes up 25% of the entire primate spinothalamic tract (Apkarian and Hodge, 1989a). Tract neurons are located in laminae 2-3 and 4-6 (Fig. 1.2b, 1.3c) and axons cross the midline at the same level, to ascend through the dorsolateral funiculus to reach the ventral posterolateral nucleus of the thalamus as Ralston and Ralston (1992) and Martin et al. (1990) demonstrated. The thalamic terminations of the dorsolateral spinothalamic tract convey mechanical, noxious, and cutaneous thermosensory information. The terminal fields of dorsolateral and ventral spinothalamic tracts are superimposed in the thalamus (Apkarian and Hodge, 1989c).

Nathan et al. (2001) reported that the spinothalamic tract decussates transversely in the dorsal funiculus to then reach the ventrolateral funiculus and ascend rostralwards and not diagonally as previously thought. Brenner and Pendl (1966) showed that there are also variations of the human spinothalamic tract as shown by a rare case of an uncrossed pathway posterior to the denticulate ligament

(Moffie, 1975). Craig et al. (2002) hypothesised that the tract neurons in lamina 1 give rise to the lateral spinothalamic tract, which ascends forming a calbindin immunoreactive bundle in the middle of the lateral funiculus of primates. Aδ and C primary afferent fibres innervate neurons in lamina 1 and they respond to thermal, noxious and mechanical stimuli, whereas laminae 4-5 (Fig. 1.3c) receive terminations of Aδ fibres which synapse on excitatory interneurons in the deep layers of lamina 2. These interneurons are wide-dynamic-range nerve cells, meaning that they are characterised by large receptive fields and can be activated by both innocuous and noxious stimuli. Blair et al. (1984) reported that spinothalamic tract neurons can also be activated by noxious visceral stimuli, such as those evoked after coronary artery occlusion. The lateral part of the thalamus receives afferents from spinothalamic tract neurons situated in laminae 1-6 (Fig. 1.3c), whereas the intralaminar and medial nuclei of the thalamus receive projections from deeper spinothalamic tract neurons. Aversive behaviours connected to nociception are the result of the integration at the level of these deep spinothalamic tract neurons whereas the superficial neurons process, integrate and transfer sensory-discriminative aspects of pain (Martin et al., 1990).

The ventral and lateral spinothalamic tracts are composed of large axons that cross in the ventral white commissure to ascend through the ventrolateral funiculus. Axons constituting the former may ascend though a couple of segments before they decussate, whereas the latter crosses at the same level of the spinal cord where it arises (Stevens et al., 1991). About 10% of the fibres that constitute the spinothalamic tracts remain uncrossed. Zhang et al. (2000) demonstrated a somatotopic organisation of its axons in monkeys. As they ascend throughout the

length of the spinal cord the axons constituting the tract migrate laterally so that fibres coming from the caudal segments are placed laterally, whereas the medial part of the spinothalamic tract is formed by fibres from more rostral levels. At mid-thoracic segmental levels in primates, spinothalamic axons are found within the dorsolateral funiculus in proximity to the denticulate ligament. Zhang et al. (2000) also found that the ventrolateral funiculus hosts fibres of the spinothalamic tract arising from the deep dorsal horn (Fig. 1.3c). As the axons move upwards to more rostral levels and reach the level of the cervical enlargement, the axons forming the spinothalamic tract shift ventrally to be placed entirely within the ventrolateral funiculus. At the level of the pontine tegmentum, the ventral spinothalamic tract shifts posterolaterally to the medial lemniscus and posteriorly through the mesencephalic tegmentum (Hong et al., 2010a).

The spinal lemniscus is the continuation of the lateral spinothalamic tract in the brainstem (Fig. 1.2b). Spinothalamic axons terminate in the ventral posterolateral, ventral posteromedial, posterior nuclear group and central lateral nucleus of the intralaminar nuclei. Blomqvist et al. (2000) found thermoreceptive-specific and nociceptive neurons in the posteromedial and ventral posterolateral nuclei. Motivational affective responses to nociception are processed and unleashed by the central lateral nucleus of the thalamus where spinothalamic tract projections terminate. The ventrobasal complex, which projects to the lateral thalamus, plays a key role in sensory-discriminative characteristics of nociception. In addition, collateral projections distributing inputs from the spinothalamic tract to a variety of brainstem sites such as the reticular formation of the medulla, periaqueductal grey, nucleus accumbens and parabrachial area (Hylden et al., 1989) may set off

descending-nociceptive mechanisms to modulate autonomic and affective responses (Kevetter and Willis, 1983).

Dum et al. (2009) demonstrated termination of the nociceptive pathways contralaterally in the granular insular cortex, cingulate cortex, as well as the secondary somatosensory cortex. Hong et al. (2010b) used diffusion tensor tractography to trace connections from the ventral posterolateral nucleus of the human thalamus through the posterior limb of the internal capsule to reach the posterior portion of the corona radiata and terminate in the primary somatosensory cortex.

In summary, the ascending pathways transfer different types of sensory information through an intricate network of projections with termination in supraspinal centres. These supraspinal centres (neocortex, thalamus, hypothalamus, cerebellum) described above, integrate the information from the periphery in order to modulate secondary motor and autonomic responses to external stimuli.

1.7 Integration of pyramidal and extrapyramidal systems to control posture and movement

Posture is defined as the stance assumed by the body and various body segments during the course of muscular activity, and is the result of coordinated contraction of skeletal muscles in order to maintain balance. The human body has the ability to retain posture without conscious effort, thus the perception of the position and movement of the body also called proprioception is imperative. Since posture and body movements are the result of coordinated muscle contractions, it is essential

to understand how the motor system integrates information to ensure proper motor control (Cramer et al., 2018). The motor system can be defined as a set of peripheral structures and central parts of the nervous system, which integrate information to support motor function. Peripheral structures comprise skeletal muscle fibres and muscle spindles. Central parts comprise the neocortex, brainstem, cerebellum, spinal cord, and the pyramidal and extrapyramidal systems (Purves et al., 2018, Augustine, 2007). The pyramidal system also called pyramidal tract (corticobulbar and corticospinal tracts) is involved in the control of motor functions in the body (Marmarou, 2011). The lateral corticospinal tract terminates at each level of the spinal cord where its fibres synapse on lower motor neurons that control gross and fine motor movements. The anterior (non-decussating) corticospinal tract controls the proximal muscles and the trunk (Saladin, 2018, Marfeo, 2010). The extrapyramidal system consists of motor-modulation centres such as the substantia nigra, subthalamic nucleus of Luys, red nucleus, reticular formation and the cerebellum. From these centres a variety of subcortical extrapyramidal fibres stem out and terminate in the spinal cord. The extrapyramidal tract is a polysynaptic network of fibres. It is composed of the rubrospinal, reticulospinal, tectospinal and vestibulospinal tracts. These centres send information to the lower motor neurons (Fig. 1.3c) in an indirect way (de Oliveira-Souza, 2012). The rubrospinal tract originates from the red nucleus. The cerebellum transmits a signal to the spinal nerves through this tract. Information flows from the cerebellar cortex through the scp to the red nucleus (dentato-rubral tract) and from the red nucleus to the spinal cord through the rubrospinal tract. At the level of the spinal cord the fibres of the rubrospinal tract synapse onto α and γ motor neurons located in the ventral horn,

which in turn stimulate the flexor muscles, the muscles of the hands and fingers. The rubrospinal tract is responsible for the maintenance of muscle tone. In addition, this tract is responsible for rudimentary motor skills, which in turn are refined by the pyramidal tract (Williams et al., 2014). The reticulospinal tract transmits motor commands from the reticular nuclei of the pons and medulla to the spinal cord. This tract terminates into α and γ motor neurons, which control extensor muscles. The tectospinal tract originates from the superior colliculus and terminates into the ventral horn of the cervical and upper thoracic segments of the spinal cord. It's function is involved in the orientation of the eyes, head, neck and upper extremities in response to bright light, noises and sudden movement (Rose and Abrahams, 1978). Finally, the vestibulospinal tract originates in the medial vestibular nuclei and mainly terminates on spinal interneurons of the ventral horn in the spinal cord. These vestibulospinal inputs have excitatory effects extensor muscles that oppose gravity while exerting some inhibitory effects on flexor motoneurons (Grillner et al., 1970, McCall et al., 2017).

This integrated circuit between pyramidal (corticospinal tract) and extrapyramidal (rubrospinal tract) systems explains the decorticate rigidity where the upper extremities assume a rigid flexion pattern whereas the trunk and lower extremities assume a rigid extension pattern. The decorticate rigidity indicates a transection at the level of the diencephalon resulting in a lesion within the corticospinal tract with subsequent interruption of the pyramidal control, whereas the brainstem motor centres are working but there is no modulation of these centres from the corticospinal tract. In particular, there is disinhibition of the red nucleus, which causes subsequent overactivation of the rubrospinal tract. The rubrospinal and

medullary reticulospinal tracts have an excitatory effect on motor neurons in the cervical spinal cord, which supply the flexor muscles of the upper extremities. The second component that explains the decorticate posturing is the disruption of the lateral corticospinal tract which causes flexor muscles of the lower extremities to be impaired. Since the corticospinal control is interrupted, the pontine reticulospinal as well as the medial and lateral vestibulospinal tracts facilitate the extensor muscles of the lower extremities (Kawai et al., 2017). The decerebrate rigidity on the other hand indicates a transection below the red nucleus, at the brainstem resulting again in a lesion within the corticospinal tract and also the subsequent elimination of the function of the rubrospinal tract. In this way there is no type of regulation or modulation of the vestibulospinal and reticulospinal tracts, as a result the motor neurons within the spinal cord are over-activated with total loss of inhibition from the neocortex and basal ganglia. This brainstem lesion explains why the patient is rigid and with clenched teeth. Moreover, this brainstem lesion causes the head to arch posteriorly, rigid extension of elbows in addition to extension and internal rotation of all extremities. If there is further advancement of the lesion and the function of the vestibulospinal and reticulospinal tracts is eliminated the patient becomes flaccid. Further progression may lead to increased intracranial pressure and a subsequent tonsillar herniation which compresses the autonomic respiratory and cardiovascular centres in the pons and medulla oblongata that leads steadily towards death (Sherrington, 1898, Plum and Posner, 1972, Riddle et al., 2009).

To summarise, the motor system must take into account the distribution of body mass and make postural adjustments through the equilibrium of the pyramidal,

on one hand, and the extrapyramidal control on the other, in order to execute refined movements (Zaretsky, 1982).

Postural adjustments are performed through two mechanisms: 1) anticipatory mechanisms, or feed-forward mechanisms and 2) compensatory mechanisms, or feed-back mechanisms. Thus, the central nervous system maintains balance in an erect posture. The anticipatory mechanisms generate pre-programmed responses responsible for the final product of stability and are anticipatory, meaning that they are responsible for the beginning of voluntary movements. The compensatory mechanisms, on the other hand, consist of extremely rapid responses which can be improved by exercise and learning (Santos et al., 2010).

To conclude, in order to finalise posture, information is integrated at three hierarchical levels; the spinal cord; brainstem; and cerebral cortex.

The spinal cord is a crucial hierarchy for the execution of movement. It is well established that the spinal cord cannot generate movement without an external input. This external input derives from the descending fibre bundles (supraspinal centres in the brainstem and cortex). In addition, the spinal cord receives external input as sensory feedback from the periphery. More specifically, the motorneurons within the spinal cord neural network are subjected to afferent feedback from the muscles. In this way supraspinal cortical signals (pyramidal and extrapyramidal systems) are tuned in order to provide appropriate activation patterns at the level of spinal α and γ motorneurons (Teka et al., 2017). The most striking demonstration of this is the fact that patients with spinal cord injury can modify, initiate and maintain execution of movement in the absence of supraspinal control when external afferent inputs

(functional electrical stimulation) are applied to the spinal cord below the level of lesion (Dimitrijevic et al., 2015).

The brainstem comprises circuits that are represented by the medial indirect system such as the vestibulospinal, reticulospinal and tectospinal tracts (extrapyramidal system) which controls the proximal muscles, as well as by the lateral indirect system such as the rubrospinal tract which controls the distal muscles (Martini and Nath, 2009).

Finally, the cerebral cortex is responsible for the anticipatory mechanisms (pyramidal system), which are evocated by visual, cutaneous, vestibular, and muscular receptors.

More specifically, the inputs from the cerebral cortex are subjected to elaborate processing through a crucial feedback loop known as the cerebrocerebellar circuit and described below.

The cerebrocerebellar circuit

The cerebrocerebellar circuit is a feedback loop that bidirectionally connects the cerebral cortex and the cerebellum. The circuit consists firstly of a descending limb which originates in the cerebral cortex and terminates via the pontine grey matter into the cerebellum, and secondly, an ascending limb which originates in the cerebellum (dentato-rubro-thalamic tract (drt)) and projects via the ventral tier of the thalamus, to cortical motor areas (Fig. 1.4); (Gray et al., 1999, Brodal, 1981). The anatomical pathways in these descending and ascending limbs are discussed further

below. In Chapter 5, I also investigate part of the ascending limb of this circuit with ultra-high-resolution DTI and postmortem deterministic tractography.

The cerebrocerebellar circuit, connecting the neocortex and the cerebellum and most particularly through the coordination of the cerebrocerebellum (or pontocerebellum), plays a crucial role in a variety of somatic functions including motor coordination, motor learning and planning, and verbal working memory (Rosenbaum, 2009, Houk and Mugnaini, 2003, Marvel and Desmond, 2010). In addition, Ramnani (2006) reported evidence of cerebellar connections to the prefrontal cortex suggesting that the cerebellum also contributes to higher cognitive function. Moreover, Dow (1988) reported that electrical stimulation of the cerebrocerebellum evokes electrical potentials not only in cortical areas such as the prefrontal cortex, but also in language areas, suggesting that the cerebellum plays a key role also in cognitive function and speech.

Various anterograde and retrograde tracing techniques, MRI and diffusion tractography studies (Palesi et al., 2017) all concur that the white matter tracts originating from nuclei within the cerebrocerebellar circuit form distinct groups of bundles, giving rise to the concept of multichannel organisation of the cerebrocerebellar circuit (Buckner et al., 2011). This concept assumes that these fibre bundles form multiple, parallel but functionally diverse neuronal channels that can form loops between the cortex and the cerebellum. For example, descending neuronal channels from specific areas of the cerebral cortex convey information to specific regions of the cerebellum, which in turn, and through diverse ascending parts of the cerebrocerebellar circuit, convey information back to the same areas of

the cerebral cortex where the neuronal information originated (Benagiano et al., 2018).

The descending limb of the cerebrocerebellar circuit

The descending limb of the cerebrocerebellar circuit consists of the corticopontine tract (proximal segment), and the pontocerebellar tract (distal segment). The pontocerebellar tract originates from the precerebellar nuclei (pontine grey matter), and synapses onto the cerebellar cortex as *mossy* fibres (Fig. 1.4). Subsequently, the cerebellar cortex projects into the deep cerebellar nuclei, see below (Benagiano et al., 2018).

The proximal segment of the descending limb (corticopontine tract)

The corticopontine tract provides a line of communication between the neocortex and the cerebellum, contributing to the coordination of motor functions (Fig. 1.4).

Brodal and Bjaalie (1997) used sensitive anterograde tracing techniques in monkeys to highlight the organisation of the corticopontine and pontocerebellar terminal fields in non-human primates. The most substantial input to the pontine grey matter in the monkey derived from primary motor and primary somatosensory cortices, superior parietal lobule (Broadman areas 4, 3, 1 and 2, most of area 5) and finally some part of the inferior parietal lobule (area 7), frontal eye field (area 8), dorsolateral prefrontal cortex (area 9), extrastriate visual cortex and insular cortex

(areas 13 and 14). Subsequently, Kamali et al. (2010) used probabilistic tractography to further track the descending bundles of the cerebrocerebellar circuit. Their data presented the relationship between different descending cortical bundles, showing a clear separation of bundles from the frontal (areas 6, 4), parietal (areas 3, 1, 2, 5, 39) and occipital (area 17) cortices. This topography was maintained at different levels of the descending limb, including at both proximal (e.g., at the internal capsule and crus cerebri) and at the distal parts, (e.g., basilar pons and cerebellum).

A number of autoradiographic studies in the monkey have used radiolabelled tracers (e.g., tritiated amino acids or WGA-HRP) to identify the terminations of corticopontine fibres from the prefrontal cortex. These fibres terminate mainly in the rostral half of the basilar pons, in ventromedial, medial, and dorsomedial regions of pontine grey matter (Brodal, 1978a, Hartmann-von Monakow et al., 1981, Stanton et al., 1988, Schmahmann and Pandya, 1997). Corticopontine fibres from the frontal and supplementary eye fields were found to terminate in medial regions of pontine grey matter (Huerta et al., 1986, Huerta and Kaas, 1990). Corticopontine projections from the supplementary eye field and prearcuate cortex have also been traced in the dorsolateral pontine fields (Shook et al., 1990, Leichnetz and Gonzalo-Ruiz, 1996). Finally, Brodal and Bjaalie (1997) emphasised a striking feature of the corticopontine projection which is the so-called ‘’patchy divergence’’ observed at the level of the basilar pons. This means that a very small area of the neocortex projects to widespread parts of pontine grey matter, and on the other hand, retrograde tracing experiments showed a considerable convergence of the projection within the cerebellum. For example, axons from many parts of pontine grey matter converge into a very small volume of cerebellar cortex.

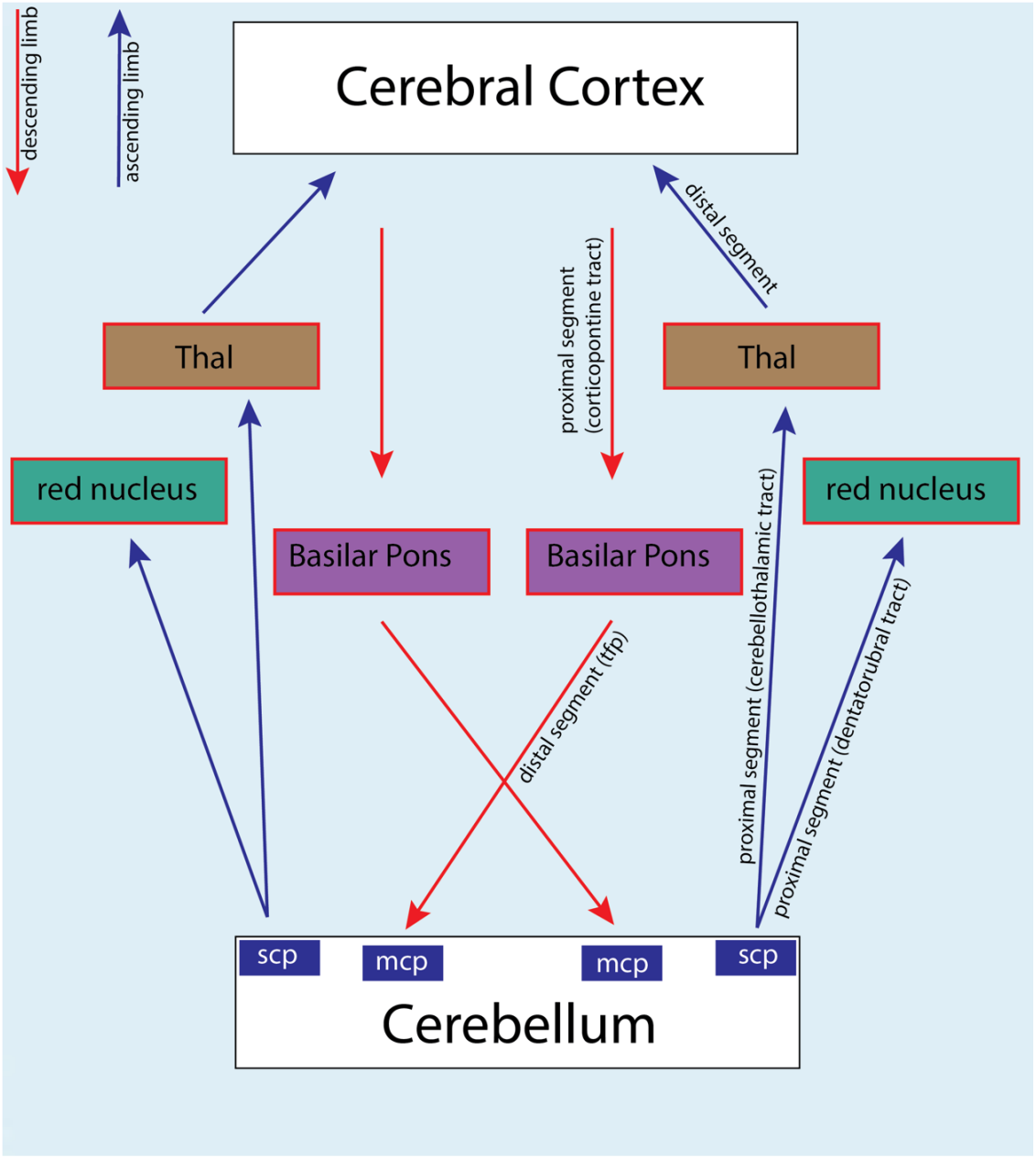
descending limb
ascending limb
Cerebral Cortex
distal segment
proximal segment (corticopontine tract)
Thal
Thal
red nucleus
red nucleus
Basilar Pons
Basilar Pons
distal segment (tfp)
proximal segment (cerebellothalamic tract)
proximal segment (dentatorubral tract)
scp
mcp
mcp
scp
Cerebellum

Fig. 1.4. Schematic diagram of the cerebrocerebellar circuit. *The descending limb (red arrows) which consists of a proximal segment (corticopontine tract) and a distal segment (transverse fibres of the pons) connects the cerebral cortex to the cerebellum via the pontine nuclei and through the middle cerebellar peduncles. The ascending limb (blue arrows) which consists of a proximal segment (dentato-rubro-thalamic tract) and a distal segment (thalamocortical projections) connects the cerebellum with the cerebral cortex passing through the superior cerebellar peduncles, red nucleus, and thalamus. Abbreviations: scp: superior cerebellar peduncle, mcp: middle cerebellar peduncle, tfp: transverse fibres of the pons, Thal: thalamus. Picture extensively modified by original taken from: Palesi et al. (2017)*

The distal segment of the descending limb (pontocerebellar projection)

Much less is known in primates regarding the transverse fibres of the pons that constitute the distal part of the descending limb of the cerebrocerebellar circuit. The transverse or pontocerebellar fibres cross the midline to form the middle cerebellar peduncles towards the cerebellum. The termination of these pontocerebellar fibres was classically thought to be diffuse or at least as multiple longitudinal aggregates (Voogd, 1969). Serapide et al. (2001) injected the pontine nuclei in the rat with anterograde tracer and observed zonally arranged projections to the paraflocculus and most of the other lobules of the cerebellum. Larger injections in the pontine nuclei, however, showed a diffuse labelling and the authors were not able to explain this phenomenon. Nevertheless, this observation was consistent with the so-called ‘’patchy divergence’’ that Brodal and Bjaalie (1997) reported. Voogd (1967) also reported that the pontine nuclei project to the entire cerebellum apart from the nodulus (lobule X) and the ventral uvula (lobule IX).

The overall topography of the pontocerebellar projection has been identified in the cat, where the anterior lobe of the cerebellum receives most (about 80%) of the fibres from the caudal half of the basilar pons (Brodal and Bjaalie, 1997) while the dorsal paraflocculus receives most (about 70%) of the projections from the rostral half of the basilar pons. The crus I, crus II (posterior lobe of the cerebellum), and the paramedian lobule of the cerebellum receive 68 %, 58 %, and 47 % respectively.

The cerebellar circuitry

The projections from pontine grey matter terminate into the cerebellar cortex as *mossy* fibres. These are fibres that emanate primarily from the pontine nuclei and from nuclei associated with the reticular formation such as the basal pontine reticulotegmental and lateral reticular nuclei. This circuitry also includes spinocerebellar and trigeminocerebellar *mossy* fibres conveying proprioceptive inputs from the trunk, limbs and face (Molinari, 2002). Each of the *mossy* fibres divides when the subcortical white matter of the cerebellum is reached, into branchlets which then course into the granular layer of the cerebellar cortex and generate two or three synaptic rosettes (or synaptic buttons) within the cerebellar glomeruli. Therefore, one *mossy* fibre may terminate onto the dendrites of about 400 cerebellar granule cells. The axon of the granule cells ascends to reach the molecular layer of the cerebellum and subsequently the axon bifurcates to two parallel branches projecting in opposite directions and finally synapsing on the dendrites of around 400 Purkinje cells (Palkovits et al., 1972, Benagiano et al., 2018). Subsequently, the Purkinje cells which are all inhibitory GABAergic neurons, project from the cerebellar cortex to the ipsilateral dentate nucleus, the largest of the deep cerebellar nuclei (Benagiano et al., 2001). The cerebellar dentate nucleus is placed bilaterally in the centrum midollare, deep in the lateral hemispheres. It is the main source of efferent projections out from the cerebrocerebellum, and these project to the red nucleus in the midbrain and to the ventral tier of the thalamus (Brodal, 1981). In the monkey, the dentate nucleus is subdivided into two functional and anatomical regions: the rostrodorsal region receives corticonuclear projections associated with motor regions of the cerebellar cortex such as the simplex and paramedian lobule,

and the anterior lobe - while the caudoventral region of the dentate receives projections from Purkinje cells in non-motor regions of the cerebellar cortex such as crus I, II, and the paraflocculus (Strick et al., 2009). There are three more deep cerebellar nuclei, from lateral to medial these are the emboliform, globose and fastigial nuclei. These nuclei may also contain neurons which project to subcortical motor centres such as the parvicellular red nucleus, the vestibular nuclei, the reticular formation and finally via the ventral tier of the thalamus to motor areas of the neocortex (Kievit and Kuypers, 1977, Stanton, 1980).

The ascending limb of the cerebrocerebellar circuit

The ascending limb of the cerebrocerebellar circuit is the return constituent of the loop, through which the processed information from the cerebrocerebellum is conveyed back to the cerebral cortex. The ascending limb consists of two segments, a proximal segment which originates from the deep cerebellar nuclei and projects to the red nucleus and thalamus (as already touched on above), and a distal segment which originates from thalamic nuclei and projects to the cerebral cortex (Fig. 1.4); (Granziera et al., 2009, Meola et al., 2016a).

The proximal segment of the ascending limb (dentato-rubro-thalamic tract (drt))

The proximal segment arises from the deep cerebellar nuclei and most particularly from the dentate nucleus. The fibres form the superior cerebellar peduncle, a fibre tract that travels rostrally to partially decussate in the midbrain. The fibres that cross over at the level of the superior cerebellar decussation (decussating

drt), and those that ascend ipsilaterally (non-decussating drt) further project to the red nucleus where they synapse onto its parvicellular part (Meola et al., 2016a). These fibres connecting the dentate and red nuclei are the dentato-rubral tract. The cerebellothalamic tract on the other hand, ascends towards the ventral tier of the thalamus (postcerebellar nuclei); (Stanton, 1980, Granziera et al., 2009). Together these tracts form the dentatorubrothalamic tract (drt), further investigated in Chapter 5.

The red nucleus

An additional regulatory centre of the cerebrocerebellar circuit is the red nucleus, and in particular the parvicellular part is anatomically and functionally connected to the cerebrocerebellum (Robak et al., 2000, Ralston and Milroy, 1989, Habas et al., 2010). The parvicellular red nucleus receives firstly, dentato-rubral axons from the cerebellar nuclei (nucleorubral fibres), and secondly, neocorticorubral fibres that project from the primary motor area (Burman et al., 2000b), the premotor area (von Monakow et al., 1979), the parietal and prefrontal areas (Leichnetz, 1981), and finally, the frontal eye field (Burman et al., 2000b). The neurons within the parvicellular red nucleus thereafter send fibres to 1) the ipsilateral inferior olivary complex, forming the rubro-olivary tract which controls the activity of the cerebello-olivary circuit (Nioche et al., 2009, Burman et al., 2000a), 2) the pontine nuclei forming the rubropontine tract (Nathan and Smith, 1982, Holstege and Tan, 1988), and 3) the precerebellar reticular nuclei forming the rubroreticular tract (Nioche et al., 2009). Both of these latter two tracts regulate the firing frequency of the *mossy*

fibre inputs back to the cerebellum, forming a complex loop. Therefore, the *mossy* fibres are crucial within the cerebellar circuitry forming complex branched axons that innervate the granule cells of the cerebellar cortex.

The distal segment of the ascending limb

The distal segment of the cerebrocerebellar circuit consists of the thalamocortical projection (Fig. 1.4). The fibres of this projection originate in the postcerebellar thalamic nuclei and ascend through the internal capsule. In the internal capsule, there is some topography related to the final fibre destination. The anterior limb of the internal capsule is occupied by fibres projecting to the prefrontal cortex and some fibres to the limbic cortex; the genu and posterior limb by the fibres to motor and parietal areas; the sublenticular limb by those to the temporal cortex; the posterior limb by additional fibres to the limbic cortex; and finally, the retrolenticular limb by the fibres to the occipital cortex (Kwon et al., 2011a, Kumar et al., 2015, Behrens et al., 2003b, Palesi et al., 2015).

Behrens et al. (2003b) have identified different areas of the thalamus projecting to different cortical regions (thalamocortical connectivity). For example, the ventral lateral and ventral anterior thalamic nuclei project to the primary motor cortex and premotor cortex, a view which was also found by Jones et al. (1979) using anterograde and retrograde tracing techniques in monkeys.

Finally, Kievit and Kuypers (1977) using horseradish peroxidase in rhesus monkeys found that areas situated ventromedially in the thalamus project to the frontal lobe and most specifically along its lateral margin.

To conclude, the information descending from the cerebral cortex is subject to complex processing across different levels. The first level of processing occurs in the basilar pons by the pontine grey matter (precerebellar nuclei). At this level the information is conveyed from 1) the cerebral cortex, 2) the lamina quadrigemina, 3) the red nucleus, and finally, 4) local interneurons. The second level of processing occurs in the cerebellar cortex. Finally, the third level of processing occurs within the deep cerebellar nuclei, and along the ascending limb of the cerebrocerebellar circuit namely, the red nucleus and the ventral tier of the thalamus. These constitute a hierarchy of signal integration that provides critical feedback and fine tuning of information passing from the cerebral cortex to the cerebellum (Benagiano et al., 2018). In fact, clinical studies reported that the dysfunction of brainstem, cerebellar and thalamic centres associated with the cerebrocerebellar circuit by conditions such as pontocerebellar hypoplasia and strokes may produce a functional deficit and seizures comparable to that of the destruction of the cerebrocerebellum (Namavar et al., 2011). Therefore, the cerebrocerebellar circuit should be studied and investigated as a non-separable anatomical entity. In Chapters 3 and 5 I investigate the parts of the descending and ascending limbs of this cerebrocerebellar circuit using Diffusion Tensor Imaging (DTI) and HARDI postmortem deterministic tractography, techniques further discussed below.

1.8 Impact of DTI on clinical research and applied science

Diffusion Tensor Imaging (DTI) is a Magnetic Resonance Imaging (MRI) technique that exploits the phenomenon of anisotropic diffusion to estimate the fibre organisation of the brain. Since MRI uses a magnetic field to create detailed images of the structures within the body, DTI is a specialised imaging technique that uses MRI principles to detect the movement of water within organs and tissues of interest. More specifically, DTI provides a quantitative analysis of the magnitude and orientation of water molecules (Alexander et al., 2007, Lope-Piedrafita, 2018). DTI was first proposed as an MRI imaging technique by Basser et al. (1994a). Therefore, the introduction of DTI model permitted to characterise the shape of water diffusion between the fibre tracts in the brain giving a rotationally invariant description. Several properties of the diffusion tensor do not change when the tensor is rotated through different angles. As a result, these properties are rotationally invariant. The invariance to rotation was a pivotal principle because it allowed the investigators to unravel complex anatomy of white matter connectivity in the brain. More specifically, these rotational invariants give quantitative information, including mean diffusivity, and anisotropy within tissues. Finally, the rotational invariants are useful in comparing tensors and ellipsoids (see below); (Pierpaoli et al., 1996, Kingsley, 2006).

The applications of DTI across a wide variety of neuroscientific studies have been enormous. Some examples include investigating different white matter connectivity patterns and features in schizophrenia (Kubicki et al., 2007), multiple sclerosis (Inglese and Bester, 2010), aging (Westlye et al., 2010), traumatic brain injury and major depression (Maller et al., 2010), and finally autism (Lange et al.,

2010). Quite famously, the National Institutes of Health have funded the application of DTI to map the normal axonal connections in the brain, through an international collaboration known as "The Human Connectome Project'' (Van Essen et al., 2012). Finally, the most clinically advanced application of DTI is the preoperative DTI neuronavigation, which has been shown to increase tumour resection efficacy and post-operative survival (Wu et al., 2007, Bello et al., 2008, Golby et al., 2011, Talos et al., 2003).

Technical aspects of DTI

As indicated above DTI investigates cellular structure by measuring the diffusion of water molecules. This measurement is called diffusivity or diffusion coefficient and is a proportionality constant between diffusive flux and a concentration gradient. Diffusivity's units are expressed in area per time: mm^2/s (Bihan and Warach, 1995). This diffusivity measured in tissues such as the brain varies in relation to the orientation of various structures, thus the diffusion becomes *anisotropic*. In contrast, the diffusion measured in a glass of pure water (devoid of lipidic and protein components such as myelin), is equal in all directions (or *isotropic*); (Beaulieu, 2002). Therefore, DTI is based on mathematical principles of linear algebra where the diffusion tensor describes the diffusion of water molecules along structures such as axons, using a Gaussian model. A Gaussian model is a probabilistic model that represents distributed subpopulations within an overall population of fibres. The diffusion tensor is proportional to the covariance matrix of a 3D Gaussian distribution which measures and by extension models the

displacement of water molecules. Mathematically, the diffusion tensor is a three by three symmetric and positive-definite matrix characterised by three orthogonal and perpendicular to each other eigenvectors and by three positive eigenvalues (Szczepankiewicz et al., 2021). An eigenvector of an n x n matrix A is a linear transformation of a nonzero vector **x** which gives a scalar multiple of itself. A scalar λ is called an eigenvalue of A (Arfken, 1985). Therefore, the major eigenvector indicates towards the principal direction of diffusion. As a result, in anisotropic tissues rich of fibres such as the brain the major eigenvector also defines the axis of the bulk of fibre bundles (Basser et al., 1994b, Dibb and Liu, 2017). Finally, the three positive eigenvalues of the tensors (λ_1, λ_2, λ_3) characterise the diffusivity along the direction of each eigenvector. To conclude, the eigenvectors and eigenvalues characterise a mathematical ellipsoid which gives an isosurface of Gaussian probability of diffusion. Therefore, in areas of high anisotropy such as along white matter tracts the ellipsoid is more elongated along the major eigenvector, whereas in areas of low anisotropy the ellipsoid assumes the shape of a sphere (Mori, 2002).

Calculating DTI measurements

To create a diffusion tensor image for neural white matter analysis, magnetic field gradients are applied to a brain region to generate a diffusion sensitised image in a particular direction. This diffusion sensitising gradient produces a situation in which the magnetic field is not homogeneous at all points within a voxel, therefore, the signals emitted by the water molecules have different frequencies and phases over the period of time in which these gradients are applied. This process is called

diffusion weighting. By repeating this process in multiple directions, a 3D diffusion model which is called the tensor is estimated. Therefore, DTI involves the application of magnetic pulses to cause a random phase shift for water molecules to diffuse (Young et al., 2020). In simplified terms, fibre tracts oriented parallel to the magnetic field gradient direction will appear dark in DWI for that specific direction. Subsequently, by comparing the signal loss with the original signal the diffusion tensor is calculated (Alexander et al., 2007).

The information deduced by the diffusion tensor is condensed into one number (a scalar), or into four numbers to display further acquisitions. Firstly, the anatomical maps characterised by images with red, green, blue colours and a brightness value (Fractional Anisotropy Colour (FAC) maps); (He et al., 2014). Secondly, the diffusion tensor can be post-processed and viewed using glyphs, which represent the major eigenvector within each voxel and thirdly, DTI can be further post-processed and the investigator can estimate the course of the pathways via a 3D tracing technique called tractography. All these different post-processing analysis models are described further below.

DTI scalars

By calculating the average of the tensor's eigenvalues we can extract the simplest but very useful scalar in DTI, referred to as Mean Diffusivity (MD); (Pierpaoli et al., 1996, Le Bihan et al., 2001). The MD relates to the total quantity of diffusion within a voxel. A voxel is the basic unit of 3D data that composes an image

or any other digital information. Therefore, an MRI image consists of a number of voxels. The size of a voxel defines the spatial resolution of the image, and as each voxel typically encompasses extracellular and intracellular space, changes in MD can be a good measure of changes in the quantity of water in the extracellular space. The MD measured in tissues with pathologies such as cytotoxic edema for example, can be higher than the value of the MD measured in water due to increased perfusion (Le Bihan et al., 1986).

Another DTI scalar useful for mapping pathways and more widely used is the Fractional Anisotropy (FA). The FA measures the fraction of the diffusion that is anisotropic. As described above regarding the ellipsoid, the FA defines the divergence of the ellipsoid's shape from that of a geometric sphere. The fractional anisotropy can be considered as a normalised variance of the eigenvalues and is defined by the following equation:

$$\mathrm{FA} = \sqrt{\frac{3}{2}} \frac{\sqrt{(\lambda_1 - \hat{\lambda})^2 + (\lambda_2 - \hat{\lambda})^2 + (\lambda_3 - \hat{\lambda})^2}}{\sqrt{\lambda_1^2 + \lambda_2^2 + \lambda_3^2}}$$

Where $\hat{\lambda} = (\lambda_1 + \lambda_2 + \lambda_3)/3$ is the mean value of the three eigenvalues (Winston, 2012, Jellison et al., 2004, Basser and Pierpaoli, 1996). As a result, if the principal eigenvector and eigenvalue λ_1 is a lot higher than the other two eigenvalues λ_2 and λ_3, then the value of the FA will be very high as well, and this is evidence for the presence of a uniformly oriented fibre population along the largest eigenvector. On the other hand, in voxels with a spherical measurement, the principal eigenvector and

eigenvalue may not always align with an underlying fibre orientation (Ennis and Kindlmann, 2006).

Fractional Anisotropy Colour (FAC) maps

While FA maps unravel differences in anisotropy in a 3D space, they do not reflect any information regarding the orientation of the fibre tracts. FAC maps are useful to visualise information about the orientation of water molecules diffusion by colour-coding information deduced from the eigenvectors. For example, the colour red indicates a lateromedial diffusion of water molecules and by extension a lateromedial orientation and not direction of fibre tracts (eigenvector [1, 0, 0]). Similarly, the colour green indicates a ventrodorsal diffusion (eigenvector [0, 1, 0]), and blue indicates a rostrocaudal diffusion (eigenvector [0, 0, 1]). Finally, diffusion along the intermediate orientations are visualised by mixing the three basic colours, for example magenta for an oblique rostrocaudal and lateromedial diffusion and yellow for an oblique ventrodorsal and lateromedial orientation of the diffusion (Pajevic and Pierpaoli, 1999). As a result, the diffusion of water molecules in the brain tissue is not random, rather reflects the presence of fibres, and cellular membranes. The fibre pattern in the brain demonstrated by diffusion MRI represents fibre architecture well as compared by MRI, polarized light imaging, and histological quantitative estimates of myelin and astrocytes (Mollink et al., 2017).

Tensor Glyphs derived from diffusion tensor imaging

A common objective in computational neuroscience is to enable the inspection of anatomical maps at precise and discrete points in 3D space, and at the same time to illustrate the anatomy of larger-scale structures. Small-scale 3D objects such as sticks, ellipsoids, and superquadric tensor glyphs can be used to disclose information of fibre orientations within each voxel which derives from a tensor eigensystem (Basser et al., 1994b, Kindlmann, 2004). A tensor field is produced by plotting the tensor glyphs over a defined space, and indicates at a precise location within each voxel the eigenvector and eigenvalue as computationally visualised by the shape, orientation and colour of the glyph geometry (Zhang et al., 2016). In addition, the glyphs can assume a more precise form than a usual ‘’peanut’’ by enhancing the isotropic resolution of the diffusion images (Kindlmann and Westin, 2006). The most obvious drawback of DTI models is the fact that they work well when there is only one fibre population within each voxel. However, these models fail completely when there are two or more fibre populations characterised by different orientations in the same voxel. The only way to overcome this disadvantage is to increase the isotropic resolution of the diffusion data (Astola et al., 2014, Mulder et al., 2019).

Step-by-step approach in Deterministic vs Probabilistic Tractography

Tractography is a 3D modelling technique which uses mathematical algorithms to calculate, commence and terminate the trajectory of white matter tracts and derives from post-processed data gathered by diffusion MRI (Jones, 2008). Tractography can be categorised into two classes: Deterministic and Probabilistic tractography. The main parameter that distinguishes these two broad categories is the sampling of tract directions regarding the propagation of streamlines. In deterministic tractography, the trajectories are produced according to a fixed direction within each voxel, thus the term deterministic, whereas probabilistic tractography calculates all probable trajectories. Therefore, the algorithms used in deterministic tractography can reproduce the bulk of fibre orientations within a voxel (Mori et al., 1999, Basser et al., 2000, Conturo et al., 1999, Yeh et al., 2013).

The most represented, studied and utilised type of tractography is streamline or deterministic tractography which derives from an earlier method for detecting a tensor field known as hyperstreamlines (Mori et al., 1999). Streamline tractography generates discrete trajectories or "tracts''. Streamline tractography works by successively stepping forwards and generating the trajectory along the orientation of the major eigenvector which, as described above, is the orientation of the fastest diffusion that water molecules assume. Therefore, the eigenvectors work like tangents that touch the curve of the calculated trajectory. Deterministic tractography uses a "deterministic" approach to delineate the trajectories of the fibre bundles. After a seed mask is placed in the white matter, the algorithm follows anterogradely and retrogradely local fibre directions through a step-by-step process characterised

by recurrence until the termination criteria are met (Euler method); (Sedrak et al., 2011). The algorithm does not involve any random parameter and therefore every time a tract is calculated within a number of voxels, an identical trajectory of the fibre bundle under investigation is produced.

Generally, deterministic tracking algorithms follow the principal eigenvector as proposed by various authors (Conturo et al., 1999, Basser et al., 2000, Jones et al., 1999, Tench et al., 2002, Mori et al., 1999). Therefore, if the resolution is not high enough the available information shown by deterministic tractography could be reduced. This means that the biggest and homogeneous fibres can be visualised. As a result, the fibres that have much smaller diameter than the voxel size of the diffusion data cannot be detected.

However, deterministic tractography is not simply setting the seeds and termination points and the pathways under investigation will be automatically produced. The parameters that affect the final tracking results include the number of the seeds, the step size, the angular threshold, the anisotropy threshold, the smoothing, and finally the minimum and maximum length allowed (Caan, 2016). These are all subjected to variations connected to the isotropic spatial resolution of the diffusion (raw) data.

A number of different software programs have been developed to calculate step-by-step fibre tracts (or streamlines) from the diffusion data including DSI Studio (Yeh, 2021) and FSL (Woolrich et al., 2009); (both programs used in this thesis). The calculations use a variety of mathematical methods to perform streamline tractography, such as the Euler method which follows the eigenvector for a fixed step

size (Zhan et al., 2015, Basser et al., 2000). The Euler method is a first-order numerical procedure used by the program to calculate differential equations and by extension the trajectory of the fibre tract under investigation. In this way, in order to calculate the shape of a fibre tract which starts at a given point, the program applies a number of tangent lines along the calculated curve so that the trajectory can be computed at any point on the curve (Zhan et al., 2015). A second order Runge-Kutta method has been developed where the tangent is followed by half a step and then a new tangent is applied along the calculated curve. In addition, a fourth order Runge-Kutta, and a Fibre Assignment by Continuous Tracking (FACT) methods have been employed to introduce the so-called 'inertia' when the algorithm calculates the trajectory within regions of planar anisotropy (regions of multiple fibre crossings) by modulating the direction of the incoming tangent instead of using the principal eigenvector as the Euler method does (Weinstein et al., 1999, Lazar et al., 2003, Westin et al., 2002, Mori et al., 1999, Conturo et al., 1999, Press et al., 1986).

Advanced algorithms have been developed and created further methods as follows.

1) The region-growing and wavefront evolution method which is a white matter tractography method that determines the pathways by tracing minimum trajectories using the vector field of the resulting partial differential equation.

2) Tractography ''meta-analysis'' methods that perform clustering. In this way this proposed method identifies a pattern of white matter tracts in a group of subjects and recognises structures that correspond to expected white matter tracts.

3) Optimisation methods which use physical models such as the Gibbs tracking that reconstructs a long neuronal pathway in small successive steps. Starting from the local information about diffusion, the method calculates and follows the local voxelwise-defined direction of the fibre tract (Kreher et al., 2008, Melonakos et al., 2007, O'Donnell et al., 2009, Yushkevich et al., 2008, Jackowski et al., 2005).

The second class of tractography is probabilistic tractography which outputs probabilities of white matter connections. Probabilistic fibre tracking is characterised by a random process by which the propagation of fibre tracking is calculated. As a result, every time the same trajectory is calculated, a different result may occur. Probabilistic tractography iterates all "probable" trajectories which can be followed and defines a certain probability to each outcome (Behrens et al., 2003a). In other words, probabilistic tractography estimates the distribution of all possible fibre orientations within a voxel. A trajectory is randomly drawn from the distribution of fibre orientations, and the algorithm determines the orientation of the streamlines (Behrens et al., 2007). While this may therefore produce tracts which are false, the approach is able to detect all possible trajectories even those small tracts missed by deterministic fibre tracking (Abhinav et al., 2014).

So which approach – deterministic or probabilistic is more efficient to use. The answer comes down to the isotropic spatial resolution of the diffusion data. If this is sufficient to directly compare computed tracts with the tensor glyphs, the FAC and most importantly the structural anatomical GRE images, then any probabilistic approach can become superfluous and deterministic tractography should be used. But the tracts do need to be compared with all available image data, glyphs, FAC, GRE,

and the rest of the DTI contrasts such as the FA, Axial Diffusivity (AD), MD, Radial Diffusivity (RD) and DWI.

The Potential of Postmortem Tractography

Optimised spatial resolution is most readily achieved for postmortem tissues, and postmortem tractography has a high potential for morphological analysis of tissues and tracing of brain connectivity. Due to the fact that postmortem tractography offers the ability to scan the specimens for long periods of time (e.g., 208 hours - scanning time for the Duke diffusion data) and to apply higher fields of strength (>7 Tesla) which are not well tolerated by a living human being, these factors enable ultra-high spatial resolution both for the structural and diffusion data. This, renders possible the reconstruction and correlations between subtle white matter tracts and fine morphological features (D'Arceuil et al., 2007, Miller et al., 2011). From higher spatial resolution morphological and diffusion imaging ultra-high-field MRI, HARDI postmortem tractography, and higher order models such as the tensor glyphs can be used to identify anatomical details which were obscured from traditional histochemistry and gross anatomy. This contrasts with the lower resolution clinical MRI, which while useful for guiding surgery in the same patient, is limited to replicating what traditional anatomical methods have seen. Postmortem diffusion MRI does not require slicing or destruction of the specimen, especially valuable for tracing connectivity. Moreover, non-invasive imaging provides comprehensive 3D morphological information, therefore, MRI based techniques are efficient by offering ultra-high spatial resolution, high chemical and tissue

specificity, as well as very high structural contrast (Dominietto and Rudin, 2014). However, there are technical challenges regarding postmortem diffusion imaging modalities. Tissue deterioration after death and incomplete fixation of tissues can render inefficient postmortem diffusion imaging data obtained from scanners with low field strength. A major challenge is the reduction of the apparent diffusion coefficient (ADC) which is a measure of the magnitude of diffusion of water molecules in tissues, and of the relaxation times following excitation (T_2). Investigators have compensated for these alterations by increasing the b-value which reflects the strength and timing of the gradients used to create DWI images.

The term b-value was coined by Stejskal and Tanner (1965) when they described their pulse gradient diffusion method. This parameter measures the degree of diffusion weighting applied. The Stejskal-Tanner pulsed gradient diffusion method is still in use for modern DWI pulse sequences. The b-value is defined by the following formula: $b = \gamma^2 G^2 \delta^2 (\Delta - \delta/3)$, and expressed in units of s/mm^2. It consists of two gradient pulses of magnitude (G), both characterised by a duration (δ), and separated from each other by a time interval (Δ). Therefore, Δ is the time between the start of the first gradient and the start of the following gradient pulse. Where γ is the proton gyromagnetic ratio (MHz/Tesla); (Westin et al., 2002). As a result, a larger b-value is achieved by increasing three factors. The gradient pulse of magnitude (G), the duration (δ) of each pulse, and finally by widening the time interval between the gradient pulses. For example, to identify slow water molecules moving at small distances the b-value should increase. It is not clearly defined which is the best b-value in diffusion weighting imaging. The b-value is correlated to MRI parameters such as the field of strength and the number of signals averaged, and factors such as

predicted pathology and anatomical features. The higher the b-value is, the higher the diffusion weighting is, thereby showing brighter white matter tracts. However, the signal to noise ratio decreases when images are obtained with high b-values resulting in images with more noise (lower quality). In clinical practice, the b-values used for diffusion imaging range from 0 to 1000 s/mm^2 (Burdette et al., 2001, DeLano et al., 2000, Mori, 2007).

Therefore, higher b-values acquire more robust diffusion effects and high quality images. As a result, we now obtain similar image quality and high contrasts to *in-vivo* studies but with increasingly higher spatial resolution (Sun et al., 2003, Pfefferbaum et al., 2004, Tovi and Ericsson, 1992).

Optimisation and Limitations of DTI and Tractography

The sensitivity of MRI is highly dependent on methodology which includes the scanner field strength, acquisition parameters, pre-processing steps and the reconstruction models. To achieve a high-quality image, the scan time has to be long (for example 208 hours for the DWI; Duke Specimen one; see Chapter 2). In addition, the field of view (FOV), the acquisition matrix, and the slice thickness all determine the voxel volume (Platt et al., 2021). For example, the FOV is the size of the displayed image and defined by the size of 3D encoding areas of the magnetic resonance image. A smaller FOV gives better resolution but captures a smaller brain region. The FOV used by the Center for In Vivo Microscopy at Duke University for human specimens 1 and 2 was 80 x 55 x 45 mm. The acquisition matrix is the

number of data samples in each direction such as the number of samples in the frequency and phase-encoding directions. The acquisition matrix was 450 x 275 x 225 (Duke specimens). The slice thickness is defined as the width of a rectangular profile which is sliced with the same maximum height and area. The data used in this thesis are characterised by a 0.2 mm slice thickness. Ultimately the smaller the voxel volume the greater the spatial resolution. All these parameters need to be adjusted and experimentally combined to produce the clearest images with the given sample and available imaging equipment and software (Mayerhoefer et al., 2009, Asai et al., 2018). Details for the images used in this thesis are given in Chapter two.

The drawbacks common to all fibre tractography include firstly, the inability to distinguish afferent from efferent pathways. One can produce a fibre tract but cannot determine from tractography alone the direction in which signals are propagated along these tracts. Secondly, the tracts are orders of magnitude greater than single axons. Human diffusion MRI studies typically use voxel sizes of 2 x 2 x 2 mm^3 (Sotiropoulos et al., 2013). This means that applying the best hardware and software, the maximum resolution that can be achieved is 1,000 μm (1 mm). This limited spatial resolution prevents identification of single neuron or axon projections within a given voxel. Additionally, this limits the investigator to distinguish if the fibres follow a straight or curving trajectory (Campbell and Pike, 2014). On a more positive note, when conditions are optimal, the spatial resolution that can be achieved (e.g., the Duke specimen one in the current study) results in a 200 μm isotropic voxel size for the DWI and 50 μm for the GRE (see Chapters 3 – 6). The human pyramidal tract is composed of thin axons the diameter of which is found to be 0.3 μm (Graf and Schramm, 1984) and thick axons of 20 μm diameter (Verhaart, 1947). The

majority of thin axons (about 80%) are smaller than 2 μm. The maximal diameter of the thick axons is high possibly due to the inclusion of myelin sheath. In addition, smaller species are characterised by the presence of smaller axons versus larger species which present higher maximal axonal diameters (Leenen et al., 1982, Biedenbach et al., 1986). Moreover, Pierpaoli et al. (1996) reported that the diameter of large axons within the pyramidal tract is close to 26 μm. Kandel et al. (2000) reported that the typical range of axon diameters in the central nervous system is from 0.2 to 20 μm. Assuming a high packing density and axon diameter of 1 μm, the cross-sectional area of a single 200 μm voxel could potentially fit 200 x 200 = 40.000 axons. This neglects any extracellular space or myelination so would be an underestimate. This is high resolution given the estimated 40 million axons that compose the human corticopontine tract alone (Brodal, 2014), without counting the axons of the corticospinal and corticobulbar tracts. However, one cannot yet directly relate diffusion data to their underlying physical micro-architecture, although efforts are underway to develop post-imaging analysis routines to achieve this correlation (Easson et al., 2020, Zhang et al., 2012). Consequently, the glyphs display the principal eigenvector (λ_1), which is the largest of the three eigenvectors (λ_1, λ_2, λ_3) and measures the average orientation of diffusion within each voxel, without calculating individual orientations of small fibre populations (Mori, 2002). This reflects the validity of the interpretation regarding the fibre pattern investigated herein with the tensor glyphs (see Chapters 3 and 5). A spatial resolution of 25 μm and below, which eventually approaches that of histology (1 μm) will permit us to identify and study the fibre trajectories more precisely, for both thick highly myelinated fibres the diameter of which is approximately 20 μm and then for smaller

fibres of 1 μm diameter (Kandel et al., 2000). Finally, tractography is also limited by not being able to detect synapses. Therefore, while tracts can be identified and one may also be able to deduce where the tract stops, one cannot definitely identify to which neurons the tracts synapse onto. Ideally, one combines tractography with biological tracers or advanced histology such as polarized light microscopy or with functional measures of connectivity.

Interpretation of DTI

A challenge in the interpretation of DTI arises from the scale at which diffusion is measured being very different from the size of neuronal fibres, as indicated above. To illustrate by further examples from the human brain: the axon packing density within the corpus callosum is around 338,000/mm^2 , the diameter of large axons within the pyramidal tract is close to 26 μm (Pierpaoli et al., 1996), the typical range of axon diameters in the central nervous system is from 0.2 to 20 μm (Kandel et al., 2000). On the other hand, the voxel size in a typical diffusion MRI is that of 2.5 x 2.5 x 2.5 mm, the typical diffusion time in DTI is 30-100 ms, finally, the mean water diffusion distance is 1-15 μm in 50-100 ms (Le Bihan, 2003, Beaulieu, 2002). This means that the measured diffusion properties are averaged over each voxel which reflects the isotropic resolution of the images. Therefore, the biophysical interpretation of the microanatomy of the nervous system through a diffusion tensor is very complicated. As a result, the above diffusion parameters need to match the dimensions of the actual fibre architecture in order to suppress false positive/negative

results and we do not really know how many fibres are inside the identified trajectories.

High Angular Resolution Diffusion Imaging (HARDI)

Over the past decade, advanced higher order models such as High Angular Resolution Diffusion Imaging (HARDI) have been developed in response to the limitations of DTI and solve the crossing fibre problem (Kuhnt et al., 2013). HARDI can be combined with appropriate tracking algorithms such as the Euler method (used in this thesis) to provide improved results. HARDI is characterised by the unique high number of diffusion-weighting gradient directions (120 directions were acquired for the Duke data in this thesis) and the high number of b-value (the b-value for the data in this thesis is 4.000 s/mm^2). Therefore, HARDI has produced more robust tractography results by providing new anisotropy measures and also increasing the spatial isotropic resolution (Xie et al., 2015). In this way HARDI can produce clear anatomical images and diminish limitations such as the crossing fibre problem. More specifically, the advances in HARDI enables diffusion data to be acquired using more than the typical six diffusion directions. Thirty-two or more directions can be used (Tuch, 2004). In addition, HARDI uses a higher b-value than the standard 1,000 for DTI which means clear images and increased colour contrast (Bar-Shir et al., 2009). Finally, by using multiple b-values, higher order models such as Diffusion Spectrum Imaging (DSI) have been developed which enable multiple b-value acquisitions in order to go beyond DTI and extract important biomarkers such as axon diameter and compartmentalisation. DSI is an advanced higher order model

that displays crossing fibres and intravoxel fibre orientations more accurately than before, for example by acquiring 515 image volumes with a maximum b-value of 17.000 s/mm^2 (Wedeen et al., 2005, Tuch et al., 2002, Farquharson and Tournier, 2016).

1.9 Development of DTI to map the human brainstem

The advent of ultra-high magnetic fields heralded a golden era in brain mapping, exemplified by the Human Connectome Project; (Fan et al., 2016, McNab et al., 2013). This project represents the discovery and optimisation of methods to efficiently map the vast network of connections in the brain, in a way that was never before possible. Principle amongst this has been the development of diffusion imaging (Fan et al., 2016).

In this section I review prior literature in DTI and diffusion tensor tractography. I hope to impress how complex and time consuming it is to develop and optimise advanced technology and data processing for brain mapping. In addition, a review of previous literature is important for the reader to understand the efforts and contribution of a variety of researchers in biomedical engineering.

I present this as a mini-historical review of developments, summarising some key papers sequentially. These key papers, with a comparison of the MRI field strength power and isotropic resolution are summarised in Table 1.

Stieltjes et al. (2001) historically used diffusion tensor MRI on six healthy volunteers to demonstrate anatomical structures of the brainstem. The scanning

was performed using a 1.5T MRI scanner, achieving a 2 X 2 X 3 mm of isotropic resolution. A number of anatomical structures were identified and compared to histological data, such as the corticospinal tract, the medial lemniscus, and the superior and inferior cerebellar peduncles. Moreover, the authors subdivided the cerebral peduncle into the classical components derived from histological data: the frontopontine, corticospinal, and temporo-parieto-occipitopontine tracts. The gross anatomy of the reconstructed fibres corresponded well to classical anatomical knowledge from histology, thus validating the results obtained by MRI. As the authors pointed out, their results revealed that the different white matter tracts are characterised by a unique signature on DTI, rendering diffusion tensor MRI a valid and powerful tool to delineate fibre bundles in 3D spaces.

Hagmann et al. (2003) used a low resolution 1.5T clinical scanner on two healthy volunteers and produced images of greater resolution with voxel size 1.64 x 1.64 mm. They also identified the medial lemniscus and superior cerebellar peduncle, as well as the pyramidal tract. The authors compared their results to prior postmortem based neuroanatomical knowledge. The medial lemniscus was identified at the level of the pons as well as the gross anatomy of the pyramidal tract within the brainstem. The authors concluded that they were demonstrating a new approach of brain connectivity, and identified several tracts using DTI which opened new insights into brain anatomy and connectivity in that their work led to the identification of various tracts and showed high correlation with prior neuroanatomical knowledge.

Nagae-Poetscher et al. (2004) used high-resolution diffusion tensor imaging at 3T and acquired images of isotropic resolution of 1.8 mm and

succeeded in identifying structures such as the corticospinal tract, the optic tract, the medial lemniscus. In addition, the authors were among the first to provide details of the overall anatomical description regarding structures on the colour-coded maps turning into reality the view to use DTI in brain mapping as initially proposed by Basser et al. (1994b). However, the resolution was not significantly high enough to provide insights concerning the detailed organisation of the white matter tracts that course through the brainstem and thalamus.

Karampinos et al. (2009) used a 3T scanner to obtain 10 transverse slices covering the volume of the pons of three healthy humans. The authors acquired low resolution DTI contrasts such as the mean diffusivity (MD), fractional anisotropy (FA) and FAC maps achieving a 1.2 mm isotropic resolution and subsequently they achieved higher resolution images of 0.8 mm isotropic, regarding the same contrasts, but this resolution was a resolution after extrapolation (see below). They highlighted the gross anatomy of the pons such as the main subdivisions of the pons in basilar pons and pontine tegmentum. Moreover, they identified the different bundles using FAC, and distinguished the descending fibre bundles, the middle cerebellar peduncle, and the transverse fibres of the pons. The medial lemniscus was clearly seen within the pontine tegmentum and the superior cerebellar peduncles were identified coursing rostrally. However, the DTI contrasts were not at sufficient resolution to subdivide any of the descending and transverse fibre bundles (they were all mapped as a single anatomical entity), nor were the DTI contrasts able to highlight any organisation within the pathways under investigation (such as topography). Interestingly, the

midline of the pons attained a faint signal. However, this did not reveal any particular anatomical organisation (see *Stria Pontis*, Chapter 3).

Naidich et al. (2009) produced what became a seminal book in neuroanatomy, *Duvernoy's Atlas of the Human Brain Stem and Cerebellum.* They utilised an ultra-high-resolution 9.4 T scanner for the structural T2-weighted postmortem MR imaging achieving an in-plane resolution comparable to that of myelin and Nissl staining (up to 60 μm), and two additional 3T and 9.4T scanners for *in vivo* and *ex vivo* DTI scanning, respectively. The authors identified grey matter nuclei and white matter tracts of the brainstem, cranial nerves and correlated their anatomical delineations with clinical 3T MR images in transverse, sagittal, and coronal planes, thus revealing detailed organisation of the brainstem. This provided a detailed MRI atlas of the human brainstem but did not focus on delineating structures beyond what was already observed by histology.

Qiu et al. (2012) scanned the brains of 15 healthy humans with low resolution 3T clinical scanner across a field of view (FOV) = 220 X 220 mm and used probabilistic tractography to identify the medial lemniscus and the pyramidal tract across two oblique sections of the brain. Their results confirmed the gross anatomy of these white matter tracts, but the resolution of their data did not enable more detailed identification of anatomical features within the brainstem and thalamus.

Ford et al. (2013) used an 11T scanner and acquired images at 0.333 mm, 1 mm, and 2 mm isotropic resolution. Using tractography, the authors showed the descending fibre bundles within the pons as a single anatomical feature, not revealing any topographical subdivision of these bundles into cervical, thoracic,

lumbar and sacral components of the pyramidal tract nor any other organisation. Moreover, the resolution was also not sufficient to subdivide the transverse fibres of the pons. This despite the use of an ultra-high-field (11T) scanner, highlighting the importance of parameters such as the total number of acquired directions, repetition time, echo time, flip angle, field of view and most importantly the total acquisition time in order to achieve ultra-high resolution data that permit the investigator to reveal anatomical details. For example, the authors acquired 64 directions uniformly distributed over a sphere for their specimen. Their images were obtained with a repetition time (TR) = 5110.9 ms producing a 0.333 mm of isotropic resolution, whereas we obtained a TR = 50 ms producing a 50 μm of isotropic resolution. Finally, they acquired images with echo time (TE) = 31ms, whereas we acquired images with TE = 10 ms.

Deistung et al. (2013) used a whole-body MRI scanner at 7T and acquired structural T_2 -weighted images at 0.53 mm x 0.53 mm of isotropic resolution for the human brainstem *in vivo*, and a voxel size of 1.2 mm x 1.2 mm x 1.2 mm for the diffusion weighted imaging (DWI). Given this was an *in vivo* scan, this resolution was very high. However, although the tract-density images were calculated on an virtual isotropic resolution of 0.43 mm^3 , "the direction of the transverse pontine fibres could not be reliably segregated from the superior-inferior running corticospinal tract on the tract-density images". It is worth noting that this is pseudo-resolution because after extrapolation (Nilsson et al., 2015, Block et al., 2008) the resolution of 1.2 mm^3 becomes 0.43 mm^3, therefore the true resolution for their tract density images was 1.2 mm^3. A pseudo-resolution means to 'up-scale' a coarse image to a finer resolution image (pseudo). Extrapolation is

a method used to reduce artifacts, blurry images, and field inhomogeneities caused by air or bone interfaces. Normally it is the low resolution being extrapolated into higher resolution. In this case, the structural scan was kept at the same spatial resolution, and the DWI (with much lower resolution) was then extrapolated from being 1.2 mm^3 into 0.43 mm^3. Therefore, the resolution of their MRI was low. However, they were able to identify the red nucleus, substantia nigra, crus cerebri, central tegmental tract and medial lemniscus. As the authors specified in their discussion, it was not possible for them to completely compensate for geometric distortion, and this did not allow them to accurately depict the ventral fibre structures of the mid pons and medulla oblongata. Greater resolution would have been possible with *ex vivo* acquisitions using small animal scanners on small parts of the brain, such as the brainstem, without the surrounding structures.

Aggarwal et al. (2013) did indeed use an autopsy brain and focused just on the brainstem, proposing the implementation of a 3D stereotaxic atlas of the human brainstem based on ultra-high-resolution DTI. The scanning was performed using an 11.7 T scanner and achieved a spatial resolution of 255 X 255 X 255 μm for the diffusion data of the whole brainstem. Microscopic neuroanatomical details were identified, including the pyramidal tract within the basilar pons, the medial lemniscus in the pontine tegmentum, the middle cerebellar peduncle and its characteristic green signature on the FAC, the superior cerebellar peduncle, and finally the transverse fibres of the pons in transverse and sagittal planes. In addition, the authors identified smaller tracts such as the medial longitudinal fasciculus, and the decussation of the pyramidal tract in the caudal medulla oblongata. Finally, they compared their data with myelin-stained

histology, showing a good correspondence between the structures identified in DTI and with traditional histological brain mapping. Hence, this study made a substantial advance in mapping out the human brainstem. However, although they achieved a high resolution for the DTI, the authors used a low number of directions (only 30 independent directions were acquired) impeding them from creating high quality images for HARDI tractography.

Finally, a number of recent studies have applied tractography to clinical use. Xiao et al. (2016) generated *in vivo* subject-specific atlases of various thalamic nuclei, such as the ventral posterolateral nucleus, to improve the ability to visualise thalamic targets for invasive deep brain stimulation. The imaging was performed on seven rhesus monkey brains at 7T achieving a 1 mm isotropic resolution for DWI. The authors used probabilistic tractography and *in vivo* whole brain scanning of seven macaques and identified that the medial lemniscus and the fibres which form the superior cerebellar peduncle project to the ventral tier of thalamus and this was crossed-validated by electrophysiology. Jang and Kwak (2017) reviewed six brain injury studies regarding the pyramidal and aberrant pyramidal tracts, and concluded that patients with brain injury who developed an aberrant pyramidal tract could actually show a better recovery. Both these studies highlight the importance of diffusion tractography for patients with various traumatic brain injuries.

The above articles and others reported in this thesis have provided invaluable conclusions identifying key structures and pathways in the human brainstem and highlighting the importance of understanding human brainstem

anatomy. They lay the foundations for subsequent ultra-high-resolution brain mapping and its greater application to the clinic.

Table 1 shows the authors and year of publication in relation to the MRI strength of field, the resolution of the images, and the structures identified			
Author – Year of publication	Strength of field	Isotropic resolution of the images	Structures identified
Stieltjes et al. (2001)	1.5T MRI Scanner	2 X 2 X 2 mm isotropic resolution	Corticospinal tract, medial lemniscus (ml), superior/inferior cerebellar peduncles (scp & icp).
Hagman et al. (2003)	1.5T clinical scanner	1.64 X 1.64 mm isotropic resolution	ml, scp, pyramidal tract.
Nagae-Poetscher et al. (2004)	3T High-resolution scanner	1.8 mm isotropic resolution	Corticospinal tract, optic tract, ml.
Karampinos et al. (2009)	3T scanner	1^{rst} data set: 1.2 mm isotropic resolution 2nd data set: 0.8 mm isotropic	Basilar pons and pontine tegmentum, descending bundles, mcp, ml, scp.
Naidich et al. (2009)	3T for *in vivo* 9.4T for *ex vivo* scanning	In-plane resolution comparable to myelin and Nissl staining of up to 60 μm.	Highly detailed mapping of the brainstem and cerebellum
Qiu et al. (2012)	3T clinical scanner	NON-specified isotropic resolution, FOV = 220 X 220 mm	ml, pyramidal tract
Ford et al. (2013)	11T scanner	1st data set: 0.333 mm, 2nd data set: 1 mm, 3rd data set: 2 mm isotropic resolution	Descending bundles within the basilar pons,

Deistung et al. (2013)	7T whole-body scanner	0.53 mm X 0.53 mm for the structural data. 1.2 X 1.2 X 1.2 mm for DWI. 0.43 mm for tract density images.	Red nucleus, Substantia Nigra, crus cerebri, central tegmental tract, ml.
Aggarwal et al. (2013)	11.7T	255 X 255 X 255 µm for DWI.	Pyramidal tract, ml, mcp, scp, transverse fibres of the pons, medial longitudinal fasciculus, pyramidal tract decussation.
Xiao et al. (2016)	7T for *in vivo* scanning.	1 mm isotropic resolution for DWI.	Thalamic nuclei such as the ventral posterolateral, ml, scp

1.10 Relationship between DTI / Tractography and Classical Tracing Techniques

Diffusion tensor imaging offers the opportunity to investigate via non-invasive *in vivo* approaches the connectivity of white matter tracts in the healthy brain and in pathologies such as strokes (Visser et al., 2019). A variety of studies have designed benchmarks to explore the reliability of DTI and tractography (Schilling et al., 2019). The accuracy of a large number of tractography algorithms was assessed against these benchmarks using high-quality Human Connectome Project (HCP) whole human brain *in vivo* data sets. The results showed the ability to reconstruct most of the existing fibre tracts. A major outcome was the significance of isotropic resolution. The experiments were performed at: 2, 1.75, 1.5, 1.25, 1.0, 0.75, and 0.5 mm of isotropic resolutions and the authors pointed out that higher resolution and by extension higher image quality may improve the validity of tractography (Maier-Hein et al., 2017). Data and the results showed the ability to reconstruct most of the existing fibre tracts. However, the results showed a variety of false positives.

The gold standard for studying structural connectivity is without doubt tract-tracing experiments which use viral, bacterial, or biotinylated dextran agents (Zingg et al., 2014, Bizley et al., 2015, Bota et al., 2015). These biological tracers can act either as anterograde tracers, where the label moves from the injection site towards the synaptic terminals, or as retrograde tracers, where the label moves from the synaptic terminals to label the cell bodies. Retrograde tracers provide the ability to quantify the number of the axons in a

particular projection, assuming each labelled neuron corresponds to a single labelled axon (Ginger et al., 2015, Wickersham et al., 2007).

Hence the validity of tractography can be compared against this gold-standard tracing approach. For example, Azadbakht et al. (2015) performed probabilistic tractography on two *ex vivo* macaque brains, and compared the interconnections they found within the visual system with the tracing data derived wiring maps described by Felleman and Van Essen (1991). Seventy-four % of the connections identified with invasive tracers (Felleman and Van Essen, 1991) were reproduced with tractography. In addition, further comparison with retrograde tracing (Markov et al., 2014), suggested that the number of connections identified with tractography were true connections (Azadbakht et al., 2015).

Zhang et al. (2018b) compared diffusion MRI and tractography results obtained at a macro-scale level to integrated meso-scale information from tract-tracing data (Bakker et al., 2012), and micro-scale information from myelin staining (Mikula et al., 2007). The authors compared different tractography parameters such as the angular and quantitative anisotropy (QA) thresholds. The QA threshold is a similar termination criterion to fractional anisotropy (FA) threshold. Even with the best tractography parameters, some false positive and negative results were produced. Moreover, the study highlighted the intrinsic limitations of diffusion MRI at 1.1 x 1.1 x 1.1 mm isotropic resolution. The authors concluded that with optimal tractography parameters and MRI scales, overall diffusion MRI and tractography could

yield trustworthy results comparable to traditional tract tracing techniques such as viral tracing and myelin staining.

Using postmortem whole brain MRI diffusion data of higher isotropic resolution (0.43 mm) a high correlation (r = 0.59) was observed when a quantitative comparison was made between cortical connections from probabilistic tractography and from retrograde viral tracing studies (Donahue et al., 2016).

Calabrese et al. (2015a) also compared a reconstructed a probabilistic tractography connectome with neuronal tracer-based connectivity data obtained from the Allen Brain Atlas. Their data derived from a mouse brain and at 43 μm of isotropic resolution. The authors emphasised that tractography can provide a three-dimensional, non-destructive brain connectivity tool, although MRI acquisition parameters, low spatial resolution, brief acquisition times, and low signal-to-noise ratio have limited its potential for investigative studies. Indeed only a weak (albeit significant) correlation between viral tracing data and tractography was observed an average Spearman r-value = 0.23 + / - 0.11.

Using a small animal 7T scanner on an ex vivo ferret brain, Delettre et al. (2019) achieved 0.24 mm of isotropic resolution for the diffusion data and showed a good correlation between their cortico-cortical tractography derived wiring patterns and the connectivity data from Dell et al. (2019) obtained using retrograde tracers. Ipsilateral and contralateral corticocortical and corticothalamic connectivity regarding visual areas 17, 18, 19, and 21were described and highly correlated with Spearman's r ranging from 0.67 – 0.91.

Using an 11.7T scanner on three postmortem human brainstems Henssen et al. (2019) achieved 0.5 mm of isotropic resolution for the diffusion data and delineated the trigeminal tracts using tract density images (TDI) and tractography. As a validation the authors sectioned the same brainstems and showed the tracts under investigation using polarized light imaging (PLI); (see also Chapter 4, section 4.3).

Guberinic et al. (2020) investigated the arrangement of the fibres in the trigeminal root using polarized light microscopy at 4 μm of resolution, histochemical staining methods such as Kluver- Barrera staining and Nauta silver stain (for neurofilaments), Heidenhain-Woelke stain (which shows differences in myelination) at 60 μm of resolution, and finally ultra-high-field MRI at 11.7T of unspecified isotropic spatial resolution combined with probabilistic tractography. All three techniques demonstrated similar results identifying the ventral and dorsal trigeminothalamic tracts.

1.11 Concluding statements

In the present study, I endeavoured to anatomically and functionally describe the cerebrocerebellar circuit. The cerebro-ponto-cerebellar circuit consists of the descending fibre bundles (cortical and striatal) and the dentato-rubro-thalamic tract which closes the loop of this complex circuit. Ascending inputs from sensory systems regulate these loops.

This is one of the largest loops in the central nervous system and yet knowledge of its precise anatomy and connectivity remains elusive.

More precisely, I analyse in the third Chapter of my thesis, parts of the motor system and most particularly the cerebro-ponto-cerebellar pathway which comprises the corticopontine tract as part of the pyramidal system (see above), and the transverse fibres of the pons as part of the extrapyramidal system which course towards the cerebellum. Moreover, I topographically describe the corticobulbar and corticospinal tracts (pyramidal system) as well as the projections to the substantia nigra (striatonigral and corticonigral pathways – extrapyramidal system) as an attempt to integrate the pyramidal and extrapyramidal systems from the anatomical point of view.

In the fourth Chapter, I identified the sensory projections (dorsal column – medial lemniscus pathway, spinothalamic, ventral and dorsal trigeminothalamic tracts, as well as the sensory root of the trigeminal nerve and the sp5) through the brainstem and thalamus. I ventured out to undertake and present a novel study regarding the exact anatomical relationship between these pain pathways, but also because the neocortex necessitates feedback from the periphery in order to adjust the neuron firing frequency during the execution of movement (see above).

Finally, in the fifth Chapter, I anatomically describe the dentato-rubro-thalamic tract which is the projection that provides information to the red nucleus (dentato-rubral tract). It was of the essence for me to describe this pathway due to its connection to the red nucleus. As I described above, the rubrospinal tract is part of the extrapyramidal system which targets the spinal cord. In addition, I also describe

the projection from the cerebellum to the thalamus (dentato-thalamic tract), which is the afferent leg towards the neocortex of the cerebrocerebellar circuit, owing to the fact that the neocortex constantly requires feedback in order to adjust the neuron firing frequency.

Overall aim of the present study

The current study is largely open and investigative. However, an overarching hypothesis is that there is organisation and topography within the pathways through the brainstem and thalamus that are yet to be revealed in full detail. I hypothesise that the fibre architecture within the descending bundles in the crus cerebri and basilar pons, follows a logical and well-defined topographical pattern. I further propose this organisation extends to the relationship between the descending and transverse fibres of the pons and the decussation of the superior cerebellar peduncle. In addition, the present thesis presents novel anatomical descriptions, identification of various components of the pathways in the human and macaque brainstem made possible through the use of magnetic resonance (MR) histology made available by recent technical advances. Currently, the broad locations and somatotopy is known, but the precise detail of the fibre bundles and their relationships are not known. This thesis provides this missing information. During the study of trajectories of the fibre bundles, distinctive aspects of their patterning were defined. The *Stria Pontis*, the decussation of the superior cerebellar peduncle (xscp) and the fibre arrangement within the descending fibres bundles were three particular novel aspects revealed by this more detailed tracing. The origin of the *Stria Pontis* and its projection were

subsequently visualised using higher order tracing and image analysis (tensor glyphs). The *Stria Pontis* emanates from each of the transverse fibres of the pons leading to the conclusion that it forms part of the corticofugal pathways. The fibres of the xscp were also traced, and shown to intertwine as they decussate at the midbrain. Such details were previously elusive. The new data and fibre tracking has also revealed more precise architectural arrangement of the descending and transverse fibres of the pons. By combining the 3-D tractography results with enhanced anatomical background, the relationships between the fibre tracts, their terminations and origins, and surrounding nuclei are revealed at ultra-high resolution.

Brain mapping at the scale of 25 – 50 μm (which is the resolution of the data used in the present study) and its interpretation is a very slow, expensive, and time-consuming process, requiring the combination of descriptive anatomy, computer science and biomedical engineering. The present study opens doors for systematic investigation of connection patterns on human postmortem tissues which also expands our ability to understand brain networks. Finally, this revolution in detecting the fibre pattern within individual bundles and the ability to establish standard anatomical landmarks with precision between different pathways, opens doors for invasive and non-invasive applications in medicine and engineering.

CHAPTER 2:
General methods

This project commenced as an international collaboration between Scientia Professor George Paxinos AO, Professor G. Allan Johnson, and Professor Manisha Aggarwal. I was commissioned to carry out this project as the principal investigator for my doctoral degree by Scientia Professor George Paxinos AO. As a result, this thesis is based on volumetric datasets provided by these collaborators. The first dataset is of postmortem human brain tissue provided by Dr. Manisha Aggarwal who is an Associate Professor and MRI investigator in the Johns Hopkins Medicine Division of MR Research in the Department of Radiology and Radiological Science. The second dataset is from two more postmortem human brains and from one macaque brain, provided by the Director of the Duke Center for In Vivo Microscopy, and Charles E. Putman University Professor of Radiology, Professor of Physics, and Biomedical Engineering, Dr. G. Allan Johnson.

My above collaborators scanned the brains, created the raw data, the structural Gradient Recalled Echo (GRE) images, the Diffusion-Weighted Image (DWI) and the Fractional Anisotropy Colour (FAC) contrast. More precisely, they effectuated the specimen preparation, image acquisition and post-processing as described below.

Afterwards, I analysed the anatomical data in 3D, conceptualised the study, created the rest of the DTI contrasts such as the Fractional Anisotropy (FA), Axial Diffusivity (AD), Mean Diffusivity (MD), and Radial Diffusivity (RD). In addition, I enhanced the colour contrast of each DTI contrast in order to obtain the highest visualisation of brain structures. Furthermore, I did the fibre tracking on the FAC and all the tractographic analyses. Finally, I created the tensor glyphs from the diffusion data which allowed me to analyse the pattern of the fibres within the pathways under investigation. For completeness, I am rewriting the methods that my collaborators at Johns Hopkins and Duke Universities used in sections 2.1, 2.2 and 2.3, while the

tractography section describes the subsequent analysis technique I applied to the data. The original descriptions can be found in Calabrese et al. (2015b) for human specimens 1 and 2. In this article the authors studied the dentato-rubro-thalamic tract with probabilistic tractography and focused on the methodology, MRI registration, and surgical targeting for deep brain stimulation (DBS). Hence, the methods for the extraction of the brainstem and thalamus during autopsy and the subsequent MRI scanning are the same. The original descriptions regarding the methods for human specimens 3 and 4 can be found in Aggarwal et al. (2013). The macaque brain also used similar approaches to prepare and image the tissue as it is for human specimens 1 and 2. Further specific details of my analysis are also in each Chapter.

2.1 Johns Hopkins University human specimens

Specimen preparation

For the analysis of the fibre bundles and the surrounding anatomical structures, we used two brainstems that were extracted during autopsy from two adult humans with no abnormal neuropathology findings. The details regarding specimen preparation and image acquisition have been published (Calabrese et al., 2015b) and are summarised here. The postmortem fixation interval was less than 24 h. The specimens were obtained from the teaching collection which is part of the Department of Neurology at Johns Hopkins University, School of Medicine. In addition, the procedure was subjected to Institutional Review Board (IRB) approved protocols. Initially, the brainstems were fixed in neutral buffered formalin

(10% weight/vol) for more than 30 days before scanning (Fox et al., 1985). Prior to MRI acquisition, the specimens were immersed to phosphate buffered saline (PBS) including 2 mM gadopentetate dimeglumine (Magnevist, Berlex Imaging, Wayne, NJ, USA) for 7 days. In order to proceed with MRI scanning, the specimens were placed in polyethylene containers which were filled with perfluoropolyether oil (Fomblin®, Solvay Solexis, Thorofare, NJ, USA) for susceptibility matching and to avoid tissue dehydration (Shatil et al., 2016).

Image acquisition

A horizontal-bore 11.7 T scanner (Bruker Biospin, Billerica, MA, USA) was used to acquire MRI images of the human brainstems. In addition, this scanner was equipped with an actively-shielded gradient system (maximum gradient strength = 740 mT/m). Furthermore, a 72-mm-diameter volume coil was used to acquire the data which operated as the radiofrequency transmitter with an 8-channel receive-only phased array coil.

Diffusion MRI data were acquired using a 12-shot diffusion-weighted echo planar imaging (DW-EPI) sequence (Turner et al., 1991) with the following parameters: echo time (TE) = 27 ms, repetition time (TR) = 500 ms, diffusion gradient duration (δ) / separation (Δ) = 5/15 ms, one signal average, and partial Fourier acquisition factor of 1.4. Firstly, diffusion-weighted images were acquired along 30 independent directions. These directions were uniformly distributed over a sphere (Jones, 2004); (b-value = 4000 s/mm^2) and secondly, two non-diffusion-

weighted images were acquired at an isotropic spatial resolution of 250 µm x 250 µm x 250 µm. The total scan time in order to acquire the diffusion data was 13.5 h.

Image processing

The 3D *k*-space data were initially used to reconstruct the MRI images. The program used was *Matlab* (MATLAB (2018); Mathworks Inc., Natick, MA, USA). Prior to Fourier transformation, the *k*-space data were zero-filled in order to double the matrix size. Subsequently, the log-linear fitting function in DtiStudio (www.mristudio.org) was used to perform the Diffusion tensor reconstruction. The parametric maps of FA and primary eigenvector were calculated from the fitted tensors. The FA and primary eigenvector maps were used to generate the FAC images. More specifically, the ratio between the red, green, and blue components was equivalent to the ratio of absolute values of x, y, and z components of the primary eigenvector. Finally, the intensity was proportional to the FA contrast (Sedrak et al., 2010).

2.2 Duke University human specimens

Specimen preparation

Two more brainstems were extracted during autopsy from two adult anonymous humans with no history of neurologic or psychiatric disease. After an approximately 24 h postmortem interval, the brains were removed from the

calvarium using standard techniques. The brainstem and thalamus were dissected out, from the pyramidal decussation to the rostral extent of the diencephalon. Subsequently, the cerebral vessels were flushed with normal saline solution to which 100 IU/mL of heparin was added. This was applied via the basilar and internal carotid arteries. Specimens were then fixed in neutral buffered formalin (10% weight/vol) for two weeks. This period of time was proven to be an adequate interval to allow complete fixation of the dissected brainstems based on previous Guidelines (Dawe et al., 2009). Seven days prior to MRI scanning, the brainstems were rehydrated in a 0.1 M solution of phosphate buffered saline doped with 1% (5 mM) gadoteridol (ProHance, Bracco Diagnostics, Monroe, Township, NJ). Prior to scanning, the specimens were transferred immediately to a custom-made MRI-compatible tube and immersed in liquid fluorocarbon (Galden PFPE, Solvay Plastics, Brussels, Belgium).

Image acquisition

A 7 Tesla small animal MRI system controlled with an Agilent console (Agilent Technologies, Santa Clara, CA) was used to prepare and image the brains, and to do the initial processing and analysis of ex vivo MR imaging. Moreover, a 65 mm inner-diameter quadrature RF coil (M2M Imaging, Cleveland, OH) was used to achieve RF transmission and reception.

A 3D gradient echo pulse sequence was used to acquire anatomic images with the following parameters: (TR) = 50 ms, (TE) = 10 ms, flip angle (a) = 60^{o}, and bandwidth (BW) = 78 Hz/pixel. In addition, the field of view (FOV) was 80 x 55 x

45 mm. As a result, 3-D gradient echo images were collected at 50 μm^3 isotropic spatial resolution. Finally, the total acquisition time was 14 h.

A simple diffusion-weighted spin echo was used to acquire the diffusion data with pulse sequence (TR = 100 ms, TE = 33.6 ms, BW = 278 Hz/pixel). Subsequently, diffusion preparation was effectuated using a pair of unipolar, half sine (δ) = 4.7 ms, (Δ) = 26 ms, and gradient amplitude (G) = 50.1 G/cm. In addition, 120 unique diffusion directions were used to obtain single-shell high angular resolution diffusion imaging (HARDI) data. These directions were achieved at b = 4,000 s/mm^2 and 11 b = 0 s/mm^2 (b_0) volumes dispersed evenly throughout the acquisition. Moreover, the FOV was 90 x 55 x 45 mm, and the acquisition matrix was 450 x 275 x 225. As a result, diffusion images were collected at 200 μm isotropic voxel size. Finally, the total acquisition time was 208 h.

Image processing

Anatomic GRE and diffusion image volumes were registered to the first b0 image volume. This was achieved using a 3D affine transformation model with 12-parameters carried out in Advanced Normalization Tools (ANTs); (http:// www.picsl.upenn.edu/ ANTS/). Thus, correcting for the linear component of eddy-current-induced distortions. Subsequently, the rotational component of the affine matrices derived from registration of DWI was used to correct the diffusion gradient matrix. Furthermore, the registered diffusion data and the corrected gradient matrix were used for all diffusion reconstructions.

A Weighted Least Squares (WLS) technique was used to calculate the diffusion tensor within each voxel. Diffusion Tensor Imaging (DTI) scalars such as Apparent Diffusion Coefficient (ADC) maps, FA and FAC were generated by the diffusion tensor. Finally, the average of all DWI volumes was used to generate an isotropic DWI.

Diffusion Tensor Imaging (DTI) is an MRI-associated imaging technique which enables to trace the location and orientation of white matter tracts, based on the principles of anisotropy that water molecules assume (movement of water molecules) along axes in different directions. Fractional anisotropy (FA) is a scalar value between zero and one which defines the degree of anisotropy of the diffusion process. A value of zero indicates that the diffusion of water molecules is isotropic, for example, it is unrestricted in all directions. A value of 1 means that the diffusion is confined to the direction of the principal eigenvector alone.

Diffusion tractography

Diffusion tractography was performed on human specimen One from Duke University using DSI Studio (http://dsi-studio.labsolver.org/). A high-angular resolution diffusion MR imaging (HARDI) scheme was used, and a total of 120 diffusion sampling directions were acquired. The b-value was 4000 s/mm^2. The in-plane resolution and the slice thickness were both 0.2 mm. The diffusion tensor was calculated.

A deterministic fibre tracking (streamline Euler) algorithm (Yeh et al., 2013) was used with a step size of 0.50 mm. The step size constitutes the distance moved forward in each successive tracking interval. Diffusion measurements at each step interval are calculated and converted to a fibre tract trajectory. The default setting is half of the spatial resolution of the diffusion data. Thus, I assigned the value to 0 and the program did a random selection of the step size from 0.5 voxels to 1.5 voxel distance.

The angular threshold prevents abrupt bending of a tract and subsequent aberrant propagation along an adjacent voxel, which would result into a false positive streamline. The angular threshold values are empirically chosen by trial and error. Since the angular threshold similarly to the FA threshold constitutes a termination criterion, these two parameters should always be adjusted in relation to each other and accounting for the complexity of the structure. Therefore, for structures where some curvature is expected, I chose a low angular threshold of 20-30% for the drt (Chapter 5), whereas for the descending bundles (Chapter 3) and sensory pathways (Chapter 4), where one expects a straighter trajectory, I chose a more liberal regime of 60%. Moreover, the number of the masks and the values of the FA thresholds permitted the reconstruction of the pathways with different angular thresholds. For example, if the investigator uses one seed mask and two region of interest masks they will be able to diminish the angular threshold or the FA threshold or both, so that the tractography criteria are satisfied and the algorithm calculates the trajectory under investigation. It's always the combination of the tractographic parameters with the masks. Finally, the resulting tracts are evaluated in relation to the structural anatomical data, as further discussed and emphasised in section 2.5. The angular and

FA thresholds constitute termination criteria of fibre tracking as analysed in Soares et al. (2013); (see below).

The FA threshold is termination criterion that determines at which curvature the calculated trajectory will stop. Generally, a low FA threshold results in more trajectories identified, but at the cost of an increased occurrence of stray streamlines. In the current experiments it varied between 0.9 and 0.28 depending on the pathway under investigation. As a result, a high FA threshold was chosen for the descending bundles (FA threshold = 0.28; Chapter 3), a low value of 0.9 for the sensory projections (Chapter 4), and an intermediate value of 0.15 for the drt (Chapter 5). These different values enabled me to reconstruct the components of the descending and transverse fibre bundles because a high FA threshold appears to be too strict selecting the actual trajectories that pass from the seed to the ROI mask and thereby eliminating the false positives. On the other hand, I chose a low FA threshold = 0.9 for the sensory projections because these projections although they are vertical just as the bundles in Chapter 3, however, these are bundles that ascend from one side such as the cuneate and gracile fasciculi, cross over to ascend again as ml and further twist at the level of the midbrain to join the spth more rostrally (see Chapter 4). In addition, to avoid false positives in this pathway, I used a higher number of masks during tractography (see specific tractography methods of Chapter 4 and Appendix Fig. 19). Finally, an FA threshold = 0.15 which stands in between was optimal for the drt which ascends and has to cross over only once at the xscp, reach the red nucleus and then project to the ventral tier of the thalamus (Chapter 5). However, in the xscp the fibres intertwine, therefore, I lowered the angular threshold to enable the fibres of the drt to cross over at the xscp. These specific tractographic parameters

have to be experimented on by the investigator where they will determine which works best for each pathway under consideration without producing false positives or spurious fibres.

The final step in the tractography analysis was to set the smoothing value. The smoothing constitutes the momentum of the propagation direction. If smoothing is zero, the propagation direction is independent from the direction of the eigenvector within previous voxels. A value of smoothing equal to 0.5 indicates that each propagation step takes in consideration 50% of the direction of the tracts in the previous voxels. The smoothing was set at 1 for all 3 result Chapters as explained in specific methods and this means that the program does a random selection of the value from 0% - 95% (Yeh, 2021, Caan, 2016).

In investigating a putative pathway, a single three-dimensional manually drawn seed region was placed in a well-defined location of the pathway, and a single spherical region of interest was placed near the rostral end. Moreover, additional ROI masks were placed where necessary due to the complexity of the pathways. Tractography was seeded at random from the seed mask. The tensor glyphs displaying the first eigenvector in every voxel were generated with the framework and analysis tools provided in the FMRIB Software Library (FSL); (Woolrich et al., 2009).

2.3 Duke University macaque specimen

Specimen preparation

The (*Macaca mulatta*) brain was acquired following approved protocol from the Pathology Services and Tissue Distribution unit of the Wisconsin National Primate Research Center. The specimen was obtained at autopsy immediately following euthanasia for non-study related reasons.

After an approximately 24 h postmortem interval, the macaque brain was removed from the calvarium using standard techniques. The brainstem and thalamus were dissected out, from the pyramidal decussation to the rostral extent of the diencephalon. Subsequently, the cerebral vessels were flushed with normal saline to which 100 IU/mL of heparin was added. This was applied via the basilar and internal carotid arteries. The specimen was then fixed in neutral buffered formalin (10% weight/vol) for two weeks. This period of time was proven to be an adequate interval to allow complete fixation of the dissected brainstem based on previous guidelines (Dawe et al., 2009). One week before MRI scanning, the brainstem was rehydrated in a 0.1 M solution of phosphate buffered saline doped with 1% (5 mM) gadoteridol (ProHance, Bracco Diagnostics, Monroe, Township, NJ). Prior to scanning, the specimen was transferred immediately to a custom-made MRI-compatible tube and immersed in liquid fluorocarbon (Galden PFPE, Solvay Plastics, Brussels, Belgium).

Image acquisition

A 7 Tesla small animal MRI system controlled with an Agilent console (Agilent Technologies, Santa Clara, CA) was used to prepare and image the brains, and to do the initial processing and analysis of ex vivo MR imaging. Moreover, a 65 mm inner-diameter quadrature RF coil (M2M Imaging, Cleveland, OH) was used to achieve RF transmission and reception.

A 3D gradient echo pulse sequence was used to acquire Anatomic images with the following parameters: (TR) = 50 ms, (TE) = 10 ms, (a) = 60^{o}, and (BW) = 78 Hz/pixel. In addition, the (FOV) was 44 x 22 x 22 mm, and the acquisition matrix was 1760 x 880 x 880. As a result, 3-D gradient echo images were collected at 25 μm isotropic voxel size. Finally, the total acquisition time was 14 h.

A simple diffusion-weighted spin echo was used to acquire the diffusion data with pulse sequence (TR = 100 ms, TE = 33.6 ms, BW = 278 Hz/pixel). Subsequently, diffusion preparation was effectuated using a pair of unipolar, half sine (δ) = 4.7 ms, (Δ) = 26 ms, and (G) = 50.1 G/cm. In addition, 120 unique diffusion directions were used to obtain single-shell high angular resolution diffusion imaging (HARDI) data. These directions were achieved at b = 4,000 s/mm^2 and 11 b= 0 s/mm^2 (b_0) volumes dispersed evenly throughout the acquisition. Moreover, the FOV was 44 x 22 x 22 mm, and the acquisition matrix was 440 x 220 x 220. As a result, diffusion images were collected at 100 μm isotropic voxel size. Finally, the total acquisition time was 208 h.

Image processing

Anatomic GRE and diffusion image volumes were registered to the first b_0 image volume. This was achieved using a 3D affine transformation model with 12-parameters carried out in Advanced Normalization Tools (ANTs); (http:// www.picsl.upenn.edu/ ANTS/). Thus, correcting for the linear component of eddy-current-induced distortions. Subsequently, the rotational component of the affine matrices derived from registration of DWI was used to correct the diffusion gradient matrix. Furthermore, the registered diffusion data and the corrected gradient matrix were used for all diffusion reconstructions.

A WLS technique was used to calculate the diffusion tensor within each voxel. DTI scalars such as ADC maps, FA and FAC were generated by the diffusion tensor. Finally, the average of all DWI volumes was used to generate an isotropic DWI.

2.4 Comments regarding the different specimens

In the present study, I used the GRE of the human specimen 1 as anatomical background at 50 μm to delineate the structures of the brainstem and thalamus. In addition, I combined the tractography derived from the diffusion data of the same specimen and I showed the relationship between the pathways and the surrounding structures. Moreover, I used the FAC of human specimens 2, 3, 4, and the FAC of the macaque brainstem and thalamus (see Appendix Figs. 13 – 18) to delineate and validate the results of Chapters 3, 4 and 5. Consequently, only the human specimen

one was used for tractography due to the fact that the quality and the post-processing of this dataset was far superior than the other specimens, and this enabled me to successfully trace the projections from the caudal medulla oblongata to the thalamus. The parameters that rendered the quality of human specimen 1 as superior can be summarised and explained as follows:

1) The postmortem interval was longer for human specimens 2, 3, and 4. Thus, postmortem alterations which occurred on human specimens 2, 3, and 4 did not allow the brain tissue to achieve optimal conditions for diffusion scanning (possibly due to the formation of blood clots).

2) Only at Duke the specimens were flushed via the cerebral vessels with normal saline solution to which 100 IU/mL of heparin was added. Thus, rendering the tissue susceptible to blood clots.

3) At Johns Hopkins the diffusion images were acquired along 30 directions whereas at Duke the images were acquired at 120 directions, and this enabled me to perform HARDI tractography something which I found impossible in terms of tractographic final output if I tried to perform HARDI on data characterised by 30 directions.

4) The total scan time for the diffusion volumes at Duke was 208 hours, whereas at Johns Hopkins my colleagues scanned the specimens for only 13.5 hours. Regardless, the Johns Hopkins data are informative enough to be used for fibre architecture orientation on the FAC, although the caudal and rostral parts of the human specimens 3 and 4 were damaged possibly due to the above reasons (Appendix Figs. 15, 16).

2.5 Methodological analysis of brain mapping, anatomical delineations and fibre tracking

2.5.1 Methodology

In this Chapter, I present an extension of details regarding the step-by-step approaches used to delineate the fibre tracts presented in Chapters 3-5. Therefore, I analyse the methodological approach that I used for fibre tracking and tractography. Moreover, I describe the validity and the anatomical information provided by the DTI contrasts. Finally, I evaluate how the isotropic spatial resolution of MR-histology is essential for accurate description of fibre orientation.

2.5.2 Deterministic Tractography

The present ultra-high resolution dataset allowed me to use deterministic tractography based on high-angular-resolution diffusion imaging (HARDI) scheme and most particularly the trajectory estimation was obtained using the Euler method (Basser et al., 2000). The reason I chose to proceed with deterministic tractography is that the most plausible pathways coincide with the deterministic streamlines (Schreiber et al., 2014) and as validation I used the structural anatomical GRE contrast. For example, the nine descending bundles that I identified on the FAC and tractography (see Chapter 3) correspond and overlap with the anatomical signature in the GRE, in all three planes of section. Moreover, deterministic fibre tracking uses a "deterministic" approach to delineate the pathways. Thus, knowledge of precise

anatomy is pivotal for this approach since the investigator places a seed point in the white matter of a particular pathway and the algorithm processed by the program follows a local fibre direction both anterogradely and retrogradely. Probabilistic tractography on the other hand uses a random process designed in the propagation direction. In other words, the difference between deterministic and probabilistic tractography is that during the deterministic approach the streamlines are steered following a fixed direction per voxel, whereas the probabilistic approach outputs the distribution of all possible fibre orientations within each voxel, and random samples are reconstructed from such distributions to determine fibre propagation. In addition, highly detailed neuroanatomical knowledge is pivotal for both the accurate seeding and the accurate interpretation and validation of the tractography outputs (Abhinav et al., 2014). There are some general limitations of deterministic tractography such as problems of false continuity (stray fibres which continue through adjacent voxels into another pathway) and premature termination, and the crossing-branching problem which has been widely observed in MRI data of low isotropic resolution (higher than 1000 μm); (Jbabdi and Johansen-Berg, 2011, Yeh et al., 2019). Finally, the isotropic spatial resolution and the fact that the investigator should always validate the tractography results with the structural anatomical contrasts remains a critical component.

2.5.3 GRE intensity differences between nuclei and tracts

Gradient recalled echo T2 weighted MRI enables a high contrast between white to grey matter. When combined with fibre directionality maps (DTI), this

assisted in delineating and annotating the specific anatomical pathways presented in Chapters 3-5, including 117 anatomical parts, areas and structures of the central nervous system such as the thalamus, hypothalamus, pineal gland, as well as nuclei and fibre tracts in the transverse, sagittal and coronal planes. In addition, major tracts were identified such as the scp, mcp and icp, as well as smaller tracts such as the spth, sp5, vtt and dtt. This is illustrated by reporting an example of how the descending and transverse fibre bundles in the basilar pons were subdivided into separate anatomical entities from rhombomere two to four.

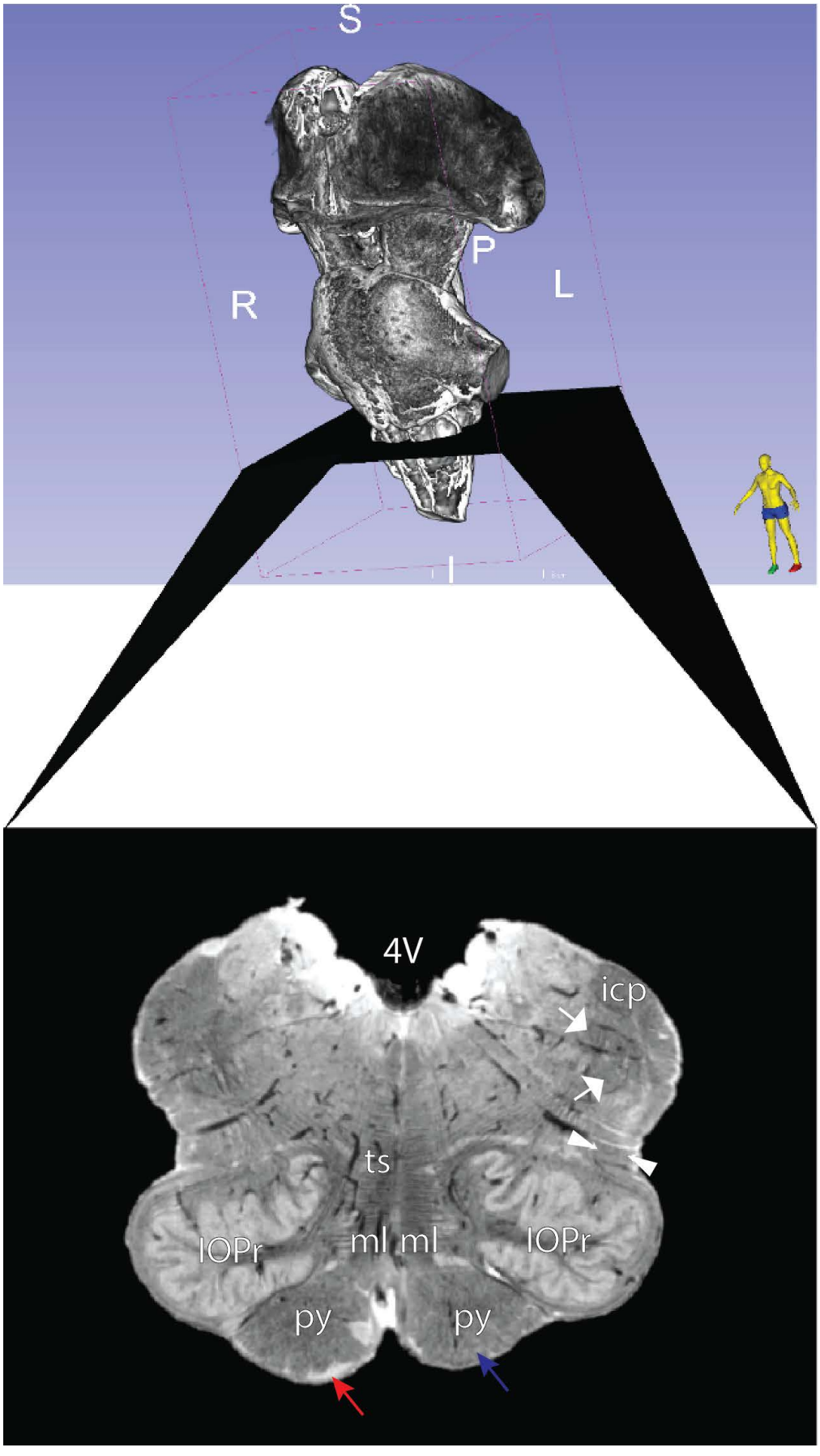
S
P
R
L
I
4V
icp
ts
IOPr
ml ml
IOPr
py
py

Fig. 2.1. Transverse section - Gradient Recalled Echo (GRE) image at 50 µm original resolution, displaying the medulla at the level of the IOPr (human specimen 1)*. White arrows: sp5, Red arrow: Arcuate nucleus, Blue arrow: pyramid, Arrowheads: spth, 4V: forth ventricle, icp: inferior cerebellar peduncle, ts: tectospinal tract, ml: medial lemniscus, py: pyramidal tract, IOPr: inferior olive, principal nucleus.*

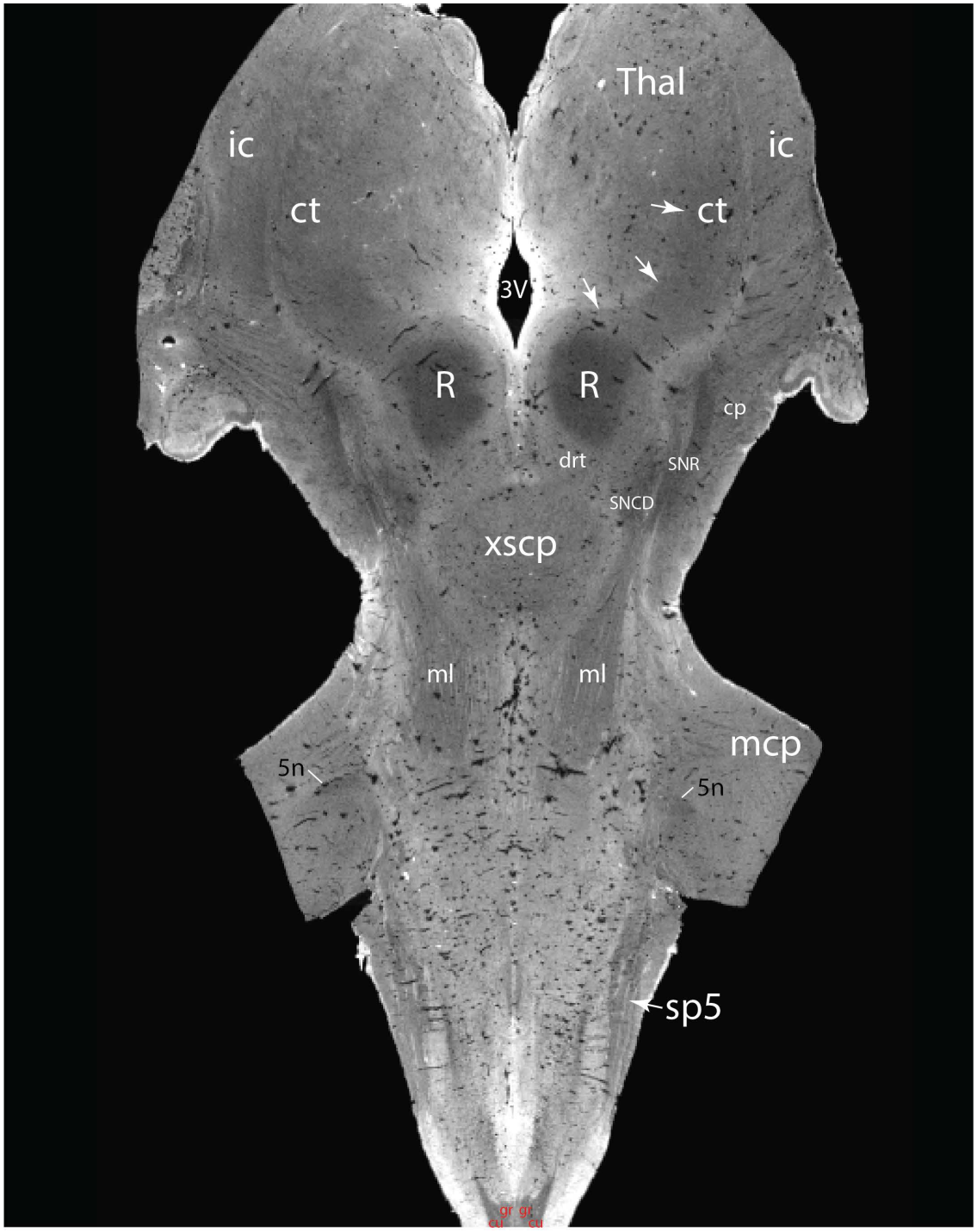
Thal
ic
ic
ct
ct
3V
R
R
cp
drt
SNR
SNCD
xscp
ml
ml
mcp
5n
5n
sp5
gr
gr
cu
cu

Fig. 2.2. Coronal section – GRE of the brainstem and thalamus (human specimen 1). *Note the hypointense fibre tracts such as the sp5 and 5n, whereas the nuclei leave a hyperintense signature. Note the 5n as it courses within the mcp and the subsequent trajectory of the sp5. Note also the trajectory of the ct as it ascends from the red nucleus to the ventral tier of the thalamus (arrows). Abbreviations: cu: cuneate fasciculus, gr: gracile fasciculus, mcp: middle cerebellar peduncle, xscp: decussation of the superior cerebellar peduncle, SNCD: substantia nigra, pars compacta, SNR: substantia nigra, pars reticulata, cp: cerebral peduncle, ml: medial lemniscus, drt: dentato-rubro-thalamic tract, R: red nucleus, 3V: third ventricle, ct: cerebellothalamic tract, Thal: thalamus.*

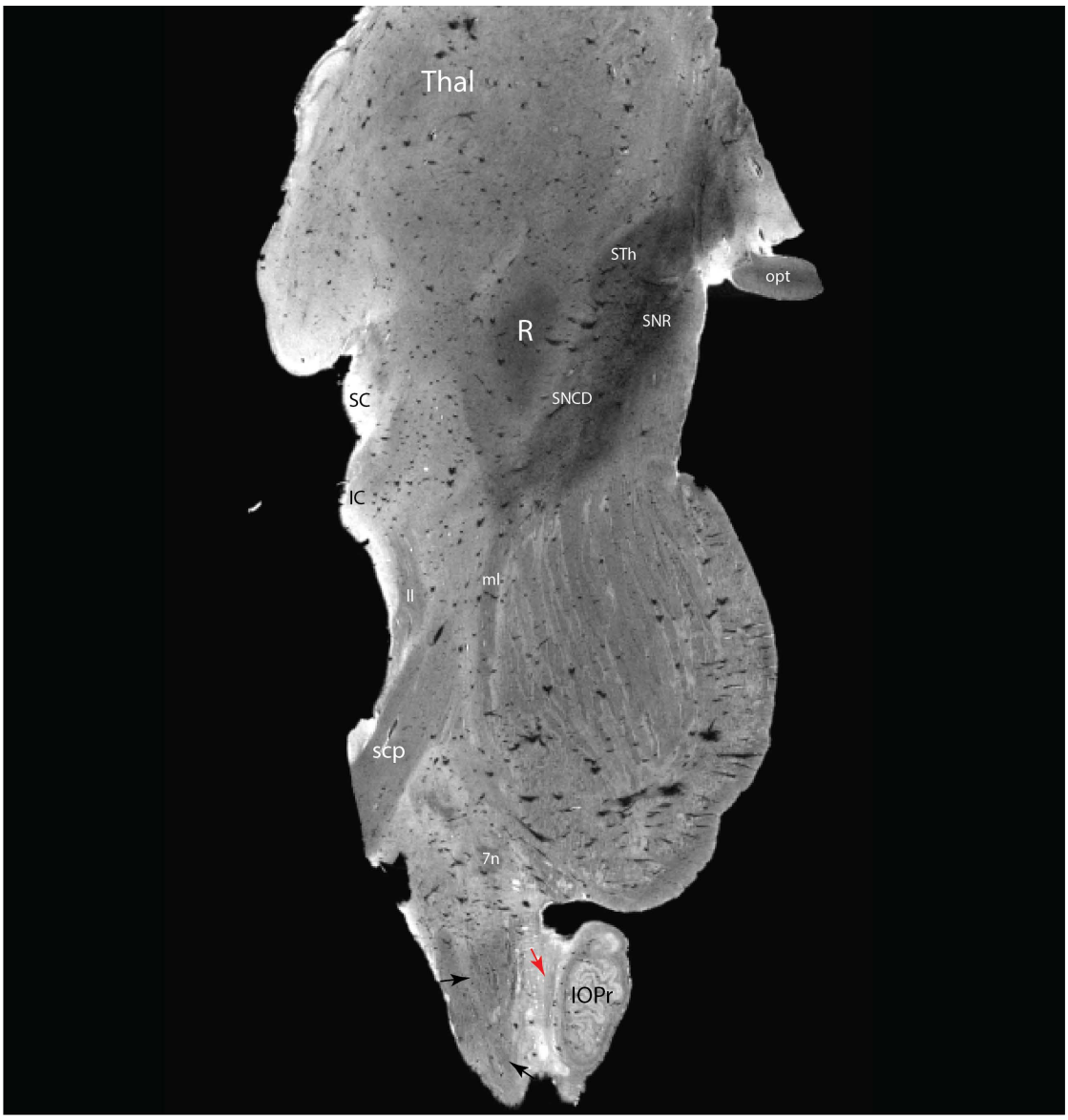
Thal
STh
opt
R
SNR
SC
SNCD
IC
ml
ll
scp
7n
IOPr

Fig. 2.3. Sagittal section – GRE shows the brainstem and thalamus (human specimen 1)*. The GRE images such as this one, are overlapped to the FAC to confirm the pattern of the descending fibre bundles. Black arrows: sp5, red arrow: spth, 7n: facial nerve, scp: superior cerebellar peduncle, IOPr: inferior olive, principal nucleus, ll: lateral lemniscus, ml: medial lemniscus, SC: superior colliculus, IC: inferior colliculus, R: red nucleus, SNR: substantia nigra, pars reticulata, SNCD: substantia nigra, pars compacta, STh: subthalamic nucleus of Luys, opt: optic tract, Thal: thalamus.*

Figs. 2.1 - 2.3 show high contrast GRE images in transverse, coronal and sagittal sections. Note the grey matter hyperintensity, where nuclei such as the Pn, the IOPr, and Ar, can be identified, contrasting with the white matter hypointensity (see Fig. 2.1 red arrow shows the Ar – blue arrow shows the py) representing the fibre tracts. In sagittal section (Figs. 2.3, and Appendix Figs. 2-FA contrast and Fig. 6-AD contrast) nine descending tracts are seen in the basilar pons where they can be followed by placing the cursor in 3D slicer on each individual bundle. These tracts are also evident in the transverse images (FAC in Chapter 3, Fig. 3.9). In this way, MR-histology offers the modern investigation and identification of white matter connectivity in 3D, and most particularly with the advantage of avoiding tissue damage when slicing it into sections.

The high contrast between grey and white matter made the determination of boundaries possible, therefore I refrained from including the actual drawings on the GRE so that I would not conceal anatomical information (see Fig. 3.15, and Fig. 2.1).

2.5.4 Tract annotations and delineations

The delineations have been conducted with a specific, colour contrast enhancing, and modern MRI software called 3D-slicer. The tracing has been done initially on the GRE, then on the FAC, and finally I overlapped both contrasts to confirm the anatomical interpretation (Appendix Fig. 23). In addition, the GRE contrast was used to estimate where the tracts are, and to guide the seed and ROI masks for tractography. The remaining DTI contrasts such as the FA, AD, RD, MD, DWI at 200 μm of isotropic resolution had high enough clarity to be complementary

tools in identifying and subdividing the above pathways. Furthermore, owing to the high resolution of these DTI contrasts, nine descending and ten transverse bundles were identified, and followed rostrally until the crus cerebri, and caudally into the pyramid so that the pattern and the way these bundles alternate in 3D space is presented herein. Finally, the sp5 and the spth were reported within the caudal brainstem using the FA as a guide (see Appendix Figs. 1-3). This 3D analysis during the tracing process was provided by the volumetric segmentation toolset in 3D slicer (http://www.slicer.org; Fedorov et al. (2012); Harvard University, National Institutes of Health).

To improve the degree of image segmentation detail between the fibre bundles as well as between fibre bundles and nuclei, two main approaches were possible. First, the investigator should carefully observe and trace the various individual bundles in the transverse plane from the rostral to the caudal end of the brainstem. Then, the same bundles should be followed in the sagittal and coronal planes. The volumetric format of the anatomical set of data renders it possible to study the brainstem and thalamus in its natural 3D space. This technique allows the investigation of fibre tracts in multiple angles simultaneously. In addition, it is possible to examine intersecting planes within a fibre bundle or nucleus in the same brainstem. Second, the investigator should observe and trace the various individual bundles in different DTI contrasts which offer different windows of observation into the brainstem anatomy. These different contrasts leave different signatures particularly for fibre bundles. For example, tracts such as the spth, vtt, dtt and also the sp5 were not clearly visible in GRE although its resolution is of 50 μm. Yet, these tracts were visible in FA, AD, MD, RD, which have a resolution of 200 μm (see

Appendix Figs. 1-12). A further parameter that rendered possible the tract annotations was the improvement of the actual colour contrast of each DTI contrast so that the white to grey matter contrast would be further enhanced.

2.5.5 Using the tensor glyphs to obtain accurate anatomical information on the FAC orientation

It is worth noting how the DTI signature illuminated in green the ventrodorsal axons at the midline of the pons and made it possible to anatomically describe though the tensor glyphs the *Stria Pontis*. More specifically, the option to generate and visualise the first eigenvector within each voxel allowed the glyph to show that the *Stria* projects bilaterally into the tegmentum (which is in alignment with the DTI signature) towards the cranial nerve nuclei. In addition, the *Stria* emanates from each of the transverse fibres of the pons and by extension I assumed that the *Stria* is part of the corticofugal pathways. Regarding the xscp the glyph showed that the fibres intertwine as they cross over. Concerning the architectural arrangement of the descending and transverse fibres of the pons, it is shown by the glyphs that the fibres coursing towards the medulla oblongata occupy a central position (see the tensors in Chapter 3; pyramidal tract) within each bundle whereas the fibres with destination to the basilar pons (corticopontine tract) are placed laterally and to some degree externally within each of the 9 descending bundles as constantly is highlighted by the glyphs from rhombomere 2 to 4 (the entire length of the basilar pons). The pathway is characterised by the fact that the bundles of the ventral group of the descending fibres anatomically and functionally correspond to the ventral group of the transverse

fibres of the pons and so on. At the crossing point where the descending projections are heading towards the pontine nuclei, the pathway is seen in the glyphs to change direction, bend and traverse the basilar pons towards the contralateral middle cerebellar peduncle (mcp).

As a result, it is reported, herein, a study of white matter connectivity and fibre tracking within the brainstem and thalamus at a resolution of 50 μm and 25 μm for the human and macaque, respectively. Moreover, deterministic tractography offered the possibility to confirm the above pathways as well as to present the various fibre bundles in 3D space interposed between the transverse, sagittal and coronal GRE delineated background.

CHAPTER 3:
Redefining the pathways in the basilar pons through ultra-high-field MRI, tractography and tensor glyphs

3.1 Introduction

The basilar pons or ventral aspect of the pons contains some of the major control pathways: those motor efferents descending through the brainstem en route to spinal cord motor circuits, and those connecting with motor nuclei in pons and medulla oblongata involved with upper body control (cranial nerve nuclei). The 1st description of this major division of the brainstem was in the 16th century by Costanzo Varolio (1543-1575), an Italian anatomist and papal physician who identified many anatomical structures such as the crus cerebri and the ileocecal valve. However, it took three centuries before the key function of this region was first revealed by the clinical manifestations of basilar pons lesions and vascular infarction. It became apparent that patients with basilar artery occlusion presented clinical manifestations that range from mild transient non-specific symptoms to fatal strokes (Hayem, 1868). Over the subsequent century, the severity of trauma, infections such as *Staphylococcus aureus* brainstem abscess, strokes within the branches of the vertebrobasilar system, tumours (pontine glioma) and autoimmune (cerebral lupus) and demyelinating diseases (multiple sclerosis) affecting the pons kindled some interest in brainstem vasculature anatomy (Duret, 1873, Biemond, 1951). Yet, the precise mapping of the neural pathways, within the human basilar pons remains incomplete.

In contrast, detail of the pathways through the basilar pons are more advanced in non-human primates. The monkey corticopontine tract has been studied utilizing for example ablation-degeneration and isotope tract tracer studies (Hartmann-von Monakow et al., 1981, Jürgens, 1984, Brodal, 1978b, Brodal, 1978a, Nyby and Jansen, 1951). Injection of retrograde tracers into the nuclei situated bilaterally

around the midline of the basilar pons reveals afferent inputs descending from primary motor cortex (M1); (Nyby and Jansen, 1951) and premotor cortices, as well as from the supplementary motor area (SMA) and corticofugal fibres from the visual cortex (Brodal, 1978b). Corticopontine projections from the M1 and SMA and premotor cortex are thought to terminate principally in the caudal two-thirds of the pons, whereas association area projections terminate predominantly in the rostral pons (MacMore et al., 2004, Schmahmann et al., 2004).

As for the corticofugal projections to the cranial nerve nuclei, the axons synapse directly, or through interneurons, on the oculomotor (extraocular muscles except for the superior oblique muscle, midbrain), trochlear (superior oblique muscle, midbrain), motor nucleus of the trigeminal (muscles of mastication, pons), abducens (lateral rectus, pons), and facial nuclei (motor innervation to the muscles of facial expression, pons). The corticobulbar tract originates from the precentral gyrus (M1), premotor cortex and SMA. The corticobulbar fibres descend from the cortex through the pons and medulla to terminate at corresponding nerve nuclei such as the ambiguous (muscles of soft palate, pharynx and larynx), spinal accessory (trapezius and sternocleidomastoid, cell bodies located in the caudal medulla and cervical spinal cord), and hypoglossal (motor innervation to the muscles of the tongue except the palatoglossus, medulla); (Young, 2007, DeMyer, 1998).

In addition to the corticopontine and corticobulbar tracts described above, the descending fibre bundles contain the cortical projections towards the spinal cord. The human corticospinal tract is composed of over one million axons, three quarters of which are myelinated (Lassek and Evans, 1946, Lassek, 1940). Most, 80% of these

corticospinal tract fibres originate from Brodmann's areas 4 (the primary motor cortex, M1) and 6 (the premotor cortex); (Kuypers, 1981). At the level of the midbrain the corticospinal projection fibres pass through the crus cerebri (which is the anterior portion of the basis pedunculi) to enter the basilar pons. These descending bundles display musculotopic arrangement, with those driving spinal motor neurons for muscles of the hand found in the ventromedial part, whereas fibres controlling motor neurons for the leg muscles are in the dorsolateral part of the basilar pons (Hong et al., 2010a). More caudally, at the level of the medulla, the corticospinal fibres congregate towards the ventral surface to form the pyramids. The fibres in the pyramids maintain the musculotopic arrangement, whereby, those driving motor neurons for the hand muscles are found medially, and those that innervate motor neurons for the muscles of the foot being found more laterally (Kwon et al., 2011b).

Therefore, the basilar pons contains both descending fibre tracts found perpendicular to the transverse fibres of the pons which in turn arise from the pontine nuclei. The precise topography of the descending bundles and their relationship with the transverse fibres of the pons remains unclear. Tracing and ablation studies, akin to those performed in experimental animals, are not feasible in humans. However, recent advanced imaging technology now enables human brain pathways to be precisely delineated. In the current Chapter, I provide tractography and analysis of the bundles and their constituent fibres (tractography outputs) through the basilar pons in postmortem human and macaque brain, defining their orientation using fractional anisotropy and delineating their interrelationships at ultra-high resolution using tensor glyphs which convey tensor variables by mapping the major

eigenvectors and eigenvalues within each voxel. I reveal specific cortico-pontine, -bulbar, and -spinal pathways with unprecedented resolution (50 μm for the human and 25 μm for the macaque). It is hoped that mapping of the corticofugal pathways through the pons, in particular, has clinical importance to enable easier and more precise targeting in neurosurgery and radiotherapy for diseases such as diffuse intrinsic pontine gliomas, lymphomas, traumatic brainstem injury and abscesses.

Finally, pharmacological treatment in medicine (i.e., by reducing the edema) would be made easier with a map of the basilar pons in conditions such as central pontine myelinolysis, Wallerian degeneration, hepatic or hypertensive encephalopathy, ischemic pathology and vasculitis (Behçet's disease and lupus); (Frazier et al., 2009). Typically, brain edema (e.g., due to tumours or other injuries) is treated with corticosteroids. For example, edema surrounding brain tumours has been extensively reduced with high doses of Dexamethasone (Rosenberg, 2012). The current topography of the pontine fibre bundles mapped in the present research, could enable improved monitoring of both brainstem tumours and their associated edema. With ongoing evaluation of the degree of peritumoral edema using standard diffusion MRI (Wick and Küker, 2004) and the subsequent overlap of our maps to accurately assess progression towards adjacent fibre bundles that would compromise function and further deterioration of the patient's neurological status, we hope to provide a useful neuroanatomical set of maps for stereotactic neurosurgery which could guide treatment, and prognosis (neuronavigation for brainstem surgery). In addition, our maps could more precisely assist brainstem edema microsurgical decompression (Zornow and Prough, 1995) by providing the topography of the pontine bundles and reducing the risk of iatrogenic damage. Finally, our maps could guide surgical

removal of tumours responsible for brainstem edema which would result in amelioration of symptomatology.

3.2 Specific methods

The data analysed below use MRI images obtained from human and macaque brains, as described in Chapter 2. Fibre bundles were traced using DTI and FA.

For the whole pathway of the descending fibre bundles a seeding region was placed at the crus cerebri with a volume (90, 90, 2.6e+02) that covers the entire crus cerebri. An additional region of interest (ROI) was placed at the level of midpons with coordinates (110, 66, 180) and a volume size of 1.6e+02 mm^3; (160 mm^3) that covers the entire basilar pons. The seeding regions and ROIs are placed on the MRI image manually and the corresponding coordinated are generated by the DSI Studio. These coordinates consist of three parts. The first part indicates the distance of the mask from the left side of the operational window in DSI Studio, starting from 0 until the value reported above. The second part indicates the precise point along the anterior-posterior plane of view, and finally the third part indicates the inferior-superior point. Each co-ordinate is an arbitrary scale. Finally, the program calculates the volume of the mask and in this case, it was 1.6e+02 mm^3 (160 mm^3). The FA threshold was 0.28. This parameter determines the threshold for fibre termination in relation to the calculated curvature of the fibre trajectory. The angular threshold was 60%. The angular threshold is initially estimated according to a priori knowledge of the trajectory curvature. This threshold serves as a termination criterion as well. For example, if two consecutive moving directions have crossing angle above this

threshold, the fibre tracking will be terminated by the program. The fibre trajectories were smoothed by averaging the propagation direction with a percentage of the previous direction. Smoothing gives the "momentum" of the propagation direction. If smoothing is 0, the propagation direction is independent of the previous direction. If smoothing is 1.0, as in the present study, the percentage is randomly selected from 0% to 95%. A total of 350,000 trajectories were calculated.

For the three components of the descending fibre bundles such as the ventral, intermediate and dorsal groups (primary subdivisions), from the original seed mask placed at the level of the crus cerebri, I selected the first two ventral lamellae (cervical), the two intermediate (thoracic), and the two dorsal (lumbar and sacral), respectively as seed regions in order to identify the patterning of the descending fibre bundles. Subsequently, I placed an additional ROI at the level of the midpons, whereas no ROI was places caudally in the pyramid (see Results section; and Appendix Figs. 20 & 22).

3.3 Results

3.3.1 Orientation of the images and specimens

The MRI images of the brainstem and thalamus from the four human specimens were followed rostrally from the internal capsule and caudally through the brainstem, so as to include midbrain, pons, medulla oblongata and the top part of the spinal cord. Streamlines and their orientations were identified at different segments and followed rostral-caudally and medial-laterally. This resulted in an extensive 3D

dataset, that can be a challenge to display in 2D. The obtained results commence by tracing the descending bundles from the internal capsule to the rostral spinal cord. In Figs 3.1 & 3.2 these bundles are displayed in pseudo-3D at different transverse levels through the thalamus and brainstem. The curvature and subdivisions of these bundles are revealed by the coding of orientation into colour, as presented by the fractional anisotropy colour (FAC) images. This orientation is particularly useful for viewing the relationship between the descending (longitudinal fibres of the pons) and transverse fibres of the pons as shown later in Figs. 3.9 to 3.11. Finally, a gradient recalled echo (GRE) sequence is used to illustrate the relationship between axonal tracts and nuclei in Fig. 3.15.

3.3.2 Overall anatomical descriptions of the subdivisions of the descending fibre bundles (corticopontine, -bulbar, -spinal tracts) traced from the internal capsule through to the medullary pyramids, including the projections to the SNR

The descending bundles from the cortex and striatum together form the internal capsule (ic), which can be seen bilaterally in Figures 3.1 a, d, g, j. The ic has been subdivided into four parts after three separate 3D masks were placed within the crus cerebri and one additional 3D mask was placed in the substantia nigra. There have been identified three external parts (Fig. 3.1 a, d, g) that descend beyond the crus cerebri, through the pons and reach the medulla oblongata as the pyramidal tract, and one additional internal part of the ic which projects to the substantia nigra pars reticulata (Fig. 3.1 j).

For the cervical component of the pyramidal tract, a 3D seed mask was created for the first two curved ventrolateral lamellae (descending bundles 1, 2, 3 and 4; Fig. 3.2a, and Appendix Fig. 22a) in the crus cerebri which revealed that the pathway originates rostrally in the external part of the internal capsule and extends caudally to the pons (Fig. 3.3). Tractographic analysis revealed that the ventral part (containing the bundles 1-4, which is the cervical component of the corticospinal tract, including corticopontine and corticobulbar fibres) assumes an external position along the long axis of the internal capsule (transverse section in Fig. 3.1a, Fig. 3.3c). As the fibres that constitute the external part of the ic descend through the diencephalon (Fig. 3.1b) and midbrain (Fig. 3.1 c) they shift, twisting to form ventrolaterally curved lamellae in the crus cerebri (Fig. 3.2a).

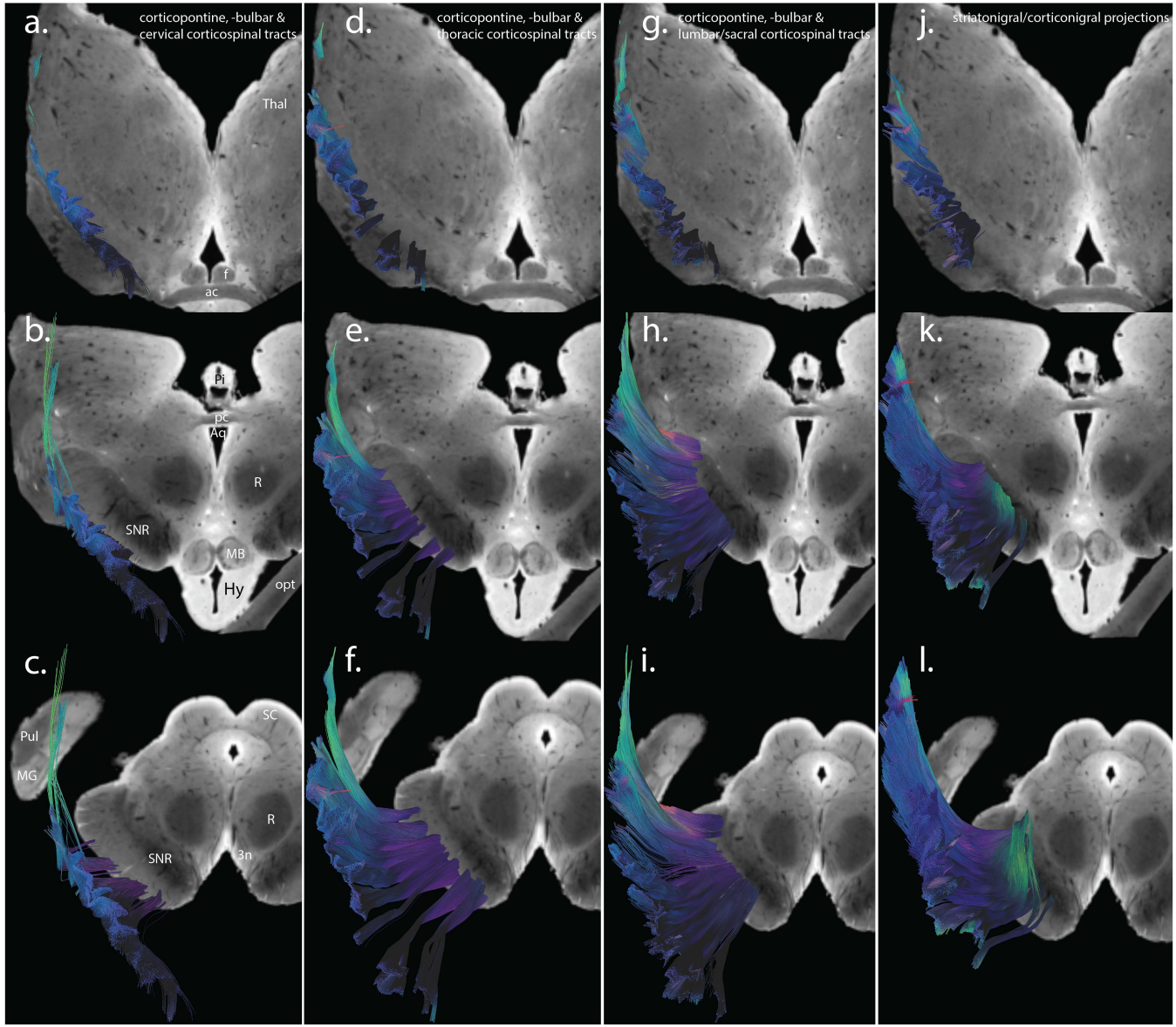
a.
corticopontine, -bulbar &
cervical corticospinal tracts
Thal
f
ac
d.
corticopontine, -bulbar &
thoracic corticospinal tracts
g.
corticopontine, -bulbar &
lumbar/sacral corticospinal tracts
j.
striatonigral/corticonigral projections
b.
Pi
pc
Aq
R
SNR
MB
Hy
opt
e.
h.
k.
c.
SC
Pul
MG
R
SNR
3n
f.
i.
l.

Fig. 3.1. Transverse sections from the thalamus to the midbrain displaying the components of the descending fibre bundles. *The four subdivisions of the internal capsule (a, d, g, j) as they are arranged from external to internal. The external in (a), intermediate in (d) and internal in (g) parts of the bundles constitute the corticopontine, -bulbar, -spinal tracts and continue through the crus cerebri (b, e, h) with the same arrangement until the junction between rhombomere one and two (c – i). The most internal component of the internal capsule (j) is occupied by the projection that does not continue beyond the nigra, the presumptive striatonigral and corticonigral pathways (j – l); this is the sector (g) that is free of corticopontine, -bulbar, -spinal tracts. The tractographic analysis was performed on human specimen 1. On the FAC (fractional anisotropy colour) maps red, blue, and green represent anisotropy along medial-lateral, rostral-caudal, and ventral-dorsal orientation, respectively. Abbreviations: Thal: thalamus, f: fornix, ac: anterior commissure, pc: posterior commissure, Aq: aqueduct, Pi: pineal gland, R: red nucleus, MB: mammillary body, SNR: substantia nigra, pars reticulata, opt: optic tract, Hy: hypothalamus, SC: superior colliculus, 3n: oculomotor nerve, Pul: pulvinar, MG: medial geniculate nucleus.*

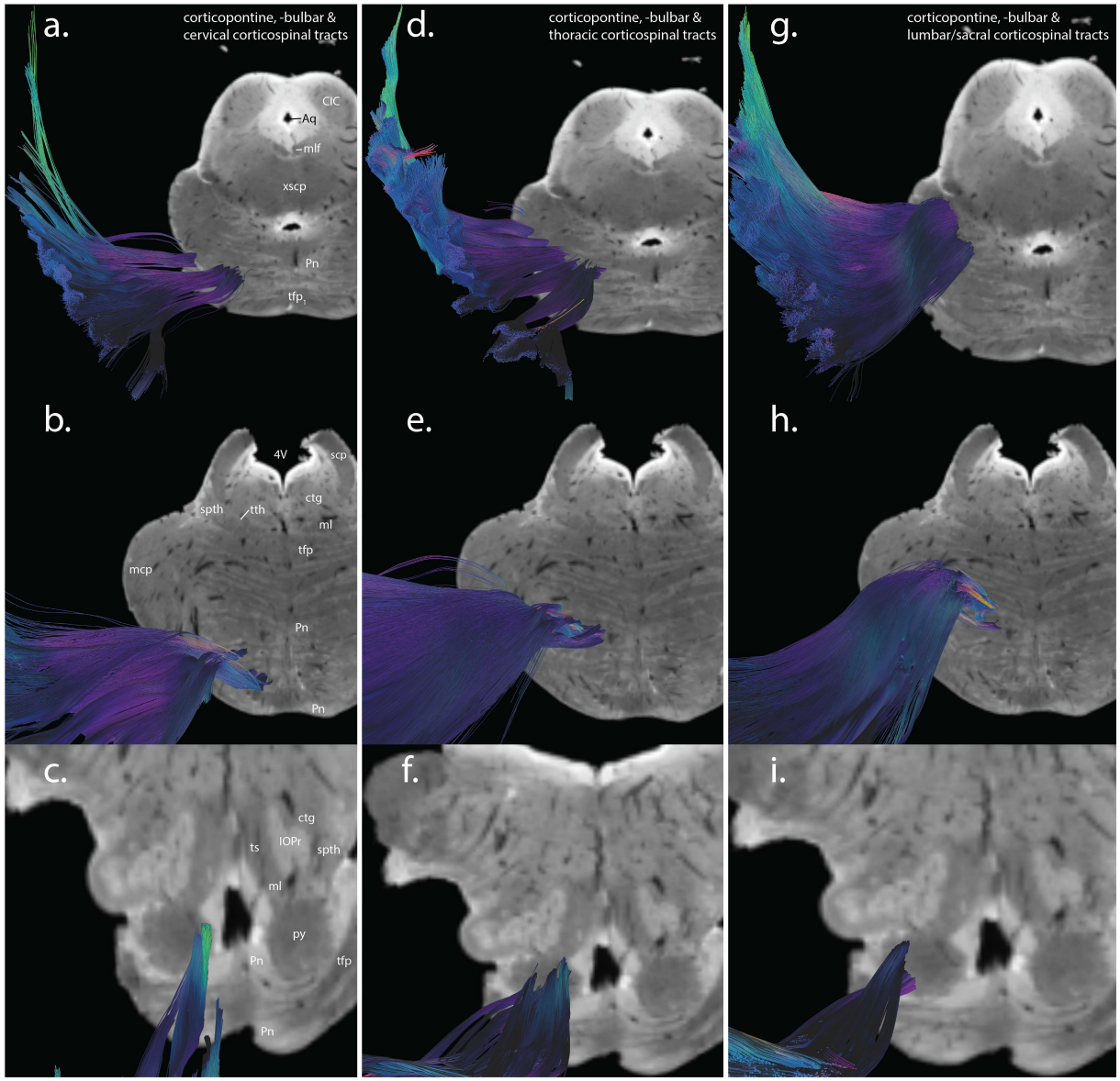
a.
corticopontine, -bulbar &
cervical corticospinal tracts
CIC
Aq
mlf
xscp
Pn
tfp
b.
4V
scp
ctg
spth
tth
ml
tfp
mcp
Pn
Pn
c.
ctg
ts
lOPr
spth
ml
py
Pn
tfp
Pn
d.
corticopontine, -bulbar &
thoracic corticospinal tracts
e.
f.
g.
corticopontine, -bulbar &
lumbar/sacral corticospinal tracts
h.
i.

Fig. 3.2. Subdivisions of the descending fibre bundles from the pons-midbrain junction to the pontomedullary junction. *At the level of the junction between rhombomere one and two (a, d, g) the descending bundles (curved lamellae) shift and occupy a ventrolateral (a), mediolateral (d), and dorsolateral (g) position. At the level of the midpons the bundles shift anticlockwise to a ventral (b), intermediate (e), and dorsal (h) position. Finally, at the level of the pontomedullary junction from (c) to (i) the ventral part of the descending bundles will eventually constitute the cervical (c), the intermediate part the thoracic (f), and finally the dorsal part the lumbar/sacral (i) components of the pyramidal tract. The tractographic analysis was performed on human specimen 1. On the FAC maps, red, blue, and green represent anisotropy along medial-lateral, rostral-caudal, and ventral-dorsal orientations, respectively. Abbreviations: CIC: central nucleus of the inferior colliculus, Aq: aqueduct, mlf: medial longitudinal fasciculus, xscp: decussation of the superior cerebellar peduncle, Pn: pontine nuclei, tfp1: most ventral transverse fibre of the pons, 4V: forth ventricle, scp: superior cerebellar peduncle, mcp: middle cerebellar peduncle, ctg: central tegmental tract, ml: medial lemniscus, tth: trigeminothalamic tract, spth: spinothalamic tract, tfp: transverse fibres of the pons, IOPr: inferior olive, principal nucleus, ts: tectospinal tract, py: pyramidal tract.*

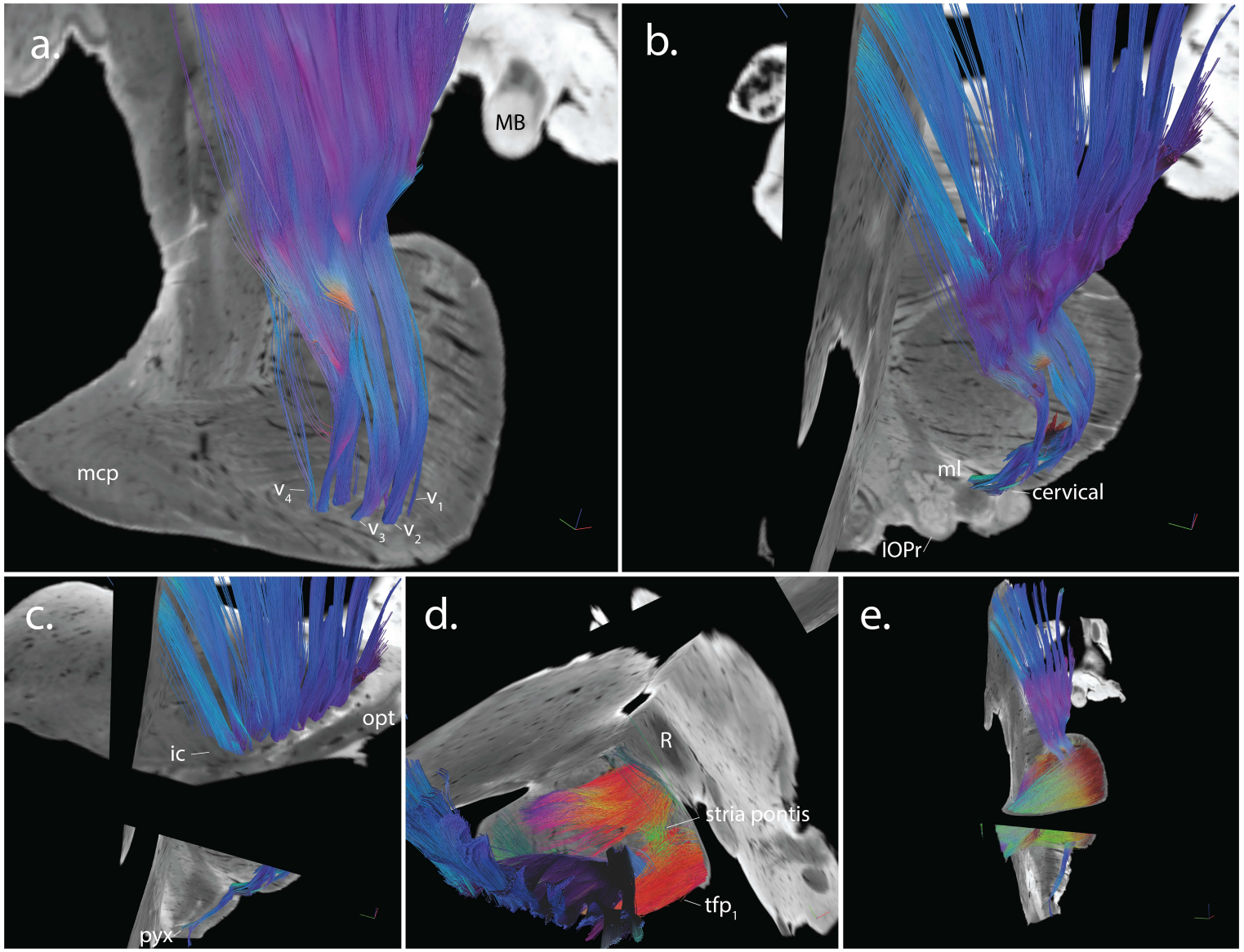
a.
MB
mcp
v4
v1
v3
v2
b.
ml
cervical
lOPr
c.
opt
ic
pyx
d.
R
stria pontis
tfp1
e.

Fig. 3.3. A 3D representation of the ventral part of the 20 fibre bundles described in the present study that constitute the descending and transverse fibres of the pons as well as the Stria Pontis. *In (a) tractographic analysis showing the v1, v2, and v3 descending bundles as well as the v4 derived from a seed mask placed on the first two most ventral descending fibre bundles (v1, v2, v3 and v4) in the crus cerebri. The bundles shift medially (b) to constitute the cervical pyramidal tract. At the level of the posterior limb of the internal capsule (c) the ventral part of the descending bundles assumes an external position along the long axis of the capsule. At the bottom of the figures, note the part of the ventral fibres that decussates as it advances towards the spinal cord. In (d) the descending and transverse bundles of the pons as well as the Stria Pontis. Note the huge most ventral and dorsal transverse bundles that cross the midline towards the opposite hemisphere. In (e) the transverse bundles originating from the rostral pons form the superior fasciculus in the middle cerebellar peduncle while the caudal pons gives rise to the inferior fasciculus. The tractographic analysis was performed on human specimen 1. On the FAC maps red, blue, and green represent anisotropy along medial-lateral, rostral-caudal, and ventral-dorsal orientations, respectively. Abbreviations: mcp: middle cerebellar peduncle, MB: mammillary body, ml: medial lemniscus, IOPr: inferior olive, principal nucleus, ic: internal capsule, opt: optic tract, R: red nucleus, tfp1: most ventral transverse fibre of the pons, pyx: pyramidal decussation.*

Through the pons they further twist and maintain a ventral position (Fig. 3.2b). By the time the external bundle of the internal capsule reaches the medulla, it twists even more (bundles 1-4 of the pons) and assumes a medial position that will go on to constitute the cervical component of the pyramidal tract (Fig. 3.2c).

For the thoracic component, a second lamella-shaped 3D seed mask was created and placed in the intermediate part of the descending bundles in the crus cerebri (Fig. 3.2b, Fig. 3.4b, and Appendix Fig. 22b). The bundles from the intermediate part (bundles 5-6, thoracic component of the corticospinal tract, including corticopontine and corticobulbar fibres) of the crus cerebri (Fig. 3.2d) assume an intermediate position rostralwards in the internal capsule (along the long axis of the internal capsule, Fig. 3.1d, Fig. 3.4a). As they descend through the diencephalon (Fig. 3.1e) and midbrain (Fig. 3.1f) they maintain an intermediate position twisting at the level of the crus cerebri (Fig. 3.2d, Fig. 3.4b) following the same pattern as the ventral part, to reach the basilar pons (Fig. 3.4c, e). As the intermediate part courses through the basilar pons it maintains an intermediate position (Fig. 3.2e, Fig. 3.4c) and continues to twist, shifting lateral to the cervical fibres, to then continue as the thoracic component of the pyramidal tract (Fig. 3.2f, Fig. 3.4d).

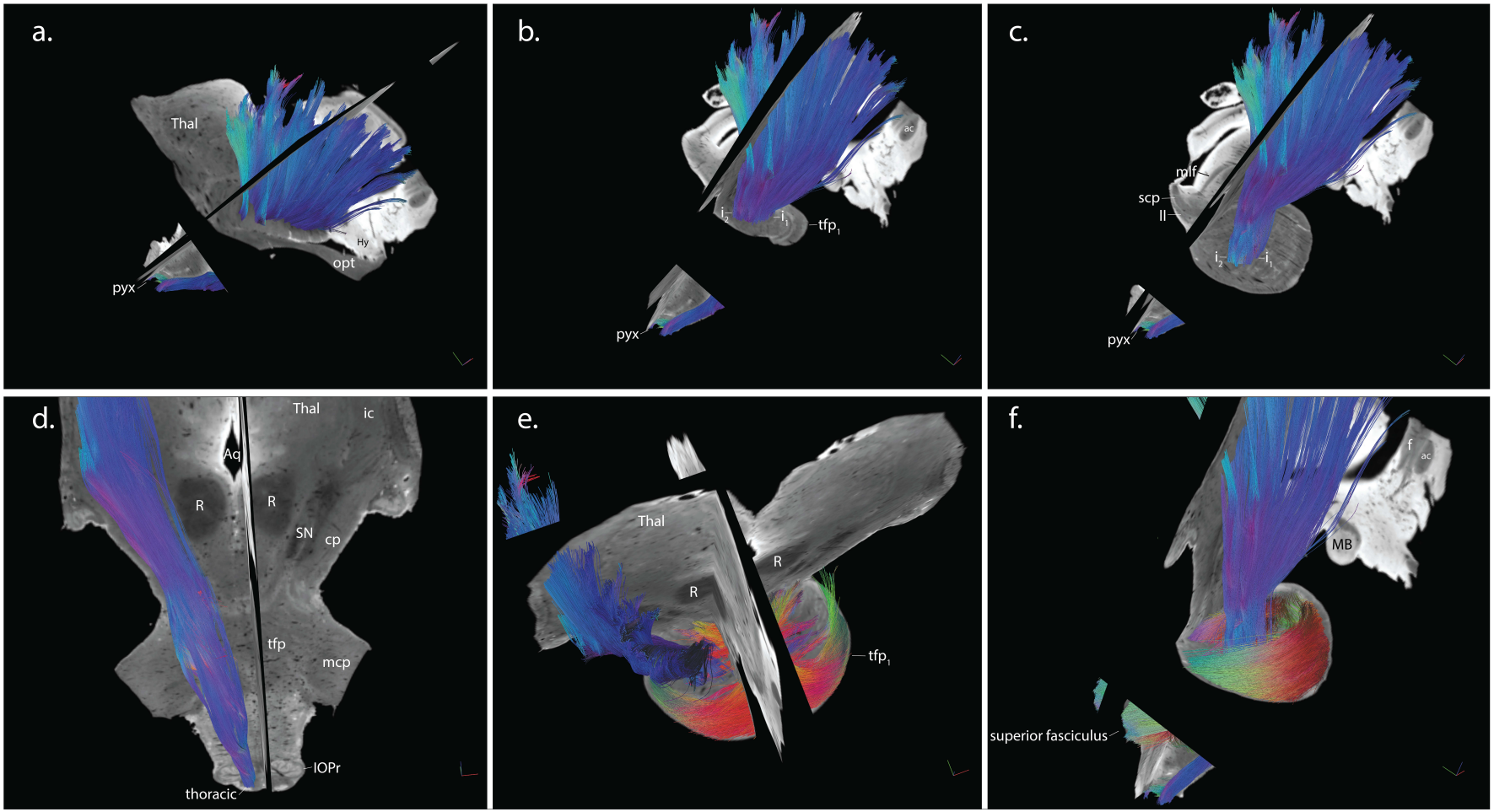
a.
Thal
Hy
opt
pyx
b.
ac
i2
i1
tfp1
pyx
c.
mlf
scp
ll
i2
i1
pyx
d.
Thal
ic
Aq
R
R
SN
cp
tfp
mcp
IOPr
thoracic
e.
Thal
R
R
tfp1
f.
f
ac
MB
superior fasciculus

Fig. 3.4. The intermediate component (thoracic) of the descending fibre bundles. *A seed mask placed on the intermediate group i1 and i2 of the descending fibre bundles in the crus cerebri (curved lamellae) projects at an intermediate position along the long axis in the posterior limb of the internal capsule. On the opposite direction of the crus cerebri, the two bundles that constitute the intermediate group (thoracic) descend through the entire basilar pons with the same pattern and twist to assume an intermediate position in the pyramids (thoracic), lateral to the cervical (d). (e) and (f) show the 3D representation of the transverse fibres of each side of the pons. The tractographic analysis was performed on human specimen 1. On the FAC maps red, blue, and green represent anisotropy along medial-lateral, rostral-caudal, and ventral-dorsal orientations, respectively. Abbreviations: Thal: thalamus, Hy: hypothalamus, opt: optic tract, pyx: pyramidal decussation, tfp1: most ventral transverse fibre of the pons, ac: anterior commissure, mlf: medial longitudinal fasciculus, scp: superior cerebellar peduncle, ll: lateral lemniscus, ic: internal capsule, Aq: aqueduct, R: red nucleus, SN: substantia nigra, cp: cerebral peduncle (crus cerebri), tfp: transverse fibres of the pons, IOPr: inferior olive, principal nucleus, f: fornix, MB: mammillary body.*

For the lumbar and sacral components, a 3D curved lamella-shaped seed mask was created and placed in the dorsolateral part of the crus cerebri (bundles 7, 8, 9, lumbar and sacral component of the corticospinal tract, including corticopontine and corticobulbar fibres); (Fig. 3.2g, Fig. 3.5b, and Appendix Fig. 22c) and showed that the projection assumes an even more internal position, compared to the thoracic component, rostralwards in the ic (Fig. 3.1g). As this part of the subdivisions descend through the diencephalon (Fig. 3.1h, Fig. 3.5a), it slices directly in front of and parallel to the long axis of the substantia nigra pars reticulata with no contact, to descend in the midbrain (Fig. 3.1i), towards the crus cerebri (Fig. 3.2g, Fig. 3.5b) occupying a dorsolateral position. Throughout the pons these subdivisions maintain a dorsal position (Fig. 3.2h, Fig. 3.5c, e) and twist lateral to the thoracic fibres (Fig. 3.2i, Fig. 3.5d) to form the lumbar and sacral components of the pyramidal tract, occupying the most lateral and external parts of the pyramid (Fig. 3.5d).

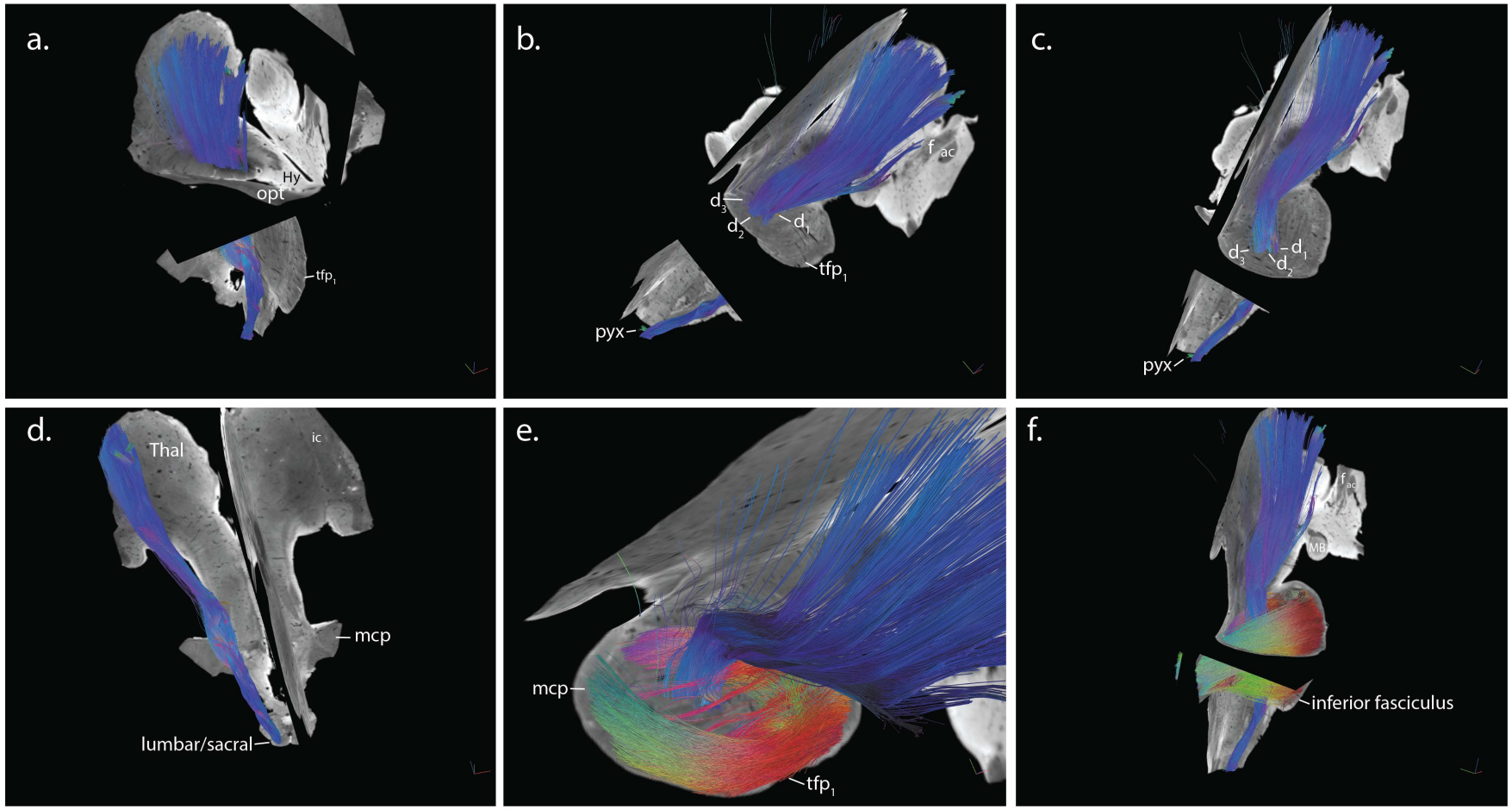
a.
Hy
opt
tfp1
b.
fac
d3
d2
d1
tfp1
pyx
c.
d3
d2
d1
pyx
d.
Thal
ic
mcp
lumbar/sacral
e.
mcp
tfp1
f.
fac
MB
inferior fasciculus

Fig. 3.5. The dorsal group (lumbar and sacral) component of the descending fibre bundles. *A seed mask placed on the dorsal group of the descending fibre bundles (bundles 7-9) allows the identification of the position that the same bundles assume in the internal capsule along its long axis between the intermediate part of the fibres externally and the striatonigral/corticonigral pathway internally (a). In (b) and (c), there can be visualised the same subdivisions in the pons whereas in (d) the dorsal group twists to assume the most lateral part of the pyramid thus, forming the lumbar and sacral pyramidal tracts. In (e) and (f) there can be visualised the transverse fibres of the pons. The tractographic analysis was performed on human specimen 1. On the FAC maps red, blue, and green represent anisotropy along medial-lateral, rostral-caudal, and ventral-dorsal orientations, respectively. Abbreviations: Thal: thalamus, Hy: hypothalamus, opt: optic tract, tfp1: most ventral transverse fibre of the pons, f: fornix, ac: anterior commissure, pyx: pyramidal decussation, mcp: middle cerebellar peduncle, ic: internal capsule, f: fornix, tfp1: most ventral transverse fibre of the pons, MB: mammillary body.*

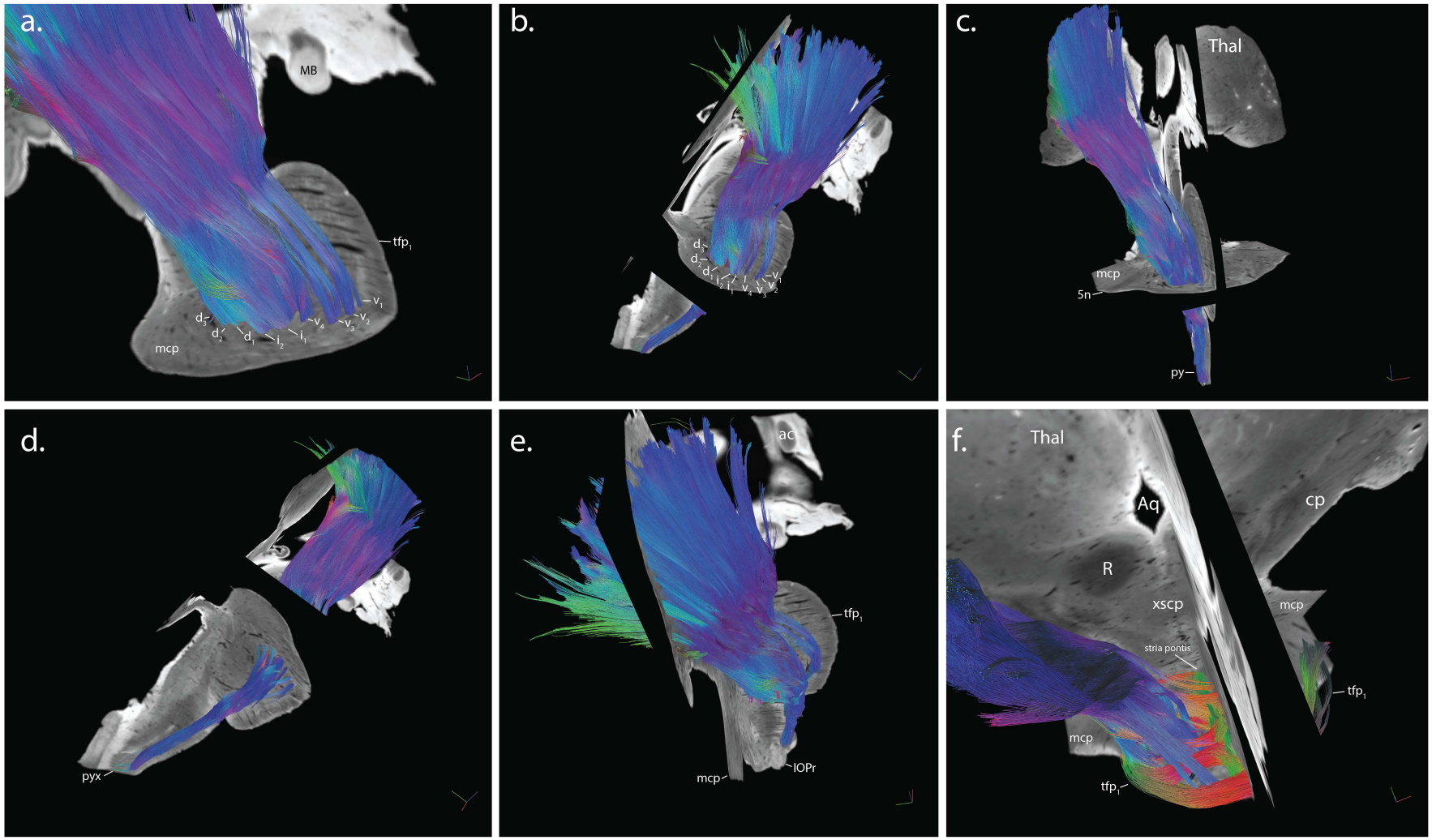
a.
MB
tfp1
d3
d2
d1
i2
i1
v4
v3
v2
v1
mcp
b.
c.
Thal
mcp
5n
py
d.
pyx
e.
ac
tfp1
mcp
lOPr
f.
Thal
Aq
cp
R
xscp
mcp
stria pontis
tfp1
mcp
tfp1

Fig. 3.6. The three groups (ventral, intermediate, dorsal; primary subdivisions) that constitute the nine descending fibres bundles (secondary subdivisions). *The entire pathway of the descending and transverse bundles is identified by tractography. The nine subdivisions of the three major groups of the descending bundles (ventral, intermediate and dorsal) through the basilar pons were traced after a seed mask was placed covering the entire surface of the crus cerebri and an additional ROI mask at the level of the midpons. The fan-like arrangement that the descending fibre bundles assume in the posterior limb of the internal capsule and the subdivisions can be clearly visualised from all perspectives. In (e) the bundles occupy the whole pyramid and in (f) the transverse fibres of the pons after they have formed (via relay in the pontine nuclei) from the lateral parts of the descending bundles cross the midline towards the opposite hemipons to reach the middle cerebellar peduncle. Note the Stria Pontis as the only pathway that courses from the ventral to the dorsal end of the pons (f). The tractographic analysis was performed on human specimen 1. On the FAC maps red, blue, and green represent anisotropy along medial-lateral, rostral-caudal, and ventral-dorsal orientations, respectively. Abbreviations: MB: mammillary body, tfp1: most ventral transverse fibre of the pons, Thal: thalamus, mcp: middle cerebellar peduncle, 5n: fifth cranial nerve, py: pyramidal tract, pyx: pyramidal decussation, ac: anterior commissure, Aq: aqueduct, IOPr: inferior olive, principal nucleus, R: red nucleus, cp: cerebral peduncle (crus cerebri), xscp: decussation of the superior cerebellar peduncle, ac: anterior commissure.*

The complete pathway is highlighted in Fig. 3.6a to f, where the entire crus cerebri was seeded. The organisation of the descending bundles from the internal capsule to the pyramids is such that all the components of the pyramidal tract (cervical, thoracic, lumbar and sacral) complete half a rotation 180º twist, clockwise for the left and anticlockwise for the right pyramidal tract.

Finally, there is one component of the internal capsule that is not featuring pyramidal tract fibres - the most internal bundle (Fig. 3.1j). To identify the possible origin and termination of this bundle, the substantia nigra was seeded (Fig 3.1l), on the assumption that this internal bundle is the striatonigral and corticonigral projections (Figs. 3.1j, k, l and Fig. 3.7a to d). Following nigral seeding, the most internal sliver of the internal capsule which was vacant of corticopontine and pyramidal fibres (Fig. 3.1g), is now occupied by a bundle that descends through the diencephalon (Fig. 3.1k) and slices right externally from the subthalamic nucleus of Luys (Fig. 3.7d) to project into the SNR at the level of the midbrain (Fig. 3.1f). Moreover, the substantia nigra pars compacta (SNCD) remains devoid of fibre bundles (Fig. 3.7d), and there were no visible projections caudal to the SNR.

In addition, I have identified and shown the relationship between the fields H2 and H1 of Forel, the mammillothalamic tract, the zona incerta (ZI), and the subthalamic nucleus of Luys, due to the importance of this region in Parkinson's disease. The subthalamic nucleus and zona incerta are traditional targets for deep brain stimulation (DBS); (Blomstedt et al., 2018, Hamani et al., 2017). The subthalamic nucleus is found approximately 7 mm rostral to the SNR (Fig. 3.1c) which I propose as a target for DBS (see page 188).

The field H2 of Forel descends lateromedially as a projection from the pallidum (lenticular fasciculus) towards the ventral lateral nucleus of the thalamus (Hamani et al., 2017). After having crossed obliquely the internal capsule, the field H2 of Forel arches over the rostral border of the subthalamic nucleus (Appendix Fig. 30a, d) to descend lateromedially and ventrodorsally between the subthalamic nucleus ventrally, and the zona incerta dorsally. The field H2 encircles the zona incerta at its most mediodorsal (Appendix Fig. 30g) and caudal (Appendix Fig. 30h) border to ascend as field H1 of Forel posterolateral to the mammillothalamic tract and projects towards the ventral lateral (VL) nucleus of thalamus.

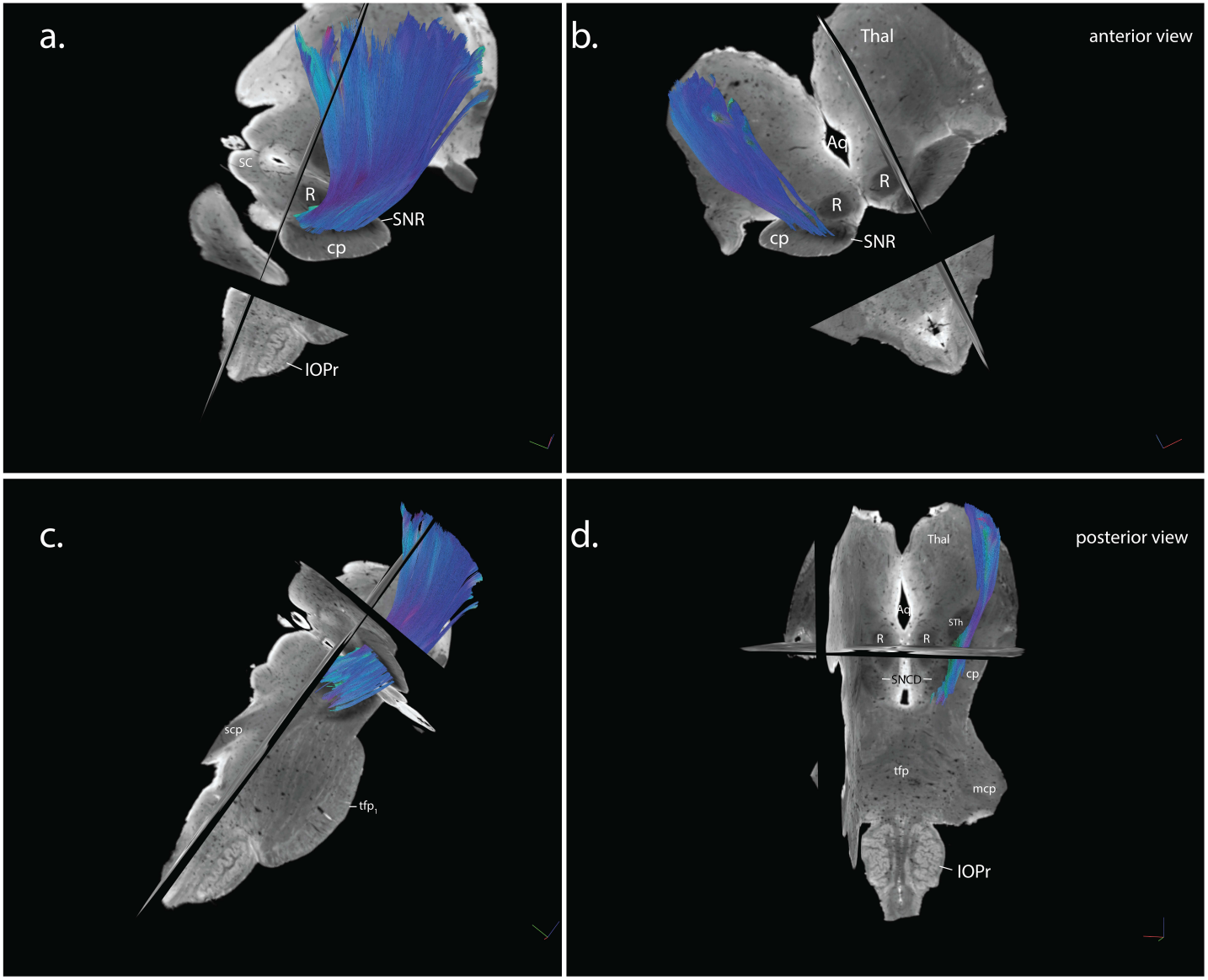
a.
SC
R
SNR
cp
IOPr
b.
Thal
anterior view
Aq
R
R
cp
SNR
c.
scp
tfp1
d.
Thal
posterior view
Aq
STh
R
R
SNCD
cp
tfp
mcp
IOPr

3.7. The projections to the substantia nigra pars reticulata. *From (a) to (d) the characteristic fan-like arrangement of the fibres that assume the most internal part of the internal capsule along its long axis as they descend into the substantia nigra pars reticulata. In (d) posterior perspective of the brainstem where the projections surge right externally from the subthalamic nucleus of Luys to terminate into and until the caudal pole of the pars reticulata. The tractographic analysis was performed on human specimen 1. On the FAC maps red, blue, and green represent anisotropy along medial-lateral, rostral-caudal, and ventral-dorsal orientations, respectively. Abbreviations: SNR: substantia nigra, pars reticulata, SNCD: substantia nigra, pars compacta dorsalis, STh: subthalamic nucleus of Luys, Thal: thalamus, SC: superior colliculus, R: red nucleus, IOPr: inferior olive, principal nucleus, cp: cerebral peduncle, scp: superior cerebellar peduncle, mcp: middle cerebellar peduncle, tfp1: most ventral transverse fibre of the pons.*

3.3.3 Subdivisions of the crus cerebri and of the descending fibre bundles in the basilar pons (longitudinal fibres of the pons); (Pontine Homunculus)

The FAC provided clear contrasts to delineate and subdivide the rostrocaudally-oriented fibre bundles (blue) and the interleaving mediolaterally-oriented transverse fibres of the pons (red); (Figs. 3.8 to 3.10).

The longitudinal fibres of the pons can be subdivided into three main groups traced from the crus cerebri (Fig. 3.8) to the end of the pons. In the four human specimens, the bundles display similar organisation (Fig. 3.9), with the exception that some fibres of a bundle peel off (interdigitations) to join an adjacent bundle (Fig. 3.10b, arrows). These bundles can be divided into ventral (1-4), intermediate (5-6), and dorsal (7-9) groups. This nomenclature is also in alignment with the schematic segmentation of the pontine nuclei proposed by Nyby and Jansen (1951) and Schmahmann and Pandya (1989). These subdivisions can also be seen in tractography in Figs. 3.3 to 3.6.

Moreover, the most ventral bundles in the basilar pons have not been identified or traced before. The four bundles that constitute the ventral group are traced on one side of four brainstems (Fig. 3.8 to 3.10). This ventral group was present in each of the four specimens. Indeed the nine bundles (4 ventral, 2 intermediate, and 3 dorsal) are always present, although there is a degree of instability. For example, in specimens (c) and (e) the v1, v2, v3 bundles of the ventral group arise from two consecutive descending bundles in the crus cerebri instead of one bundle as seen in (b) and (d). In addition, the number of the bundles may vary between the two sides of the brainstem, their precise anatomical location relative to

the midline and the thickness of respective bundles between the specimens can be different (Fig. 3.9).

Fig. 3.8 shows the components of the crus cerebri as they become the longitudinal fibres of the pons (Fig. 3.9). At the level of the junction between rhombomere one and two, the cervical component is condensed to form two ventrolateral lamellae (Figs. 3.8, 3.10). Caudalwards, the two ventrolateral lamellae reach the midpons as two separable anatomical entities. At this level the most ventral lamella further divides into three fibre bundles (Fig. 3.9b to e; bundles: v1, v2, v3) maintaining a separate trajectory until they merge again and twist medially to form the cervical component of the pyramid tract (Figs. 3.10, 3.11 and Fig. 3.13c to e).

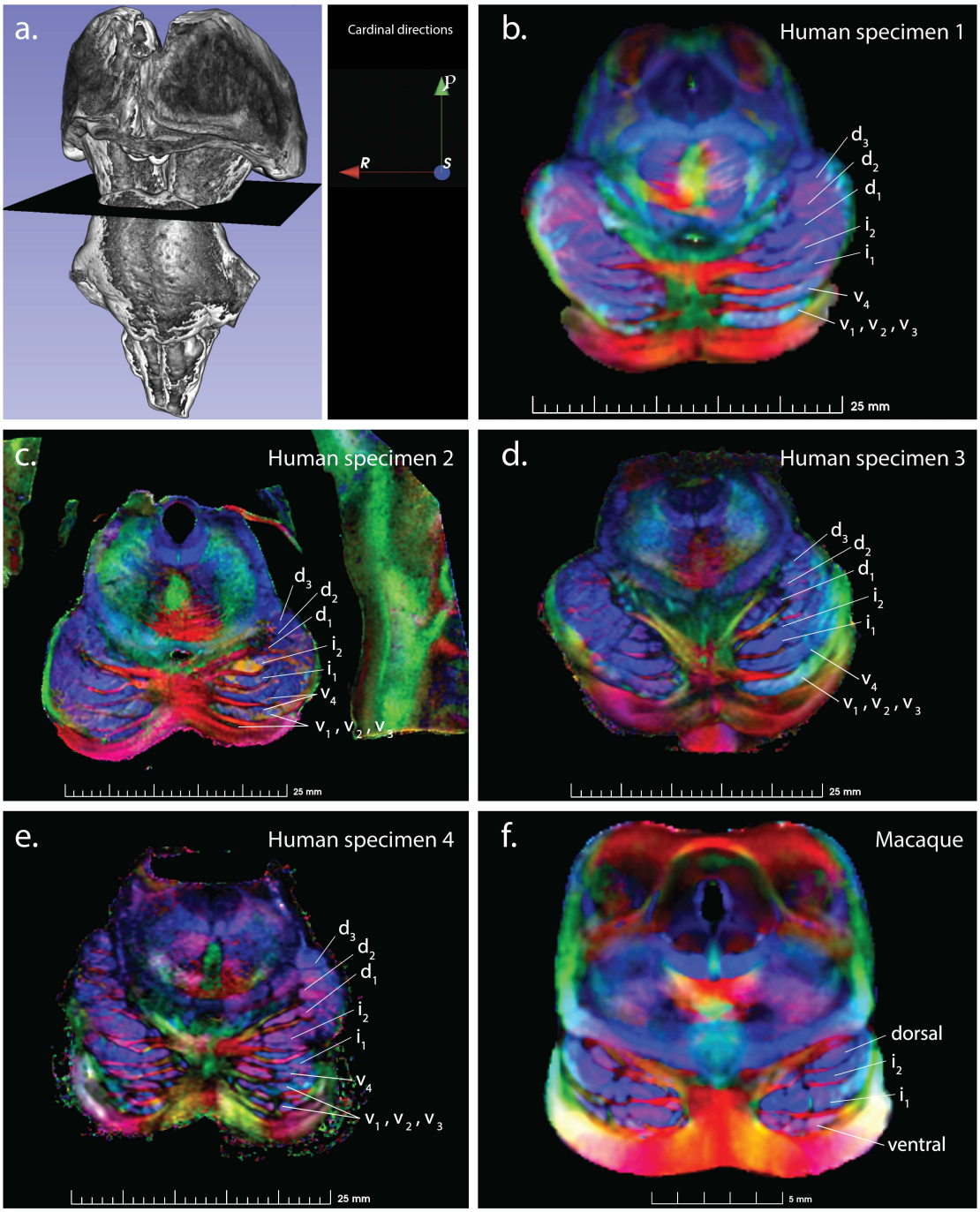
a.
Cardinal directions
P
R
S
b.
Human specimen 1
d3
d2
d1
i2
i1
v4
v1 , v2 , v3
25 mm
c.
Human specimen 2
d3
d2
d1
i2
i1
v4
v1 , v2 , v3
25 mm
d.
Human specimen 3
d3
d2
d1
i2
i1
v4
v1 , v2 , v3
25 mm
e.
Human specimen 4
d3
d2
d1
i2
i1
v4
v1 , v2 , v3
25 mm
f.
Macaque
dorsal
i2
i1
ventral
5 mm

Fig. 3.8. Cross sections at the level of the pons-midbrain junction as shown by DTI scalars-directionally coloured fractional anisotropy (FAC) of the four ex vivo human brainstems and one macacque. *The FAC shows the subdivisions of the descending bundles as well as the subdivisions of the first most ventral five transverse fibres of the pons as they form from the pontine nuclei interspersed between the descending fibre bundles. This study revealed that the descending bundles fan out in the rostral pons (rhombomere one and two) forming curved lamellae which alternate in sequence with the transverse fibres of the pons. Transverse sections, at the level shown in (a) from the fractional anisotropy colour (FAC) derived from the DTI are shown. On the FAC maps red, blue, and green represent anisotropy along medial-lateral, rostral-caudal, and ventral-dorsal orientations, respectively. The crus cerebri has been subdivided into three groups of fibre bundles (curved lamellae). The ventral group is composed by two ventral curved lamellae v1, v2, v3 (which are merged at this level and constitute the most ventral lamella), and v4 (cervical component of the pyramidal tract). The intermediate group i1 and i2 (thoracic component of the pyramidal tract) follows as we proceed from the ventral to the dorsal end of the transverse plane. Finally, the dorsal group is composed by the d1, d2 and d3 (lumbar and sacral components of the pyramidal tract) curved lamellae. The leader lines point at the exact location where the subdivisions in the crus cerebri, midpons, medulla oblongata correspond, in both transverse and sagittal planes. Note the ventral transverse fibres as they alternate with the descending fibres as well as the formation of the Stria Pontis, ventrally, to constitute a pathway towards the tegmentum. In samples (b) and (d) the bundles present exactly the same patterning whereas in samples (c) and (e) the fibre bundles that will constitute the v1, v2, and v3 in the pons arise from two consecutive descending bundles in the crus cerebri and this presents the only idiosyncratic difference among the four samples. In (f, Macaca mulatta) there have been identified four descending fibre bundles and five transverse fibres of the pons. The ventral lamella (cervical), i1 and i2 (thoracic component of the pyramidal tract) and finally the dorsal lamella constitutes the lumbar and sacral components of the pyramidal tract.*

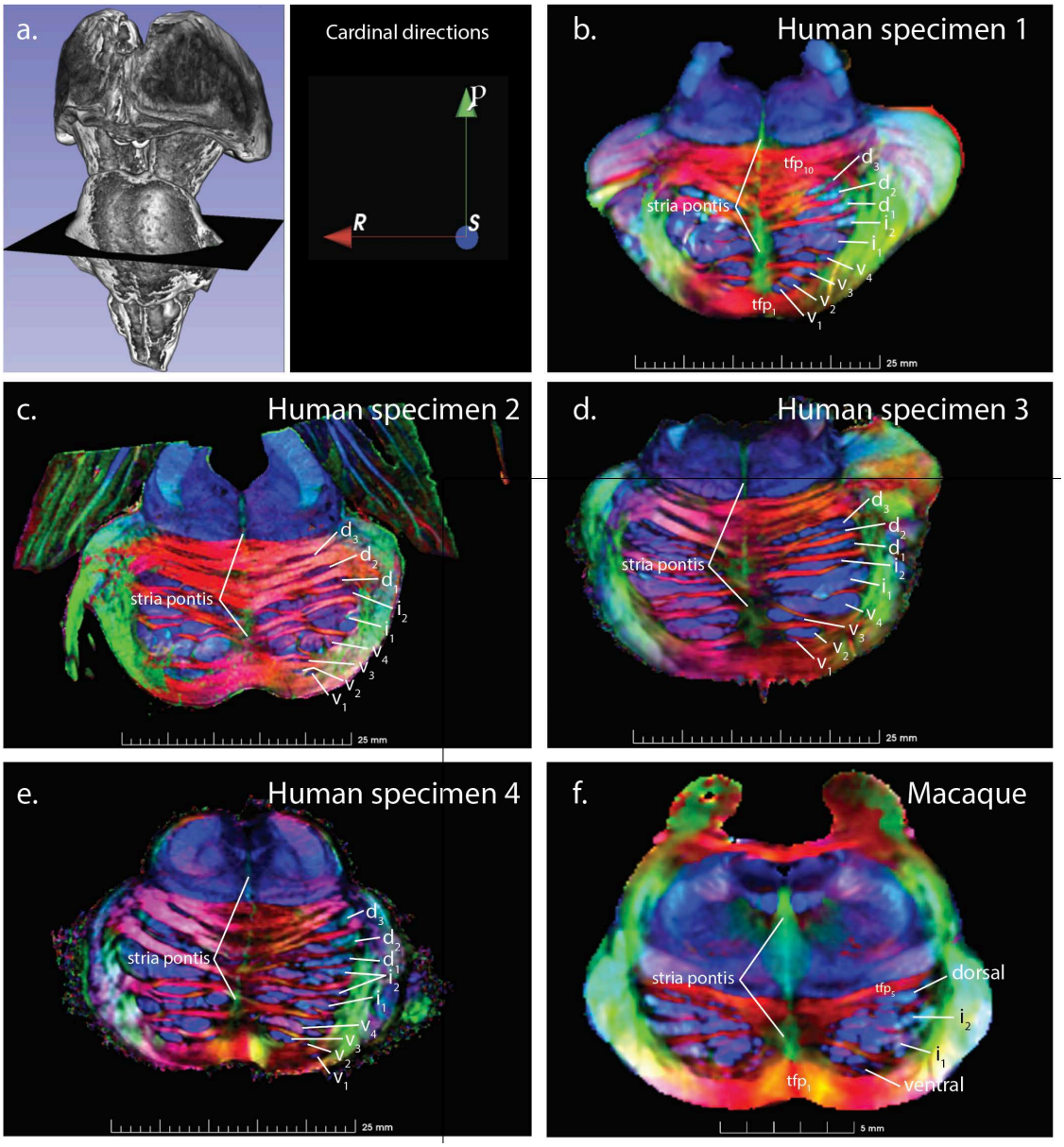
a.
Cardinal directions
P
R
S
b.
Human specimen 1
stria pontis
tfp10
tfp1
d3
d2
d1
i2
i1
v4
v3
v2
v1
25 mm
c.
Human specimen 2
stria pontis
25 mm
d.
Human specimen 3
stria pontis
25 mm
e.
Human specimen 4
stria pontis
25 mm
f.
Macaque
stria pontis
tfp2
tfp1
dorsal
ventral
5 mm

Fig. 3.9. Cross-section at the level of the midpons (a) at its maximal width showing the nine descending (in blue) cortico-pontine, -bulbar, and -spinal fibre bundles (b), and ten transverse fibres of the pons (in red) for the human, four descending and five transverse for the macaque. *Note that the v1, v2, v3 present similar patterning in all the human samples with three ventral minute fibres followed by a thicker bundle v4 (hand representation), which descend throughout the length of the basilar pons to constitute the cervical pyramidal tract. The intermediate group by two thick bundles (thoracic) followed by a thinner group of dorsal bundles (lumbar and sacral). The transverse fibres of the pons are functionally connected to the descending bundles, so that the ventral group of the descending bundles will terminate into the pontine nuclei which will then give rise to the ventral transverse fibres of the pons (in red), the intermediate group of the descending bundles is connected to the intermediate transverse bundles and finally the dorsal descending bundles are functionally connected to the dorsal transverse bundles of the pons. Subpanel (f) presents the subdivisions of the descending (four) and transverse (five) fibre bundles in the macaque brainstem where the architecture is less complex, however the anatomy of the basilar pons presents similarities in architecture between primates and a well-defined morphological pattern, ventral, intermediate and dorsal groups of bundles are homologous between the two species. On the FAC maps red, blue, and green represent anisotropy along medial-lateral, rostral-caudal, and ventral-dorsal orientations, respectively.*

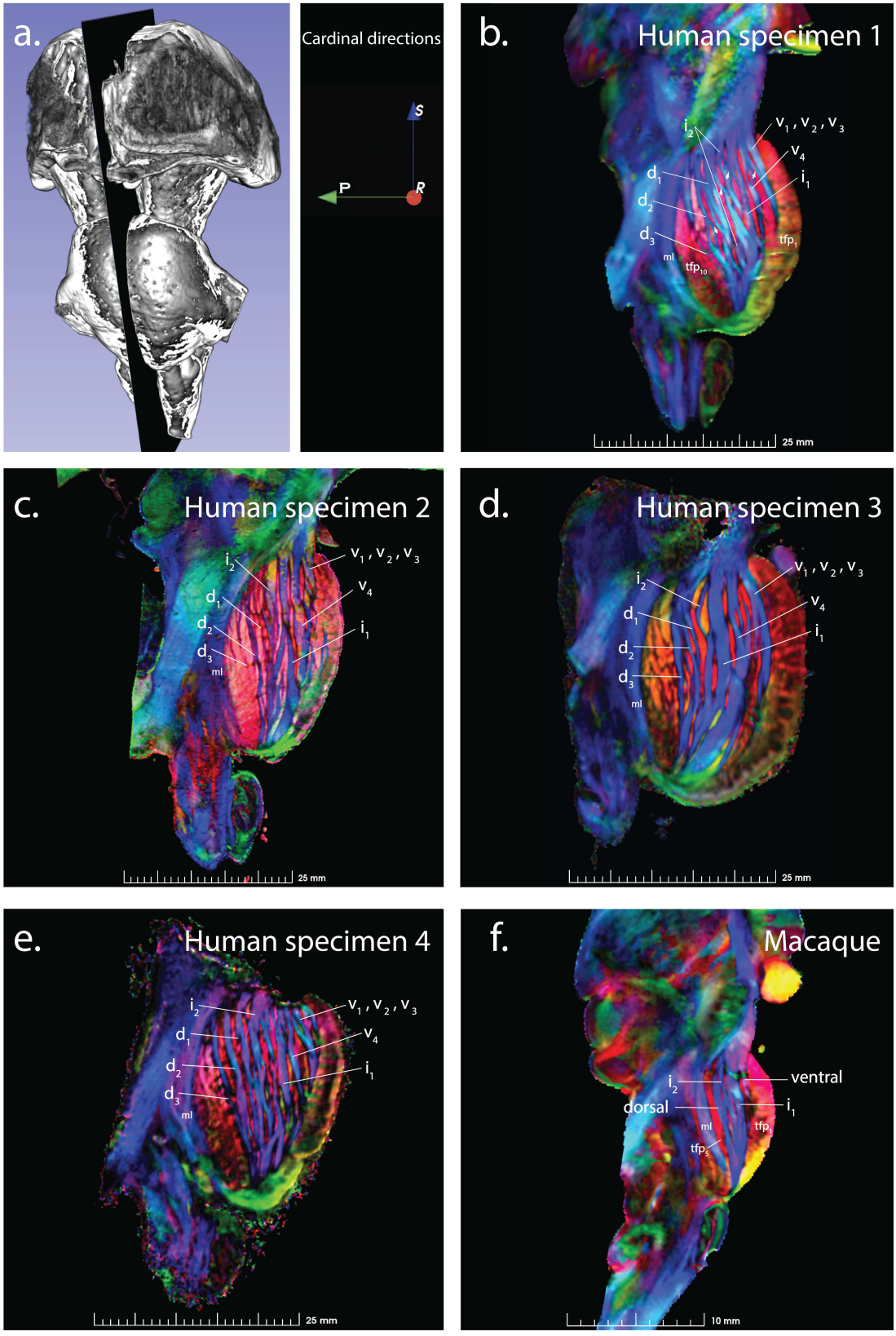
a.
Cardinal directions
S
P
R
b.
Human specimen 1
i2
v1 , v2 , v3
v4
i1
d1
d2
d3
ml
tfp10
tfp1
25 mm
c.
Human specimen 2
i2
v1 , v2 , v3
v4
i1
d1
d2
d3
ml
25 mm
d.
Human specimen 3
i2
v1 , v2 , v3
v4
i1
d1
d2
d3
ml
25 mm
e.
Human specimen 4
i2
v1 , v2 , v3
v4
i1
d1
d2
d3
ml
25 mm
f.
Macaque
ventral
dorsal
i2
i1
ml
tfp1
tfp3
10 mm

Fig. 3.10. Sagittal sections show the nine descending bundles (in blue) that alternate with the ten transverse fibres of the pons (in red) for the human specimens and the four descending that alternate with the five transverse bundles for the macaque. *The subdivisions of the descending bundles in the four samples are presented from (b) to (e). Note that there are always interdigitations (arrows) between the descending bundles, for example, in (b) between the v1, v2, v3 and v4, as well as between the d1 and d2. These interdigitations are present in all samples, however less complex in the macaque (f). On the FAC maps red, blue, and green represent anisotropy along medial-lateral, rostral-caudal, and ventral-dorsal orientations, respectively.*

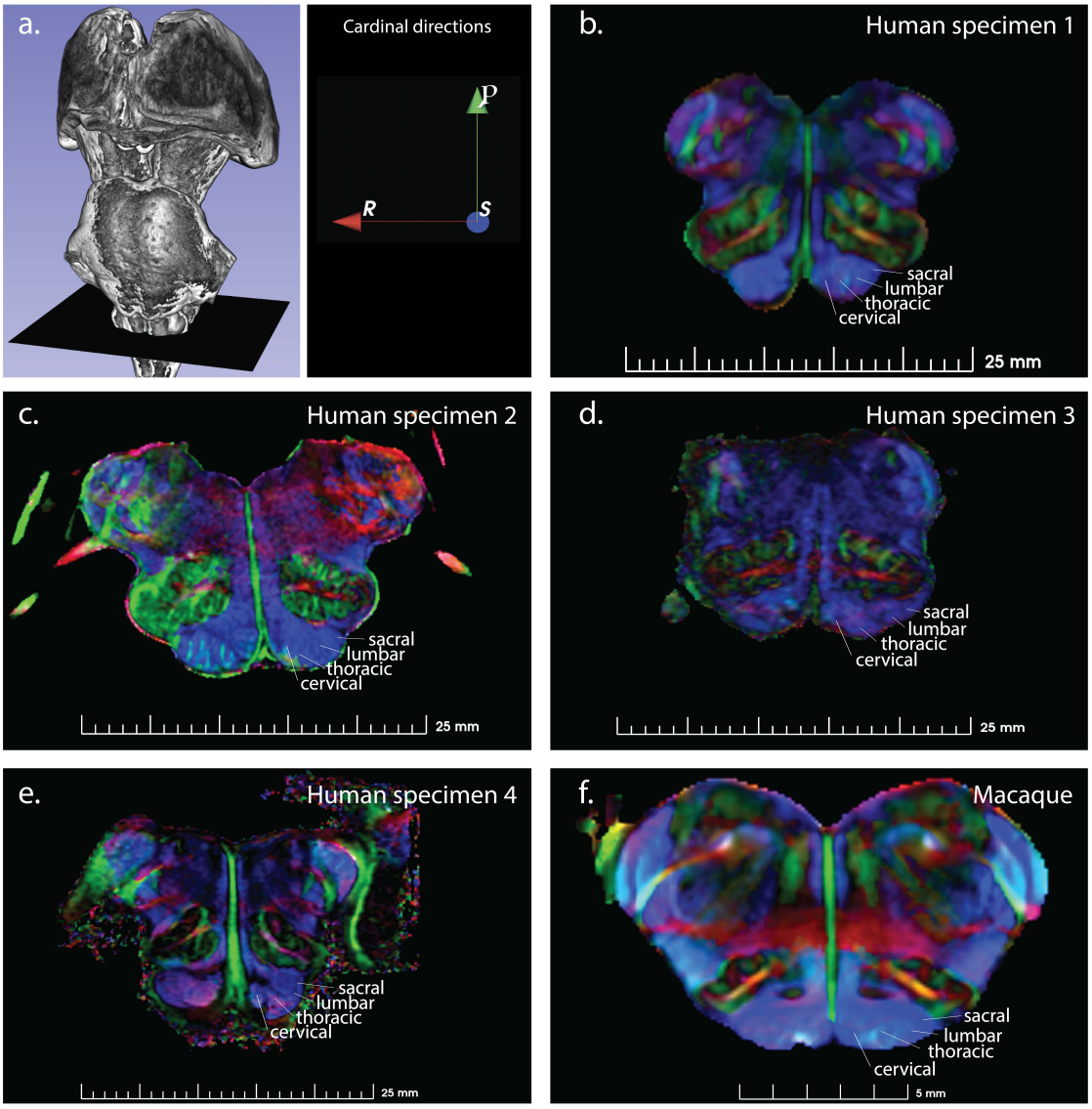
a.
Cardinal directions
P
R
S
b.
Human specimen 1
sacral
lumbar
thoracic
cervical
25 mm
c.
Human specimen 2
sacral
lumbar
thoracic
cervical
25 mm
d.
Human specimen 3
sacral
lumbar
thoracic
cervical
25 mm
e.
Human specimen 4
sacral
lumbar
thoracic
cervical
25 mm
f.
Macaque
sacral
lumbar
thoracic
cervical
5 mm

Fig. 3.11. Cross-sections at the level of the pyramids. *The descending fibre bundles have been traced after the maximal width of the pons and started to converge and shift to assume a mediolateral direction forming the cervical (v1, v2, v3, v4), thoracic (i1 and i2) and lumbar/sacral (d1, d2, and d3) portions of the pyramidal tract as confirmed by tractography in Figs. 3.1 to 3.5. Approximately, a 20% of the volume of the descending bundles that form the crus cerebri will continue onto the pyramids, the rest 80% will terminate into the basilar pons. In the macaque (f) the ventral lamella in the crus cerebri will eventually occupy the medial part of the pyramid where the leader line points as cervical component of the pyramidal tract and so on. On the FAC maps red, blue, and green represent anisotropy along medial-lateral, rostral-caudal, and ventral-dorsal orientations, respectively.*

3.3.4 Subdivisions of the transverse fibres of the pons

Similarly to the descending bundles, the transverse fibres can also be aggregated into three broad groups, ventral, intermediate, and dorsal, in correspondence with the aggregation of the descending bundles (Figs. 3.3 to 3.6, Figs. 3.10 to 3.12).

Note how the descending and transverse fibres of the pons follow a pattern where they alternate with each other; for example in a transverse plane through the basilar pons, starting ventrally, there is one transverse fibre bundle, followed by one descending bundle, then followed by another transverse fibre bundle, then another descending bundle, and so on. This is seen across Figs. 3.8 to 3.10, and perhaps most clearly in the sagittal sections shown for the specimens in Fig. 3.10. Finally, note how the first and tenth transverse fibres of the pons found on the extremities are always stable between the two sides of the brainstem and between the specimens (Figs. 3.9 & 3.10), thereby are named herein as ventral arcuate (tfp_1) and dorsal arcuate (tfp_{10}), due to the shape they assume in transverse and sagittal sections (see Appendix Fig. 28).

The inspection of the vectors and tractography indicates that the transverse fibres of the pons arise from pontine grey matter that receives axons from the ventral, intermediate and dorsal parts of the descending bundles (Fig. 3.12, Fig. 3.14).

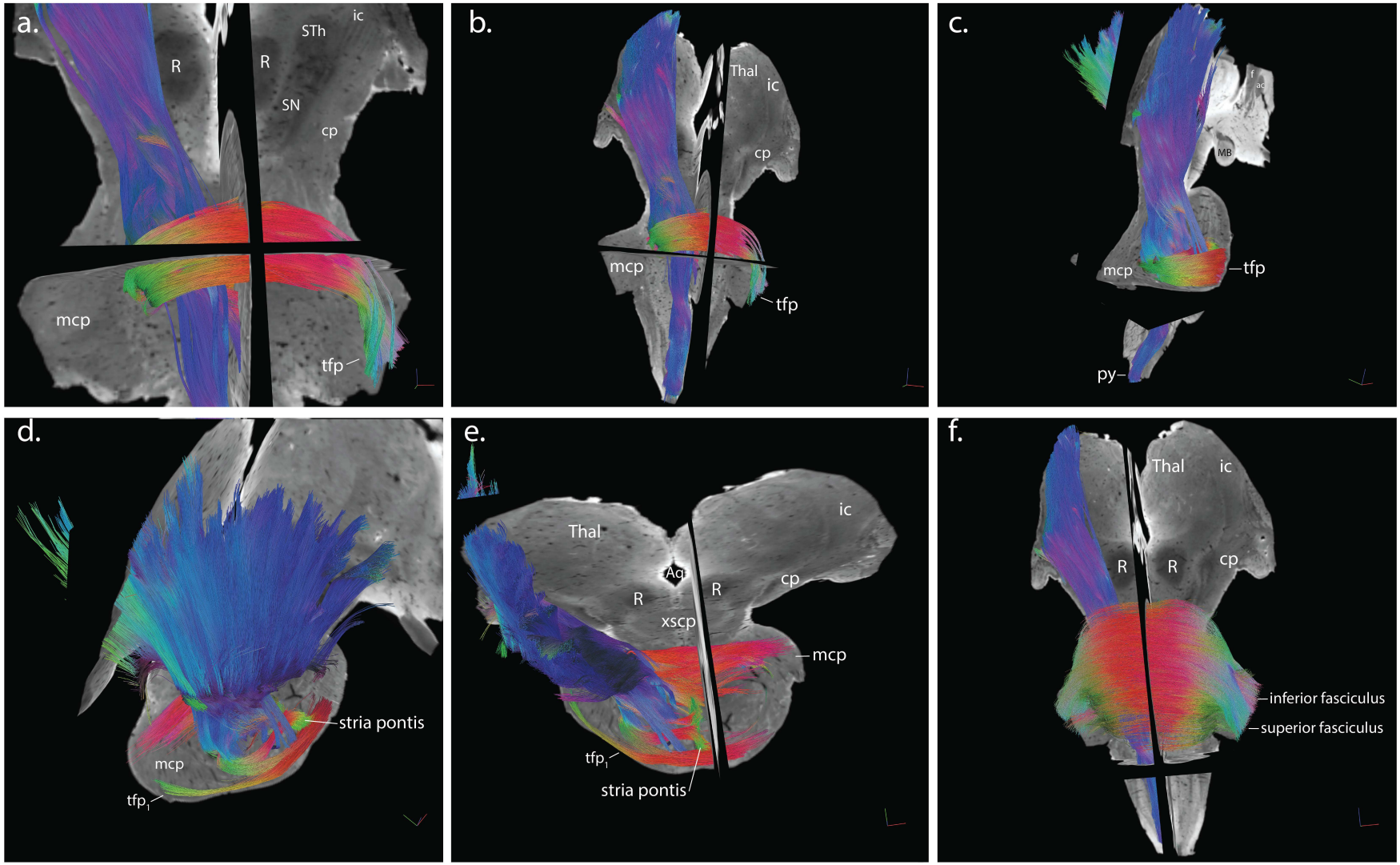
a.
ic
STh
R
R
SN
cp
mcp
tfp
b.
Thal
ic
cp
mcp
tfp
c.
f
ac
MB
mcp
tfp
py
d.
stria pontis
mcp
tfp1
e.
Thal
ic
Aq
R
R
cp
xscp
mcp
tfp1
stria pontis
f.
Thal
ic
R
R
cp
inferior fasciculus
superior fasciculus

Fig. 3.12. A more extensive view of the patterning of the transverse fibres of the pons. *These fibre bundles arise from the pontine nuclei that receive the lateral and external parts of the descending bundles. The transverse fibres of the pons are characterised by the most ventral and dorsal transverse bundles (transverse fibres of the pons 1 and 10) that start to form in the rostral pons and are always stable between the human samples and in the monkey (transverse fibre bundle 1 & 5). In between, there can be identified eight more transverse bundles, in the human, which present variability between the samples and between the right and left side of the pons. The transverse bundles cross the midline and congregate towards the mcp to form part of the superior fasciculus that conveys information from the rostral pons. In (d) and (e) are visible fibres that cross from the opposite hemipons as well, forming part of the most ventral transverse bundle. In (f) the subdivisions of the mcp in superior and inferior fasciculus (left) where the deep transverse fibres form the underneath deep fasciculus as seen on the right mcp. The tractographic analysis was performed on human specimen 1. On the FAC maps red, blue, and green represent anisotropy along medial-lateral, rostral-caudal, and ventral-dorsal orientations, respectively. Abbreviations: R: red nucleus, STh: subthalamic nucleus of Luys, SN: substantia nigra, ic: internal capsule, cp: cerebral peduncle, mcp: middle cerebellar peduncle, tfp: transverse fibres of the pons, py: pyramidal tract, Aq: aqueduct, xscp: decussation of the superior cerebellar peduncle.*

As a validation of the tractography architecture of the herein delineated pathways, four structural GRE images were overlapped with four FAC (Figs. 3.8 to 3.10, and Appendix Fig. 23). The descending bundles can be observed and followed in GRE and FAC images, and traced via tractography, from the internal capsule to the crus cerebri and on to the pyramids. Similarly, the transverse fibres of the pons are visualised in GRE, FAC and tractography (Figs. 3.6f, 3.9, 3.10).

3.3.5 Subdivisions of the descending fibre bundles/subdivisions of the transverse fibres of the pons in the macaque

Figures 3.8 to 3.10 compare the descending fibre bundles between the four human specimens and the single macaque brainstem. In this macaque specimen, only four discrete descending fibre bundles are identified at the crus cerebri (Fig. 3.8f) and throughout the basilar pons (Fig. 3.9f). These however, can be similarly subdivided into ventral, intermediate (i_1, i_2) and dorsal groups. Note also how the fibre bundles in the macaque are less complex than those in the human specimens, with only minor interdigitations seen in the sagittal sections (Fig. 3.10f). The fibre architecture is less complex in this species, forming curved lamellae at the level of the pons-midbrain junction (Fig. 3.8f) that then fan out and subsequently the transverse fibres of the pons arise from pontine nuclei interspersed between the descending bundles. As in the human, the transverse bundles from one side of the macaque pons, cross the midline and curve to pass between the descending fibre bundles of the opposite hemipons (Fig. 3.9f). The five transverse fibres of the pons identified in this macaque

specimen, therefore also less complex than in the human. Similarly, however, the macaque transverse fibres alternate in sequence with the descending fibre bundles.

3.3.6 Subdivisions of the pyramidal tract

Figure 3.11 shows the pyramidal tract in a transverse plane at the level of the medulla oblongata. The characteristic organisation of the descending bundles shift from a dorsoventral to a mediolateral disposition. Specifically, within the medullary pyramids, the ventral group (bundles 1, 2, 3 & 4) forms the cervical pyramidal tract, and the intermediate (bundles 5 & 6) and dorsal groups (bundles 7, 8 & 9) form the thoracic and lumbar-sacral subdivisions of the pyramidal tract, respectively (see also tractography in Figs 3.3 to 3.5).

3.3.7 The corticopontine tract

As Fig. 3.13 demonstrates, there is no evidence for a distinct corticopontine tract that terminates in the ventral pons as accepted ideas used to indicate (see 3.4.1 & 3.4.2 discussion). At the point where the transverse and sagittal display sections intersect (Fig. 3.13a), the most ventral descending bundle (bundle no 1) is seen. This fibre bundle and the rest of the ventral group, (bundles $v_{1\text{-}3}$) fan out in the rostral pons (rhombomere two), while they descend, to constitute the first three ventral fibre bundles of the basilar pons (Figs. 3.3, 3.6, 3.8 to 3.10, 3.12 and Fig. 3.13a to e). As also clearly seen in Fig. 3.10 (sagittal view, fibre bundles $v_{1\text{-}3}$) and Fig. 3.13 the ventral bundles descend through the whole length of the pons. In Fig. 3.13a, and 13b,

the cursor is placed more medially towards the midline and the two thirds of the caudal part of the most ventral bundle (v_1) begin to appear, revealing the entire pathway from the crus cerebri to the medullary pyramids. In fig. 3.13c & 13d, the pathway is more visible where the most ventral bundle shifts from a ventral (more rostral levels) to a more medial and dorsal position (more caudal levels) to form with the rest of the bundles of the ventral group, the cervical part of the medullary pyramids, which will eventually reach the ventral horn of the cervical spinal cord (innervation of the muscles of the hand (Kwon et al., 2011b)).

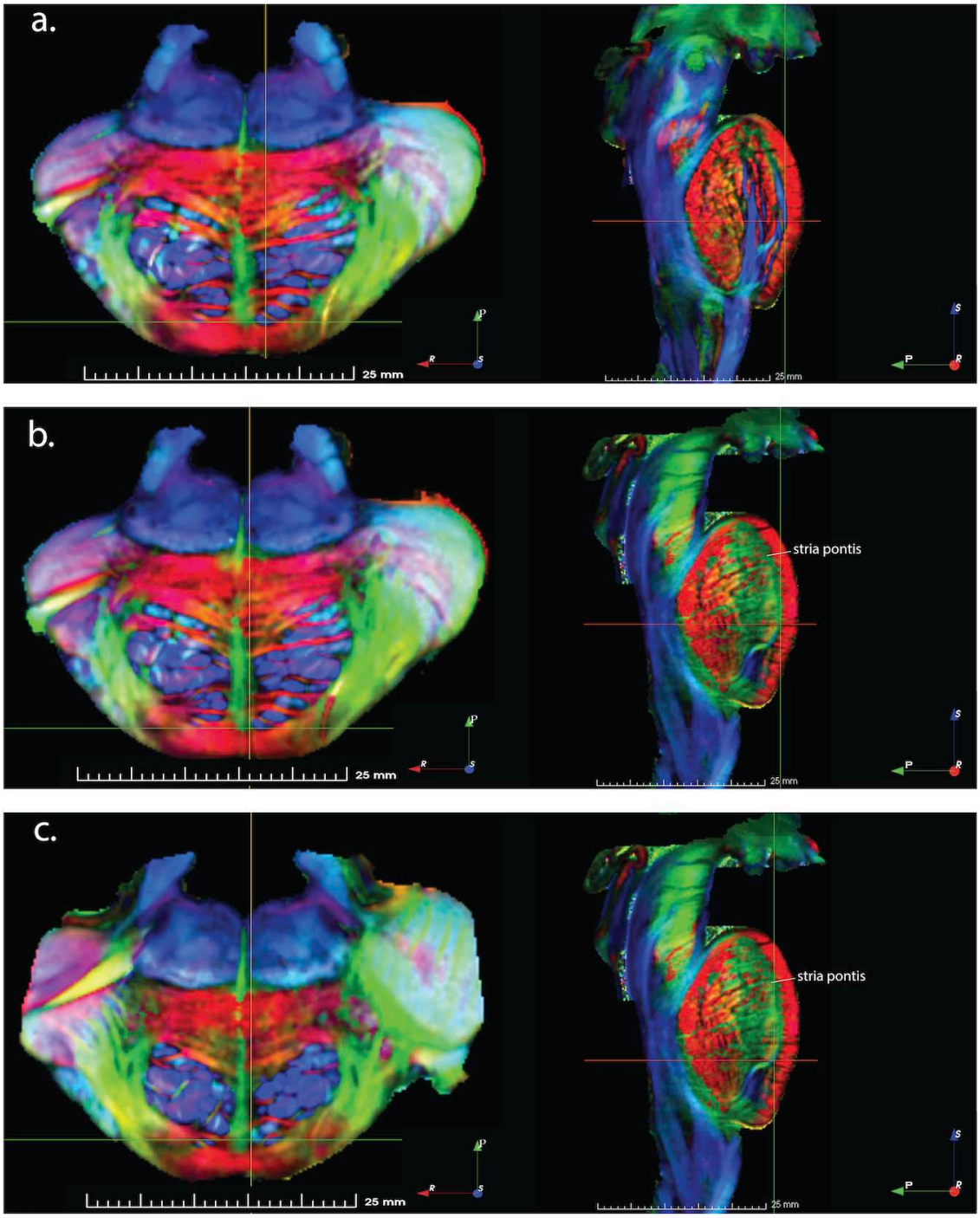
a.
25 mm
25 mm
b.
stria pontis
25 mm
25 mm
c.
stria pontis
25 mm
25 mm

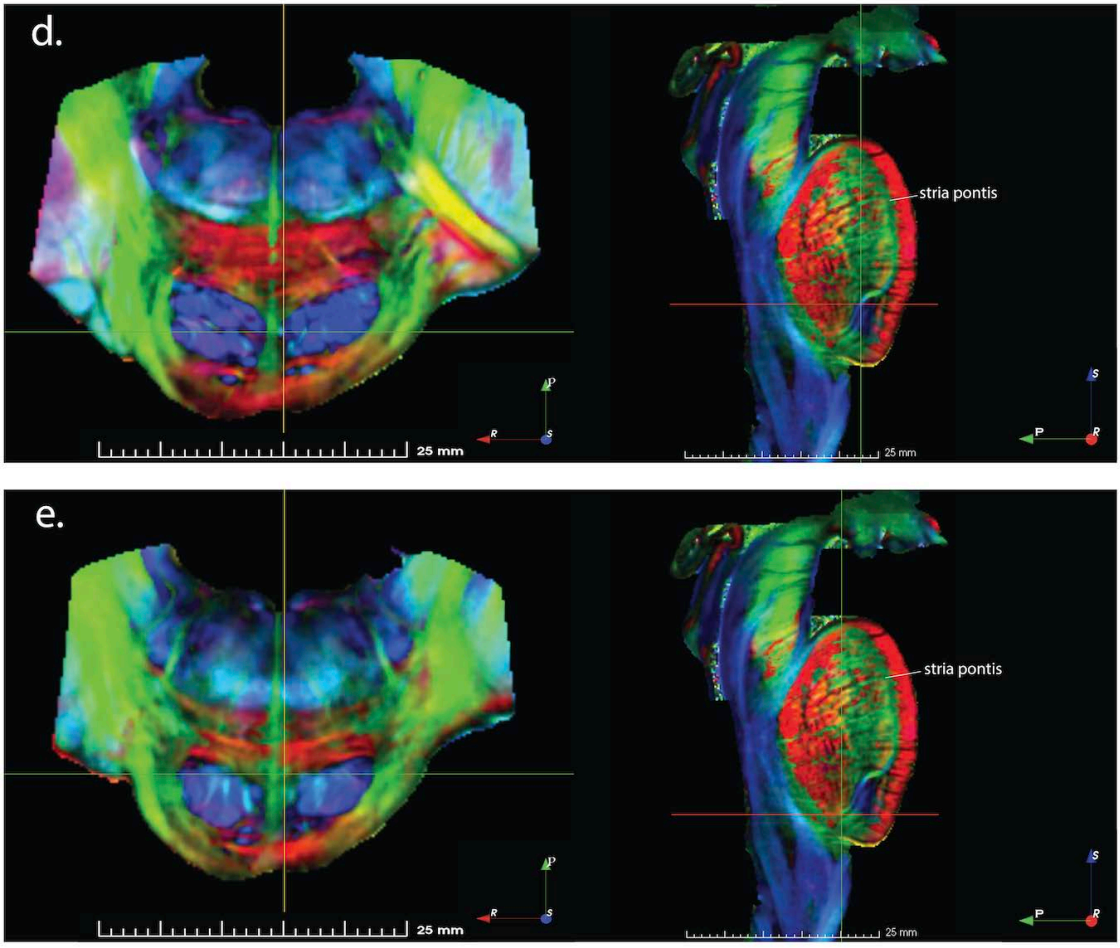

Fig. 3.13. The most ventral descending fibre bundle identified until the pontomedullary junction. *Transverse and the corresponding sagittal sections from (a) to (e) showing that the v1 bundle descends from the crus cerebri ventrally throughout the entire length of the basilar pons and characteristically shifts dorsally while it descends onto the pyramids, where the intersections are visualised from (a) to (e), to form the cervical component of the pyramidal tract. Note in (b), (c), (d), (e)(sagittal view) the extension of the Stria Pontis (in green) throughout the length of the pons. As a result, the accepted concept of a distinct corticopontine tract that courses ventrally and terminates within the pons seems to be incorrect. Note the extent of the Stria Pontis (rhombomere two to four; in green) in sagittal view. On the FAC maps red, blue, and green represent anisotropy along medial-lateral, rostral-caudal, and ventral-dorsal orientations, respectively.*

Finally, in Fig. 3.13e, the remaining fibres which formed the most ventral bundle (v_1) in the basilar pons are found medially in the pontomedullary junction to further descend as the part of the cervical component of the pyramidal tract (see intersections). All the above is evidence that the corticopontine tract does not course solely through the ventral basilar pons, rather as demonstrated, herein, all nine subdivisions (ventral, intermediate and dorsal groups) of the longitudinal fibres of the pons project into the pyramid and thusly, none of these bundles exclusively terminate in the pons. The tensor glyphs obtained at this microscopic resolution (200 μm for the diffusion imaging) demonstrate that all the nine subdivisions collectively shed fibres in the pons with a specific topographic arrangement (see below).

3.3.8 The principle of topology

Based on the tractographic analysis and tensor glyphs (Fig. 3.12 and Fig. 3.14) there is a topographic distribution within each bundle which constitutes the longitudinal fibres of the pons. The crus cerebri has now been subdivided into three groups of curved lamellae that disaggregate to give rise to nine distinct descending fibre bundles. These bundles become less compact and spread out as pontine cell bodies intersperse between them and maintain their curved lamellae shape while they descend until they reach the midpons and their maximum spatial spread.

It has been identified herein by analysing the course and the orientation of the tensors (first eigenvector) within each voxel (Fig. 3.14 a to c) that the fibres of the

lateral and external parts of each bundle separate from their main body, and curve to terminate into the pontine nuclei.

These fibres constitute the corticopontine tract that synapse into the pontine nuclei. The projections from the pontine nuclei, in turn give rise to the transverse fibres of the pons. From the inspection of the tensors (a technique which gives no information about synapses and highlights only the pathway) I identified streamlines emanating from all ten transverse fibres to form the *Stria Pontis* (see below). Therefore, all three primary subdivisions of the crus cerebri and basilar pons (ventral, intermediate and dorsal groups), and by extension all the nine descending bundles (secondary subdivisions), contain cortico-bulbar, -pontine and -spinal projections with a precise topographical distribution (Fig. 3.14). Thus, the fibres found in lateral and external parts of the descending bundles $v_{1\text{-}4}$ bend, break off, synapse onto pontine grey matter and from there the transverse fibres of the pons (transverse bundles 1-5; Fig. 3.14) form. Similarly, the intermediate group of the descending bundles $i_{5\text{-}6}$ contribute to transverse bundles 5-7, and the dorsal descending bundles $d_{7\text{-}9}$ contribute to transverse bundles 7-10 (Fig. 3.10 and 3.14 b & c). Each of the descending bundles projects into pontine nuclei which in turn give rise to two adjacent transverse bundles. For example, fibres of the v_1 synapse onto pontine nuclei which form the tfp1 & 2. In this way the same information from the cortex is conveyed to two adjacent transverse fibres. As a result, from one descending bundle which terminates on pontine nuclei, two transverse fibres of the pons arise and so on.

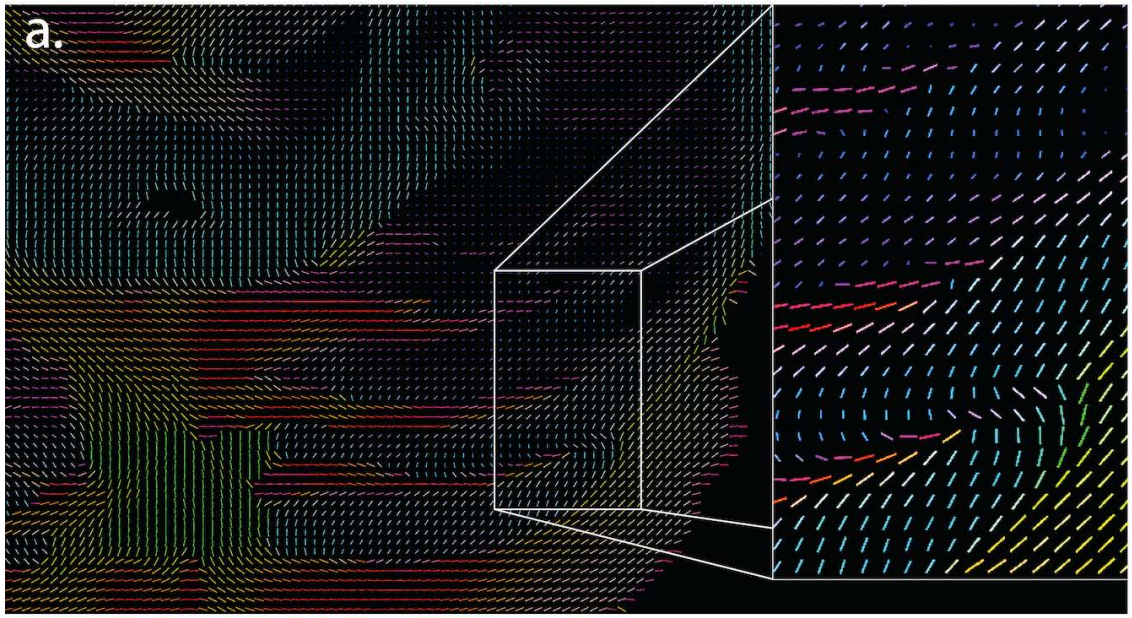
a.

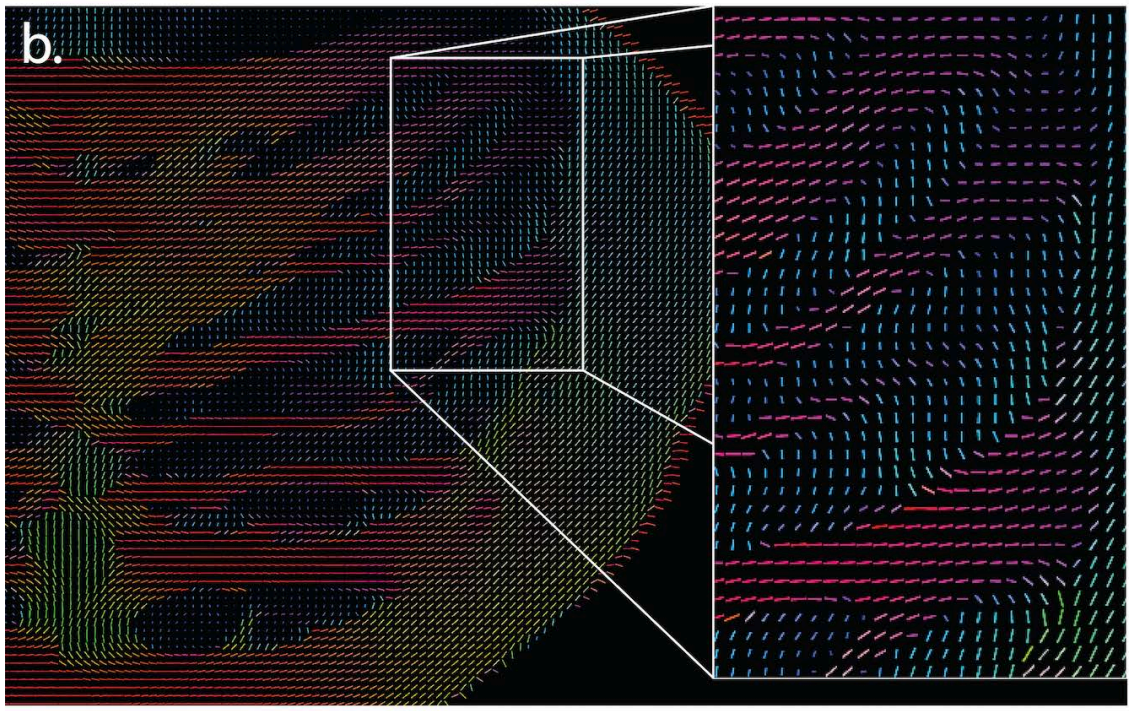
b.

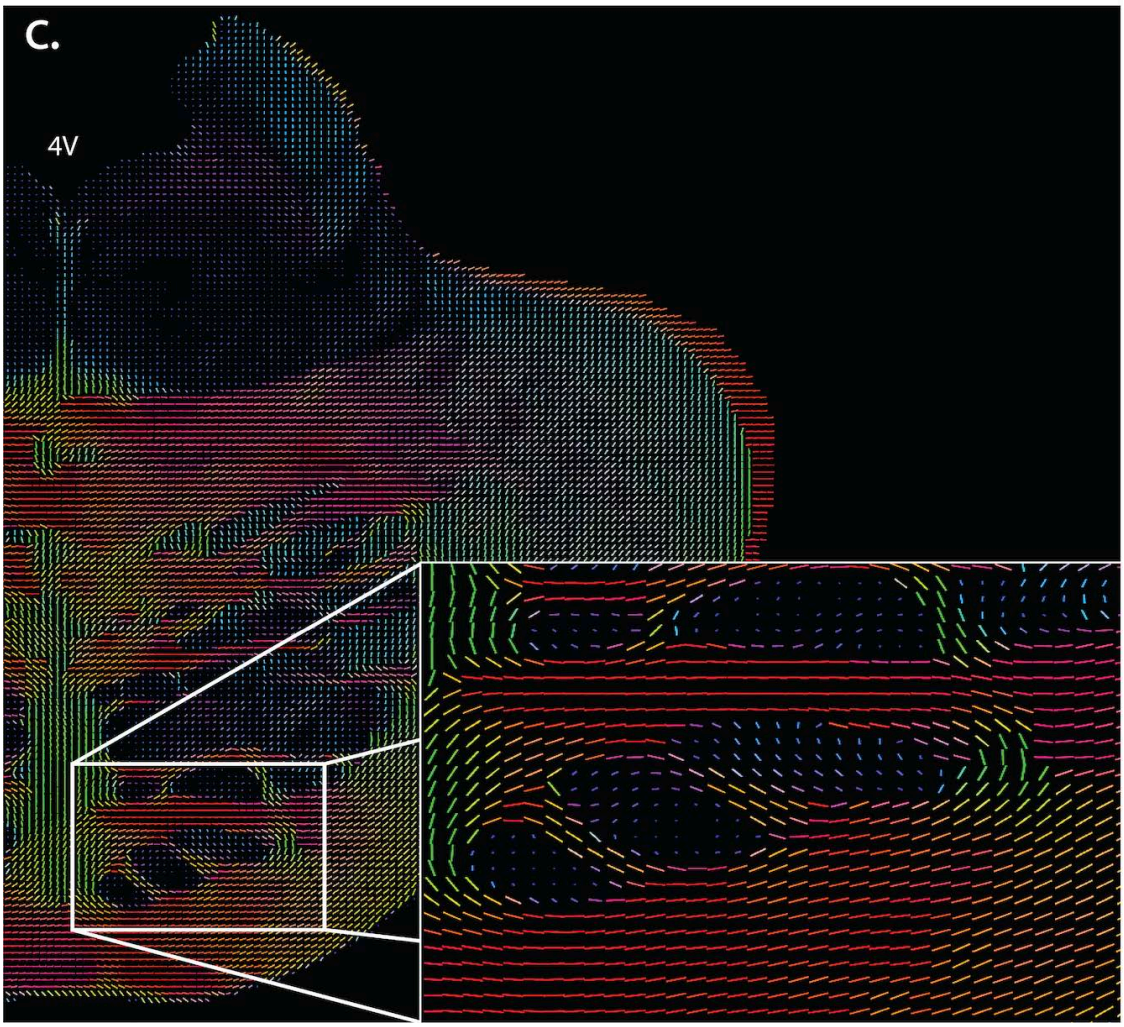
C.
4V

Fig. 3.14. Colour-coded Vector Map of First Eigenvector. *The tensor glyph illustrates the principal direction of the fibres by colour and vectors. Each vector is contained within an individual voxel, and the line within (the vector) represents the orientation of the fibres, i.e., if the fibre(s) courses from lateral to medial or vice versa then the vector is horizontal and red, from ventral to dorsal or vice versa it is vertical and green, and from rostral to caudal it is a dot and blue. In (a) at the level of rhombomere one and two (crus cerebri) the central part of the descending subdivisions projects rostrocaudally (as inferred by the shape of the vectors) throughout the brainstem whereas the lateral parts bend (higher magnification) change direction and synapse onto the pontine nuclei which, in turn, form the transverse fibres of the pons. In (b) tensor glyph and fibre tracking in the midpons as seen through this higher order DTI technique. In (c) at a more caudal level, a tensor glyph was created from diffusion data at 200 μm isotropic resolution (human specimen 1). Note the orientation of the tensors (fibres) and most particularly (in magnification) how the lateral parts of the ventral group of the descending bundles (v1, v2, v3, and v4) break off and bend to synapse into the pontine nuclei. From there the five ventral transverse fibres of the pons (in red) form and traverse horizontally to the opposite hemipons. Abbreviation: 4V: fourth ventricle.*

Hence, the ventral group of the descending bundles is anatomically and functionally related to the ventral group of the transverse fibres of the pons and so on (after an obligatory synapse in the pontine nuclei). In other words, in the basilar pons, not only is there a somatotopic representation akin to the homunculus of the cortex, and a topographic arrangement (as mapped herein), but there is also a consistent topography within the descending bundles so that the centromedial part is occupied by the cortico-bulbar and -spinal tracts whereas the lateral and external parts is occupied by the corticopontine projections (Fig. 3.14). This topology is also supported by the structural GRE image (Fig. 3.15) at the level of rhombomere one and two where the pontine nuclei are found between the descending and transverse fibres of the pons.

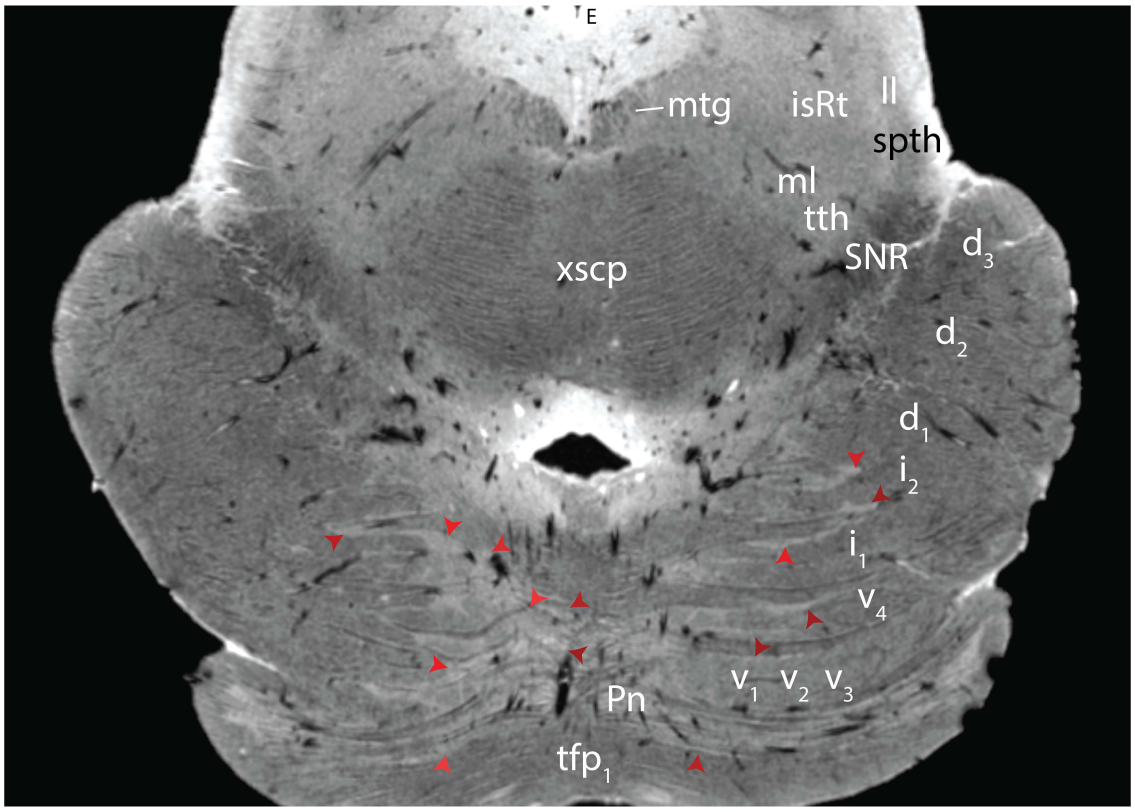

3.15. GRE (gradient recalled echo) sequence at 50 µm, at the level where the crus cerebri meets the pontine nuclei (border between rhombomere one and two). *The pontine nuclei (arrow heads) are principally found not inside the descending or transverse bundles but between them. As the descending fibre bundles fan out, the pontine nuclei can be identified assuming a lateral position between the descending bundles that alternate with the transverse fibres of the pons. Abbreviations: mtg: mammillotegmental tract, xscp: decussation of the superior cerebellar peduncle, ml: medial lemniscus, ll: lateral lemniscus, tth: trigeminothalamic tract, spth: spinothalamic tract, SNR: substantia nigra, pars reticulata, Pn: pontine nuclei, tfp1: most ventral transverse fibre of the pons, isRt: isthmic reticular formation, E: ependyma.*

3.3.9 The Stria Pontis

In addition to the descending and transverse fibre bundles, an additional fibre bundle has been identified which is now named as the *Stria Pontis.* This pathway is most clearly seen in Fig. 3.16, where it runs ventral to dorsal (green in FAC), but can also be seen in Figs. 3.3d, 3.5e, 3.6f, 3.8, 3.9, 3.12d & e, 3.13, 3.14, and Appendix Fig. 31. The *Stria Pontis* forms a vertical ridge at the midline of the basilar pons and pontine tegmentum which extends throughout the entire length of the pons (Fig. 3.16a at a more rostral pontine level, 3.16b at a more caudal pontine level). It is formed in the rostral pons (Fig. 3.8, level of rhombomere two) from the first ventral transverse fibres of the pons. The first bundle to give rise to the *Stria Pontis* is the most ventral transverse fibre of the pons (transverse fibre bundle no. 1, Figs. 3.8, 3.14a). Subsequently, the remaining transverse fibre bundles begin to form from the spaces between the fanning descending fibre bundles (where the pontine nuclei are). Each one of these transverse fibre bundles is seen to contribute (Figs. 3.14a to c) to the formation of the *Stria Pontis*. It extends caudally until the pontomedullary junction where the most ventral transverse bundle (transverse fibre bundle no. 1) begins to disappear (at the level of rhombomere four), just prior to the medullary pyramids (Fig. 3.13e, sagittal view).

The eigenvector analysis (Fig. 3.14c) is consistent with the observation made on the FAC that the *Stria Pontis* veers laterally once the fourth ventricle (4V) is reached.

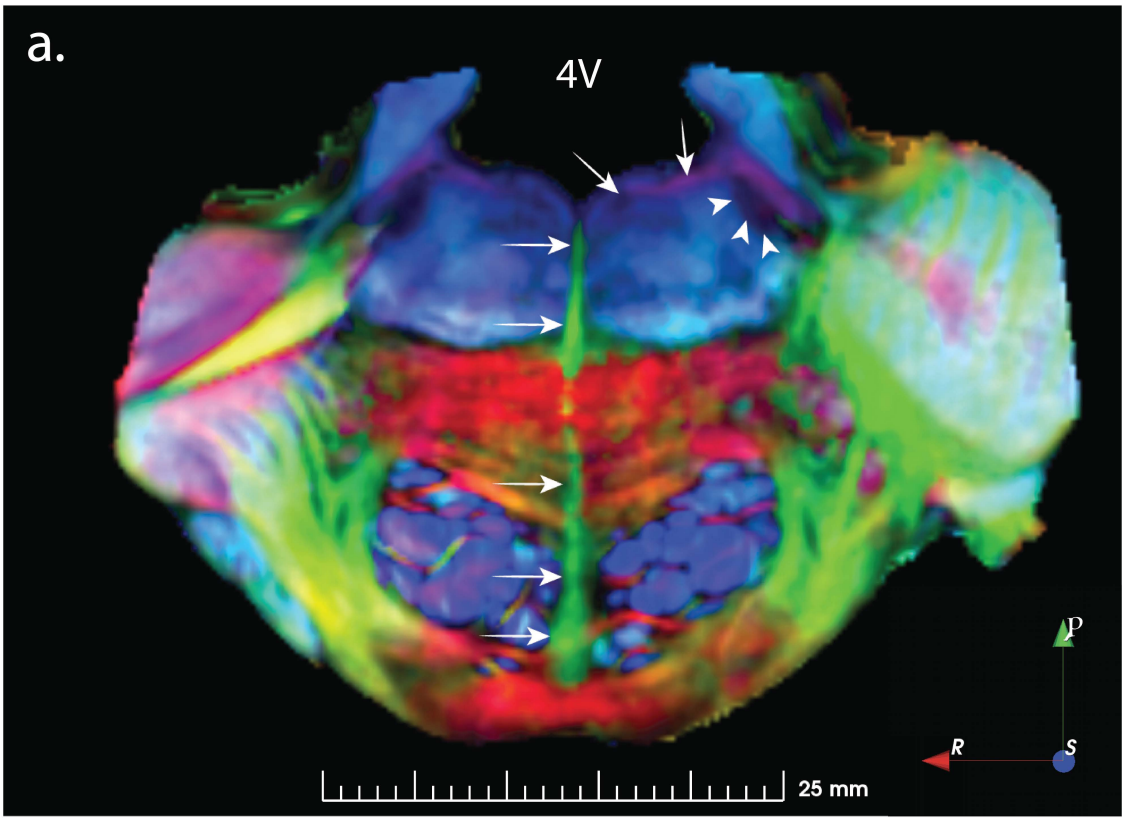
a.
4V
P
R
S
25 mm

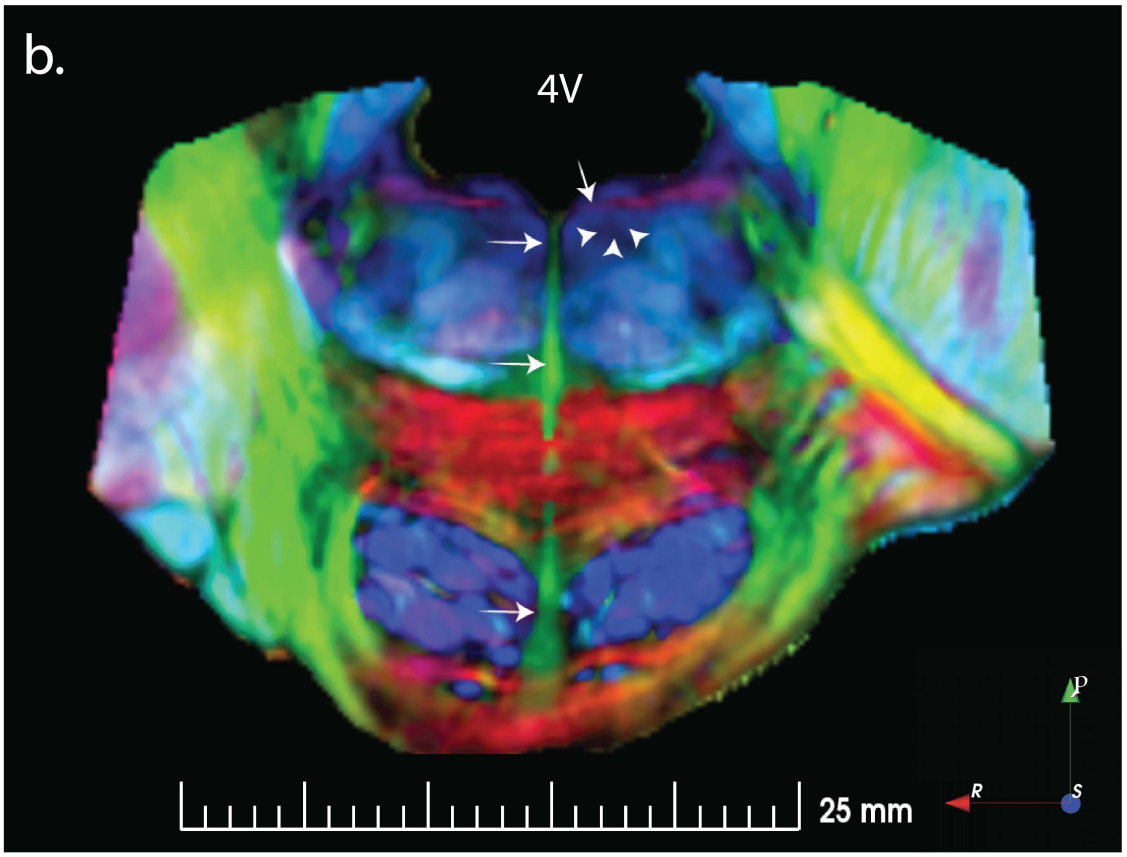
b.
4V
P
R
S
25 mm

Fig. 3.16. Ultra-high-resolution FAC map at 200 µm. *This highly detailed approach of fibre tracking revealed how the Stria Pontis (arrows) in green traverses the entire pons from the ventral to the dorsal end where it bends just before it reaches the floor of the 4th ventricle (4V; magenta in DTI) to project (a) and dorsally surround the motor trigeminal nucleus (arrow heads) in the pontine tegmentum. Similarly, the Stria Pontis (arrows) identified in this study as the presumptive pathway that conveys information from cortical areas, courses through the basilar pons towards the pontine tegmentum where it bends (magenta in DTI) at the level of the floor of the 4th ventricle in (b) and maintains its course within approximately 500 µm from the abducens nucleus (arrow heads). On the FAC maps red, blue, and green represent anisotropy along medial-lateral, rostral-caudal, and ventral-dorsal orientations, respectively.*

Moreover, DTI reveals that the fibres that constitute the *Stria Pontis* arch bilaterally just before they reach the floor of the fourth ventricle, forming the corticotegmental pathway; (magenta in Fig. 3.16). The stria fibres are subsequently lost in the vicinity of the motor trigeminal nucleus (5N; Fig. 3.16a). At a more caudal level, the fibres that emanate from the transverse fibres of the pons (the presumptive corticotegmental pathway) continue to form the *Stria Pontis* at the midline to then progress towards the nuclei of the cranial nerves in the pontine tegmentum. More specifically, the *Stria* courses within 500 μm from the dorsal part of the abducens nucleus (6N) ventrally, and the floor of the fourth ventricle dorsally (Fig. 3.16b).

3.4 Discussion

The present study uses ultra-high-resolution MRI datasets derived from four human and one macaque postmortem specimens to map the fibre bundles in the internal capsule, crus cerebri, basilar pons and medulla oblongata. Four subdivisions of these descending fibre bundles were applied within the internal capsule, from internal to external. The most internal bundle terminates in the substantia nigra pars reticulata (SNR), the striato- and corticonigral pathways. The three external bundles of the internal capsule contain cortico-pontine, -bulbar, and, -spinal projections, but with topography. The fibres with cervical spinal terminations were most external and those with lumbar/sacral terminations were most internal. The external three bundles of the internal capsule continue in the crus cerebri and appear as ventrolateral curved-lamellae in cross section. Therefore, the crus cerebri has been subdivided herein into three groups of bundles (four ventral, two intermediate and three dorsal). These

lamellae twist and assume a ventrodorsal orientation as they descend and form ventral, intermediate and dorsal groups of bundles in the basilar pons with further subdivision into four, two and three bundles, respectively. The lateral part of these nine bundles peels off into the pontine grey matter, while the central and medial parts continue to form the pyramid. The topography and somatotopy is maintained in the pyramids, with the ventral bundles twisting medially as the cervical component of the pyramids; the intermediate bundles are found lateral to the cervical and are the thoracic component; similarly, the dorsal bundles twist laterally to the thoracic and are the lumbar and sacral components of the pyramids. The transverse fibres of the pons have also been subdivided into three main groups and traced in relationship to the descending bundles. Finally, a midline bundle orthogonal to the descending and transverse fibres of the pons was discovered and named as the *Stria Pontis*.

As well as delineating the specific tracts descending or traversing the pons towards the cerebellum, this study is particularly novel in a number of aspects: 1) dispelling the idea about a specific ventral corticopontine tract, 2) showing the interspersed nature of the descending bundles and the fact that they alternate with the transverse fibres of the pons, and 3) discovering the *Stria Pontis* at the midline of the pons.

3.4.1 The Corticopontine tract is formed collectively by fibres peeling off from all the descending bundles

The data indicate that the transverse fibres of the pons arise from both the ventral and the dorsal parts of the crus cerebri and basilar pons, which is contrary to the classic view which states that the ventral part of the descending bundles

constitutes exclusively the corticopontine tract (first order neuron) that innervates pontine nuclei (Hurley et al., 2010, Hendelman, 2000). However, corticopontine projections in the dorsolateral pons were also reported in monkey by Shook et al. (1990) and Leichnetz and Gonzalo-Ruiz (1996) using WGA-HRP and horseradish peroxidase technique. The subsequent pontine efferents (second order neuron) then cross the midline and form the middle cerebellar peduncle to reach the cerebellum. Together the corticopontine and pontocerebellar tracts form the cerebrocerebellar pathway, the purpose of which is a line of communication between the cortex and the cerebellum to allow for the coordination of planned motor functions and for accessing of stored learned motor routines in the pontocerebellar cortex. To further test the notion of an exclusively ventral corticopontine tract, I specifically traced the ventral group of the descending fibre bundles (Fig. 3.13). The most ventral bundle (v_1), descended through, the crus cerebri to the basilar pons and continued onto the pontomedullary junction it then twists medially. The intermediate and dorsal descending bundles were traced in all five specimens with similar results. They all appeared to shed fibres in the pons rather than exclusively terminating within the basilar pons. The tensor glyphs (Fig. 3.14) suggest that each of the descending bundles sheds fibres to the pons. This was consistent with tractography (Fig. 3.3) where the ventral group of the descending bundles (cervical) courses from the external part of the internal capsule, descends through the brainstem (ventrally) to twist and project into the pyramids (medially), and finally to form part of the pyramidal decussation (Fig. 3.3c and e). Moreover, I did not find any evidence that robust fibres course the basilar pons from the ventral to the dorsal end, and this evidence would be to identify green fibres on the FAC. The only pathway that

courses the pons ventrodorsally seems to be the *Stria Pontis* at the midline. To conclude, the present study shows that the ventral part of the descending fibres (bundles 1-4) does not terminate as a distinct corticopontine tract. Instead, after shedding fibres in the pons it descends, shifts from ventral to medial, and enters the pyramids to constitute the cervical pyramidal tract. Therefore, none of the descending fibre bundles exclusively terminates in the pons, and this was seen across all human and macaque specimens. As a result, the classic view of a distinct ventral corticopontine tract is not supported by the present study. Instead, all the bundles contribute to the pons (Figs. 3.3 to 3.6, 3.9, 3.10 and Figs. 3.13, 3.14).

In proposing these new anatomical patterns, it is important to consider the possibility of error during the tractographic analysis (this is also further discussed for the dorsal trigeminothalamic tract in Chapter 4). One possibility is that oligodendrocytes myelinating multiple axons resulting in perpendicular or angled myelin sheathing, for example. However, I do not believe that these oligodendrocytes would have a major effect on the consistent pattern of the ultra-high-resolution tensor glyphs because the glyphs calculate and show the major eigenvector which reflects the trajectory of the major fibre population within each voxel. Therefore, the glyphs could provide a reliable tool for fibre identification, neglecting small fibre populations that may be present within each voxel. (see also Ch 1.8 - Optimisation and Limitations of DTI and Tractography). Nevertheless, to more definitively demonstrate that the corticopontine tract terminates into the pontine nuclei according to the pattern proposed herein, it would help to actually see the synapses – of course, we do not see these with DTI. The tensor glyphs do show the transition from the descending to the transverse fibres which occurs locally, from one individual

descending bundle to adjacent transverse bundles and it would be helpful to see the synapses and pontine nuclei that receive the descending bundles and project the transverse fibres of the pons. Ultimately tracing methods targeting individual descending and transverse fibres or fibre bundles could support the fibre architecture within the pons proposed.

3.4.2 The topography of the fibre bundles in the crus cerebri and basilar pons

The classical descriptions of the crus cerebri (Hurley et al., 2010, Haines, 1987) show the descending bundles within the crus cerebri into orthogonal groups adjacent to each other of frontopontine, corticobulbar, corticospinal, parieto-occipital and temporopontine fibres. The current higher resolution GRE, DTI, and tractography suggest different organisation, for both the human and the macaque. The present study found that the descending bundles course in the crus cerebri, before fanning out in rhombomere two (basilar pons) while maintaining the shape of curved lamellae that alternate with the transverse fibres of the pons (Figs. 3.8 to 3.10, 3.14 and Fig. 3.15). This architectural model in the human is also consistent with that noted by Brodal and Bjaalie (1997) in the monkey, where they observed lamellae-like subspaces using WGA-HRP to identify the organisation of corticopontine terminal fields. Wheat germ agglutinin coupled with horseradish peroxidase (WGA-HRP) is a protein extracted from wheat, coupled to an enzyme which has high affinity for the soma and axon of a neuron and has been extensively used as retrograde and anterograde tracer. The authors identified terminal fields within the

pons which are arranged in a lamellar pattern and this is in alignment with the shape of the descending bundles observed herein.

The classical view, also depicted that the longitudinal fibres of the pons are concentrated in the central region of the basilar pons called peduncular nucleus. This view has been espoused even recently (Morecraft et al., 2018, Schmahmann and Pandya, 1997) and is based on the original segmentations of the pontine nuclei by Nyby and Jansen (1951). The ultra-high-resolution data and the fibre tracking in the present study again suggest an alternative organisation that the longitudinal and transverse fibres occupy the entire territory of the basilar pons (Figs 3.9 & 3.10).

3.4.3 The Stria Pontis

The pontine nuclei that receive fibres from the descending bundles give rise to the transverse fibres of the pons, which in turn gather together into a newly discovered fibre tract that runs ventrodorsally, which I termed the *Stria Pontis* (from Latin: the stripe of the pons). Traditional histologic techniques, cytoarchitectonic and myeloarchitectonic data (Olszewski and Baxter, 1954, Mihailoff et al., 1981, Martin, 2016) have not routinely identified this structure before. It may be that the nature of the stains used hindered the identification of this pathway. The traditional histopathology stains rely on a specific chemical signature which may be challenging for the *Stria Pontis*. Typical nuclear or soma stains, such as Nissl will not detect fibre tracts (Kádár et al., 2009). Another common stain, Luxol fast blue, can stain the myelin sheath but may have failed to reveal the *Stria* because the transverse fibres of

the pons obscure the midline which the current data readily illuminated due to the colour-coded orientations (green) of the ultra-high-resolution DTI. Furthermore, the basilar pons and the tegmentum are negative for immunofluorescent staining of the Glial Fibrillary Acidic Protein (GFAP); (The Human Protein Atlas, 2019a, Uhlén et al., 2015), and this indicates that the midline of the pons where the *Stria* is located is devoid of astrocytes. Some stains however have been able to access this region - the midline of the pons is highly positive for Myelin Basic Protein (MBP) - indicating that the axons of the *Stria* are myelinated (The Human Protein Atlas, 2019b, Uhlén et al., 2015). However, these latter studies failed to report the midline structure of the *Stria Pontis,* probably due to the fact that there was not high enough contrast between the various pathways (only possible in DTI). Both the descending and transverse bundles are myelinated and leave the same signature, making it challenging to discern between all these fibre tracts in the absence of orientation data (i.e., the FAC). Interestingly, in Golgi stained preparations, Cajal (1899) in the newborn pup and later Valverde (1998) in the postnatal mouse included diagrams of the brainstem, and also in some myelin fibre stained images (Sudheimer et al., 2013), one can see, retrospectively, vertical fibres along the midline of the pons, consistent with the pathway identified in the present study as the *Stria Pontis.* However, the authors did not refer to this fibre bundle in their texts. Moreover, the signature of the *Stria* can be also seen with polarized light microscopy in the recent article by Henssen et al. (2019).

It should be acknowledged that DTI does not detect the direction of the axons (only the orientation) and, therefore, some of the fibres that form the *Stria Pontis* could theoretically originate from the reticular formation within the pons and project

on the opposite direction towards the spinal cord. This could in theory be part of the reticulospinal tract. Further research using biological tracers, polarized light microscopy and/or, CLARITY techniques, should specifically examine this, however, this seems unlikely because one end of the *Stria Pontis* fibres (starting point) appears as emanating from the transverse bundles of the pons, while the other end (ending point) of the *Stria* projecting fibres is through the cranial nerve nuclei within the pontine tegmentum.

It is also worth noting that MRI/DTI exploits a physical phenomenon (diffusion) that is different from detecting chemical signatures in histology. The higher sensitivity of the present MRI, in comparison to histology for fibre tracking, in combination with the FAC maps at the isotropic spatial resolution of 200 μm has provided sufficient contrasts and resolution to delineate rostrocaudally (blue), mediolaterally (red) and ventrodorsally (green) oriented bundles. This ultra-high-resolution DTI scalar allowed the *Stria Pontis* to be revealed. In addition, the deterministic tractography based on high-angular-resolution diffusion imaging (HARDI) combined with higher order models such as tensors glyphs, confirmed the identification and anatomical description of this hitherto unknown pathway at the midline of the pons. Finally, the *Stria Pontis* seems to be the only major pathway that courses the basilar pons and the tegmentum in a ventrodorsal orientation.

The glyphs are based on mathematical principles that reflect the principal eigenvector (λ_1), which is the largest of the three eigenvectors (λ_1, λ_2, λ_3) and measures the average orientation of diffusion within each voxel, without calculating individual orientations of small fibre populations (Ennis and Kindlmann, 2006). This

reflects the validity of the interpretation regarding the pattern that the fibres assume to form the *Stria Pontis* but also regarding the interpretation of the tensor glyphs for the topography of the corticopontine fibres within the descending bundles (see 3.3.8 The principle of topology). However, to further validate the above findings, Golgi staining, CLARITY technique, and biological tracers should be used to perform targeted tracking from single descending bundles to see if they maintain the topographical arrangement proposed herein. Finally, when superconducting electromagnets achieve resolutions 4 – 10 fold greater, then tractography could analyse the fibre architecture more precisely.

3.4.4 Possible Functional Consequences of the Inter-relationship Between the Longitudinal and Transverse fibres of the Pons

This architectural model of nine descending that alternate with ten transverse fibres of the pons and one vertical pathway at the midline (the *Stria Pontis*) could provide redundancy and alternate neural routes. Therefore, I propose the following neural framework: 1) three groups of descending bundles which are always stable (primary subdivisions), all of which contain corticobulbar and -spinal projections centromedially, and corticopontine projections laterally and externally. 2) Three groups of transverse fibres of the pons which are functionally and anatomically related to the descending ones which are always stable (no anatomical variation between specimens). In addition, the transverse fibres found on the extremities of the basilar pons tfp_1 & tfp_{10} are stable. 3) A vertical bundle at the midline of the pons which emanates from all the transverse bundles and projects into the pontine

tegmentum bilaterally. Moreover, as I report in Fig. 3.10, we can clearly see that between the main ventral bundles there are interdigitations (see arrows in Fig. 10). The same can be seen for i_1 and i_2, d_1, and d_2, but also between i_1, and d_1. I speculate that these may offer communication between adjacent bundles but I do not have any further evidence for this. I hypothesise that the same information that travels through one bundle could be conveyed to an adjacent bundle. Therefore, the interdigitations and the higher number of the descending and transverse bundles in the human, could provide a mechanism of adaptation after lesions such as lacunes in the basilar pons so that the cerebrocerebellar pathway is not interrupted.

3.4.5 Comparative Anatomy

In the rat, there is a less complex architectural plan for the descending, transverse fibres of the pons and pontine nuclei. The descending bundles are situated immediately ventral to the medial lemniscus (ml, containing ascending sensory fibres, see Chapter 4), leaving virtually no space to be populated by pontine nuclei. The transverse fibres in the rat congregate at the external part of the pons as a solid bundle (Paxinos et al., 2015). For the marmoset, the descending bundles are not as compact as in the rat although pontine nuclei are still found dorsal to the descending bundles, and below the ml, rather than interspersed (Paxinos et al., 2012). The complexity appears to increase for the human, with the descending bundles exhibiting higher degrees of interdigitations (Figs. 3.8 to 3.10b, arrows) and, alternating with pontine grey matter and multiple transverse fibres of the pons. In spite of this, in the humans the most ventral and dorsal transverse bundles are also

the most compact (as seen in Figs. 3.9 & 3.10). The complexity of the cerebrocerebellar pathway in humans and in particular the higher number of descending bundles and interdigitations between them, including the increased number of transverse fibres of the pons could reflect the higher level of dexterity assumed by humans through evolution. The subdivisions of the cervical, thoracic and lumbar/sacral components of the human pyramidal tract are composed of a higher number of bundles and interdigitations between them compared to other species (compare with macaque in subpanels: Figs. 3.8f, 3.9f, 3.10f). Therefore, the information conveyed from the cortex to the spinal cord may be more resistant in the human to interruptions by a lacunar stroke. A higher number of bundles and interdigitations may confer an evolutionary advantage in providing greater flexibility in the flow of electrical impulses.

3.4.6 The striatonigral and corticonigral projections

There has been much investigation of the inputs to the substantia nigra, given the clinical significance in Parkinson's disease and its therapies. Monosynaptic fibre tracing techniques, biological tracing, and cell-specific transgenic mice have identified afferent inputs from the striatum and cortex in experimental animals. For example, Royce and Laine (1984) showed after injecting horseradish peroxidase into the caudate nucleus that in cats the head of the caudate nucleus projects through the internal capsule to the SNR. This striatonigral projection is the major input to the nigra, but there is evidence for a corticonigral pathway (Foix and Niculescu, 1925, Rinvik, 1966, Afifi et al., 1974, Naito and Kita, 1994, Cacciola et al., 2016). In the

present study, the most internal sector of the internal capsule distinguishes itself by the lack of any pyramidal tract fibres (Fig. 3.1j). Instead, the internal sector features a pathway that ends at the level of the nigra, presumably the striatonigral and corticonigral pathways which terminate in the SNR. To our knowledge, this is the first study in humans which identifies the fibre inputs to the SNR at a microscopic resolution of 50 μm for the GRE and 200 μm for the diffusion data. Although it was not possible to identify with precision the islands of substantia nigra, pars compacta which are present within the pars reticulata, it has been demonstrated herein that the projections under consideration concentrate in the ventral part of the nigra where the SNR is mainly found (Fig. 3.1i).

3.4.7 Clinical relevance

The enhanced resolution of the descending and transverse bundles identified here has clinical relevance.

Above I discussed the idea and explanation based on evidence delivered by GRE, DTI, tractography and tensor glyphs that the interdigitations and the topology provided redundancy should there be a discrete lesion. Moreover, the somatotopic arrangement in the basilar pons is such that hand coordination and dexterity occupies the ventral group of the primary subdivisions of the descending bundles. The thoracic component is in alignment with the intermediate group, and finally leg coordination has a dorsolateral concentration (MacMore et al., 2004, Bassetti et al., 1996, Schneider and Gautier, 1994, Hong et al., 2010c). Thus, targeting the individual

bundles as mapped herein, may offer a more precise therapeutic approach that could, for example, minimise off target damage to adjacent tracts during radiotherapy or surgery.

In addition, identification of the course of the striatonigral and corticonigral pathways may provide more precise targeting for possible therapeutic treatment of movement disorders. The corticonigral pathway could work in parallel with the corticopallidal system which is an additional route to the basal ganglia (Smith and Wichmann, 2015), and the striatonigral pathway to provide direct cortical regulation to the SNR as an additional route for motor control. By producing cortical modulation, therapeutic interventions aimed at disinhibition of the SNR including repetitive Transcranial Magnetic Stimulation (rTMS) and transcranial Direct Current Stimulation (tDCS); (To et al., 2018) could provide auxiliary treatments for Parkinson's disease, additionally, I propose by inserting an electrode for further stimulation targeting exclusively the SNR.

Brainstem surgery remains a challenge despite recent improvements in neuroimaging (Párraga et al., 2016). As emphasised by Párraga et al. (2016), a detailed knowledge of brainstem anatomy to plan microsurgical or any other invasive therapeutic approach is mandatory. The white matter tracts that I have mapped through the basilar pons extend such knowledge, thereby providing an important tool for neurosurgical specialists diagnosing and planning therapeutic approaches.

3.4.8 Implications for Specific Surgical Procedures

Various neurosurgical approaches are used to target lesions such as tumours, hematomas and/or cysts in the brainstem (Meola et al., 2016b). In treating such lesions, Recalde et al. (2008) recommend a peritrigeminal approach to reach the ventral pons. This neurosurgical approach corresponds to a triangular area, confined inferiorly by the pontomedullary sulcus, medially by a line which corresponds to the lateral margin of the descending fibre bundles in the ventral pons, and laterally by a line connecting the origin of the trigeminal root with the medial aspect of the facial (7n) and vestibulocochlear (8n) nerves (cerebellopontine angle). These landmarks are seen at greater resolution in the data presented here, specifically in Fig. 4.1 panel f, where the 8n is identified, and Fig. 4.2 panel e, for the identification and microanatomy of 7n, and the root of the trigeminal nerve (5n). As suggested by Recalde et al. (2008) this peritrigeminal approach should proceed gradually and lateral to the ventral descending bundles, and as the surgeon reaches deeper levels, they should advance more posterolaterally (Meola et al., 2016b). The termination point of the invasive corridor is formed by the dorsal transverse fibres of the pons (tfp_{10} – dorsal arcuate); (see Fig. 3.9) found ventral to the pontine tegmentum. Therefore, ventral, intermediate, and dorsal lesions in the basilar pons which would compromise the functionality of upper, torso, and lower limbs respectively, can be effectively and more precisely targeted by using the maps presented in this thesis to direct this neurosurgical approach.

The only impractical procedure proposed is the median sulcus approach which is a dorsal approach to the pons and has limited clinical use because of the

narrow space between the medial longitudinal fasciculi and the risk of iatrogenic injury (Giliberto et al., 2010).

Regarding the neurosurgical approach to the midbrain and by extension to the SNR, various invasive approaches have been classically used. The supracollicular, infracollicular, perioculomotor, and lateral mesencephalic approaches (Bricolo and Turazzi, 1995, Giliberto et al., 2010).

The supracollicular approach is performed right above the superior colliculus. Thus, targeting all the components of the crus cerebri and the substantia nigra, the dorsal longitudinal fasciculus (dlf), the rostral part of the medial longitudinal fasciculus (mlf), and the central tegmental tract (ctg). In order to preserve these tracts without any damage the termination point of this approach is a plane dorsal to the dlf, one level lower to the floor of the cerebral aqueduct (Aq); (Fig. 3.1c). Therefore, the medial border of this neurosurgical approach is the cerebral aqueduct (Aq), and the lateral border is confined by the spinothalamic tract (spth); (Giliberto et al., 2010); The landmarks of this approach can be better observed in higher resolution in Fig. 4.6.

The infracollicular neurosurgical approach is performed through a corridor located one plane lower to the inferior colliculi maintaining the same landmarks as for the supracollicular approach. These two approaches are performed through the dorsal mesencephalic tegmentum, that is the lamina quadrigemina (superior and inferior colliculi); (see Fig. 3.1c, f, i, l, Fig. 3.2a, d, g).

In addition, the perioculomotor approach targets ventrally the midbrain with the entry point between the descending fibre bundles and the oculomotor nerve (3n);

(Fig. 3.1c, 4.6c), rostral to the superior cerebellar artery and caudal to the posterior cerebral artery (Bricolo and Turazzi, 1995). The surgical corridor is directed towards the decussation of the superior cerebellar peduncle, and its termination point should be confined by the red nucleus.

Finally, the lateral mesencephalic approach opens a corridor through the lateral mesencephalic sulcus, that is through the lateral surface of the mesencephalic tegmentum. The direction is obliquely oriented towards the ventral part of the midbrain. This corridor is formed by the crus cerebri laterally, by the medial lemniscus (ml) medially, whereas the ventromedial termination point of the corridor is formed by the 3n (Recalde et al., 2008, Meola et al., 2016b).

CHAPTER 4:
Sensory pathways in the human and macaque brainstem and thalamus

4.1 Introduction

During evolution, animals developed their ability to perceive and learn about the internal and external environment through a series of sensory receptors. In mammals, these receptors are embedded within the skin to respond to external stimuli such as nociception, crude and fine touch and temperature, and within internal organs to respond to different joint position and muscle tension (proprioception) or from chemical signals within the body (Iggo, 1985, Dubin and Patapoutian, 2010). Together these somatic and visceral receptors transfer sensory information via the axon of the neuron through the posterior root, into the posterior horn of the spinal cord, and then through the posterior column to supraspinal centres such as the brainstem, diencephalon and neocortex (see Chapter 1,6 & 1.7); (Todd, 2010). This Chapter investigates three of these sensory pathways as they ascend through the brainstem and thalamus: the dorsal column afferent pathway, the spinothalamic pathway and the sensory pathways which originate from the trigeminal nerve (5n) such as the spinal trigeminal tract (sp5) and the ventral and dorsal trigeminothalamic tracts (vtt & dtt).

The dorsal column – medial lemniscus pathway (dcml) consists of two large and discrete ascending bundles, the gracile (gr) and cuneate (cu) fasciculi in its caudal portion (dorsal funiculus in the spinal cord, and caudal medulla until the gracile and cuneate nuclei), and one discrete bundle the medial lemniscus (ml) from the sensory decussation rostralwards (Willis et al., 1999, Rodríguez-Mena and Türe, 2017). The gr conveys information from the trunk and extremities that are lower than the sixth thoracic segment; the cu, which is situated more lateral to the gr within the

dorsal funiculus, conveys information from the upper trunk and extremities (Mai and Paxinos, 2012). These fasciculi consist of 1st-order neurons, with their mechanoreceptor terminals such as the tactile corpuscles or Meissner corpuscles (discriminative sensation) which lie in the dermis of skin close to the epidermis (Paré et al., 2001); the muscle spindles which are responsible for proprioception (Macefield and Knellwolf, 2018); the Merkel-Ranvier cells for light touch (Boulais and Misery, 2007); the bulbous corpuscle or Ruffini ending for skin stretch, kinesthetic sense, control of finger position and movement (Paré et al., 2003); the Pacinian corpuscles for vibration and pressure (Biswas et al., 2015) and finally the peritrichial endings which are hair follicle receptors for touch sensation (Carlson, 2019). The cell bodies from all these afferents are located in the dorsal root ganglia, and their central projections terminate into the gracile (Gr) and cuneate (Cu) nuclei within the dorsal part of the medulla oblongata in the brainstem. From there, the internal arcuate fibres (second-order neurons) cross the midline in the sensory decussation and ascend as the ml. These ascending ml projections finally synapse in the ventral posterolateral nucleus (VPL) of the thalamus (Watson et al., 2008). The entire projection conveys proprioceptive, tactile (crude or light touch which yields information such as contact with an object and discriminative touch which enables awareness of shape, size and texture (Ackerley et al., 2014)) and finally vibratory information. Destruction of the cu for example, prevents the control of fine finger movements and causes subsequent hypotonia of the fingers in primates (Leonard et al., 1992, Glendinning et al., 1992).

The spinothalamic pathway (spth) conveys neural activity related to nociception, temperature, pressure and crude or non-discriminative touch to the corresponding somatosensory region of the thalamus. Within the spinal cord, this

sensory tract can be subdivided into a ventral or anterior part (the paleo-spinothalamic pathway) and a lateral (or neo-spinothalamic) tract. The ventral and lateral spth are both composed of the large axonal projections of second-order neurons that originate from cell bodies in the dorsal horn (see also Chapter 1.6; the spinothalamic tract); (Kerr, 1975, Ralston and Ralston, 1992). The axons cross in the ventral white commissure of the spinal cord to ascend through the ventrolateral funiculus (Gildenberg, 2009). Axons of the ventral spth can ascend through a couple of spinal cord segments before they decussate, whereas the lateral spth crosses at the same spinal level of the soma (Stevens et al., 1991). The spth in the spinal cord and caudal medulla is very difficult to be thoroughly subdivided, rather, it has always been grouped broadly within a region defined as the anterolateral system which also encompasses the spinoreticulothalamic and spinotectal tracts (Mendoza and Foundas, 2008). According to accepted ideas, as this anterolateral system fibres ascend to the brainstem, the fibre bundle is reported to be located between the inferior olive, principal nucleus (IOPr) and the nucleus of the spinal trigeminal tract (Sp5) in the medulla oblongata (Mense, 2004, Willis and Westlund, 1997). In addition, current knowledge reports that in the pons and midbrain, the spinothalamic projections course dorsolateral to the ml, however the precise topographical distribution particularly within the midbrain or any distinction between the borders of the spth, ml and trigeminothalamic tract (tth) still remains vague; (Purves et al., 2001, Kayalioglu, 2009, Kerr, 1975). As a result, the detailed topography of the spth and its relationship to the ml and tth as it travels through the medulla, pons and midbrain en route to the VPL of the thalamus is unclear. At the VPL, the spth synapses onto grey matter and

subsequently gives rise to the third-order neurons that ultimately project to the somatosensory cortex (Brodmann areas 3, 2, 1; Khalid and Tubbs (2017)).

Orofacial nociceptors and thermoreceptors convey information from the mouth and face to the brainstem via the trigeminal nerve, the 5th cranial nerve (Go et al., 2001). These are first-order axons originate largely from the trigeminal ganglion cells, but also from ganglia associated with other cranial nerves, including the VII, IX, and X. The projections are believed to synapse into the trigeminal sensory nucleus complex within the ipsilateral brainstem (García-Guillén et al., 2021, Ziyal et al., 2004). The sp5 which is a vertical sensory bundle located in the lateral pons and medulla oblongata courses caudalwards in parallel to the corresponding nucleus (Sp5); (Devoize et al., 2010). This sensory tract is considered to be the cranial homologue of the dorsal root afferents, whereas the vtt would be homologous to the spth. The sp5 similar to the spth conveys information about deep/crude touch, nociception and temperature from the ipsilateral face to the Sp5 (Devoize et al., 2010). From there, second order-neurons cross the midline and ascend as the tth to convey integrated information to the ventral posteromedial nucleus (VPM) of the thalamus (Sessle, 2000, Ralston, 2005). In humans, functional magnetic resonance imaging (fMRI) provides strong evidence that noxious information ascends bilaterally towards the thalamus and by extension to the primary sensory cortices (Nash et al., 2009, Nash et al., 2010), the exact topography of the trigeminal pathway remains elusive.

A number of clinical pathologies are associated with disruptions to these afferent pathways as they traverse the brainstem and thalamus. For example,

unilateral lesions such as ectatic vessels or plaques of demyelination affecting the dorsal column – medial lemniscus pathway above the sensory decussation may lead to impairment of discriminative touch, proprioception and vibration on the contralateral half of the body (Seo et al., 2019). Unilateral lesions affecting the spth such as atherosclerotic disease, multiple sclerosis, or infections (West Nile virus, poliomyelitis) usually cause contralateral anaesthesia. Brainstem lesions disrupting the vtt or dtt result in sensory changes in the contralateral face (Noback et al., 2005). Decompression surgery is the gold standard for patients with traumatic injury, tumor, abscess or aneurisms which cause compression of the ascending sensory pathways (Choudhri et al., 2017). Trigeminal neuralgia can be caused by a dysfunction of the trigeminal nerve root itself, by a lesion within the brainstem or by demyelination of sensory projections (Maarbjerg et al., 2017). These lesions of the pain pathways are typically treated with Gamma knife surgery where in the case of trigeminal neuralgia 69% of patients are pain free without further medical or surgical interventions (Obermann, 2010). However, different types of neuralgia which are refractory to classical neurosurgical treatment (microscopic vascular decompression) can be more efficiently treated by localised radiofrequency rhizotomy, where the surgeon goes down to the level of the brainstem to induce a loss of afferent input (Charalampaki et al., 2008, Obermann, 2010). These surgical and radiotherapeutic approaches will benefit from greater knowledge of the precise topography of these sensory pathways and their relationships to each other and to other landmarks in the brainstem. This Chapter aims to provide advanced mapping of these sensory pathways.

4.2 Specific tractography methods

For the ml: a seed region was placed at the midpons with a volume size of 11 mm^3. A ROI was placed within the sensory decussation with a volume size of 1.4 mm^3. An additional ROI was placed dorsolaterally to the red nucleus with a volume size of 6.8 mm^3. In this way the program calculated all the tracts which pass from a well known region of the ml (at the level of the midpons) and project to the sensory decussation caudalwards and the vicinity of the red nucleus rostralwards.

For the spth: A seeding region was placed at midpons, laterally to the ml with a volume size of 12 mm^3. A ROI was placed in the caudal medulla dorsolateral to the IOPr with a volume of 1.4 mm^3. An additional ROI was placed rostrally in the isthmus laterally to the ml, with a volume size of 1.7 mm^3. In this way, I used the previously known ml coordinates such as the well-defined ml topography at midpons (Paxinos et al., 2020) as anatomical landmarks to help define and identify in the other DTI scalars the precise location of the spth and then create the corresponding masks.

Subsequently:

1) For the 5n, vtt and dtt: A seeding region was placed at 5n within the mcp, with a volume size of 13 mm^3.

2) For vtt and dtt a bilateral ROI was placed approximately 4 mm more rostrally and within the pons with a volume size of 17 mm^3. The bilateral ROI masks occupied the entire territory of the ml and trigeminothalamic tracts. To define only the trigeminothalamic projections, I placed two additional ROI masks rostralwards within the thalamus, in the vicinity of and dorsolaterally to the red nucleus. These

two were placed bilaterally. For the dtt: the mask occupied a volume size of 2.2 mm^3. For the vtt: the mask occupies a volume size of 2.9 mm^3.

3) For the sp5 no ROI mask was used because the projection was clearly identified as a vertical bundle heading towards the caudal medulla. Note that the caudal part of the sp5 is reported by the program (DSI Studio) as two broken bundles because I use high FA thresholds in order to identify vertical and horizontal tracts. In reality the sp5 is a parabola open towards the midline (crescent shaped in transverse cross section) which encircles the corresponding nucleus (Sp5); (see DTI scalars in the Appendix Figs. 1, 4, 7, 10 and additional specimens in Appendix Figs. 13 (Human specimen 2), 15 (Human specimen 3), 16 (Human specimen 4), 17 (macaque)).

For all trajectories, common DTI parameters were used as follows. The angular threshold was 60%, and an FA threshold of 0.9 was applied. The step size was randomly selected from 0.5 voxel to 1.5 voxels. The fibre trajectories were smoothed by averaging the propagation direction with a percentage of the previous direction. The percentage was randomly selected from 0% to 95% (smoothing = 1.0). A total of 75,000 trajectories were calculated for ml, 45.000 trajectories for 5n, sp5, vtt and dtt, and finally 15,000 trajectories for spth. The trajectories were not manually edited and are presented exactly as generated.

4.3 Results

4.3.1 Anatomical details of the dorsal column – medial lemniscus pathway in the medulla oblongata

Fig. 4.1 shows the sensory pathways in relationship to the pons and medulla. The cu and gr fasciculi were identified as separate anatomical entities and traced ascending through the dorsolateral medulla oblongata. The cu is located lateral to the gr, posterior to the sp5, with its fibres enclosing its synaptic target, the Cu, together forming the cuneate tubercle (Fig. 4.1a, b, and Appendix Figs. 13a, b, & 17a, b). This topography of the caudal medulla is shown in slightly greater detail in Fig. 4.2a. The gr ascends in a more dorsomedial position compared to the cu, in proximity to the midline, to synapse into the Gr and form the gracile tubercle (Fig. 4.2a, Fig. 4.7, and Appendix Figs. 13a, b, & 17a, b). The second-order neuronal projections from these nuclei join together, forming the internal arcuate fibres (ia) which course as one distinct fibre bundle (Fig. 4.1c, Fig. 4.2a, b, and Appendix Fig. 13b), progressively shift dorsoventrally and lateromedially as they ascend. The ia cross the midline behind the pyramids to form the sensory decussation (xml) just prior and at the level of the inferior pole of the IOPr (Fig. 4.1c, 4.1d, and Appendix Figs. 13b, 17b). From this level the projection ascends as the ml throughout the length of the medulla oblongata between the midline and the IOPr mediolaterally, the pyramids and the tectospinal tract (ts) ventrodorsally (Fig. 4.1d to f, Fig. 4.2c, d, and Appendix Figs. 13c, d, 15a, b, 16a, b, 17c, d).

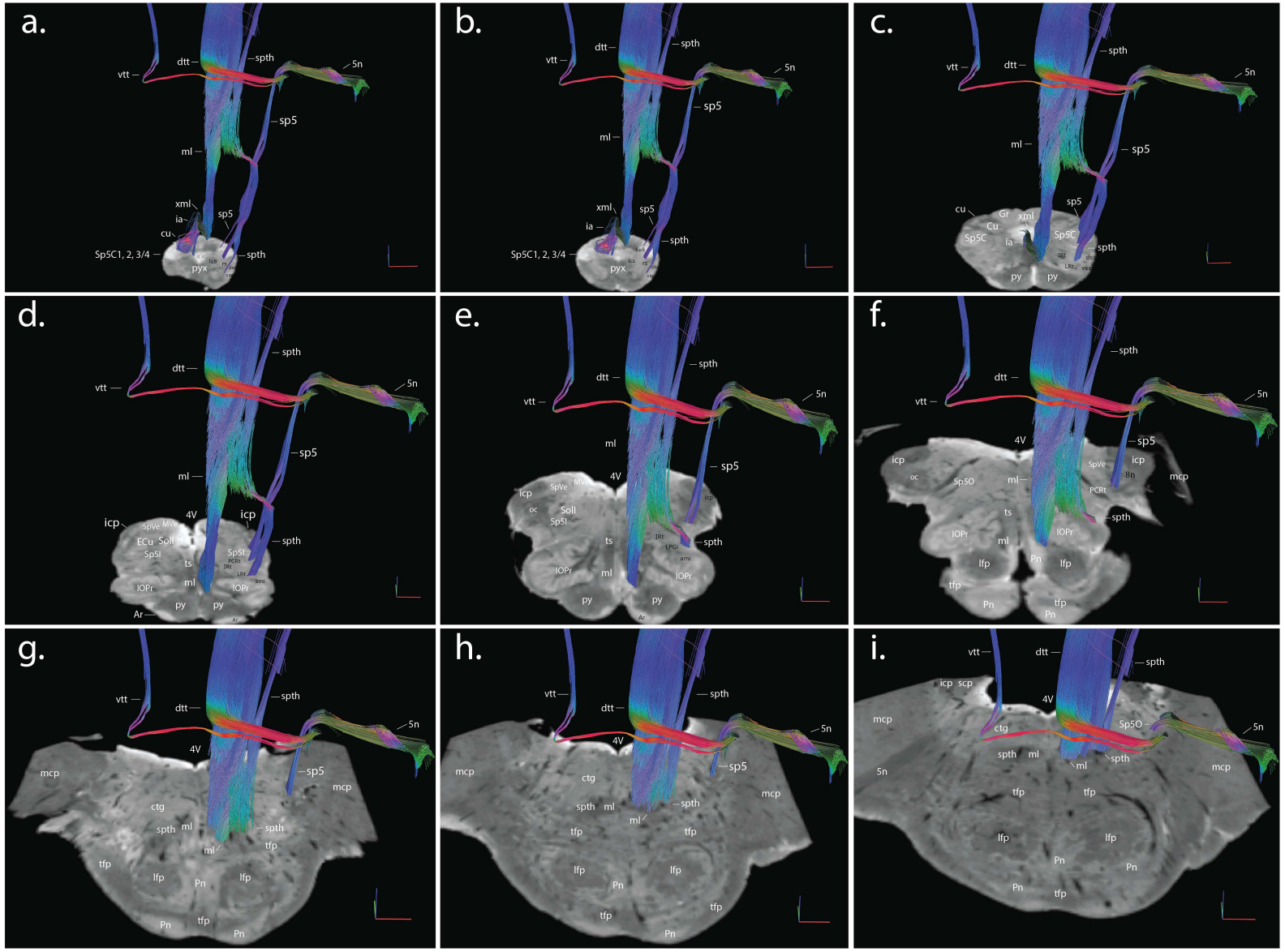
a.
vtt
dtt
spth
5n
sp5
ml
xml
ia
sp5
cu
Sp5C1, 2, 3/4
cc
pyx
spth
b.
vtt
dtt
spth
5n
sp5
ml
xml
sp5
ia
Sp5C1, 2, 3/4
pyx
spth
c.
vtt
dtt
spth
5n
ml
sp5
cu
Gr
Cu
xml
sp5
Sp5C
ia
Sp5C
spth
py
py
d.
spth
vtt
dtt
5n
sp5
ml
icp
4V
icp
spth
Ar
e.
dtt
spth
vtt
5n
ml
sp5
4V
icp
oc
Sp5I
ts
spth
IOPr
ml
IOPr
py
py
f.
spth
dtt
vtt
5n
4V
sp5
icp
oc
Sp5O
ml
icp
mcp
ts
spth
IOPr
ml
IOPr
lfp
Pn
lfp
tfp
tfp
Pn
Pn
g.
vtt
dtt
spth
5n
4V
sp5
mcp
mcp
ctg
spth
ml
spth
ml
tfp
tfp
lfp
Pn
lfp
Pn
tfp
Pn
h.
vtt
dtt
spth
5n
4V
mcp
sp5
ctg
mcp
spth
ml
spth
ml
tfp
tfp
lfp
lfp
Pn
tfp
tfp
Pn
i.
vtt
dtt
spth
icp
scp
4V
mcp
ctg
Sp5O
5n
5n
spth
ml
ml
spth
mcp
tfp
tfp
lfp
lfp
Pn
Pn
Pn
tfp

Fig. 4.1. The trajectories of the sensory pathways. *Dorsal column – medial lemniscus pathway, spth, sp5, 5n, vtt and dtt overlaid on transverse sections of the caudal part of the medulla oblongata, (a) through to the pontomedullary junction (f) and the caudal pons (g) to (i). Tractography, GRE and the remaining DTI scalars identified tracts which are colour oriented from rostrocaudal (blue), lateromedial (red) and ventrodorsal (green). The intermediate oblique orientations assume the corresponding shades (i.e yellow as the dtt in (h), ascends towards the diencephalon). The tractographic analysis was performed on human specimen 1. Abbreviations: vtt: ventral trigeminothalamic tract, dtt: dorsal trigeminothalamic tract, spth: spinothalamic tract, 5n: trigeminal nerve, sp5: spinal trigeminal tract, ml: medial lemniscus, xml: sensory decussation, ia: internal arcuate fibres, pyx: pyramidal decussation, CC: central canal, Sp5C,1,2,3/4: spinal trigeminal nucleus, caudal part, laminae one to four, Cu: cuneate nucleus, cu: cuneate fasciculus, Gr: gracile nucleus, py: pyramidal tract, Sp5C: spinal trigeminal nucleus, caudal part, icp: inferior cerebellar peduncle, scp: superior cerebellar peduncle, mcp: middle cerebellar peduncle, MVe: medial vestibular nucleus, SpVe: spinal vestibular nucleus, ECu: external cuneate nucleus, SolI: solitary nucleus, interstitial part, Sp5I: spinal trigeminal nucleus, interpolar part, ts: tectospinal tract, IOPr: inferior olive, principal nucleus, 4V: fourth ventricle, oc: olivocerebellar tract, Sp5O: spinal trigeminal nucleus, oral part, lfp: longitudinal fibres of the pons, tfp: transverse fibres of the pons, Pn: pontine nuclei, PCRt: parvicellular reticular nucleus, IRt: intermediate reticular nucleus, LRt: lateral reticular nucleus, LPGi: lateral paragigantocellular nucleus, ami: amiculum, ctg: central tegmental tract, Ar: arcuate nucleus, 8n: vestibulocochlear nerve.*

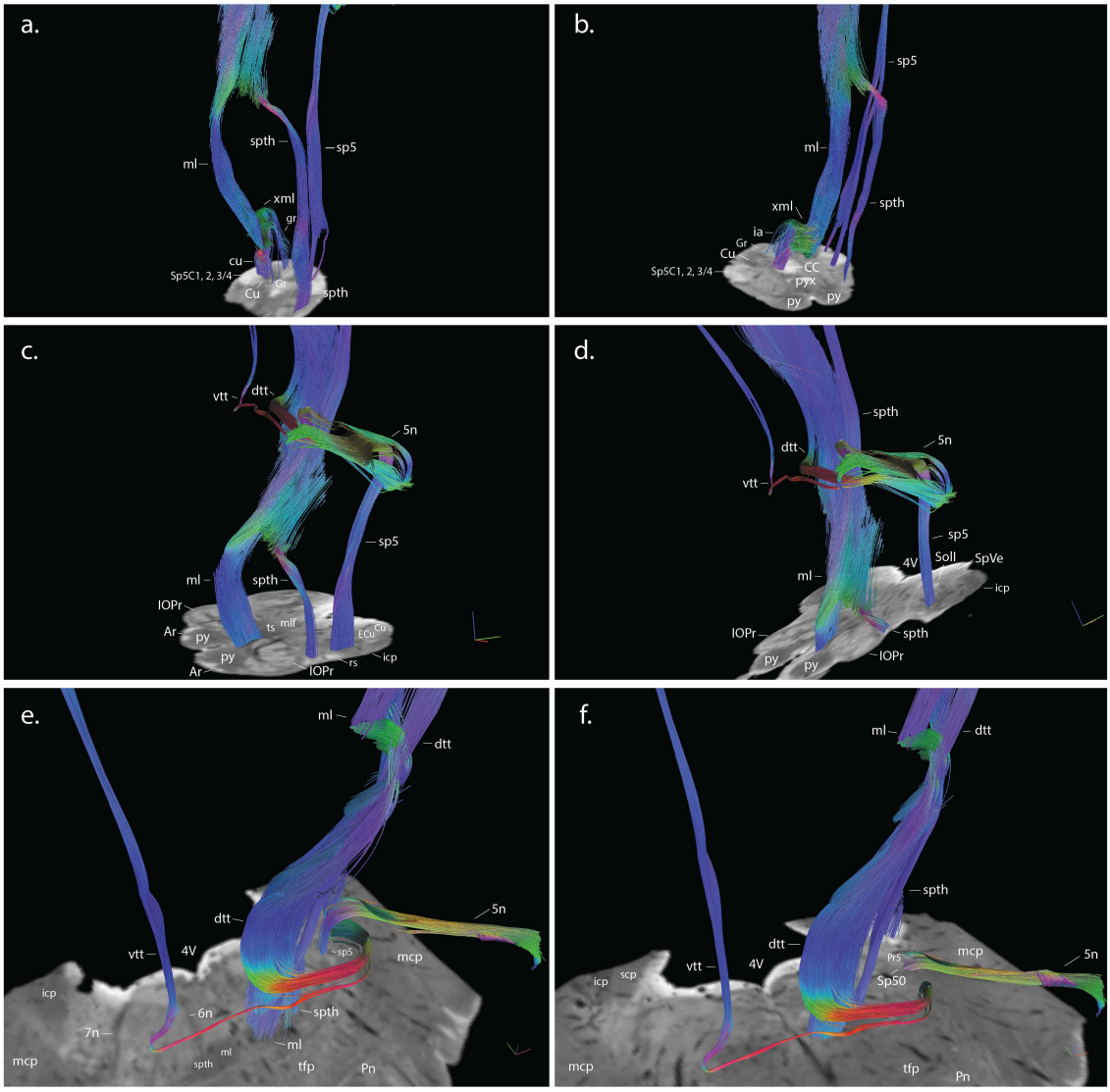
a.
spth
sp5
ml
xml
gr
cu
Sp5C1, 2, 3/4
Gr
Cu
spth
b.
sp5
ml
xml
spth
ia
Gr
Cu
Sp5C1, 2, 3/4
CC
pyx
py
py
c.
vtt
dtt
5n
sp5
ml
spth
IOPr
Ar
py
ts
mlf
Ecu
Cu
py
icp
Ar
IOPr
rs
d.
spth
dtt
5n
vtt
sp5
4V
Soll
SpVe
ml
icp
IOPr
spth
py
py
IOPr
e.
ml
dtt
dtt
5n
vtt
4V
sp5
mcp
icp
6n
spth
7n
ml
ml
spth
mcp
tfp
Pn
f.
ml
dtt
spth
dtt
mcp
5n
vtt
4V
Pr5
icp
scp
Sp5O
mcp
tfp
Pn

Fig. 4.2. Oblique sections through the brainstem starting from the caudal medulla oblongata until the level of the sensory root of the 5n in the pons. *The cu and gr fasciculi (a) are shown traced on one side of the brainstem, whereas the spth ascends ventrally and sp5 dorsally, on the other side. In (b) the gr and cu as they ascend and terminate into the Gr and Cu and from there the internal arcuate fibres (in green) course ventromedially to cross and ascend in (c) as ml. Note the precise boundaries in (c) of the ml behind the pyramids and in front of the ts. The spth is placed laterally and the sp5 dorsally. In (d) the ml and spth begin to converge as the two projections ascend rostralwards. From the rostral pole (d) of the IOPr the two projections ascend as adjacent anatomical entities. In (e) we identified the sensory root of the 5n, the vtt (which crosses on the other side) and dtt (which ascends ipsilaterally). In (e) it has been identified the topography of the rostral part of the sp5 and in (f) note the relationship at the most precise level, between the Pr5, Sp5O and sp5 (magenta fibres). The leader line points at the exact location of the Sp5O. The tractographic analysis was performed on human specimen 1. On the FAC maps red, blue, and green represent anisotropy along medial-lateral, rostral-caudal, and ventral-dorsal orientations, respectively. Abbreviations: vtt: ventral trigeminothalamic tract, dtt: dorsal trigeminothalamic tract, spth: spinothalamic tract, 5n: trigeminal nerve, sp5: spinal trigeminal tract, ml: medial lemniscus, xml: sensory decussation, ia: internal arcuate fibres, cu: cuneate fasciculus, pyx: pyramidal decussation, CC: central canal, Sp5C,1,2,3/4: spinal trigeminal nucleus, caudal part, laminae one to four, Cu: cuneate nucleus, Gr: gracile nucleus, py: pyramidal tract, icp: inferior cerebellar peduncle, scp: superior cerebellar peduncle, mcp: middle cerebellar peduncle, SpVe: spinal vestibular nucleus, ECu: external cuneate nucleus, SolI: solitary nucleus, interstitial part, ts: tectospinal tract, mlf: medial longitudinal fasciculus, IOPr: inferior olive, principal nucleus, 4V: fourth ventricle, Sp5O: spinal trigeminal nucleus, oral part, Pr5: principal sensory trigeminal nucleus, lfp: longitudinal fibres of the pons, tfp: transverse fibres of the pons, Pn: pontine nuclei, Ar: arcuate nucleus, rs: rubrospinal tract, 6n: abducens nerve, 7n: facial nerve.*

4.3.2 Anatomical details of the spth in the medulla oblongata

The spth ascends through the ventrolateral funiculus in the caudal medulla where it is confined by the lateral corticospinal tract medially, by the rubrospinal (rs) and spinocerebellar tracts (vsc, dsc) dorsolaterally (Fig. 4.1a, Fig. 4.2a, and Appendix Figs. 13a, b, 17a). As it ascends, more rostrally, through the caudal medulla it is confined by the territories occupied by the lateral reticular nucleus (LRt) and intermediate reticular nucleus (IRt) ventromedially, while maintaining the same topography (rs, vsc, dsc) dorsolaterally (Fig. 4.1b, c, Fig 4.2b, Fig. 4.7, and Appendix Figs. 13b, 17b). At more rostral levels, while the territory occupied by the LRt is being displaced by the IOPr, the spth is topographically placed behind the IOPr and lateral to the IRt, whereas dorsolaterally is confined by the vsc, dsc, (Figs. 4.1d to f, Figs 4.2c, d, and Appendix Figs. 13c, 15a, 16a, 17c). As the spth courses through the mid and rostral medulla, it is situated dorsolateral to the IOPr and in proximity to the lateral parts of the lateral paragigantocellular (LPGi) and IRt (Fig. 4.1e and Appendix Figs. 13d, 15b, 16b, 17d). At the level of the rostral pole of the IOPr while the territory occupied by the same nucleus is obliterated (as the IOPr is no longer present), the spth begins abruptly to shift medially and converges with the fibres that constitute the ml (Fig. 4.1e to g, Fig. 4.2a to d, Fig. 4.3, and Appendix Figs. 13e, f, 15c, 16c, 17e).

Note the discontinuities in the ascending fibres in Figs, 4.2 a,c,d and 4.7, just where the spth ascends at the level of the rostral pole of the IOPr. Such discontinuities can occur in deterministic tractography where the deterministic tensor generates several broken streamlines ((Sarwar et al. (2019); Fig. 3 of their article)

that fail to traverse the intersecting trajectories within various voxels. These discontinuities may also arise from various bundles changing the degree of compactness or direction. In this case, the ascending spth is more compact while courses the medulla and becomes wider when it courses more rostrally. The bundles also twist, for example the ml and spth, through the pons and midbrain (see Fig. 4.1 & Fig. 4.4). This discontinuity was seen regardless of different FA thresholds applied during the experiments.

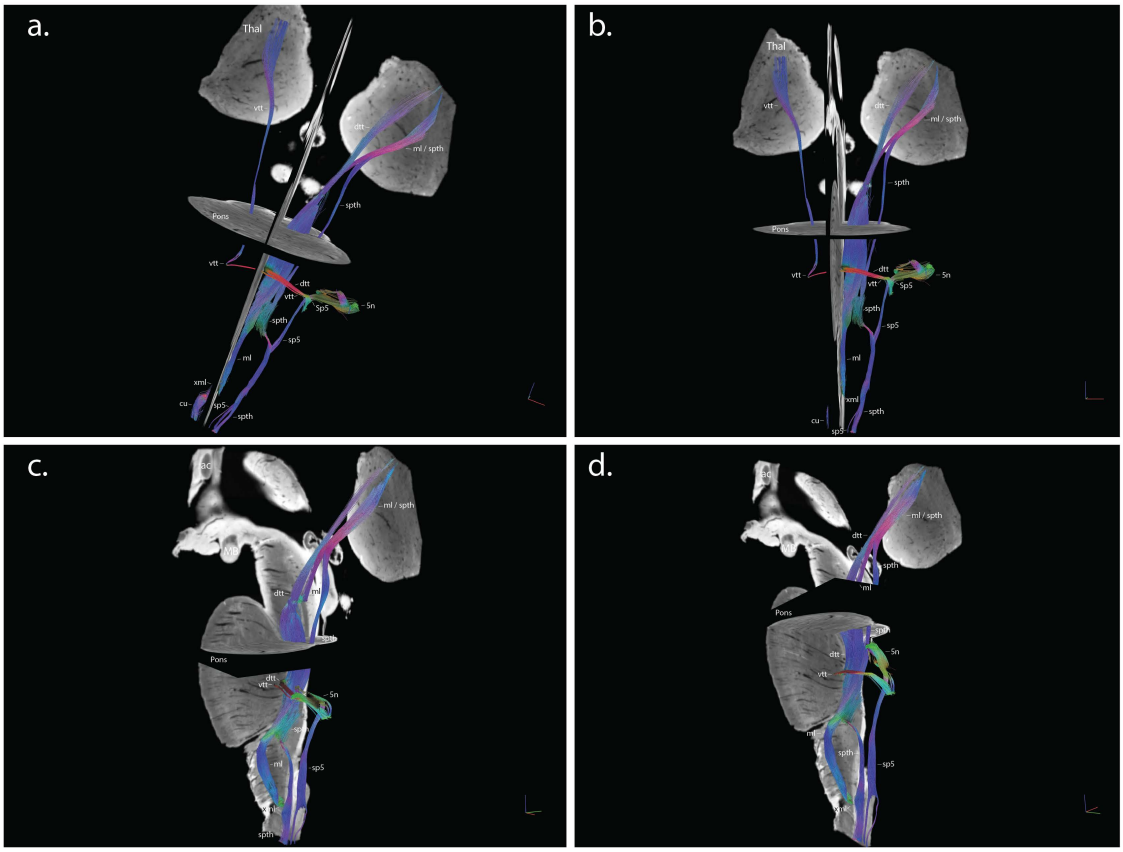

Fig. 4.3. Sensory pathways shown in longitudinal and oblique axis. Note the anatomical information shown by the GRE background in sagittal, transverse and coronal MRI planes as they intersect and interrelate with the tractography bundles. *Note in (a) and (b) the xml at which level the internal arcuate fibres cross from one side of the medulla to the other and ascend as ml. In (c) and (d) note the level where the vtt crosses to join the contralateral pain pathways and ascend towards the thalamus. In addition, note that the caudal part of the sp5 assumes the form of a parabola which is open towards the midline (see Appendix Figs. 1, 4, 7, 10 - DTI contrasts). The tractographic analysis was performed on human specimen 1. Abbreviations: vtt: ventral trigeminothalamic tract, dtt: dorsal trigeminothalamic tract, spth: spinothalamic tract, 5n: trigeminal nerve, sp5: spinal trigeminal tract, ml: medial lemniscus, xml: sensory decussation, ia: internal arcuate fibres, cu: cuneate fasciculus, ac: anterior commissure, MB: mammillary body.*

4.3.3 Topography of the spinal trigeminal tract (sp5) from the pons to the caudal medulla oblongata

The most rostral part of the sp5 is confined by the middle cerebellar peduncle laterally, by the transverse fibres of the pons ventrally, by the spinal trigeminal nucleus, oral part (Sp5O) and principal sensory trigeminal nucleus (Pr5) medially (Fig. 4.1i, and Appendix Figs. 13f, e, 15d, c, 16d, c, 17e). As it ipsilaterally descends the sp5 progressively shifts medioventrally in proximity to the Sp5O and parvicellular reticular nucleus (PCRt) until it reaches the pontomedullary junction to be confined by the 8th cranial nerve laterally, and by the solitary tract (sol) and spinal vestibular nucleus (SpVe) dorsally (Fig. 4.1h, g, f, Fig. 4.2f, e, d, and Appendix Figs. 13,e, 15c, 16c, 17e, d). At the level of the rostral pole of the IOPr, the sp5 further shifts medially while it descends. It is confined by the spth ventrally, by the spinal trigeminal nucleus, interpolar part (Sp5I) medially, by the SpVe, the solitary nucleus, interstitial part (SolI) dorsally, by the inferior cerebellar peduncle (icp) dorsolaterally (Fig. 4.1f, e, d, Fig. 4.2d, c, and Appendix Figs. 13d, 15b, a, 16b, a, 17d, c). Caudal to the xml the sp5 approaches even more the spth ventrally, whereas it is confined by the cu and external cuneate nucleus (ECu) dorsally, and by the icp and dsc dorsolaterally. Finally, in the caudal part of the medulla the sp5 courses in the vicinity of the spth ventrally, the spinal trigeminal nucleus, caudal part (Sp5c) medially, the complex territory occupied by the lateral pericuneate (LPCu), cu, ECu and Cu dorsally, and icp laterally (Fig. 4.1c, b, a, Fig. 4.2a, b, and Appendix Figs. 13c, b, a, 17b, a). Note that in my tractographic analysis the caudal part of the sp5 is presented split due to the high FA threshold that I use for the vertical bundles.

4.3.4 Anatomical details of the ml, spth, 5n, vtt and dtt in the pons

After the pontomedullary junction the bundles that form medially the ml and laterally the spth, begin to converge as adjacent anatomical entities and shift progressively dorsally while ascending to more rostral levels throughout the pons, to occupy a position behind the transverse fibres of the pons. The ml and spth are confined dorsally by the pontine reticular nucleus, oral part (PnO) until the midpons, by the superior cerebellar peduncle (scp) from mid to rostral pons. Dorsolaterally the two projections are confined by the ventrolateral tegmental area (VLTg) and the lateral lemniscus (ll), throughout the pontine tegmentum. The spth constitutes about $1/4^{th}$ of the entire territory of the three projections (Fig. 4.1f to I, Fig. 4.2e, f, Fig. 4.3, Fig. 4.4d, and Appendix Figs. 13f, g, h, 15d, e, f, 16d, e, f, 17e, f, g).

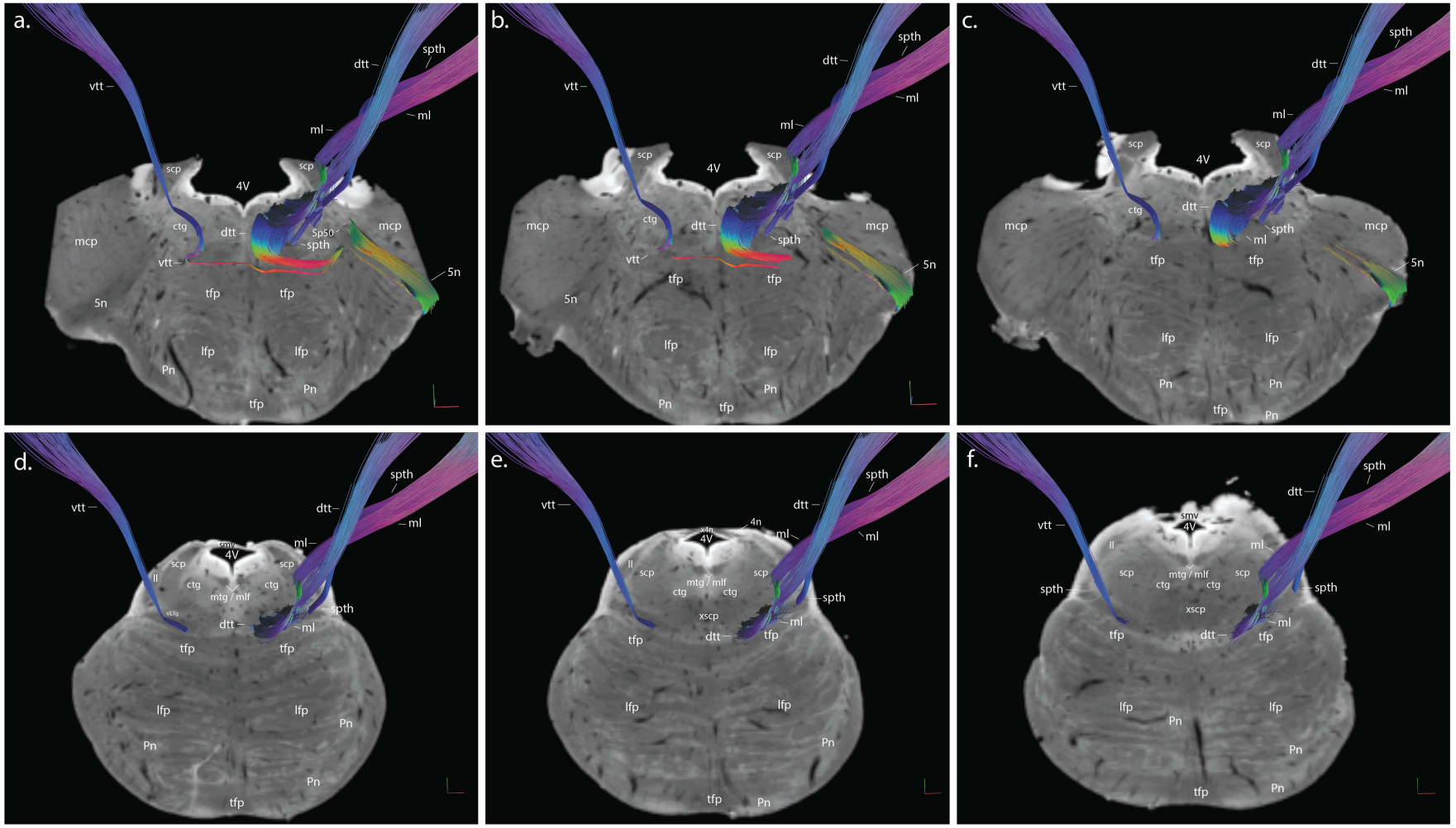
a.
vtt
dtt
spth
ml
scp
4V
ctg
mcp
Sp50
5n
tfp
lfp
Pn
b.
c.
d.
smv
mtg / mlf
vtfg
e.
4n
xscp
f.

Fig. 4.4. Cross sections through the pons Varolii. *Representative images showing the relationship between the ipsilateral and contralateral pain pathways. In (a) and (b) the sensory root of 5n (in green) as slices through the mcp to approach the Pr5 and Sp5. The course of the vtt and dtt (in red) has been identified within the transverse fibres of the pons. The two projections finally bend (the vtt after having crossed on the other side of the pons) and ascend towards the thalamus. From (d) to (f) while the fibre bundles that constitute the pain pathways approach the rostral pons they begin to shift from a mediolateral to a more oblique ventrodorsal direction. The tractographic analysis was performed on human specimen 1. Abbreviations: vtt: ventral trigeminothalamic tract, dtt: dorsal trigeminothalamic tract, spth: spinothalamic tract, 5n: trigeminal nerve, ml: medial lemniscus, scp: superior cerebellar peduncle, mcp: middle cerebellar peduncle, 4V: fourth ventricle, Sp5O: spinal trigeminal nucleus, oral part, lfp: longitudinal fibres of the pons, tfp: transverse fibres of the pons, Pn: pontine nuclei, PCRt: parvicellular reticular nucleus, ctg: central tegmental tract, 4n: trochlear nerve, x4n: decussation of the trochlear nerve, ll: lateral lemniscus, smv: superior medullary velum, mtg: mammillotegmental tract, mlf: medial longitudinal fasciculus, VLTg: ventrolateral tegmental area.*

At about 6 millimetres (mm) more rostrally from the pontomedullary junction in the human, and 3 mm more rostrally in the macaque, the sensory root of the trigeminal nerve (5n) enters obliquely the pons following a rostrocaudal, ventrodorsal and lateromedial direction, surging through the middle cerebellar peduncle (mcp) to convey its sensory root (s5) to both the Pr5 and the Sp5 which is located ventrally to the former (Fig. 4.2e, f, Fig 4.4a to c, a, and Appendix Figs. 13g, 15e, 16e, 17f, e). The vtt and dtt course in the vicinity of Pr5. Tractography showed that the fibres that constitute these two tracts (vtt and dtt) travel within the transverse fibres of the pons (Fig. 4.2e, f, Fig 4.4a, b). The vtt is placed ventrally, whereas the dtt runs dorsally to the former. As the dtt reaches the midline bends and ascends, ipsilaterally, to interweave with the fibres of the ml, occupying a mediodorsal position throughout the length of the pons, whereas the vtt crosses the midline to ascend contralaterally within the fibres of the contralateral ml and follows the same direction as the ipsilateral dtt until the thalamus (Fig. 4.2e, f and Fig. 4.4a to c). In the rostral pons, all three projections (tth, ml and spth) begin to shift obliquely anticlockwise from a mediolateral to a ventrodorsal direction until meeting the junction of rhombomere one and two, where the xscp is found (pontomesencephalic junction; Fig. 4.4d to f, Fig. 4.5a, and Appendix Figs. 13h, i, 15f, g, 16f, g, 17g. h).

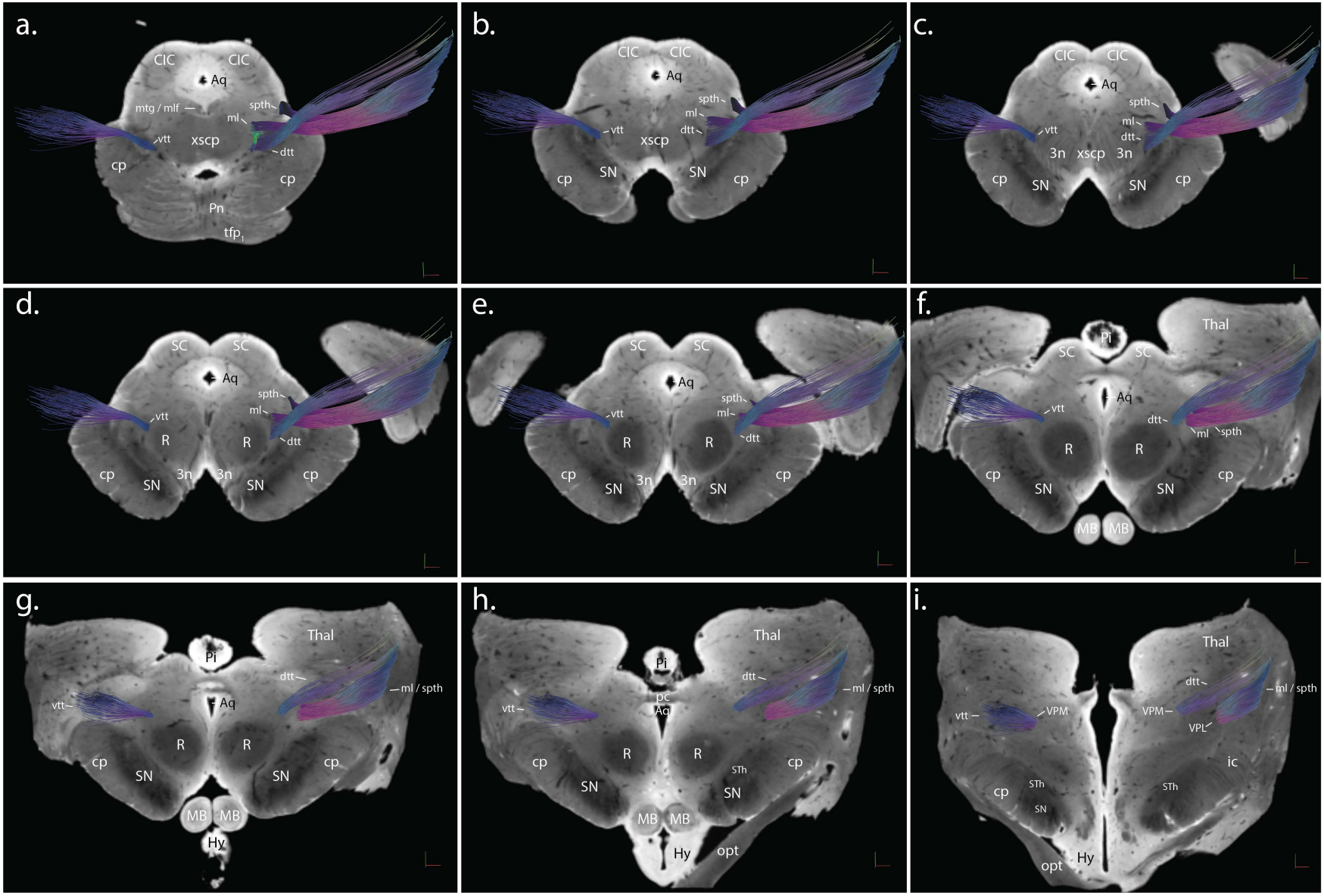
a.
CIC
CIC
Aq
mtg / mlf
spth
ml
vtt
xscp
dtt
cp
cp
Pn
tfp$_i$
b.
CIC
CIC
Aq
spth
ml
vtt
dtt
xscp
cp
SN
SN
cp
c.
CIC
CIC
Aq
spth
ml
vtt
dtt
3n
xscp
3n
cp
SN
SN
cp
d.
SC
SC
Aq
spth
ml
vtt
R
R
dtt
cp
SN
3n
3n
SN
cp
e.
SC
SC
Aq
spth
ml
vtt
R
R
dtt
cp
SN
3n
3n
SN
cp
f.
Thal
Pi
SC
SC
Aq
vtt
dtt
ml
spth
R
R
cp
SN
SN
cp
MB
MB
g.
Thal
Pi
dtt
ml / spth
vtt
Aq
R
R
cp
SN
SN
cp
MB
MB
Hy
h.
Thal
Pi
dtt
ml / spth
pc
vtt
Aq
R
R
STh
cp
cp
SN
SN
MB
MB
Hy
opt
i.
Thal
dtt
ml / spth
vtt
VPM
VPM
VPL
ic
cp
STh
STh
SN
opt
Hy

Fig. 4.5. Cross sections through the brainstem, starting from the pontomesencephalic junction (rhombomere one and two) until the diencephalon and the nuclei of termination of the pain pathways. *In (a) the ml begins to shift dorsally while the tth ascends internally to the SNC. The spth has shifted more dorsolaterally in front of the ll. Note the symmetrical position that the vtt (contralateral) and dtt (ipsilateral) occupy while they ascend towards the thalamus. In (b) and (c) the projections pass through the isthmus. Note the anatomical relationships between the bundles and the 3n in (c). From (d) to (f) the ml begins to converge with the spth while ascending through the mRt, laterally to the red nucleus and finally the tth shifts dorsally so that the three projections align mediolaterally (f). From (g) to (i) the tth ascends and synapses into the VPM, whereas the ml and spth as a single anatomical entity terminate into the VPL. The tractographic analysis was performed on human specimen 1. Abbreviations: vtt: ventral trigeminothalamic tract, dtt: dorsal trigeminothalamic tract, spth: spinothalamic tract, 5n: trigeminal nerve, ml: medial lemniscus, Aq: aqueduct, Pn: pontine nuclei, tfp1: most ventral transverse fibre of the pons, 4V: fourth ventricle, Sp5O: spinal trigeminal nucleus, oral part, lfp: longitudinal fibres of the pons, tfp: transverse fibres of the pons, PCRt: parvicellular reticular nucleus, ctg: central tegmental tract, x4n: decussation of the trochlear nerve, ll: lateral lemniscus, smv: superior medullary velum, mtg: mammillotegmental tract, mlf: medial longitudinal fasciculus, SC: superior colliculus, CIC: central nucleus of the inferior colliculus, cp: cerebral peduncle, xscp: decussation of the superior cerebellar peduncle, R: red nucleus, 3n: oculomotor nerve, SN: substantia nigra, MB: mammillary body, Thal: thalamus, VMP: ventral posteromedial nucleus, VPL: ventral posterolateral nucleus, STh: subthalamic nucleus of Luys, opt: optic tract.*

4.3.5 Topography of the ml, spth and tth in the isthmus, midbrain and thalamus

As the fibre bundles project through the isthmus, the tth shifts ventrally to ascend internally to the substantia nigra pars compacta (SNC) and laterally to the decussation of the superior cerebellar peduncle (xscp), whereas the ml and spth are located more posteriorly between the isthmic reticular formation (isRt) medially, the ll, dorsally (Fig. 4.5a to c, Fig. 4.6a, b, and Appendix Figs. 13i, j, 15g, h, 16g, i, 17h, i). Furthermore, I observe that the fibres that constitute the ml detach and deviate from the main bulk of the ascending sensory pathways and progressively shift posteriorly while ascending throughout the isthmus, in proximity to the xscp, (Fig. 4.5a to c, Fig. 4.6b and Fig. 4.7). Similarly, the spth shifts to occupy the most lateral and external position between the ml ventrally, the ll dorsally, and the brachium of the inferior colliculus (bic) laterally, through the isthmus passing the xscp until the level of the exit of the third cranial nerve (3n), (Fig. 4.5c, Fig. 4.6c, Fig. 4.7, and Appendix Figs. 13j, 17i). At the level of the red nucleus the ascending sensory pathways maintain the same pattern as they ascend through the mesencephalic reticular formation (mRt), whereas at the rostral pole of the red nucleus the tth shifts more dorsally (Fig. 4.5e) to align mediolaterally with the ml and spth (Fig. 4.5f, Fig. 4.6d, and Appendix Figs. 13k, 17j).

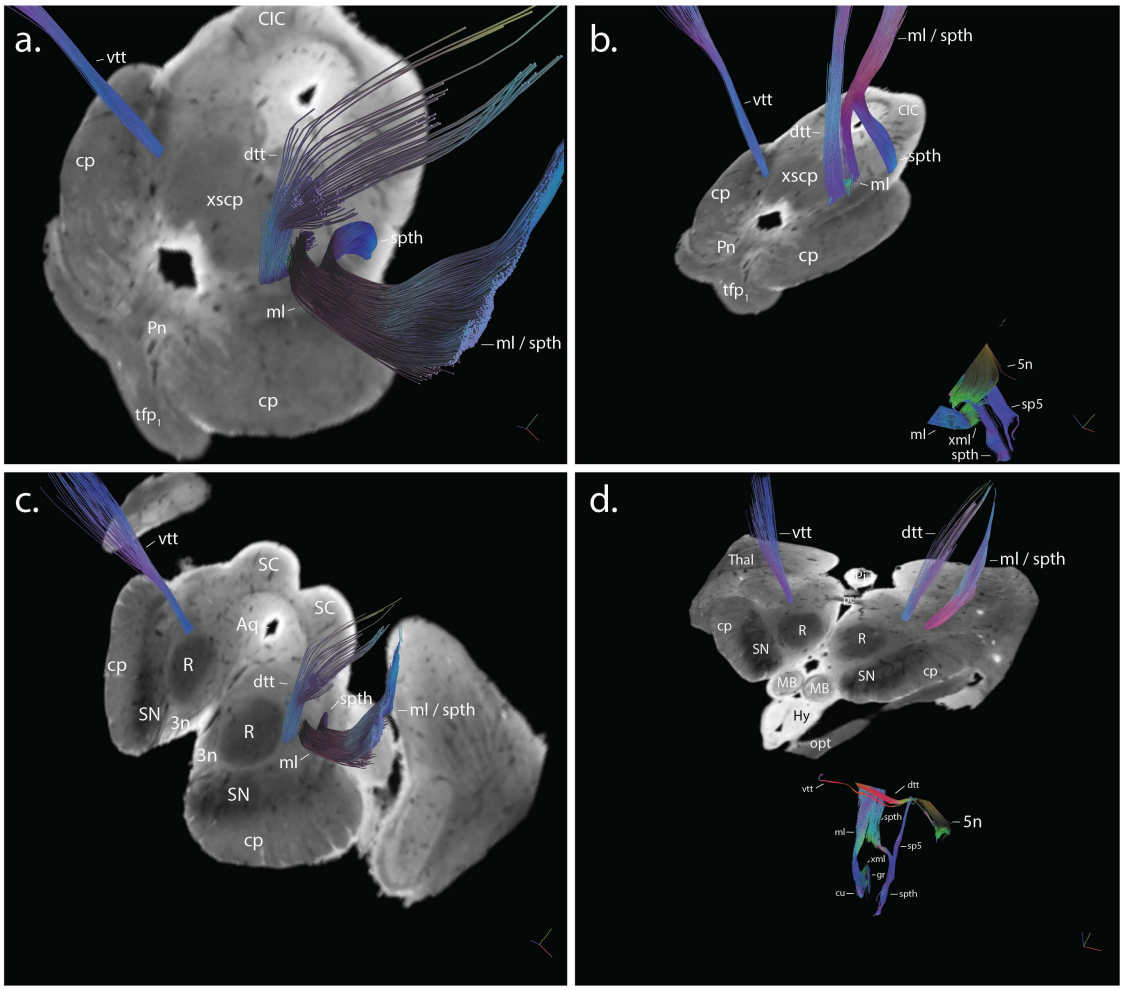

Fig. 4.6. Oblique sections from the pons-midbrain junction in (a) and (b) through the midbrain in (c) to the diencephalon in (d) that show the relationship between the pain pathways and the adjacent anatomical structures only feasible with this technique. *The tractographic analysis was performed on human specimen 1. Abbreviations: vtt: ventral trigeminothalamic tract, dtt: dorsal trigeminothalamic tract, spth: spinothalamic tract, 5n: trigeminal nerve, sp5: spinal trigeminal tract, ml: medial lemniscus, xml: sensory decussation, cu: cuneate fasciculus, gr: gracile fasciculus, pc: posterior commissure, MB: mammillary body, Pi: pineal gland, Hy: hypothalamus, SN: substantia nigra, opt: optic tract, R: red nucleus, CIC: central nucleus of the inferior colliculus, xscp: decussation of the superior cerebellar peduncle, Pn: pontine nuclei, tfp1: most ventral transverse fibre of the pons, cp: cerebral peduncle.*

In the diencephalon, at the level where the mamillary bodies align with the pineal gland (Fig. 4.5f) the ml and the spth begin to converge as they ascend through the prosomere 1 reticular formation (p1Rt) and form a single anatomical entity from the level of the caudal pole of the hypothalamus heading rostralwards (Fig. 4.5g and Fig. 4.6d). As the three pathways ascend, they progressively shift posterolaterally until the tth reaches its target at the VPM whereas the ml alongside the spth terminates as a united bundle into the VPL of the thalamus (Fig. 4.7, and Appendix Figs. 13l, 17k).

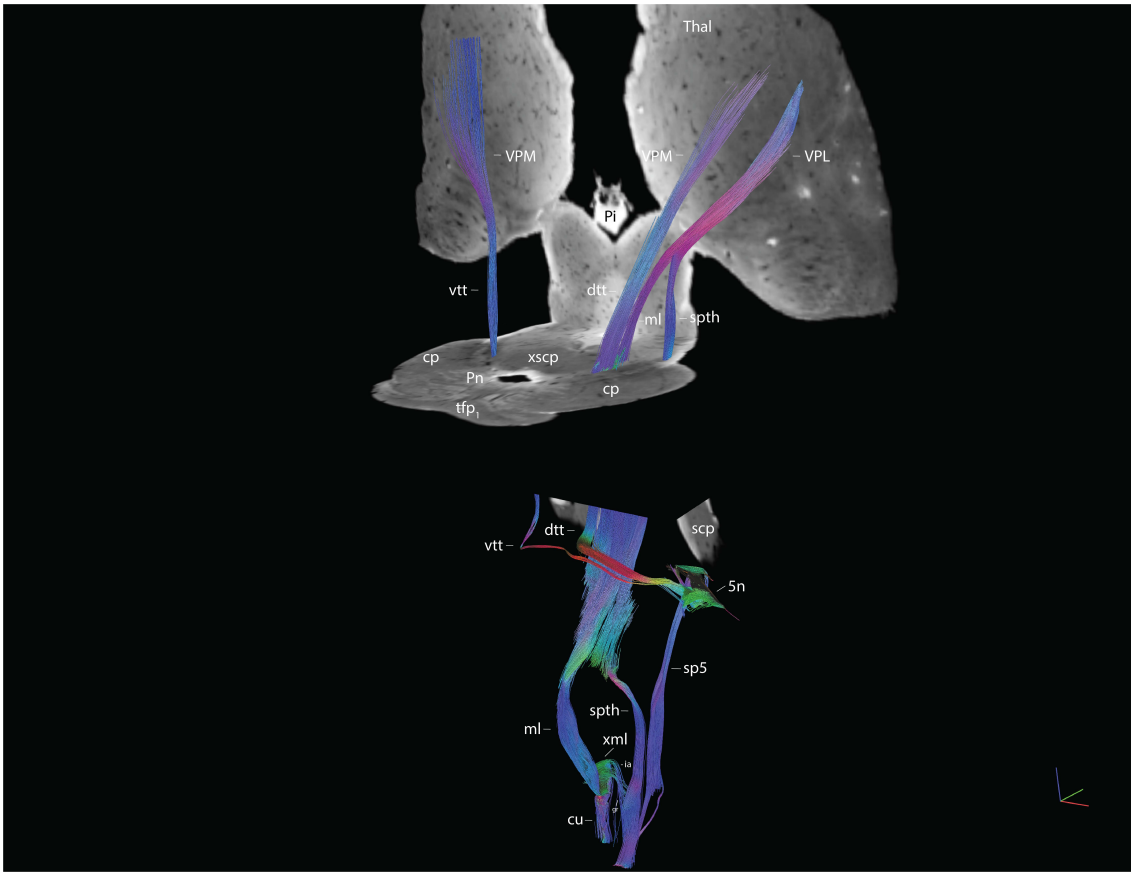

Fig. 4.7. 3D overview of the dorsal column – medial lemniscus pathway, spth, 5n, sp5, vtt and dtt throughout the brainstem and thalamus. *The tractographic analysis was performed on human specimen 1. Abbreviations: vtt: ventral trigeminothalamic tract, dtt: dorsal trigeminothalamic tract, spth: spinothalamic tract, 5n: trigeminal nerve, sp5: spinal trigeminal tract, ml: medial lemniscus, xml: sensory decussation, cu: cuneate fasciculus, gr: gracile fasciculus, ia: internal arcuate fibres, scp: superior cerebellar peduncle, MB: mammillary body, Pi: pineal gland, Thal: thalamus, VPM: ventral posteromedial nucleus, VPL: ventral posterolateral nucleus, xscp: decussation of the superior cerebellar peduncle, Pn: pontine nuclei, tfp1: most ventral transverse fibre of the pons, cp: cerebral peduncle.*

4.4 Discussion

4.4.1 Implications for surgical treatment of pain and brain trauma

The present study maps the sensory pathways such as the dorsal-column medial lemniscus pathway (dcml), the spinothalamic tract (spth), the segment of the trigeminal nerve within the brainstem, the spinal trigeminal tract (sp5), and trigeminothalamic tracts (tth) through ultra-high field MRI and tractography on human and macaque postmortem tissue. The aforementioned projections also known as pain pathways because of the morbidity associated with a lesion throughout their course (Kitahata, 1993), have been identified, herein, in the medulla oblongata, basilar pons, midbrain and thalamus. The cuneate (cu) and gracile (gr) fasciculi are identified as separate anatomical entities. The internal arcuate fibres that arise after the cu and gr synapse into the corresponding nuclei cross the midline behind the pyramids to form the sensory decussation (xml). From this level, the projection ascends as medial lemniscus (ml) throughout the pons, midbrain and finally terminates into the ventral posterolateral nucleus (VPL) of the thalamus. The pathway transiting via these general landmarks through the medulla, pons, midbrain and then finally terminating in the ventral tier of the thalamus is in alignment with previous studies (Xiao et al., 2016, Hagmann et al., 2003, Qiu et al., 2012). The course of the ml, spth, and tth through the pons to their final terminations in the thalamus correspond with the most detailed atlas of the human brainstem (Paxinos et al., 2020). This thesis presents a 3D detailed topography of these sensory pathways and the relationship between the adjacent structures. In addition, the present study shows in detail the course and topography of the spth as it ascends through the caudal medulla to reach the pons and midbrain and finally it converges with the ml to

terminate into the VPL. The termination of the spth in the thalamus is consistent with conclusions from experimental lesions in the spinal cord of *Macaca mulatta* (Hodge and Apkarian, 1990, Kerr, 1975). Moreover, the course of the sensory root of the trigeminal nerve and the spinal trigeminal tract (sp5) as it descends towards the medulla are precisely mapped. This course of the sp5 is consistent with that in the *Macaca mulatta* (Warren and May, 2013). In this paper, the authors injected the Pr5 (principal sensory trigeminal nucleus) with WGA-HRP and identified labelled neurons through the dorsolateral pons and medulla oblongata, and ultimately within the dorsal horn of the spinal cord (DH). Interestingly, we confirm this finding on the FAC of the macaque (Appendix Fig. 17a). Finally, the ventral and dorsal trigeminothalamic tracts (vtt, dtt) were also traced, being bilateral bundles ascending towards the ventral posteromedial (VPM) nucleus of the thalamus. The topography of the final segment of the trigeminothalamic tract in the thalamus was also consistent with Friedberg et al. (2004) who specifically followed the sensory information pathway from neurons which innervate the whisker follicles in the rat's face, through the Sp5 and Pr5 to the VPM of the thalamus.

The complexity of the fibre architecture in the human brainstem and the inability to precisely map in 3D the pain pathways due to the lack of sophisticated methods are some of the reasons which make chronic pain often difficult to treat (Dia Tine et al., 2009). More precisely, surgical interruption of a particular tract in order to mitigate chronic pain is not always effective in reducing pain symptoms due to our lack of knowledge about the anatomical relationship between the major sensory pathways (dorsal column – medial lemniscus pathway, spth, 5n, sp5, vtt and dtt). For example, microscopic decompression or interruption of a particular tract of the entire

pathway (in cases of trigeminal neuralgia associated with a solitary pontine lesion; Tohyama et al. (2020)) within the brainstem could be used in cases of chronic pain refractory to classical pharmacological or surgical procedures such as brain stereotactic radiosurgery.

The present study may also have clinical benefits in relation to brainstem traumatic lesions. Various authors report a narrowing of the spth after two weeks in patients with head trauma that can subsequently result in partial tearing of the spth in the lower brainstem. While MRI scanners and subsequent tractography were able to identify narrowing of the spth compared to normal controls, the resolution of the images was not high enough for the authors to identify the topography of the spth thus enabling neurosurgical intervention (Jang et al., 2016). The detailed maps reported herein, which offer a precise location of the pain pathways could be combined with in vivo MRI in such patients to study the topography and detect silent lesions in relation to symptomatology, obtain prognostic information, follow up and guide rehabilitation in relation to neuronal proliferation during recovery, and potentially aid therapeutic interventions such as transcranial magnetic stimulation (TMS) for pain alleviation (George et al., 2003).

4.4.2 Advances in knowledge of the sensory tracts

Our knowledge obtained with histology and microdissection techniques about the anatomy of the ml described that the neurons of the dorsal column nuclei cross over (sensory decussation) to the other side of the medulla oblongata as internal

arcuate fibres to form the ml (Rodríguez-Mena and Türe, 2017, Romanowski et al., 2011). In the pons the ml had been shown to ascend in front of the trigeminal lemniscus and behind the transverse fibres of the pons, whereas for the rest of the brainstem the axons were known to ascend behind the red nucleus to finally synapse into the VPL nucleus of the thalamus (Xiao et al., 2016, Kamali et al., 2009, Qiu et al., 2012). All these studies validate the gross anatomy of the ml within the brainstem and thalamus, and are in alignment with my current findings of a detailed 3D map of the sensory projections from the caudal medulla until the thalamus, highlighting the relationship between these pain pathways.

To a minor degree it was known about the descriptive anatomy of the spth in the human brainstem and thalamus. Various authors report that the spth as part of the anterolateral system in the medulla oblongata courses without precise boundaries between the IOPr and the Sp5. In the pons and midbrain the spth was reported to course dorsolaterally to the ml and finally terminates into the VPL of the thalamus (Kerr, 1975, Khalid and Tubbs, 2017).

This thesis provides a detailed study in which I used ultra-high-field MRI, deterministic tractography and DTI scalars alongside the structural anatomical GRE contrast to define standard anatomical landmarks between the sensory pathways and the adjacent nuclei and fibre bundles. The current dataset provides advanced anatomical knowledge unspecified at this precise level anywhere else in literature, combining the sensory tracts with more than 117 anatomical areas, parts and structures through the brainstem and thalamus.

4.4.3 Advanced resolution of the trigeminal pathways

Finally, the course of the sensory root of the trigeminal nerve, the vtt and the dtt in the human brainstem has been mapped, herein, using tractographic analysis derived from ultra-high resolution diffusion weighted imaging (DWI). This study identifies two bundles. One bundle crosses the midline and ascends contralaterally as the vtt, and a second bundle runs dorsally to the former and ascends ipsilaterally as dtt. In support of the presence of two discrete fibre bundles, it has been documented in kittens ascending bilateral projections from the Pr5 to the thalamus with the uncrossed component being smaller than the crossed one (Torvik, 1957). Subsequently, Rausell and Jones (1991) identified in the monkey, bilateral somatosensory afferents through distinct compartments of the VPM, with these afferents then projecting to the primary somatosensory cortex. Finally, functional MRI (fMRI) in humans has shown that unilateral noxious stimulation of the orofacial region activates both the ipsilateral and contralateral thalami, insulae, and primary somatosensory cortices (Nash et al., 2010) which is consistent with the identification in the present study of bilateral ascending ventral and dorsal trigeminothalamic projections.

While the above studies are supported by the present work, there has been some controversy surrounding the course of the vtt and dtt. Henssen et al. (2019) used ultra-high-field MRI and FAC sections combined with polarized light microscopy (PLM) in human postmortem tissue to identify the vtt and dtt. The authors reported that the sensory root of the trigeminal nerve bifurcates into the ventral and dorsal trigeminothalamic tracts (vtt & dtt). Subsequently, the vtt is

reported to project medially in a red region in which the authors delineated as medial lemniscus (ml). This disagrees with our delineations in which the red region is part of the transverse fibres of the pons, whereas we find the ml to project rostrocaudally (blue fibres) in the pontine tegmentum. Our delineations are also consistent with Paxinos et al. (2020). Therefore, those red fibres that cross from lateral to medial constitute the dorsal part of the transverse fibres of the pons. The ml courses rostro-caudally, as a result it cannot leave a red signature on the FAC, but only a blue signature. The red fibres that cross lateromedially (see Fig. 4A in Henssen et al. (2019)) constitute the dorsal part of the transverse fibres of the pons in which I also found the vtt and dtt. More recently, Guberinic et al. (2020) using polarized light microscopy combined with postmortem MRI, identified two branches peeling off from the trigeminal nerve -one ventral and one dorsal, and they confirm that the vtt projects towards the transverse fibres of the pons. However, both Henssen et al. (2019) and Guberinic et al. (2020) reported that the dtt courses dorsally and lateromedially through the pontine tegmentum to ascend towards the thalamus. This latter finding is in contrast to our observations, where there was no evidence of clear projection which courses lateromedially through and within the pontine tegmentum to ascend, afterwards, behind the ml as the ipsilateral tth. Despite many attempts using a vast variety of seeds and ROI masks, there was no evidence of a lateral-to-medial projection through the pontine tegmentum. The reasons for this discrepancy are unclear. My tracking results regarding the precise pathway of the vtt is based on higher resolution data images, however this high resolution is from a single human specimen. It remains possible that the pathway I traced had some aspects unique to this human. Clearly, further

ultra-high-resolution brainstem samples are needed, and additional techniques such as Gallyas staining and biological tracers should be used to elucidate the topography of the vtt and dtt at this level.

While the anatomical landmarks have been corroborated by the additional three human FAC and macaque images in Appendix Figs. 13 - 18, I acknowledge that the suggested surgical pathways derive from tractography of the best human specimen 1. Deviations, however, from the reported tractography would have most likely been evident on the DTI of these other specimens. As a result, the sensory projections identified in this Chapter are solid bundles which leave a corresponding signature between the structural anatomical GRE (50 μm) contrast and the other DTI contrasts (200 μm) such as the MD, AD, RD, DWI and most particularly the FAC (see Appendix Figs. 1 – 18, the pattern of the projections is consistent across five specimens), and the fact that different contrasts leave such a similar signature allowed me to use the background GRE of the images and most particularly the opposite side of the same GRE as further validation.

The DTI image samples included four human brains and one macaque, all at the resolution sufficient for GRE and FAC analysis of gross structures and major pathways.

4.4.4 Comparing macaque and human brainstem structures

A couple of key points emerged in comparing human and macaque.

Firstly, the medulla oblongata in the macaque seems to be compressed ventrodorsally and elongated lateromedially, compared to the medulla in the human (see and compare Appendix Figs. 13, 15, 16, and Fig. 17).

Secondly, in the human the IOPr protrudes ventrolaterally, whereas in the macaque the IOPr does not extend beyond the curve which forms between the py ventrally, and the spth, vsc, dsc, and icp dorsally. On the other hand, the IOPr seems to be more elongated rostrocaudally in the macaque, therefore I encounter at the level of the pyx and xml the caudal pole of the IOPr in the macaque (Appendix Fig. 17a, b) whereas in the human the caudal pole of the IOPr emerges at more rostral levels (Fig. 4.1d and Appendix Fig. 13c).

Thirdly, a lateromedial bundle-like structure (red on the FAC) was apparent in the macaque (100 μm of isotropic resolution for the FAC); (Fig. 17f), behind the ml and spth in the pontine tegmentum, which was absent in the human (200 μm of isotropic resolution for the FAC). This could be the trapezoid body, hence further research and tracing is needed to identify if this structure connects the superior olivary nucleus to the cochlear nucleus.

Fourthly, I observed in the macaque the butterfly-pattern of the grey matter of the spinal cord projecting up until the medulla oblongata (Appendix Fig. 17a). This colourful pattern consists of red, green, and azure on the FAC and is confined ventrally by the py, pyx, IOPr, spth, rs, and dsc, whereas dorsally is confined by the

cu, on both sides. In addition, in the dorsolateral region of this butterfly-pattern within the caudal medulla I found the sp5 and Sp5C1, 2, 3/4 to project into the dorsal horn of the spinal cord (DH) and this is in alignment with what was reported by Warren and May (2013). This observation is also in alignment with what proposed by Martinez-de-la-Torre et al. (2018) that the pyx is located in a zone which is defined as part of the spinal cord, and our data show that the pyx is indeed located at the same level as the level at which the sp5 projects into the DH. However, this anatomical configuration was not observed in the human (Appendix Fig. 13a). I cannot give a plausible explanation regarding this difference, and again it should be validated in additional macaque and other primate samples.

CHAPTER 5:
The dentato-rubro-thalamic tract in the human and macaque

5.1 Introduction

One of the challenges in connectomics is to find methods which are accurate enough to elucidate the specific pathways in the human brain at a sufficient resolution to allow for a comprehensive understanding of their role in physiology as well as in pathologies. One such example is the pathway between the cerebellum and thalamus, the dentato-rubro-thalamic tract (drt). The drt is the major output tract of the cerebellum, connecting the dentate nucleus (which is the largest, most lateral, and phylogenetically most recent of the cerebellar nuclei) with the red nucleus in the midbrain, before ascending to synapse into the ventral lateral nucleus (VL); (ventral tier) of the thalamus (Akakin et al., 2014). The VL then projects to the primary motor and premotor areas as well as prefrontal and posterior parietal areas of the cerebral cortex (Dum and Strick, 2003).

The drt is involved in a range of cerebellar functions, including fine movement control and gait coordination while it maintains posture, muscle tone and voluntary muscle activity (Roostaei et al., 2014). Dysfunction of the drt or its targets is implicated in movement disorders including essential tremor and multiple sclerosis (Alesch et al., 1995, Torres et al., 2010). Essential tremor is the most common neurologic cause of postural or action tremor. The upper limbs are usually symmetrically involved, however the head and voice can also be involved. The etiology of essential tremor is mostly elusive. About half of the cases appear to result from a genetic mutation (familial tremor), however a specific genetic locus has never been identified. In addition, various cases of traumatic brain injury reported symptoms such as resting and intentional tremor as well as ataxic gait, some time

following the incident. These types of disfunction of the drt caused by traumatic brain injury are only now highlighted through diffusion tensor tractography (Jang and Kwon, 2015), as a result, analysis of the drt could be useful in elucidating the exact location of a lesion which causes post-traumatic abnormal movements.

Deep-brain-stimulation (DBS) is the most common, effective and safe surgical treatment for essential tremor. This invasive surgical procedure traditionally targets the ventral tier of the thalamus and achieves a one-year tremor reductions ranging from 66% to 78% for bilateral DBS. The overall quality of life of such patients is significantly improved, however transient symptoms such as paraesthesia, dysarthria and ataxia are commonly reported as adverse effects (Dallapiazza et al., 2019). Use of pre-operative MRI imaging and diffusion tractography to trace the thalamic afferents of the drt has enabled more precise and successful DBS for tremor suppression, both in case reports and post-hoc analysis. Despite subtle anatomical variations that might be present between individuals, by directly targeting the drt and subsequent placement of electrode contacts within the pathway, seems to be a more effective strategy for tremor suppression (Fenoy and Schiess, 2017).

Diffusion tensor tractography (DTT) derives from diffusion tensor imaging (DTI) and allows the visualisation in 3D of white matter tracts. Historically, tractography was limited by low spatial resolution, difficulty in estimating fibre orientations and crossing fibres within each voxel and low signal-to-noise ratio. However, with the advent of ultra-high field magnetic resonance imaging and more sophisticated post-processing algorithms (Calabrese et al., 2015a), it is now widely applied preoperatively in patients with tumours because it is the only reliable non-

invasive technique which allows for the identification of the fibre bundles both adjacent to and inside the tumour (Mori et al., 2002). More recently, a variety of diffusion studies using ultra-high-field scanners have compared their tractography results with traditional histology (myelin staining and polarized light microscopy) and demonstrated high spatial accuracy of postmortem tractography when compared to a histological reconstruction (Mollink et al., 2016, Henssen et al., 2019).

Given the importance of the drt in movement and other disorders, a number of recent studies have attempted to better define the drt. Earlier work, using anterograde degeneration studies after lesions into the dentate nucleus of the macaque (*Macaca mulatta*), reported that the drt fibres course through the superior cerebellar peduncle (scp) or *Brachium Conjunctivum*; as used by the *Terminologia Anatomica* (Allen, 2009) until they reach the isthmus where the majority of the fibres cross, contralaterally, through the superior cerebellar decussation (xscp), whereas some non-crossing fibres ascend ipsilaterally towards the red nucleus (Petersen et al., 2018). Further tractography studies with MRI at 1.5T attempted to trace the scp or parts of the drt (Kwon et al., 2011a) however, the long and disynaptic nature of this decussating and non-decussating pathway meant such low resolution studies were not clinically useful. Using a single postmortem brain specimen of an 87 year old woman at higher resolution (7T), Mollink et al. (2016) demonstrated that the DTI had reasonable success in accurately delineating white matter tracts as correlated with 3D histological reconstruction, although the extent of overlap differed at different levels of the drt precluding full, accurate delineation of this pathway. Delineation was particularly poor in the xscp where the fibres mingled, and in the red nucleus which is characterised by a precise topographical distribution of fibre populations.

The 7T MRI material of postmortem brainstem from the Duke Center for In Vivo Microscopy provides the highest resolution images to date of brainstem pathways (see Table 1, p 82). As described in Chapters 1 & 2, the advanced postprocessing algorithms and optimised MRI acquisition parameters, including the prolonged scanning time (208 hours for DWI - Duke) resulted in these high quality images. Although the drt has been previously mapped by a number of authors, the much higher isotropic resolution of human specimen 1 enables deterministic tractography and higher order investigative models such as the tensor glyphs to delineate the drt at a more precise level. The aim of this Chapter is to provide this higher resolution mapping of the entire drt projection and its surrounding structures. It is hoped this more precise topography may assist targeting the drt during neurosurgery or aid invasive insertion of an electrode within its fibres for deep brain stimulation.

5.2 Specific methods

The results have been achieved using deterministic tractography based on high-angular-resolution diffusion imaging (HARDI) and a higher-order tensor glyph model. Human specimen 1 was selected for all the tractography studies in this Chapter due to the high quality of this dataset (see section 2.4). These high resolution GRE and tractography images from Duke specimen 1 are complemented by the FAC maps derived from three more human specimens and one macaque (see Appendix Figs. 13 to 18). Since the drt constitutes a long ascending projection, it is particularly

challenging to obtain tractography results through the whole course of the pathway, thus only human specimen 1 achieved this.

Regarding the masks and tractography parameters, I used, a seed region placed bilaterally in the superior cerebellar peduncle with a volume size of 11 mm^3. The seed and ROI masks of all the result Chapters are shown in the Appendix Figs. 19 – 22). A ROI was placed within the red nucleus with a volume size of 23 mm^3.

The angular threshold was 20%, and an FA threshold of 0.15 was applied. The step size was randomly selected from 0.5 voxel to 1.5 voxels. The fibre trajectories were smoothed by averaging the propagation direction with a percentage of the previous direction. Smoothing gives the "momentum" of the propagation direction. If smoothing is 0, the propagation direction is independent of the previous direction. If smoothing is 1.0, as in the present Chapter, the percentage is randomly selected from 0% to 95%. No tracts were discarded. A total of 75,000 trajectories were calculated. The trajectories were not manually edited and are presented exactly as generated.

The tensor glyph in Fig. 5.3 displaying the first eigenvector in every voxel was generated with the framework and analysis tools provided in the FMRIB Software Library (FSL; Woolrich et al. (2009)).

5.3 Results

5.3.1 Topography of the scp and analysis of the fibre arrangement from caudal pontine levels to the isthmus

The output fibres of the cerebellum heading towards the cerebral cortex pass through the scp, hence the 3D masks were manually drawn on the structural MRI contrast within the caudal scp bilaterally. The borders of the scp could be clearly delineated from the MRI / FAC images by combining the transverse, sagittal and coronal sections (see intersections in Fig. 5.1a). Subsequently, two ROI masks were placed bilaterally, in the red nucleus while no masks were created for the thalamus. In Fig. 5.1, and Appendix Figs. 13, 15, 16, 17, 18 the borders of the scp and the orientation of the fibres within the scp are delineated using FAC. The scp begins to form at caudal pontine levels (Fig. 5.1a, Fig. 5.2, and Appendix Figs. 13g, 15e, 16e, 17e, 18c) and constitutes the side walls of the fourth ventricle. Topographically, the scp is confined medially from the central tegmental tract (ctg) which courses through the pontine tegmentum, ventrally from the medial, spinal and trigeminal lemnisci, and laterally from the lateral lemniscus (Fig. 5.1a, b, and Appendix Figs. 13h, 15e, f, 16 e, f, 17g). While the scp ascends, it assumes an oblique lateromedial and dorsoventral direction reminiscent of the lateral surface areas of a triangular prism (Fig. 5.1a, sagittal and coronal sections, Fig. 5.2). Until the midpons, the scp ascends on both sides as a wedge-shaped compact fibre bundle pointing ventrolaterally (Fig. 5.1a, and Appendix Figs. 13g, 15e, 16e, 17f).

At the level of the midpons, the ventral fibres of the scp begin to swift ventromedially (Fig. 5.1b, and Appendix Figs. 13h, 15f, 16f, 17f, g) into the pontine tegmentum, until they reach the level of the xscp in the isthmus (Fig. 5.1c, Fig. 5.2c, d, and Appendix Figs. 13i, 15g, 16g, 17h, 18b), having a cross-section that bears a resemblance to a parabola, crescent or scimitar shape (medial-side U-shaped or banana-shaped anatomical entity; see also arrows in Fig. 5.1) which is open towards the midline.

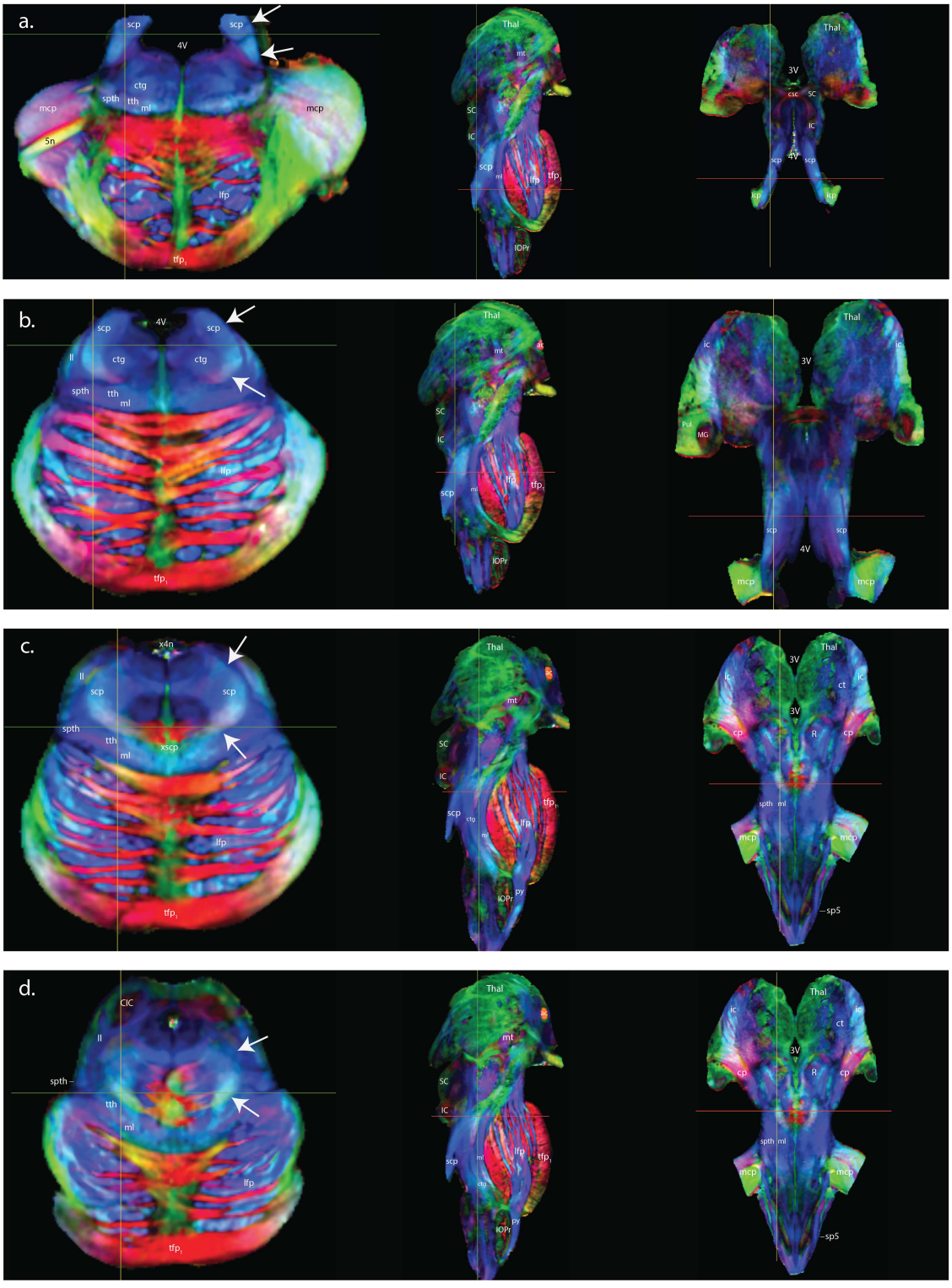
a.
scp
scp
4V
ctg
spth
tth
ml
mcp
mcp
5n
lfp
tfp1
Thal
mt
SC
IC
scp
ml
lfp
tfp1
lOPr
Thal
3V
csc
SC
IC
4V
scp
scp
icp
lcp
b.
scp
4V
scp
ll
ctg
ctg
spth
tth
ml
lfp
tfp1
Thal
mt
SC
IC
scp
ml
tfp1
tfp1
lOPr
Thal
ic
ic
3V
Pul
MG
scp
scp
4V
mcp
mcp
c.
x4n
ll
scp
scp
spth
tth
ml
xscp
lfp
tfp1
Thal
mt
SC
IC
scp
ctg
ml
tfp1
lfp
py
lOPr
Thal
3V
ic
ic
ct
3V
cp
R
cp
spth
ml
mcp
mcp
–sp5
d.
CIC
ll
spth
tth
ml
lfp
tfp1
Thal
mt
SC
IC
scp
ml
lfp
tfp1
ctg
py
lOPr
Thal
ic
ic
ct
3V
cp
R
cp
spth
ml
mcp
mcp
–sp5

Fig. 5.1. Mapping out the borders of the superior cerebellar peduncle (scp) from directionally coloured fractional anisotropy (FAC) of the whole ex vivo human brainstem at the level of midpons in (a), rostral pons in (b) and (c), and in the mesencephalon (isthmus) in (d). *The left, centre and right columns show the transverse, sagittal and coronal sections of the brainstem and thalamus, respectively. Where the perpendicular lines intersect is the exact point of the scp in the transverse, sagittal and coronal sections. The spatial distribution of the fibres of the scp is that of the lateral surface areas of a triangular prism in (a), sagittal and coronal sections. Note how the fibres that constitute the scp shift ventromedially to form a parabola that assumes a shape similar to a U-like structure which is open towards the midline until they decussate in the isthmus. In (b) the first fibres to decussate are the most ventral ones and gradually the intermediate and dorsal ones follow the crossing in (c). The dorsal part of the scp assumes a deep blue colour where gradually it becomes azure and magenta ventrally as the fibres shift dorsoventrally and lateromedially to decussate. In red (c) are the decussating fibres, in yellow (d) are the fibres of the xscp that obliquely shift while they cross over. The arrows show the borders of the scp from the caudal pons to the midbrain. FAC sections from human specimen 1. On the FAC maps red, blue, and green represent anisotropy along medial-lateral, rostral-caudal, and ventral-dorsal orientations, respectively. Abbreviations: tth: trigeminothalamic tract, spth: spinothalamic tract, 5n: trigeminal nerve, sp5: spinal trigeminal tract, ml: medial lemniscus, scp: superior cerebellar peduncle, MB: mammillary body, Pi: pineal gland, Thal: thalamus, mcp: middle cerebellar peduncle, lfp: longitudinal fibres of the pons, xscp: decussation of the superior cerebellar peduncle, Pn: pontine nuclei, tfp1: most ventral transverse fibre of the pons, cp: cerebral peduncle, ac: anterior commissure, CIC: central nucleus of the inferior colliculus, SC: superior colliculus, IC: inferior colliculus, ll: lateral lemniscus, ic: internal capsule, ctg: central tegmental tract, R: red nucleus, Aq: aqueduct, 3V: third ventricle, 4V: fourth ventricle, IOPr: inferior olive, principal nucleus, x4n: decussation of the trochlear nerve, csc: commissure of the superior colliculus, mt: mammillothalamic tract, ct: cerebellothalamic tract.*

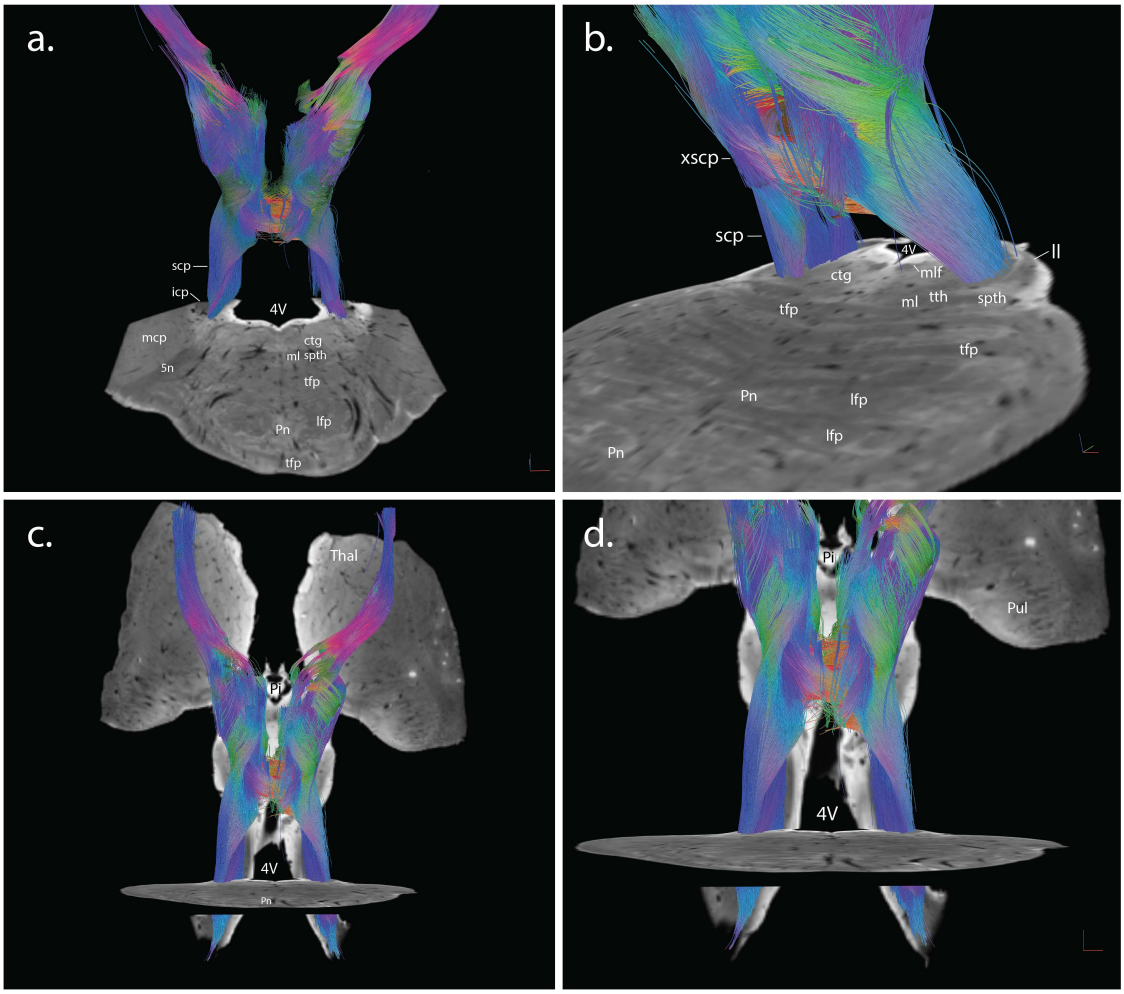

Fig. 5.2. 3D representation of the drt at lower (left) and higher (right) magnification. *In (a) and (b) the scp and xscp as seen through oblique planes. In (c) and (d) the drt is shown from a horizontal perspective. The drt is traced from the caudal scp to the xscp and red nucleus which eventually terminates into the VL nucleus of the thalamus. The tractographic analysis was performed on human specimen 1. On the FAC maps red, blue, and green represent anisotropy along medial-lateral, rostral-caudal, and ventral-dorsal orientations, respectively. Abbreviations: tth: trigeminothalamic tract, spth: spinothalamic tract, 5n: trigeminal nerve, sp5: spinal trigeminal tract, ml: medial lemniscus, scp: superior cerebellar peduncle, icp: inferior cerebellar peduncle, Pi: pineal gland, Thal: thalamus, Pul: pulvinar, xscp: decussation of the superior cerebellar peduncle, Pn: pontine nuclei, tfp: transverse fibres of the pons, ll: lateral lemniscus, ctg: central tegmental tract.*

Note in Fig. 5.1a, coronal view, herein, the myelinated axons are identified for the first time (magenta in DTI – rostrocaudal and mediolateral orientation) which form the circuit that conveys and integrates information between the inferior and superior colliculi. In addition, note how these axons converge into the commissure of the superior colliculus (csc) to cross over.

5.3.2 Analysis of the fibre arrangement of the drt into the xscp

The first fibres to decussate from the drt occur at the level of the isthmus (red tracts in Fig. 5.1c, right to left orientation) being the most ventral fibres. Subsequently, at more rostral levels the U-shaped arrangement of the fibres of the scp begin to shift more medially (Fig. 5.1d) and gradually the intermediate and dorsal fibres decussate (obliquely) from both sides. This can also be seen for the tracts in Fig. 5.2d where some of the ventral fibres coming from one side intertwine with the intermediate fibres crossing from the opposite side and assume an orange colour prior to the midline due to their oblique orientation (see also Fig. 5.1d). At the midline, the fibres shift more obliquely and assume a yellow colour in FAC and the tensor glyph (Fig. 5.2d, 5.3).

The tensor glyph in Fig. 5.3 analyses the orientation of the fibres in the xscp in greater detail. The pathway of the drt at this level assumes a lateromedial intertwined arrangement and the tensor glyph provides a powerful mathematical language to analyse this complex and elusive architecture. Some of the ventral fibres from each side can cross horizontally (red in FAC). Other fibres from the ventral part decussate to an intermediate position. Subsequently, fibres from the intermediate part

can cross over to an intermediate position, while other fibres decussate more ventrally or intertwine dorsally on the other side. Similarly, the dorsal fibres that decussate from one side can assume a dorsal or intermediate position on the opposite side to later ascend towards the red nucleus (Fig. 5.3). This arrangement comprises only the decussating drt. The non-decussating drt ascends more laterally (blue fibres in FAC and tensor glyph). Although I was unable to determine the exact percentage of the ipsilateral (non-decussating) and contralateral (decussating) drt I observed the existence of both, where the vast majority of the fibres decussate as it can be deduced by the volume of the tracts within the xscp (Figs. 5.1d & 5.3).

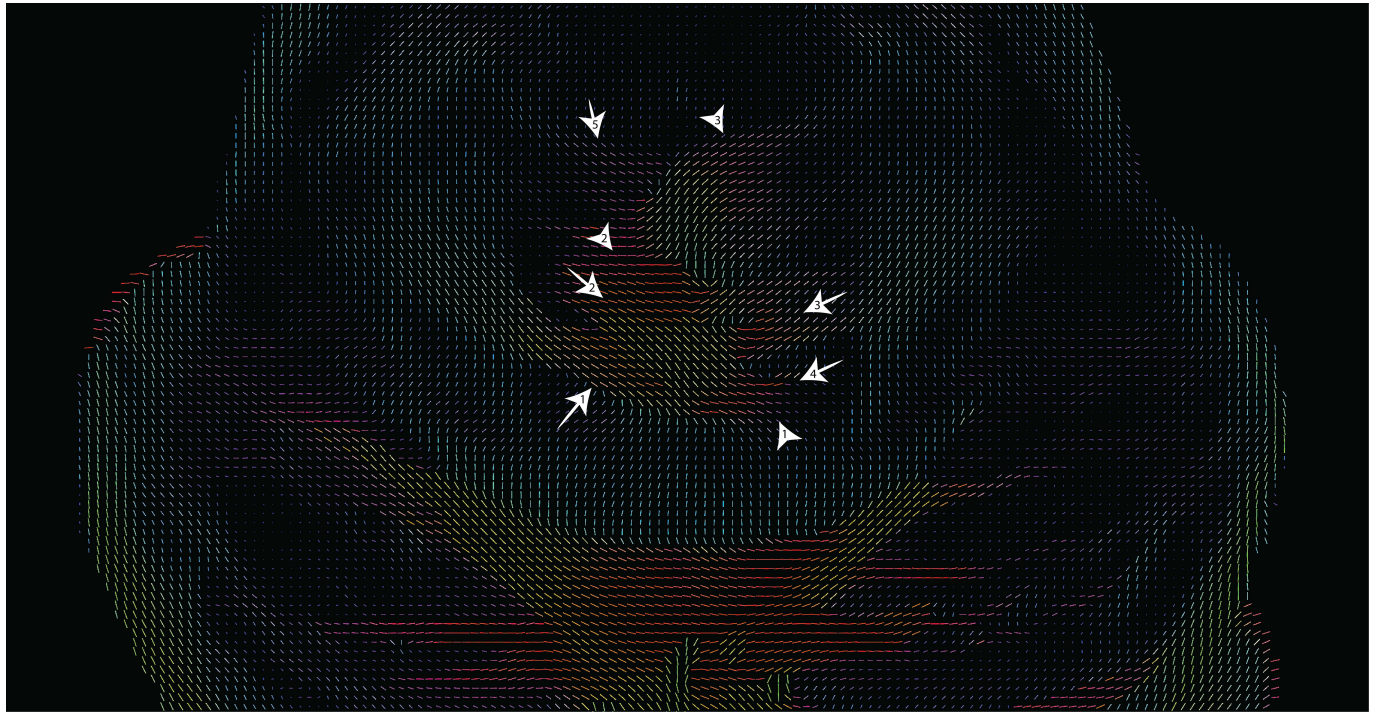

Fig. 5.3. Glyph-based fibre visualisation of diffusion tensor fields from human specimen 1 are seen at the level of the xscp*. The fibres can be clearly seen in the xscp intertwine. Some of the ventral fibres (arrow-head 1) cross ventrally to the opposite side (arrow 1), whereas other fibres are branching off while crossing obliquely and assume an intermediate position (more dorsally) on the opposite side (arrow 2). Similarly, some of the intermediate fibres (arrow-head 2) decussate and assume an intermediate position (arrow 3), others course obliquely (yellow in FAC, Fig. 1d), to a ventral position (arrow 4), others can be displaced dorsally (arrow-head 3). Finally, some of the dorsal fibres (arrow-head 3) can decussate dorsally (arrow 5) whereas other fibres intertwine to an intermediate position (arrow-head 2).*

5.3.3 Topography of the drt from the xscp to the red nucleus

After having crossed at the level of the isthmus (Fig. 5.2, 5.6c), the drt ascends for approximately two mm in the human, and one mm in the macaque on both sides to reach the red nucleus. This can be seen in the FAC images of Fig. 5.4, and Appendix Figs. 13j, k (arrows), 14b, 18b. At this level, the fibres surrounding the red nucleus are shown as green in FAC (Fig. 5.4a), also due to the presence of the fasciculus retroflexus (fr); (see also Appendix Fig. 17j, k). Note also at this level a small and clearly defined cross-commissural fibre pathway connecting the bilateral superior colliculi (csc, red in Fig. 5.4a). The drt is topographically identified between the parabrachial pigmented (PBP) nucleus ventrally, the ctg dorsally, the mesencephalic reticular formation (mRt) dorsolaterally, and the rostral linear nucleus (RLi) medially (Fig. 5.4, Fig. 5.5a, and Fig. 5.6d).

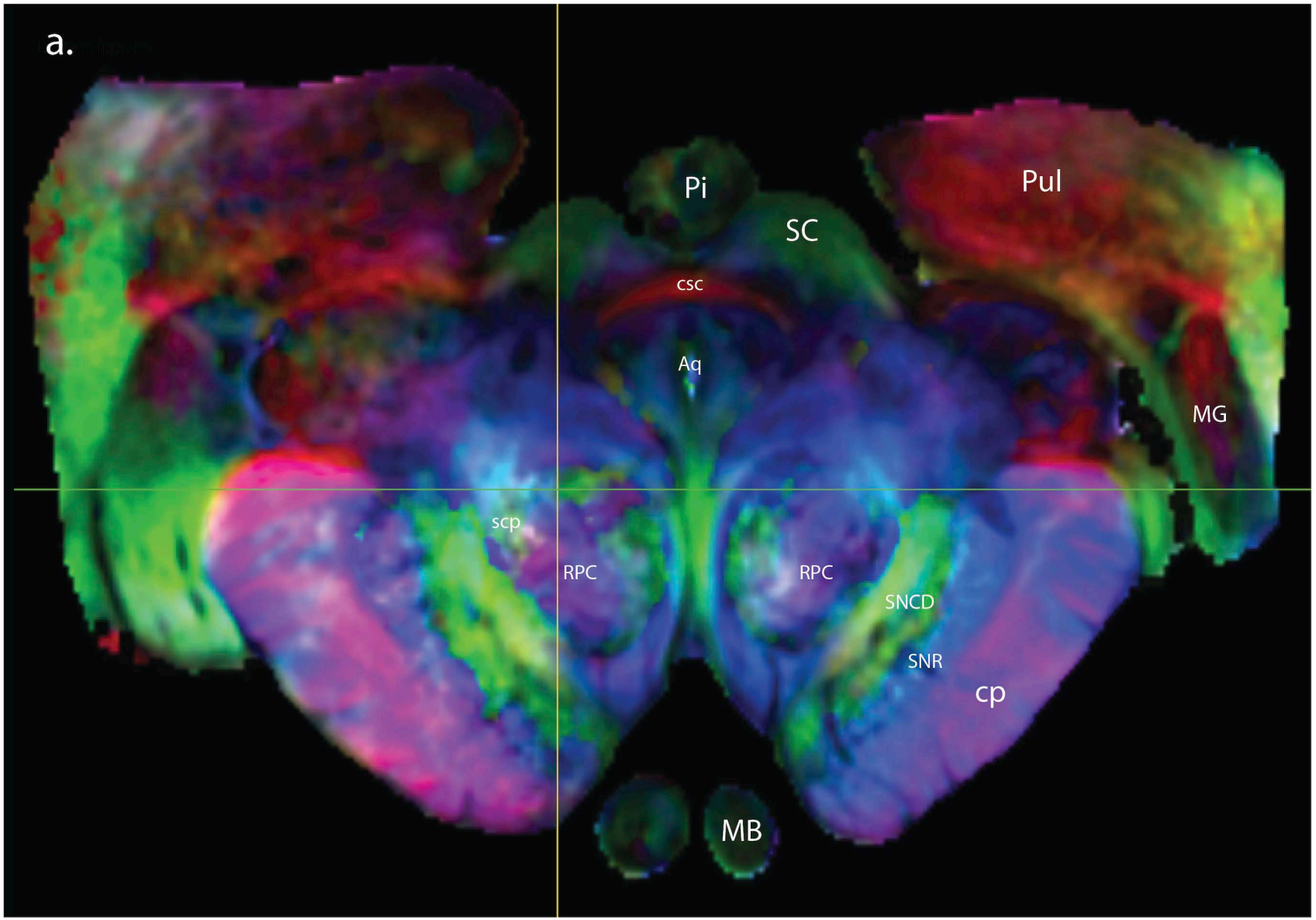
a.
Pi
SC
Pul
csc
Aq
MG
scp
RPC
RPC
SNCD
SNR
cp
MB

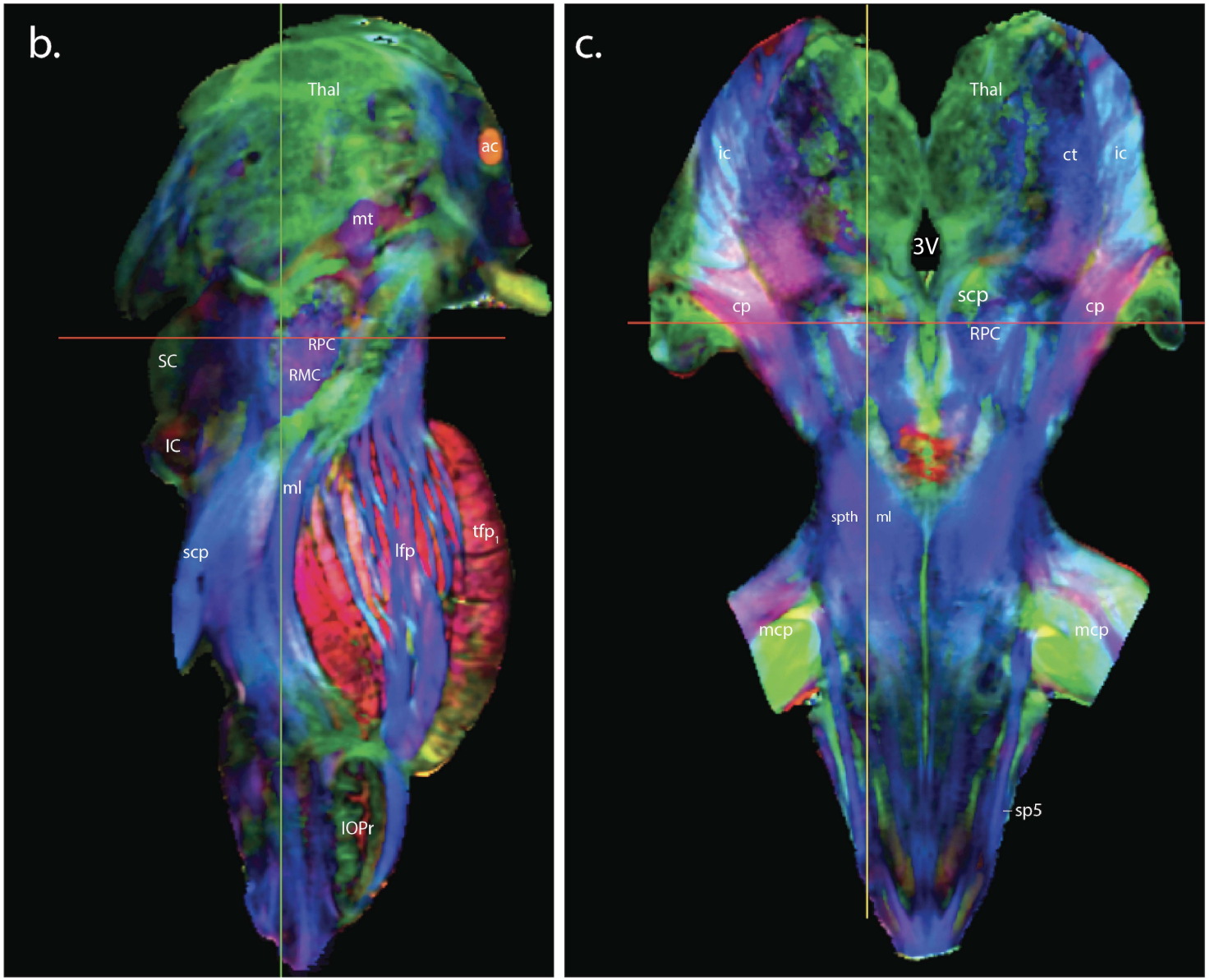
b.
Thal
ac
mt
RPC
SC
RMC
IC
ml
scp
tfp1
lfp
lOPr
c.
Thal
ic
ct
ic
3V
cp
scp
cp
RPC
spth
ml
mcp
mcp
sp5

Fig. 5.4. Spatial distribution of drt fibres as they course the red nucleus. FAC images from human specimen 1 at the level of midbrain in transverse (a), sagittal (b) and coronal (c) sections. *The scp fibres are shown (greenish colour) surrounding the red nucleus (intersections) to ascend as cerebellothalamic tract, whereas the vast part of the fibres that terminate as the dentato-rubral tract are found more centrally (blue). Note in (a) the csc as a lateromedial interhemispheric commissural connection (red) between the two superior colliculi (SC). On the FAC maps red, blue, and green represent anisotropy along medial-lateral, rostral-caudal, and ventral-dorsal orientations, respectively. Abbreviations: Pi: pineal gland, spth: spinothalamic tract, sp5: spinal trigeminal tract, ml: medial lemniscus, scp: superior cerebellar peduncle, MB: mammillary body, Thal: thalamus, mcp: middle cerebellar peduncle, lfp: longitudinal fibres of the pons, tfp1: most ventral transverse fibre of the pons, cp: cerebral peduncle, ac: anterior commissure, SC: superior colliculus, IC: inferior colliculus, ic: internal capsule, 3V: third ventricle, IOPr: inferior olive, principal nucleus, csc: commissure of the superior colliculus, RPC: red nucleus, parvicellular part, SNR: substantia nigra, pars reticulata, SNCD: substantia nigra, pars compacta dorsalis, RMC: red nucleus, magnocellular part, MG: medial geniculate, Pul: pulvinar, mt: mammillothalamic tract, ct: cerebellothalamic tract.*

5.3.4 Arrangement of the drt at the level of the red nucleus

For approximately 9 mm in the human (see also coronal view in Fig. 2.2 and Appendix Fig. 14b) and 4.5 – 5 mm in the macaque (Appendix Fig. 18b) the drt courses through the red nucleus to ascend towards the thalamus. The spatial distribution of the fibres that constitute this pathway is such that the fibres from the dentate to the red nucleus (dentato-rubral tract) are placed more centrally and terminate into the red nucleus (Fig. 5.5a & b, blue fibres in the centre of the red nucleus) compared to those that will eventually constitute the cerebellothalamic pathway (greenish fibres in the periphery of the red nucleus in Fig. 5.5a & b). Thus, the projections en route to the thalamus are located more externally (Fig. 5.5b, c) and continue to ascend towards more rostral levels beyond the rostral pole of the red nucleus which obliterates at the level of the caudal pole of the STh (Fig. 5.5d, Fig. 5.6e).

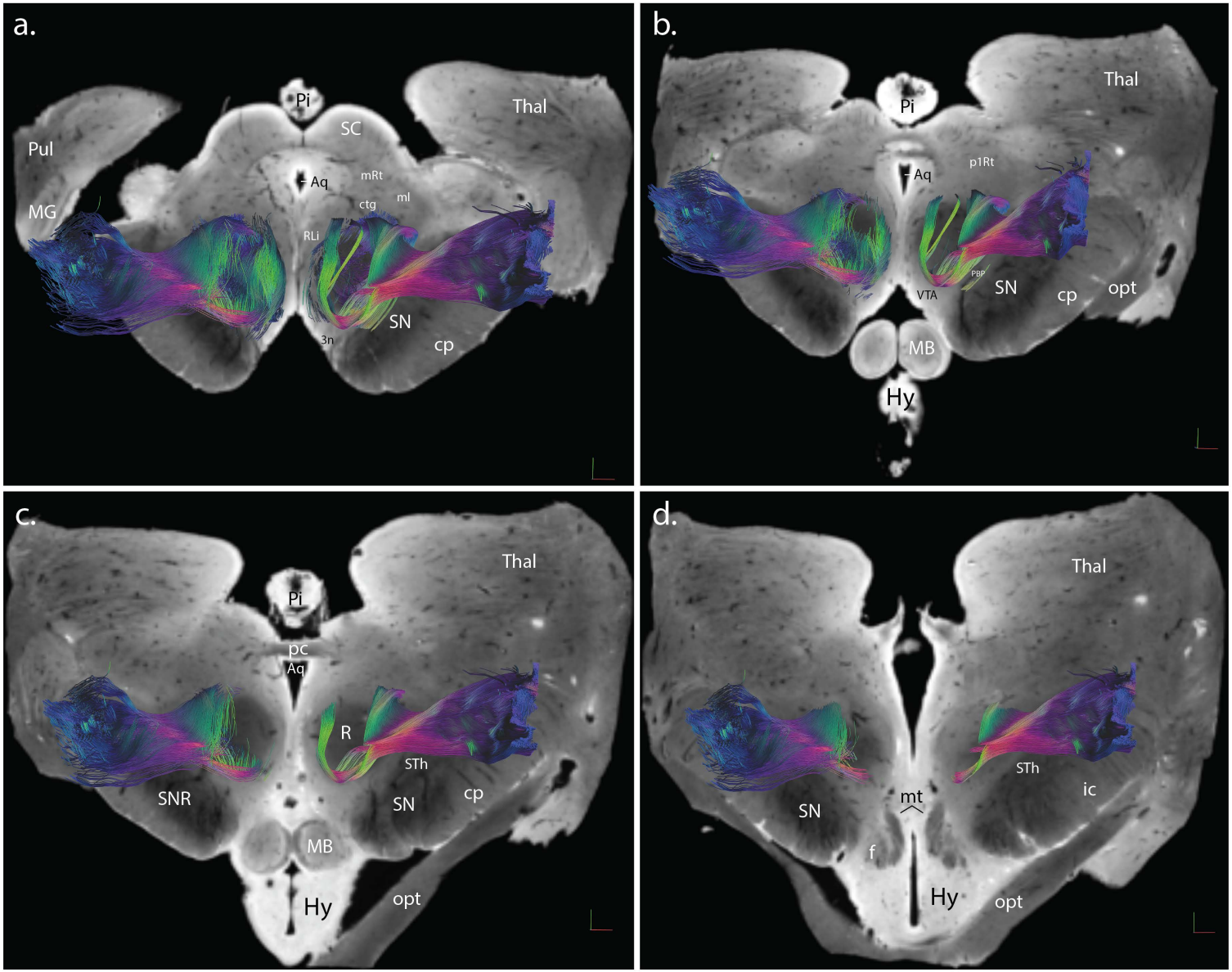
a.
Pi
SC
Thal
Pul
Aq
mRt
ml
ctg
MG
RLi
SN
3n
cp
b.
Thal
Pi
Aq
p1Rt
PBP
VTA
SN
cp
opt
MB
Hy
c.
Thal
Pi
pc
Aq
R
STh
SNR
SN
cp
MB
Hy
opt
d.
Thal
STh
ic
mt
SN
f
Hy
opt

Fig. 5.5. Architectural arrangement of the drt through the red nucleus from the midbrain to the diencephalon. *The course of the cerebellothalamic fibres surrounding the red nucleus is shown from (a) to (d)***.** *Note in (a) and (b) how the dentato-rubral tract terminates into the central part of the rostral red nucleus (diencephalic part of the red nucleus) whereas the rest of the projection ascends towards the VL nucleus of the thalamus in (c) and (d). The tractographic analysis was performed on human specimen 1. Abbreviations: Pi: pineal gland, MB: mammillary body, Thal: thalamus, cp: cerebral peduncle, ac: anterior commissure, Hy: hypothalamus, SC: superior colliculus, ic: internal capsule, STh: subthalamic nucleus of Luys, pc: posterior commissure, Aq: aqueduct, opt: optic tract, R: red nucleus, SN: substantia nigra, f: fornix, mt: mammillothalamic tract, SNR: substantia nigra, pars reticulata, MG: medial geniculate, Pul: pulvinar, VTA: ventral tegmental area, RLi: rostral linear nucleus, mRt: mesencephalic reticular formation, p1Rt: prosomere 1 reticular formation, PBP: parabrachial pigmented nucleus.*

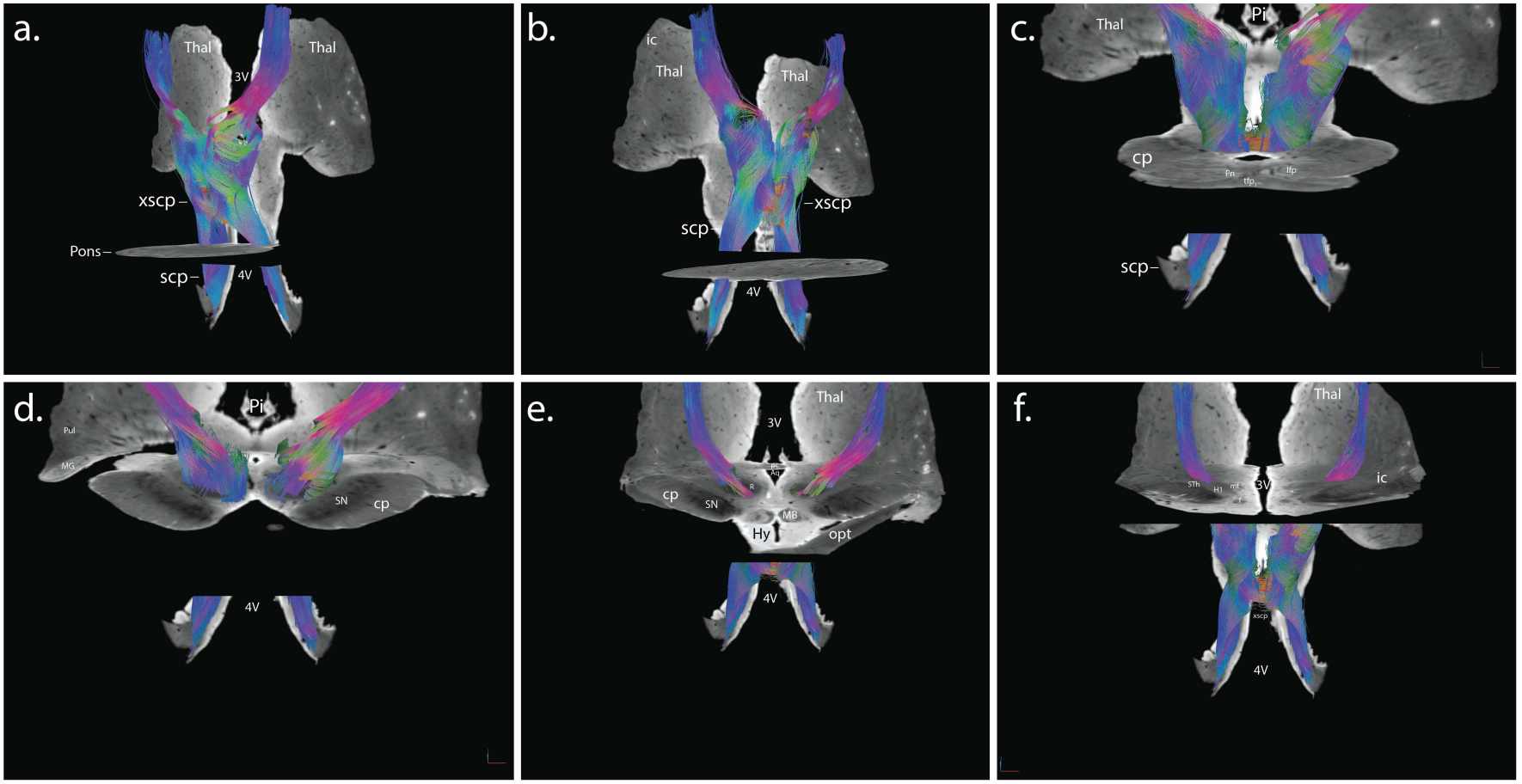
a.
Thal
Thal
3V
xscp
Pons
scp
4V
b.
ic
Thal
Thal
xscp
scp
4V
c.
Thal
Pi
cp
Pn
lfp
tfp
scp
d.
Pi
Pul
MG
SN
cp
4V
e.
Thal
3V
cp
SN
MB
Hy
opt
4V
f.
Thal
STh
H1
mt
3V
ic
xscp
4V

Fig. 5.6. Tractographic analysis combined with the structural GRE background reveals the complexity of the patterning that the fibres assume, and their relationship with the surrounding structures from the pons in (a) to the diencephalon in (f). *Note in (c) the external limit of the xscp in the vicinity of the substantia nigra at the level between rhombomere one and two. In (d) and (e) the cerebellar projections course through the red nucleus towards the diencephalon in (f). The tractographic analysis was performed on human specimen 1. Abbreviations: Pi: pineal gland, Thal: thalamus, 3V: third ventricle, 4V: fourth ventricle, cp: cerebral peduncle, Pn: pontine nuclei, tfp: transverse fibres of the pons, tfp1: most ventral transverse fibre of the pons, Hy: hypothalamus, SC: superior colliculus, ic: internal capsule, STh: subthalamic nucleus of Luys, pc: posterior commissure, Aq: aqueduct, opt: optic tract, R: red nucleus, SN: substantia nigra, f: fornix, mt: mammillothalamic tract, SNR: substantia nigra, pars reticulata, MG: medial geniculate, Pul: pulvinar, xscp: decussation of the superior cerebellar peduncle, H1: field H1 of Forel.*

5.3.5 Topography of the cerebellothalamic tract through the diencephalon

After having coursed through the entire length of the red nucleus the cerebellothalamic (ct) fibres ascend and course through the fields of Forel (Fig. 5.6e, Fig. 5.7a). The fibres are topographically distributed behind the subthalamic nucleus and ansa lenticularis, whereas the mammillothalamic tract ascends more ventromedially (Fig. 5.7a, and Appendix Figs. 13 final panel, 17k, 18b). The cerebellothalamic tract terminates into the VL nucleus of the thalamus which is found internally to the posterior limb of the internal capsule and ventrally to the lateral posterior thalamic nucleus (Fig. 5.7b, c, and Appendix Figs. 14, 17l).

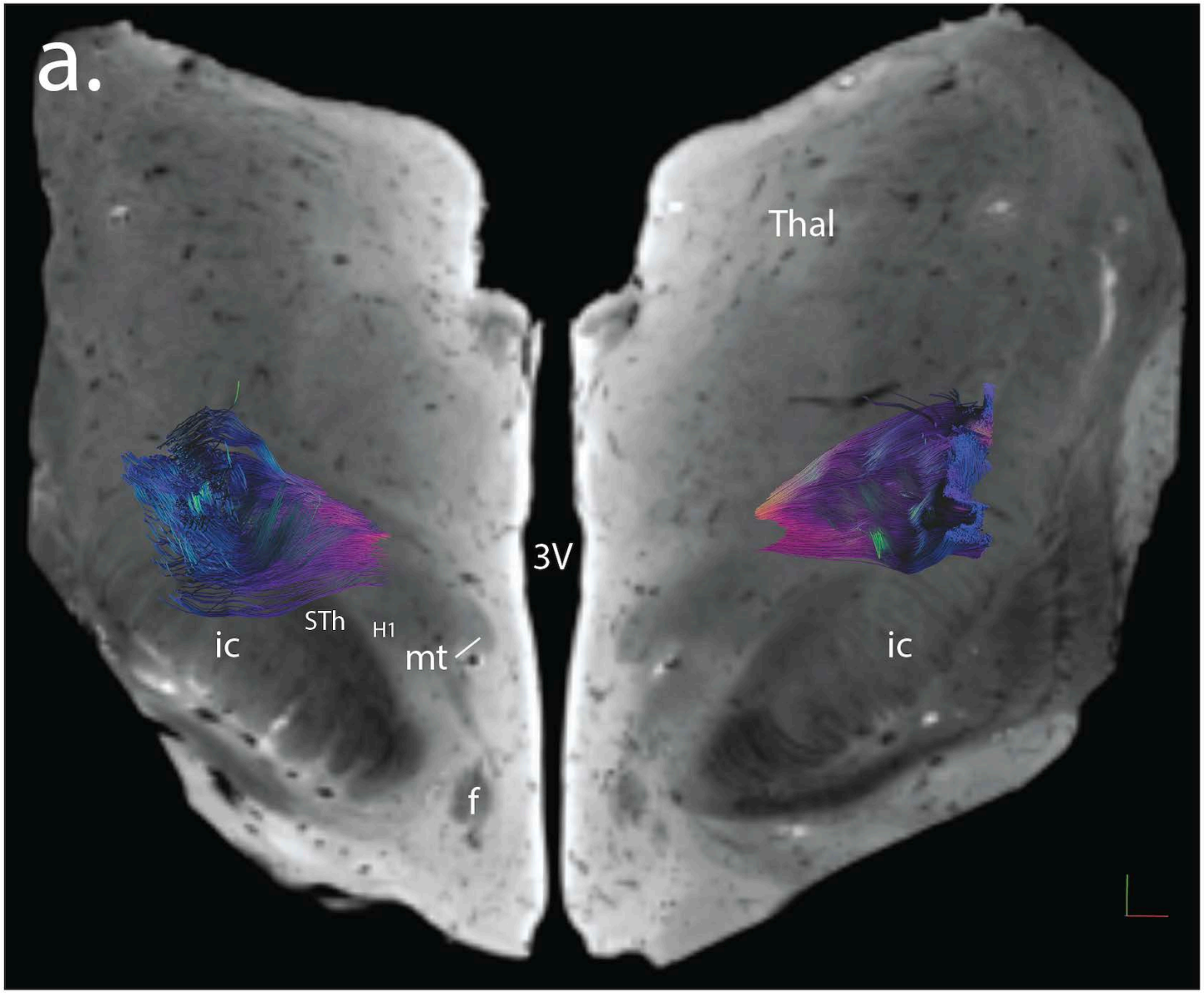
a.
Thal
3V
STh
H1
ic
mt
f
ic

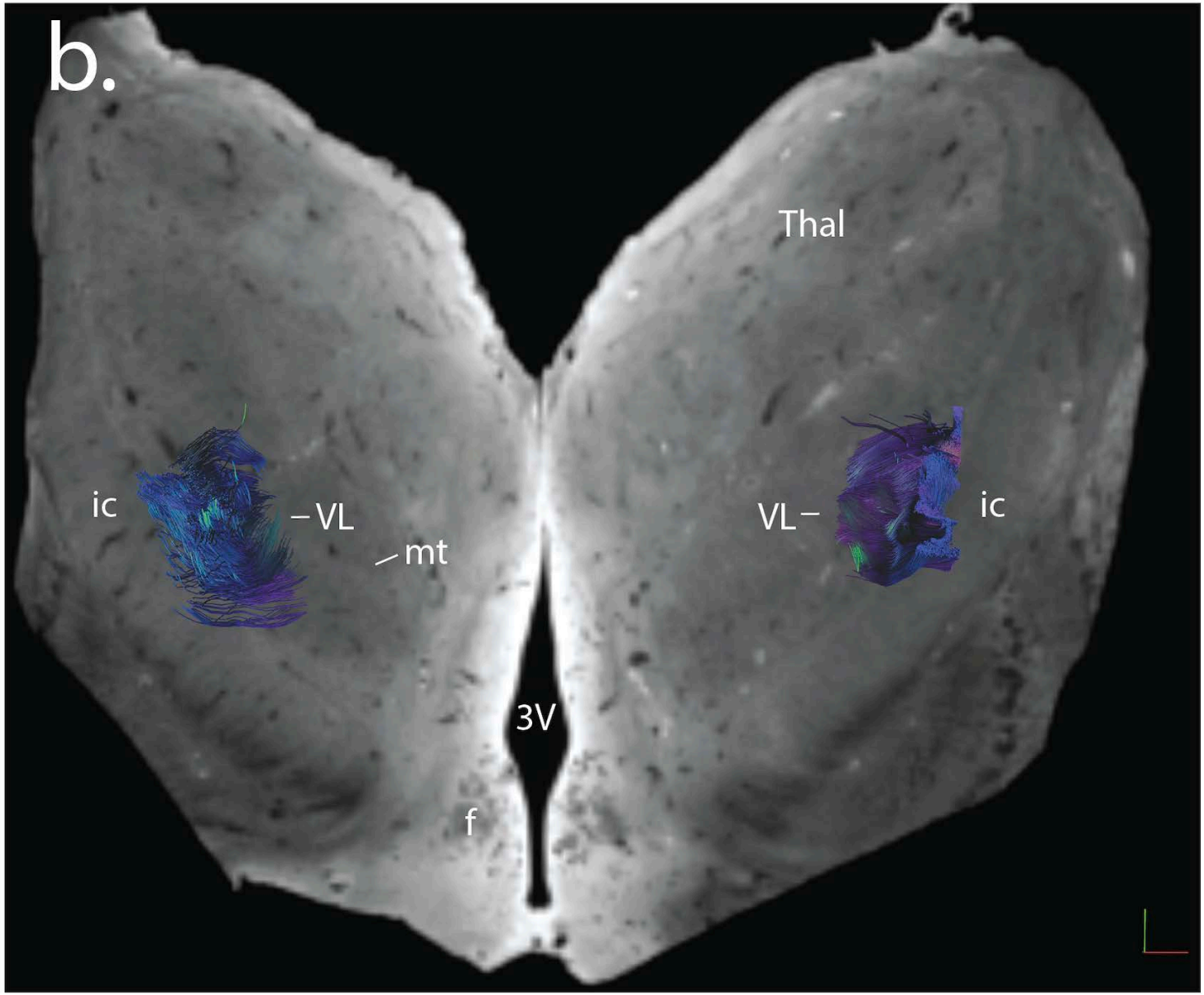
b.
Thal
ic
VL
mt
VL
ic
3V
f

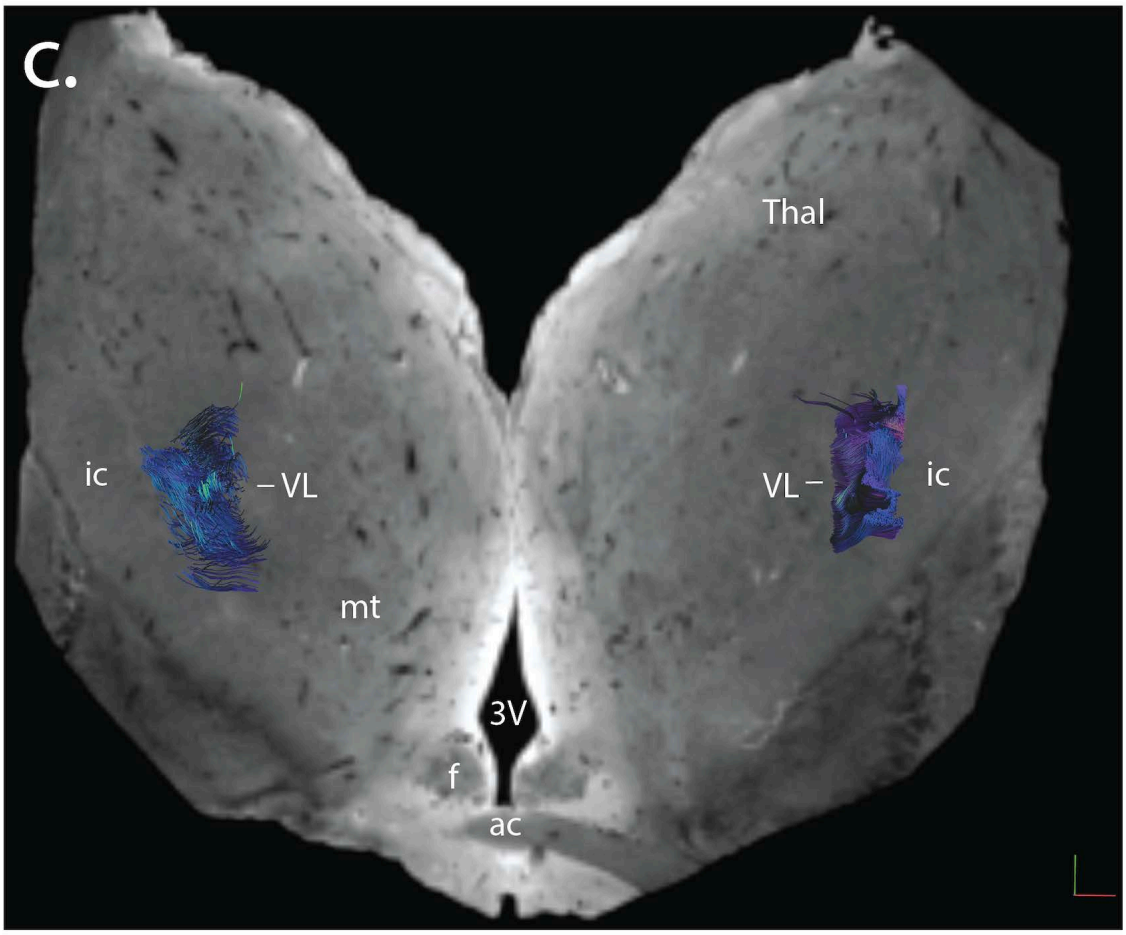

Fig. 5.7. Cross sections at the level of the diencephalon from caudal (a) to rostral (c). *Through the fields of Forel, the cerebellothalamic pathway courses behind the subthalamic nucleus of Luys in (a) and ansa lenticularis, whereas in the ventromedial part of the thalamus the mammillothalamic tract and the fornix ascend. Finally, in (b) and (c) the afferent leg of the cerebrocerebellar circuit terminates into the VL nucleus of the thalamus. The tractographic analysis was performed on human specimen 1. Abbreviations: Thal: thalamus, 3V: third ventricle, ic: internal capsule, STh: subthalamic nucleus of Luys, f: fornix, mt: mammillothalamic tract, H1: field H1 of Forel, VL: ventral lateral nucleus, ac: anterior commissure.*

5.4 Discussion

The dentato-rubro-thalamic (drt) is the output tract from the cerebellum to the thalamus and from there to the neocortex. The drt originates in the dentate nucleus of the cerebellum and its fibres course via the scp to decussate and ascend towards the red nucleus in the mesencephalon. Finally, the drt ascends and terminates into the VL nucleus of the thalamus (Kwon et al., 2011a).

The current study uses ultra-high resolution MRI, deterministic tractography and tensor glyphs to map the course of the fibres that constitute the drt in the human and macaque brains. Derived from a high quality brainstem tissue and sophisticated post-processing, the current results characterised and anatomically described this white matter tract at a resolution level beyond that previously reported (see also table 1 in Ch 1, and Appendix Fig. 26).

Calabrese et al. (2015b) used the same human specimen 1 as analysed here. They undertook probabilistic tractography of the drt and then used this as a template to estimate the precise site of electrodes inserted in twelve patients for deep brain stimulation (DBS) to treat tremor, where these patients had low resolution clinical MRIs to mark electrode sites. The work analysed herein presents a number of differences from that conducted by Calabrese et al. (2015b). Firstly, as my work is predominantly a descriptive anatomy study, I present a series of transverse, coronal, and sagittal sections from the caudal pons to the red nucleus (Fig. 5.1 and Fig. 5.4) using the FAC to anatomically describe the drt in 3D. Secondly, my work includes HARDI deterministic tractography combined with the annotated GRE background, providing the drt within the surrounding structures. Finally, I used the tensor glyph

(obtained with the FSL program) to unravel the fibre architecture of the drt within the superior cerebellar decussation. In summary, my work extends that of Calabrese et al. (2015b) by providing more detailed descriptive anatomy of the drt and surrounding brainstem and thalamic structures.

5.4.1 Decussating vs non-decussating pathway

Although the drt has been classically described as a decussating pathway, debate exists as to the extent in which it decussates or ascends ipsilaterally. A variety of studies have demonstrated a non-decussating (ipsilateral) drt in the rat (Aumann and Horne, 1996), in the cat (Flood and Jansen, 1966), in the monkey (Wiesendanger and Wiesendanger, 1985), and finally, in the human (Meola et al., 2016a). The significance of a bilateral projection is highlighted by the fact that when a lesion such as stroke, tumour or arteriovenous malformation involves a cerebellar hemisphere and by extension the dentate nucleus, bilateral limb motor impairment was observed (Fisher et al., 2006). Just as the corticospinal tract decussates and projects bilaterally heading towards the spinal cord, the same occurs for the corticopontine tract (Morecraft et al., 2018), the ventral and dorsal trigeminothalamic tracts and finally, for the drt. As a result, the same information processed in the dentate nucleus, projects at each cerebral hemisphere. This bilateral projection pattern could be advantageous in cases of neurological damage so that the information is being preserved. In the present study, I have observed the existence of both an ipsilateral and contralateral drt by using two seed masks at the same level, one for each of the two scp's. Moreover, I observed that the vast majority of the fibres decussate, whereas the lateral fibres of the xscp (blue fibres in periphery of xscp in FAC; Fig.

5.1d) do not decussate, rather they ascend ipsilaterally on both sides as non-decussating drt. However, I was unable to determine the exact percentage of the decussating fibres because in order to trace this complex pathway it was necessary to use two additional bilateral 3D ROI masks at the level of the red nucleus. As a result, any attempt to calculate the quantity of both ipsilateral and contralateral projections would be erroneous (Fig. 5.2). Although quantitative determination of nerve fibre density is challenging, to resolve this enigma an investigator could use the traditional way of counting fibres manually via fluorescence immunolabeling methods, or more sophisticated line intensity scan analysis (Sathyanesan et al., 2012). Nevertheless, further research is needed to determine whether or not these techniques are applicable for the xscp quantification.

5.4.2 Terminations of the drt

Our results regarding the projection from the dentate nucleus, through the scp, until the midbrain and the nucleus of termination (VL) in the thalamus are compatible with what was found in the monkey following WGA-HRP injections into the dentate nucleus (Sakai et al., 1996). Although the authors traced the projection from the dentate nucleus, through the scp to the red nucleus, they were unable to map the fibre tracts at the level of the xscp nor did they determine the exact portion of the red nucleus that receives the dentato-rubral projection. On the other hand, Stanton (1980) found that the dentate nucleus projects to the parvicellular red nucleus (RPC) and more precisely, that there is a projection from the rostroventral dentate to the lateral hindlimb areas in the RPC. I confirm and extend these results with my

tractography studies, observing that fibres which occupy the central parts of the drt terminate within the rostral red nucleus whereas the rest of the cerebellar projection continue through the scp towards the thalamus (see sagittal and coronal location of RPC in Fig. 5.4, and dentato-rubral fibres within the central part of the rostral red nucleus in Fig. 5.5a &b).

5.4.3 Implications for DBS treatment of tremor

The major implications of our study is that *ex vivo* MR histology obtained by ultra-high-field scanners produces anatomically accurate results that can be exploited for precise neurosurgical planning. As I described in the introduction (Ch 5.1), invasive deep brain stimulation for essential tremor traditionally targets the ventral tier of the thalamus, where it can achieve a reduction in tremor score one year post surgery ranging from 66% - 78% decrease as compared to pre-surgical scores (Dallapiazza et al., 2019). Adverse effects related to neurosurgery and DBS in the ventral tier of the thalamus include paraesthesia, ataxia and dysarthria, however it remains an effective strategy for tremor suppression.

A number of studies using clinical MRI and tractography have suggested that the drt is the locus of therapeutic benefit for tremor reduction. A correlation has been found between proximity to the drt and therapeutic benefit (Calabrese et al., 2015b, Fenoy and Schiess, 2017, Coenen et al., 2020, Coenen et al., 2011b, Coenen et al., 2014, Barkhoudarian et al., 2010, Coenen et al., 2011a, Henderson, 2012). In addition, Coenen et al. (2014) reported that electric fields applied on the anterior border and on the centre of the drt presented moderate and excellent

reduction in tremor, respectively. More specifically, Fenoy and Schiess (2017) used both clinical tractography and traditional atlas (Schaltenbrand, 1977) to identify the placement of electrode contacts for tremor control. Stereotactic coordinates ranging from 1 mm (caudal to the intercommissural line) to 2.9 mm (rostral to the intercommissural line) within the drt fibres resulted in effective tremor control (suggesting a direct drt targeting). Fenoy and Schiess (2017) suggest that the total rostrocaudal length in which the electrodes can be placed is 3.9 mm within the drt. Hence, mapping the drt with improved resolution, achieved here on human specimen 1, 2 and the macaque (see also Appendix Figs. 13, 14, 17, 18 regarding the rostral part of the drt), is highly important. Although this high resolution tractography was conducted on human specimen 1, the FAC of human specimen 2 and the macaque corroborated the rostral part of the drt identified with tractography in the present study. Therefore, my current results identify this 3.9 mm length as starting from the rostral pole of the red nucleus in which its parvicellular subdivision is defined (Fig. 5.5c), up until the ventral lateral nucleus of the thalamus at the level of the fornix, ventrally (Fig. 5.7c). Therefore, the landmarks for DBS in this segment of the drt can be defined ventrally in relation to the mammillary bodies, hypothalamus and optic tract as seen in Fig. 5.5c, until the fornix and the rostral part of the anterior commissure as seen in Fig. 5.7c. Moreover, the brainstem and thalamus in the present thesis were sectioned perpendicularly to their long axis, aligning with the configuration used in the most detailed and up-to-date chemoarchitectonic and myeloarchitectonic atlas of the human brainstem (Paxinos et al., 2020). Given that the drt and its nucleus of termination including the above landmarks are found ventrally throughout the

midbrain and thalamus, cutting the dataset perpendicularly to its long axis (and not according to the MNI space) could not be subjected to major morphological variations which are connected to the angle between the sagittal and transverse sections (perpendicular vs MNI space).

Therefore, the current work offers a 3D anatomical map of the drt which could more efficiently guide electrode placement directly within its fibres for future neurosurgical studies and applications regarding deep brain stimulation. Other more caudal key landmarks identified in this 3D map may also be possible targets for tremor reduction.

5.4.4 The complexity of the drt

The drt shows marked complexity, due to the fact that it is a disynaptic pathway with specific topography within the red nucleus on one hand and on the other it crosses over in the xscp to ascend as decussating and non-decussating projection. Moreover, not only does it decussate but as I demonstrated with the tensor glyphs the fibres within the decussation intertwine from both sides so that the information from the dentate nucleus disperses through various parts of the drt. This renders the identification and anatomical description of this pathway and its various components more complex than the descending and ascending pathways described in Chapters 3 and 4. This complexity may reflect the function of the cerebellum to integrate neuronal input and transmit this integrated information to the cerebral cortex for modulation and refinement of motor control. This complexity is also consistent with the intricate anatomical arrangement of the cerebrocerebellar circuit

as described in Chapter 3, since the drt represents the afferent leg from the cerebellum to the thalamus.

This observation regarding the complexity of the drt seems to be connected to the role that the cerebellum undertook during evolution. For over two hundred years, it has been understood and scientifically accepted that lesions of the cerebellum impair movement coordination. Luciani (1893) summarised the cerebellar syndrome and by extension the function of the skeletomotor cerebellum as a triad of symptoms: atonia (loss of muscle tone), ataxia (poor coordination), and astasia (inability to stand unassisted and loss of continuity of movement). Tasks that make the human species unique compared to non-human primates such as the ability to employ finer motor skills (dexterity), visuomotor functions through visual inputs to the cerebellum (vestibulo-ocular reflex by the flocculus, saccades, optokinetic and pursuit by the oculomotor vermis); (Glickstein et al., 1998), as well as non-motor functions of the cerebellum such as neurocognition (Stoodley and Schmahmann, 2018), are connected to the development and evolution of a complex organisation of the cerebrocerebellar circuit in *Homo sapiens*. The organisation of the cerebrocerebellar circuit is less complex in non-human primates (*Macaca mulatta*), for example the longitudinal fibres of the pons are four in the macaque vs nine in the human (see Chapter three), the interdigitations between these bundles are less in the macaque, the transverse fibres of the pons are five in the macaque vs ten in the human, and finally the same volume of the pons, crus cerebri but also the volume of the brainstem itself is smaller in the macaque. As we further analyse the change in the anatomical structures and characteristics of one species over another, we observe that the cerebrocerebellar circuit is rudimentary in the rat (Paxinos et al., 2015) and virtually absent in the bird

which lacks cerebellar hemispheres and has virtually no neocortex (Puelles et al., 2018). Finally, it may be that the complexity of the drt and most particularly the fibre intertwining within the xscp and fibre arrangement in the red nucleus is also greater in the human, than in non-human primates, and may even depend on the extent of skill and dexterity of the specific individual, however further research is needed.

5.4.5 Clinical Implications

Tractography of white matter connectivity is widely applied before neurosurgical procedures (Fernandez-Miranda et al., 2012). For example, applying this technique to ultra-high resolution postmortem data provides anatomical accuracy high enough for us to use as an investigative tool in order to map uncharted territories such as the scp, the xscp and red nucleus which could be used in neurosurgery and further propose possible anatomical sites for invasive insertion of electrodes.

Identification of the fine architecture of the drt will aid in understanding diseases associated with tremor and poor motor control, and to assist in their surgical treatments by offering a map for deep brain stimulation. This has been achieved using firstly, fractional anisotropy colour maps (FAC), secondly, deterministic tractography and thirdly, a higher-order tensor glyph.

This thesis provides evidence that there is no *a priori* reason to support the proposition that resolution is the main parameter for clearer brain visualisation. Thereby, diffusion imaging proves to be inherently a more sensitive and specific method for identification of fibres versus histology. The anatomical information that we obtained from the Duke specimen 1 at 200 μm of resolution for the diffusion data,

enabled us to create higher order models (HARDI, tensor glyphs) in order to elucidate structures and pathways previously concealed from traditional histology methods (1 μm), but also from more sophisticated and modern techniques developed in the last two decades such as polarized light microscopy (Axer et al., 2011). Although the drt is a larger projection compared to the tracts identified in Chapter four (dorsal column – medial lemniscus pathway, spth, 5n, sp5, vtt, dtt), it is expected that idiosyncratic differences will be present between human samples. However, the descriptive anatomy reported in the present thesis and the anatomical delineations regarding the drt correspond (in areas in which the FAC rendered the delineations possible) between human specimens 1, 2, 3, 4 and the macaque (see Appendix Figs. 13 – 18).

Chapter 6:
Conclusions

This thesis applied advanced DTI and tractography approaches to ultra-high-resolution MRI data from postmortem human and macaque brains to map out the brainstem and thalamus. In Chapter 2, I analyse the methodology and technical approaches such as the use of different DTI contrasts which open corresponding windows of view and shed light into brain anatomy regarding this novel method of brain mapping in its natural 3D space. In addition, I emphasise the importance of isotropic spatial resolution both in fibre tracking on the anatomical GRE, DTI contrasts and in tractography as the final output in investigative studies. I indicate that an investigator should always confirm and be guided in relation to structural anatomical contrasts in the transverse, sagittal and coronal sections. In Chapter 3, I mapped the internal capsule, crus cerebri, basilar pons and pyramids. In Chapter 4, I identified the sensory pathways such as the dorsal column-medial lemniscus pathway (dcml), the spth, the 5n, the sp5, the vtt and dtt projections from the caudal medulla until the corresponding nuclei of termination in the thalamus. The major contribution of this Chapter is the identification at the most precise level of the spth throughout the brainstem and thalamus, and the establishment of anatomical landmarks between the pain projections and the adjacent structures. In Chapter 5, I mapped the return leg of the cerebrocerebellar circuit from the most caudal part of the scp until the VL nucleus of the thalamus. Throughout this pathway, the precise topography and anatomical arrangements of the scp, xscp, the fibre arrangement within the red nucleus, and the pattern of the drt projection within the diencephalon have been unravelled for more comprehensive knowledge in neuroscience and neurosurgery.

6.1 Synopsis of Discoveries

Tractography analysed the pathways as they course through the thalamus and brainstem. More specifically, the internal capsule was subdivided into four parts along its long axis. The most external three parts are all occupied by cortico-pontine, -bulbar, -spinal projections with precise anatomical distributions. Moreover, the fourth most internal part of the internal capsule is occupied by the motor pathways that ultimately project to the substantia nigra (striatonigral and corticonigral projections). In this way there is a topographical organisation of the descending fibre bundles at this level such that (a) the most external part is occupied by the fibres that will eventually constitute the cervical component of the pyramidal tract, (b) the intermediate part by fibres of the thoracic component and (c) the internal part by fibres of the lumbar and sacral components. In addition, all the above three external parts contain corticopontine and corticobulbar projections. Finally, (d) the most internal part of the internal capsule is occupied by fibres en route to the substantia nigra pars reticulata. As the fibre bundles which constitute the three most external parts of the internal capsule descend beyond the diencephalon, they shift and assume a ventrolateral position in the shape of curved lamellae which fan out in the pontomesencephalic junction (rhombomere 2 & 1) where pontine grey matter and transverse fibres of the pons afterwards alternate between these curved lamellae.

Through the basilar pons, the lamellae descend in three groups of bundles (primary subdivisions; ventral, intermediate, dorsal) which can be further subdivided into nine distinct fibre bundles (secondary subdivisions) with a certain degree of interdigitations. All the subdivisions contain corticobulbar and corticospinal fibres within their medial parts, and corticopontine fibres within their most lateral and

external aspects, maintaining the same spatial distribution as in the crus cerebri. This study was the first to demonstrate such a topographic distribution. At each level, as the bundles descend caudally, the corticopontine fibres break off and bend to then synapse onto the pontine nuclei, which constitute the somata of origin of the transverse fibres of the pons. The ventral bundles in the basilar pons twist medially and are the cervical component of the pyramids; the intermediate bundles are found lateral to the cervical and are the thoracic component; similarly, the dorsal bundles twist laterally to the thoracic and are the lumbar and sacral components of the pyramid.

A novel fibre bundle (herein named the *Stria Pontis*) anatomically described, and suggested to convey cortical information to the pontine tegmentum. The *Stria Pontis* is a collection of transverse fibre tracts along the midline of the pons, identified from the rostral (rhombomere 2) to the caudal pons (rhombomere 4). In addition, I have been able to identify its termination fibres coursing within approximately 500 μm of the motor trigeminal and abducens nuclei in the pontine tegmentum at caudal pontine levels, hence I presume that the *Stria* is the final segment of the corticotegmental pathway. All these descending pathways mapped in Chapter 3 were seen across four human specimens, and were contrasted with a less complex pattern in a single macaque specimen.

Using the best quality and resolution obtained for specimen 1, Chapter 4 and 5 visualised in 3D, for the first time, the exact topography of the pain pathways in the human brainstem and the output pathway of the cerebellum to the thalamus (the dentato-rubro-thalamic tract). The results were validated where possible by the FAC of three more human specimens and one macaque. Prior research using viral tracing

techniques in animals and neuronal electrophysiology combined with fMRI studies in humans, identified the pain pathways but their detailed topography remained largely elusive (Yang et al., 2009, Jang and Seo, 2015, Yen et al., 1991, McGovern et al., 2015). I succeeded in tracing the spinothalamic and dorsal column – medial lemniscus pathways through the brainstem and thalamus, including defining the trigeminal nerve, sp5, vtt and dtt within the brainstem as they project towards the thalamus. In Chapter 5, I traced the dentato-rubro-thalamic tract from the caudal part of the scp to the VL nucleus of the thalamus. A couple of key points emerged in Chapter 5: the complexity of the superior cerebellar decussation has been revealed, for the first time, using higher order models such as the tensor glyphs, and tractography identified the part of the red nucleus that receives the cerebello-rubral projection which is in alignment with viral tracing studies. I detected both an ipsilateral and contralateral drt projection, nevertheless, I was unable to evaluate the precise percentage of an ipsilateral versus a contralateral drt, although the majority of the fibres decussate centrally whereas the minority ascend laterally through the midbrain.

6.2 Complex mathematical algorithms and sophisticated higher order techniques promote modernised fibre tracking

In Chapter 2, I provided a set of stepwise instructions for fibre tracking using deterministic tractography, FAC, and tensor glyphs. Although much trial and error and optimising is needed, the resolution of the MRI data enabled us to verify the tracts directly, something that cannot be applied to this extent in vivo MRI studies. In

addition, this work highlights the significance and validity of ex vivo ultra-high field MRI and sophisticated post-processing techniques such as high angular resolution diffusion imaging (HARDI) deterministic tractography which can be used as an investigative tool in connectomics (Boukadi et al., 2019, Wang et al., 2012, Van Essen et al., 2013). However, to date HARDI scheme in ex vivo specimens at microscopic resolution is performed in very few centres across the world and only now its major exploitation will reverberate in medicine. Just to mention an example, the number of the MRI scanners operating at 7T only now exceeds 70 around the world (Clarke et al., 2020). Tractography, based on diffusion tensor imaging (DTI), is a technique with great potential to indicate and highlight the in vivo integrity of white matter tracts and for this reason it is widely used for neurosurgical planning (Essayed et al., 2017, Panesar et al., 2019, Zoli et al., 2021, Shukla et al., 2017, Henderson et al., 2020). Moreover, tractography offers the ex vivo investigation of the pathways within the brain (Ellingson et al., 2008), also demonstrated herein, which can be used as an explorative tool to identify the patterning and integrity of brain fibre bundles. This has been accomplished since the advent of ultra-high-field MRI scanners and more detailed MRI post-processing, thus permitting us to achieve a resolution (50 μm for the human GRE and 25 μm for the macaque) that gradually approaches that of histology (1 μm; Yilmazer-Hanke et al. (2020)). Deterministic tractography allowed us to use a "deterministic" approach to investigate the brain pathways (Tan et al., 2015), the anatomical GRE permitted us to show the relationship of these pathways with the adjacent nuclei and most particularly we were able to shed light within the same pathways by exploiting the FAC at 200 μm and higher order techniques such as the tensor glyphs (for example, the topography

within the basilar pons, also within the descending bundles, xscp, red nucleus and so on).

Regarding the overarching hypothesis of this work, I conclude from the results reported herein, that there is indeed a further organisation and topography within the pathways through the brainstem and thalamus beyond that previously appreciated. The current work attests to the fact that as we develop sophisticated techniques, the more we will shed light on the structural and functional organisation of the brain.

6.3 Implications of the work

My overarching aim of the present studies was not only to verify previous studies nor was it to create new scientific theories but it was descriptive anatomy. I wanted to provide insights into the anatomy of the above pathways in humans, using some of the highest resolution data available (see table 1 in Ch 1). This work could significantly contribute to creating new knowledge and may consolidate diffusion imaging even more as a significant tool for basic brain research (Morita et al., 2016). Furthermore, this is applied science and can be clinically used to aid neurosurgery and stereotactic radiotherapy (Wang et al., 2019). For example, the motor pathways described in Chapter 3 can be disrupted in cases of pontine gliomas (Janjua et al., 2020), ischemic pathology (Calabrò et al., 2009), vasculitis (Razek et al., 2014), traumatic brainstem injury (Al-Sarraj et al., 2012), abscesses (Sclar et al., 2007) and finally central pontine myelinolysis (Martin, 2004); the pain and sensory pathways in Chapter 4 disrupted in lesions such as ectatic vessels (Savitz et al., 2006) or multiple

sclerosis (Skorić et al., 2014), infections (Hall, 1993), atherosclerotic disease (Feng et al., 2013) and most particularly in trigeminal neuralgia (Hughes et al., 2016), while the dentato-rubro-thalamic tract disrupted in essential tremor (Schlaier et al., 2015) and multiple sclerosis (Torres et al., 2010). I hope this work can provide a detailed map which includes the identification of anatomical landmarks in order to be used for invasive and non-invasive therapeutic techniques. In the immediate term, clinicians could be able to more accurately diagnose neurological upper or lower limb impairments associated with a tumour in the ventral or dorsal basilar pons respectively (Cavalheiro et al., 2015), and enabling a more targeted therapy (antiedema treatment, key-hole neurosurgery, gamma knife stereotactic radiotherapy, targeted therapy based on molecular biological markers) at the most precise level with minimal damage to adjacent nuclei and bundles (Shcherbenko, 2015).

6.4 Future Perspectives

I see this work progressing in a number of different ways. Firstly, the FAC volumetric dataset from the Center for In Vivo Microscopy, my tractography scripts and my maps can be incorporated into a database so surgeons and oncologists could overlay my subdivisions on their lower resolution clinical MRI of their patient brain, and thereby guide neurosurgery or deliver radiotherapy. Secondly, we may extend the research on the *Stria Pontis* by using electrophysiology in rodent brain and fMRI in humans to further validate, if possible, the function or implications for cranial nerve output. In addition, Golgi staining could be used to identify and follow each axon from the soma which is placed in the basilar pons and projects towards the

midline and further to the pontine tegmentum. This is a particular and time-consuming technique because Golgi staining allows the identification of a relatively small percentage of cells, and the selection process remains elusive (Di Cristo and Chattopadhyaya, 2020). Moreover, polarized light microscopy in humans, CLARITY technique, and recombinant viral tracing in non-human primates could be used as further investigative tools (Oldenbourg, 2013, Zhang et al., 2018a, Nectow and Nestler, 2020). Finally, the development of stronger magnetic fields and more sophisticated data post-processing will yield higher resolution images to affirm the topography within the descending bundles (corticopontine vs cortico-bulbar, -spinal tracts), and the origin and termination of the *Stria Pontis.*

6.5 Final Comment

Technologies that probe neural circuitry herald the golden age of brain science. Prior to the advent of superconducting magnets, visual examination of brain connections by expert neuroanatomists was limited to shades of grey and in two dimensions. By comparison, my work could set the threshold for a high quality three-dimensional colourful novel brain exploration in a way that brain mapping will take on a new dimension. In the long term, the development of more powerful magnetic fields capable of generating higher resolution images and increasingly sophisticated data post-processing will bring about a deeper insight for researchers and clinicians to fathom the pathways in the brain.

“The brain is a world consisting of a number of unexplored continents and great stretches of unknown territory”. Santiago Ramon y Cajal (1852-1934)

“Since the initial suggestion by Lauterbur (*Nature*, 1973) that the technique of nuclear magnetic resonance could be used to produce images of intact biological materials”, the first researcher to bring this vision to practice was Dr. G. Allan Johnson.

References

ABHINAV, K., YEH, F.-C., PATHAK, S., SUSKI, V., LACOMIS, D., FRIEDLANDER, R. M. & FERNANDEZ-MIRANDA, J. C. 2014. Advanced diffusion MRI fiber tracking in neurosurgical and neurodegenerative disorders and neuroanatomical studies: A review. *Biochimica et Biophysica Acta (BBA) - Molecular Basis of Disease,* 1842**,** 2286-2297.

ACKERLEY, R., CARLSSON, I., WESTER, H., OLAUSSON, H. & BACKLUND WASLING, H. 2014. Touch perceptions across skin sites: differences between sensitivity, direction discrimination and pleasantness. *Frontiers in behavioral neuroscience,* 8**,** 54-54.

AFIFI, A. K., BAHUTH, N. B., KAELBER, W. W., MIKHAEL, E. & NASSAR, S. 1974. The cortico-nigral fibre tract. An experimental Fink-Heimer study in cats. *Journal of anatomy,* 118**,** 469-476.

AGGARWAL, M., ZHANG, J., PLETNIKOVA, O., CRAIN, B., TRONCOSO, J. & MORI, S. 2013. Feasibility of creating a high-resolution 3D diffusion tensor imaging based atlas of the human brainstem: a case study at 11.7 T. *Neuroimage,* 74**,** 117-27.

AKAKIN, A., PERIS-CELDA, M., KILIC, T., SEKER, A., GUTIERREZ-MARTIN, A. & RHOTON, A., JR. 2014. The dentate nucleus and its projection system in the human cerebellum: the dentate nucleus microsurgical anatomical study. *Neurosurgery,* 74**,** 401-24; discussion 424-5.

AL-SARRAJ, S., FEGAN-EARL, A., UGBADE, A., BODI, I., CHAPMAN, R., POOLE, S., SWIFT, B., JERREAT, P. & CARY, N. 2012. Focal traumatic brain stem injury is a rare type of head injury resulting from assault: a forensic neuropathological study. *Jornal of Forensic Legal Medicine,* 19**,** 144-51.

ALESCH, F., PINTER, M. M., HELSCHER, R. J., FERTL, L., BENABID, A. L. & KOOS, W. T. 1995. Stimulation of the ventral intermediate thalamic nucleus in tremor dominated Parkinson's disease and essential tremor. *Acta Neurochirurgica,* 136**,** 75-81.

ALEXANDER, A. L., LEE, J. E., LAZAR, M. & FIELD, A. S. 2007. Diffusion tensor imaging of the brain. *Neurotherapeutics : the journal of the American Society for Experimental NeuroTherapeutics,* 4**,** 316-329.

ALLEN, J. D. 2008. Human Physiology - the Basis of Medicine. *The Ulster Medical Journal,* 77**,** 216-216.

ALLEN, W. E. 2009. Terminologia anatomica: international anatomical terminology and Terminologia Histologica: International Terms for Human Cytology and Histology. *Journal of Anatomy,* 215**,** 221-221.

AMMONS, W. S. 1987. Characteristics of spinoreticular and spinothalamic neurons with renal input. *Journal of Neurophysioly,* 58**,** 480-95.

ANGELES FERNÁNDEZ-GIL, M., PALACIOS-BOTE, R., LEO-BARAHONA, M. & MORA-ENCINAS, J. P. 2010. Anatomy of the brainstem: a gaze into the stem of life. *Seminars in Ultrasound, CT and MRI,* 31**,** 196-219.

ANTAL, M., SHOLOMENKO, G. N., MOSCHOVAKIS, A. K., STORM-MATHISEN, J., HEIZMANN, C. W. & HUNZIKER, W. 1992. The termination pattern and postsynaptic targets of rubrospinal fibers in the rat

spinal cord: a light and electron microscopic study. *Journal of Comparative Neurology,* 325**,** 22-37.

APKARIAN, A. V. & HODGE, C. J. 1989a. Primate spinothalamic pathways: I. A quantitative study of the cells of origin of the spinothalamic pathway. *Journal of Comparative Neurology,* 288**,** 447-73.

APKARIAN, A. V. & HODGE, C. J. 1989b. Primate spinothalamic pathways: II. The cells of origin of the dorsolateral and ventral spinothalamic pathways. *Journal of Comparative Neurology,* 288**,** 474-92.

APKARIAN, A. V. & HODGE, C. J. 1989c. Primate spinothalamic pathways: III. Thalamic terminations of the dorsolateral and ventral spinothalamic pathways. *Journal of Comparative Neurology,* 288**,** 493-511.

ARAVAMUTHAN, B. R., MUTHUSAMY, K. A., STEIN, J. F., AZIZ, T. Z. & JOHANSEN-BERG, H. 2007. Topography of cortical and subcortical connections of the human pedunculopontine and subthalamic nuclei. *Neuroimage,* 37**,** 694-705.

ARFKEN, G. 1985. *Eigenvectors, Eigenvalues. Mathematical Methods for Physics,* Orlando, Academic Press.

ARMAND, J. 1982. The Origin, Course and Terminations of Corticospinal Fibers in Various Mammals. *Progress in Brain Research.* Elsevier.

ARMAND, J., OLIVIER, E., EDGLEY, S. A. & LEMON, R. N. 1997. Postnatal development of corticospinal projections from motor cortex to the cervical enlargement in the macaque monkey. *Journal of Neuroscience,* 17**,** 251-66.

ASAI, A., OGURA, A., SOTOME, H. & FUJU, A. 2018. Effect of Slice Thickness for Apparent Diffusion Coefficient Measurement of Mass. *Nihon Hoshasen Gijutsu Gakkai Zasshi,* 74**,** 805-809.

ASTOLA, L., SEPASIAN, N., HAIJE, T. D., FUSTER, A. & FLORACK, L. 2014. A Simplified Algorithm for Inverting Higher Order Diffusion Tensors. *Multidisciplinary Digital Publishing Institute,* 3**,** 369-379.

ATTA, H. M. 1999. Edwin Smith Surgical Papyrus: the oldest known surgical treatise. *American Journal of Surgery,* 65**,** 1190-2.

AUGUSTINE, J. R. 2007. *Human Neuroanatomy,* San Diego, Academic press.

AUMANN, T. D. & HORNE, M. K. 1996. Ramification and termination of single axons in the cerebellothalamic pathway of the rat. *Journal of Comparative Neurology,* 376**,** 420-430.

AXER, H., BECK, S., AXER, M., SCHUCHARDT, F., HEEPE, J., FLÜCKEN, A., AXER, M., PRESCHER, A. & WITTE, O. W. 2011. Microstructural analysis of human white matter architecture using polarized light imaging: views from neuroanatomy. *Frontiers in neuroinformatics,* 5**,** 28-28.

AZADBAKHT, H., PARKES, L. M., HAROON, H. A., AUGATH, M., LOGOTHETIS, N. K., DE CRESPIGNY, A., D'ARCEUIL, H. E. & PARKER, G. J. 2015. Validation of High-Resolution Tractography Against In Vivo Tracing in the Macaque Visual Cortex. *Cerebral Cortex,* 25**,** 4299-309.

BAKER, S. N. 2011. The primate reticulospinal tract, hand function and functional recovery. *The Journal of physiology,* 589**,** 5603-5612.

BAKER, S. N. & PEREZ, M. A. 2017. Reticulospinal Contributions to Gross Hand Function after Human Spinal Cord Injury. *Journal of Neuroscience,* 37**,** 9778-9784.

BAKKER, R., WACHTLER, T. & DIESMANN, M. 2012. CoCoMac 2.0 and the future of tract-tracing databases. *Frontiers in Neuroinformatics,* 6(30).

BAR-SHIR, A., DUNCAN, I. D. & COHEN, Y. 2009. QSI and DTI of excised brains of the myelin-deficient rat. *Neuroimage,* 48**,** 109-16.

BARKHOUDARIAN, G., KLOCHKOV, T., SEDRAK, M., FREW, A., GORGULHO, A., BEHNKE, E. & DE SALLES, A. 2010. A role of diffusion tensor imaging in movement disorder surgery. *Acta Neurochirurgica (Wien),* 152**,** 2089-95.

BARRETT, K. E., BOITANO, S., BARMAN, S. M., BROOKS, H. L. & GANONG, W. F. 2015. *Ganong's review of medical physiology*.

BASBAUM, A. I. & FIELDS, H. L. 1979. The origin of descending pathways in the dorsolateral funiculus of the spinal cord of the cat and rat: further studies on the anatomy of pain modulation. *Journal of Compative Neurology,* 187**,** 513-31.

BASSER, P. J., MATTIELLO, J. & LEBIHAN, D. 1994a. Estimation of the effective self-diffusion tensor from the NMR spin echo. *Journal of Magnetic Resonance B,* 103**,** 247-54.

BASSER, P. J., MATTIELLO, J. & LEBIHAN, D. 1994b. MR diffusion tensor spectroscopy and imaging. *Biophysics Journal,* 66**,** 259-67.

BASSER, P. J., PAJEVIC, S., PIERPAOLI, C., DUDA, J. & ALDROUBI, A. 2000. In vivo fiber tractography using DT-MRI data. *Magnetic Resonance in Medicine,* 44**,** 625-32.

BASSER, P. J. & PIERPAOLI, C. 1996. Microstructural and physiological features of tissues elucidated by quantitative-diffusion-tensor MRI. *Journal of Magnetic Resonance B,* 111**,** 209-19.

BASSETTI, C., BOGOUSSLAVSKY, J., BARTH, A. & REGLI, F. 1996. Isolated infarcts of the pons. *Neurology,* 46**,** 165-75.

BEAULIEU, C. 2002. The basis of anisotropic water diffusion in the nervous system - a technical review. *NMR Biomedicine,* 15**,** 435-55.

BECERRA, J. L., PUCKETT, W. R., HIESTER, E. D., QUENCER, R. M., MARCILLO, A. E., POST, M. J. & BUNGE, R. P. 1995. MR-pathologic comparisons of wallerian degeneration in spinal cord injury. *AJNR American Journal of Neuroradiology,* 16**,** 125-33.

BECKER, R., SURE, U. & BERTALANFFY, H. 1999. Punctate midline myelotomy. A new approach in the management of visceral pain. *Acta Neurochirurgica (Wien),* 141**,** 881-3.

BEHRENS, T. E., BERG, H. J., JBABDI, S., RUSHWORTH, M. F. & WOOLRICH, M. W. 2007. Probabilistic diffusion tractography with multiple fibre orientations: What can we gain? *Neuroimage,* 34**,** 144-55.

BEHRENS, T. E., WOOLRICH, M. W., JENKINSON, M., JOHANSEN-BERG, H., NUNES, R. G., CLARE, S., MATTHEWS, P. M., BRADY, J. M. & SMITH, S. M. 2003a. Characterization and propagation of uncertainty in diffusion-weighted MR imaging. *Magnetic Resonance in Medicine,* 50**,** 1077-88.

BEHRENS, T. E. J., JOHANSEN-BERG, H., WOOLRICH, M. W., SMITH, S. M., WHEELER-KINGSHOTT, C. A. M., BOULBY, P. A., BARKER, G. J., SILLERY, E. L., SHEEHAN, K., CICCARELLI, O., THOMPSON, A. J., BRADY, J. M. & MATTHEWS, P. M. 2003b. Non-invasive mapping of

connections between human thalamus and cortex using diffusion imaging. *Nature Neuroscience,* 6**,** 750-757.

BELLO, L., GAMBINI, A., CASTELLANO, A., CARRABBA, G., ACERBI, F., FAVA, E., GIUSSANI, C., CADIOLI, M., BLASI, V., CASAROTTI, A., PAPAGNO, C., GUPTA, A. K., GAINI, S., SCOTTI, G. & FALINI, A. 2008. Motor and language DTI Fiber Tracking combined with intraoperative subcortical mapping for surgical removal of gliomas. *Neuroimage,* 39**,** 369-82.

BENAGIANO, V., RIZZI, A., LORUSSO, L., FLACE, P., SACCIA, M., CAGIANO, R., RIBATTI, D., RONCALI, L. & AMBROSI, G. 2018. The functional anatomy of the cerebrocerebellar circuit: A review and new concepts. *The Journal of Comparative Neurology,* 526**,** 769-789.

BENAGIANO, V., RONCALI, L., VIRGINTINO, D., FLACE, P., ERREDE, M., RIZZI, A., GIROLAMO, F., ROBERTSON, D., BORMANN, J. & AMBROSI, G. J. T. H. J. 2001. GABA immunoreactivity in the human cerebellar cortex: a light and electron microscopical study. *The Histochemical Journal,* 33**,** 537-543.

BENNETT, G. J., SELTZER, Z., LU, G. W., NISHIKAWA, N. & DUBNER, R. 1983. The cells of origin of the dorsal column postsynaptic projection in the lumbosacral enlargements of cats and monkeys. *Somatosensory & Motor Research,* 1**,** 131-49.

BERKLEY, K. J., BLOMQVIST, A., PELT, A. & FLINK, R. 1980. Differences in the collateralization of neuronal projections from the dorsal column nuclei and lateral cervical nucleus to the thalamus and tectum in the cat: an anatomical study using two different double-labeling techniques. *Brain Research,* 202**,** 273-90.

BIEDENBACH, M. A., DEVITO, J. L. & BROWN, A. C. 1986. Pyramidal tract of the cat: axon size and morphology. *Experimental Brain Research,* 61**,** 303-310.

BIEMOND, A. 1951. Thrombosis of the basilar artery-the vascularization of the brain stem. *Brain***,** 300-17.

BIHAN, D. L. & WARACH, S. J. 1995. Diffusion and Perfusion Magnetic Resonance Imaging: Applications to Functional MRI. *Journal of Neurology, Neurosurgery & Psychiatry,* 19**,** 844.

BISWAS, A., MANIVANNAN, M. & SRINIVASAN, M. A. 2015. Vibrotactile sensitivity threshold: nonlinear stochastic mechanotransduction model of the Pacinian Corpuscle. *IEEE Transactions on Haptics,* 8**,** 102-13.

BIZLEY, J. K., BAJO, V. M., NODAL, F. R. & KING, A. J. J. J. O. C. N. 2015. Cortico-cortical connectivity within ferret auditory cortex. *The Journal of Comparative Neurology,* 523**,** 2187-2210.

BLAIR, R. W., AMMONS, W. S. & FOREMAN, R. D. 1984. Responses of thoracic spinothalamic and spinoreticular cells to coronary artery occlusion. *Journal of Neurophysioly,* 51**,** 636-48.

BLOCK, K. T., UECKER, M. & FRAHM, J. 2008. Suppression of MRI Truncation Artifacts Using Total Variation Constrained Data Extrapolation. *International Journal of Biomedical Imaging,* 2008**,** 184123.

BLOMQVIST, A., ZHANG, E. T. & CRAIG, A. D. 2000. Cytoarchitectonic and immunohistochemical characterization of a specific pain and temperature relay, the posterior portion of the ventral medial nucleus, in the human thalamus. *Brain,* 123 Pt 3**,** 601-19.

BLOMSTEDT, P., STENMARK PERSSON, R., HARIZ, G.-M., LINDER, J., FREDRICKS, A., HÄGGSTRÖM, B., PHILIPSSON, J., FORSGREN, L. & HARIZ, M. 2018. Deep brain stimulation in the caudal zona incerta versus best medical treatment in patients with Parkinson's disease: a randomised blinded evaluation. *Journal of Neurology, Neurosurgery & Psychiatry,* 89**,** 710-716.

BOTA, M., SPORNS, O. & SWANSON, L. W. J. P. O. T. N. A. O. S. 2015. Architecture of the cerebral cortical association connectome underlying cognition. *Proceedings of the National Academy of Sciences,* 112**,** E2093-E2101.

BOUKADI, M., MARCOTTE, K., BEDETTI, C., HOUDE, J.-C., DESAUTELS, A., DESLAURIERS-GAUTHIER, S., CHAPLEAU, M., BORÉ, A., DESCOTEAUX, M. & BRAMBATI, S. M. 2019. Test-Retest Reliability of Diffusion Measures Extracted Along White Matter Language Fiber Bundles Using HARDI-Based Tractography. *Frontiers in Neuroscience,* 12.

BOULAIS, N. & MISERY, L. 2007. Merkel cells. *Journal of the American Academy of Dermatology,* 57**,** 147-65.

BRENNER, H. & PENDL, G. 1966. Ipsilateral effect of chordotomy--a rare case of an uncrossed pathway of pain. *Wiener Medizinische Wochenschriff,* 116**,** 1041-2.

BRICOLO, A. & TURAZZI, S. 1995. Surgery for gliomas and other mass lesions of the brainstem. *Advances and Techical Standards in Neurosurgery,* 22**,** 261-341.

BRODAL, A. 1981. Brodal, A., Neurological anatomy in relation to clinical medicine. Third edition. New York, Oxford University Press, 10**,** 584-584.

BRODAL, P. 1978a. The corticopontine projection in the rhesus monkey. Origin and principles of organization. *Brain,* 101**,** 251-83.

BRODAL, P. 1978b. Principles of organization of the monkey corticopontine projection. *Brain Research,* 148**,** 214-8.

BRODAL, P. 2014. Pontine Nuclei. *Encyclopedia of the Neurological Sciences (Second Edition).* Oxford: Academic Press.

BRODAL, P. & BJAALIE, J. G. 1997. Chapter 13 Salient anatomic features of the cortico-ponto-cerebellar pathway. *Progress in Brain Research.* Elsevier.

BRODMANN, K. 1909. Vergleichende Lokalisationslehre der Grosshirnrinde in ihren Prinzipien dargestellt auf Grund des Zellenbaues.

BROMAN, J. & BLOMQVIST, A. 1989. GABA-immunoreactive neurons and terminals in the lateral cervical nucleus of the cynomolgus monkey. *Journal of Comparative Neurology,* 283**,** 415-24.

BRÖSAMLE, C. & SCHWAB, M. E. 1997. Cells of origin, course, and termination patterns of the ventral, uncrossed component of the mature rat corticospinal tract. *Journal of Comparative Neurology,* 386**,** 293-303.

BROWN, A. G., FYFFE, R. E., NOBLE, R., ROSE, P. K. & SNOW, P. J. 1980. The density, distribution and topographical organization of spinocervical tract neurones in the cat. *Journal of Physiology,* 300**,** 409-28.

BROWNSTONE, R. M. & CHOPEK, J. W. 2018. Reticulospinal Systems for Tuning Motor Commands. *Frontiers in neural circuits,* 12**,** 30-30.

BRYAN, R. N., COULTER, J. D. & WILLIS, W. D. 1974. Cells of origin of the spinocervical tract in the monkey. *Experimental Neurology,* 42**,** 574-86.

BUCKNER, R. L., KRIENEN, F. M., CASTELLANOS, A., DIAZ, J. C. & YEO, B. T. 2011. The organization of the human cerebellum estimated by intrinsic functional connectivity. *Journal of Neurophysioly,* 106**,** 2322-45.

BURDETTE, J. H., DURDEN, D. D., ELSTER, A. D. & YEN, Y. F. 2001. High b-value diffusion-weighted MRI of normal brain. *Journal of Computer Assisted Tomography,* 25**,** 515-9.

BURMAN, K., DARIAN-SMITH, C. & DARIAN-SMITH, I. 2000a. Geometry of rubrospinal, rubroolivary, and local circuit neurons in the macaque red nucleus. *Journal of Comparative Neurology,* 423**,** 197-219.

BURMAN, K., DARIAN-SMITH, C. & DARIAN-SMITH, I. 2000b. Macaque red nucleus: origins of spinal and olivary projections and terminations of cortical inputs. *Journal of Comparative Neurology,* 423**,** 179-196.

BURSTEIN, R., DADO, R. J. & GIESLER, G. J., JR. 1990b. The cells of origin of the spinothalamic tract of the rat: a quantitative reexamination. *Brain Research,* 511**,** 329-37.

CAAN, M. W. A. 2016. DTI Analysis Methods: Fibre Tracking and Connectivity. *Diffusion Tensor Imaging: A Practical Handbook.* New York, NY: Springer New York.

CACCIOLA, A., MILARDI, D., ANASTASI, G. P., BASILE, G. A., CIOLLI, P., IRRERA, M., CUTRONEO, G., BRUSCHETTA, D., RIZZO, G., MONDELLO, S., BRAMANTI, P. & QUARTARONE, A. 2016. A Direct Cortico-Nigral Pathway as Revealed by Constrained Spherical Deconvolution Tractography in Humans. *Frontiers in human neuroscience,* 10**,** 374-374.

CAJAL, S. R. Y. 1899. *Histology of the Nervous System,* Toronto, OXFORD UNIVERSITY PRESS.

CALABRESE, E., BADEA, A., COFER, G., QI, Y. & JOHNSON, G. A. 2015a. A Diffusion MRI Tractography Connectome of the Mouse Brain and Comparison with Neuronal Tracer Data. *Cerebral cortex (New York, N.Y. : 1991),* 25**,** 4628-4637.

CALABRESE, E., HICKEY, P., HULETTE, C., ZHANG, J., PARENTE, B., LAD, S. P. & JOHNSON, G. A. 2015b. Postmortem diffusion MRI of the human brainstem and thalamus for deep brain stimulator electrode localization. *Human Brain Mapping,* 36**,** 3167-78.

CALABRÒ, R. S., LAGANÀ, A., SAVICA, R., LA SPINA, P., MENTO, G., LONGO, M. & MUSOLINO, R. 2009. Brainstem ischemia, steno-occlusive pathology of the vertebral arteries, and alterations in the circadian blood pressure pattern: a case report. *Journal of Stroke & Cerebrovascular Disease,* 18**,** 309-12.

CAMPBELL, J. S. W. & PIKE, G. B. 2014. Potential and limitations of diffusion MRI tractography for the study of language. *Brain and Language,* 131**,** 65-73.

CANEDO, A. 1997. Primary motor cortex influences on the descending and ascending systems. *Progress in Neurobiology,* 51**,** 287-335.

CANEDO, A. 2003. Functional heterogeneity of the piramidal system: corticobulbar and corticospinal tracts. *Revue Neurologique,* 36**,** 438-52.

CAO, C. Q., DJOUHRI, L. & BROWN, A. G. 1993. Lumbosacral spinal neurons in the cat that are candidates for being activated by collaterals from the spinocervical tract. *Neuroscience,* 57**,** 153-65.

CARLSON, B. M. 2019. Chapter 3 - Skin. *The Human Body.* Academic Press.

CASTIGLIONI, A. J., GALLAWAY, M. C. & COULTER, J. D. 1978. Spinal projections from the midbrain in monkey. *Journal of Comparative Neurology,* 178**,** 329-46.

CATALA, M. & KUBIS, N. 2013. Gross anatomy and development of the peripheral nervous system. *Handbook of Clinical Neurology,* 115**,** 29-41.

CAVALHEIRO, S., YAGMURLU, K., DA COSTA, M. D. S., NICÁCIO, J. M., RODRIGUES, T. P., CHADDAD-NETO, F. & RHOTON, A. L. 2015. Surgical approaches for brainstem tumors in pediatric patients. *Child's nervous system : ChNS : official journal of the International Society for Pediatric Neurosurgery,* 31**,** 1815-1840.

CERVERO, F., IGGO, A. & MOLONY, V. 1977. Responses of spinocervical tract neurones to noxious stimulation of the skin. *Journal of Physiology,* 267**,** 537-58.

CHARALAMPAKI, P., KAFADAR, A. M., GRUNERT, P., AYYAD, A. & PERNECZKY, A. 2008. Vascular Decompression of Trigeminal and Facial Nerves in the Posterior Fossa under Endoscope-Assisted Keyhole Conditions. *Skull base : official journal of North American Skull Base Society ... [et al.],* 18**,** 117-128.

CHOUDHRI, O., CONNOLLY, I. D. & LAWTON, M. T. 2017. Macrovascular Decompression of the Brainstem and Cranial Nerves: Evolution of an Anteromedial Vertebrobasilar Artery Transposition Technique. *Neurosurgery,* 81**,** 367-376.

CLARKE, W. T., MOUGIN, O., DRIVER, I. D., RUA, C., MORGAN, A. T., ASGHAR, M., CLARE, S., FRANCIS, S., WISE, R. G., RODGERS, C. T., CARPENTER, A., MUIR, K. & BOWTELL, R. 2020. Multi-site harmonization of 7 tesla MRI neuroimaging protocols. *NeuroImage,* 206**,** 116335.

COENEN, V. A., ALLERT, N. & MÄDLER, B. 2011a. A role of diffusion tensor imaging fiber tracking in deep brain stimulation surgery: DBS of the dentato-rubro-thalamic tract (drt) for the treatment of therapy-refractory tremor. *Acta Neurochirurgica (Wien),* 153**,** 1579-85; discussion 1585.

COENEN, V. A., ALLERT, N., PAUS, S., KRONENBÜRGER, M., URBACH, H. & MÄDLER, B. 2014. Modulation of the cerebello-thalamo-cortical network in thalamic deep brain stimulation for tremor: a diffusion tensor imaging study. *Neurosurgery,* 75**,** 657-69; discussion 669-70.

COENEN, V. A., MÄDLER, B., SCHIFFBAUER, H., URBACH, H. & ALLERT, N. 2011b. Individual fiber anatomy of the subthalamic region revealed with diffusion tensor imaging: a concept to identify the deep brain stimulation target for tremor suppression. *Neurosurgery,* 68**,** 1069-75; discussion 1075-6.

COENEN, V. A., SAJONZ, B., PROKOP, T., REISERT, M., PIROTH, T., URBACH, H., JENKNER, C. & REINACHER, P. C. 2020. The dentato-rubro-thalamic tract as the potential common deep brain stimulation target for tremor of various origin: an observational case series. *Acta Neurochirurgica (Wien),* 162**,** 1053-1066.

CONTURO, T. E., LORI, N. F., CULL, T. S., AKBUDAK, E., SNYDER, A. Z., SHIMONY, J. S., MCKINSTRY, R. C., BURTON, H. & RAICHLE, M. E. 1999. Tracking neuronal fiber pathways in the living human brain. *Proceedings of the National Academy of Sciences of U S A,* 96**,** 10422-7.

COOKE, J. D., LARSON, B., OSCARSSON, O. & SJÖLUND, B. 1971. Organization of afferent connections to cuneocerebellar tract. *Experimental Brain Research,* 13**,** 359-77.

CRAIG, A. D., JR. 1978. Spinal and medullary input to the lateral cervical nucleus. *Journal of Comparative Neurology,* 181**,** 729-43.

CRAIG, A. D., JR. & BURTON, H. 1979. The lateral cervical nucleus in the cat: anatomic organization of cervicothalamic neurons. *Journal of Comparative Neurology,* 185**,** 329-46.

CRAIG, A. D., JR. & TAPPER, D. N. 1978. Lateral cervical nucleus in the cat: functional organization and characteristics. *Journal of Neurophysiology,* 41**,** 1511-34.

CRAIG, A. D., ZHANG, E. T. & BLOMQVIST, A. 2002. Association of spinothalamic lamina I neurons and their ascending axons with calbindin-immunoreactivity in monkey and human. *Pain,* 97**,** 105-15.

CRAMER, H., MEHLING, W. E., SAHA, F. J., DOBOS, G. & LAUCHE, R. 2018. Postural awareness and its relation to pain: validation of an innovative instrument measuring awareness of body posture in patients with chronic pain. *BMC musculoskeletal disorders,* 19**,** 109-109.

D'ARCEUIL, H. E., WESTMORELAND, S. & DE CRESPIGNY, A. J. 2007. An approach to high resolution diffusion tensor imaging in fixed primate brain. *Neuroimage,* 35**,** 553-65.

DALLAPIAZZA, R. F., LEE, D. J., DE VLOO, P., FOMENKO, A., HAMANI, C., HODAIE, M., KALIA, S. K., FASANO, A. & LOZANO, A. M. 2019. Outcomes from stereotactic surgery for essential tremor. *Journal of Neurology, Neurosurgery & Psychiatry,* 90**,** 474.

DAVIDOFF, R. A. 1990. The pyramidal tract. *Neurology,* 40**,** 332-9.

DAWE, R. J., BENNETT, D. A., SCHNEIDER, J. A., VASIREDDI, S. K. & ARFANAKIS, K. 2009. Postmortem MRI of human brain hemispheres: T2 relaxation times during formaldehyde fixation. *Magnetic Resonance in Medicine,* 61**,** 810-818.

DE LAHUNTA, A., GLASS, E. N. & KENT, M. 2016. Embryonic Development of the Central Nervous System. *Veterinary Clinics of North America: Small Animal Practice,* 46**,** 193-216.

DE OLIVEIRA-SOUZA, R. 2012. The human extrapyramidal system. *Medical Hypotheses,* 79**,** 843-52.

DEISTUNG, A., SCHÄFER, A., SCHWESER, F., BIEDERMANN, U., GÜLLMAR, D., TRAMPEL, R., TURNER, R. & REICHENBACH, J. R. 2013. High-Resolution MR Imaging of the Human Brainstem In vivo at 7 Tesla. *Frontiers in Human Neuroscience,* 7**,** 710.

DELANO, M. C., COOPER, T. G., SIEBERT, J. E., POTCHEN, M. J. & KUPPUSAMY, K. 2000. High-b-value Diffusion-weighted MR Imaging of Adult Brain: Image Contrast and Apparent Diffusion Coefficient Map Features, *American Journal of Neuroradiology,* 21**,** 1830-1836.

DELETTRE, C., MESSÉ, A., DELL, L.-A., FOUBET, O., HEUER, K., LARRAT, B., MERIAUX, S., MANGIN, J.-F., REILLO, I., DE JUAN ROMERO, C., BORRELL, V., TORO, R. & HILGETAG, C. C. 2019. Comparison between diffusion MRI tractography and histological tract-tracing of cortico-cortical structural connectivity in the ferret brain, *Network Neuroscience,* 517136.

DELL, L. A., INNOCENTI, G. M., HILGETAG, C. C. & MANGER, P. R. J. J. O. C. N. 2019. Cortical and thalamic connectivity of occipital visual cortical areas 17, 18, 19, and 21 of the domestic ferret (Mustela putorius furo), *The Journal of Comparative Neurology,* 527**,** 1293-1314.

DEMYER, W. 1998. *Neuroanatomy*, Williams & Wilkins.

DEVOIZE, L., DOMÉJEAN, S., MELIN, C., RABOISSON, P., ARTOLA, A. & DALLEL, R. 2010. Organization of projections from the spinal trigeminal subnucleus oralis to the spinal cord in the rat: a neuroanatomical substrate for reciprocal orofacial-cervical interactions. *Brain Research,* 1343**,** 75-82.

DI CRISTO, G. & CHATTOPADHYAYA, B. 2020. Chapter 5 - Development of neuronal circuits: From synaptogenesis to synapse plasticity. *Handbook of Clinical Neurology.* Elsevier.

DIA TINE, S., TAMBA, B., GASSAMA, B. B., NIANG, P., DIA, L., KÉBÉ NDÈYE, F., BADIANE, S. & DIALLO, B. 2009. Clinical and therapeutic aspects of trigeminal neuralgia. Apropos of 27 cases treated at the General Hospital of Grand-Yoffin Dakar. *Odontostomatologie Tropicale,* 32**,** 5-12.

DIBB, R. & LIU, C. 2017. Joint eigenvector estimation from mutually anisotropic tensors improves susceptibility tensor imaging of the brain, kidney, and heart. *Magnetic Resonance in Medicine,* 77**,** 2331-2346.

DIMITRIJEVIC, M. R., DANNER, S. M. & MAYR, W. 2015. Neurocontrol of Movement in Humans With Spinal Cord Injury. *Artificial Organs,* 39**,** 823-33.

DJOUHRI, L. & JANKOWSKA, E. 1998. Indications for coupling between feline spinocervical tract neurones and midlumbar interneurones. *Experimental Brain Research,* 119**,** 39-46.

DOMINIETTO, M. & RUDIN, M. 2014. Could magnetic resonance provide in vivo histology? *Frontiers in genetics,* 4**,** 298-298.

DONAHUE, C. J., SOTIROPOULOS, S. N., JBABDI, S., HERNANDEZ-FERNANDEZ, M., BEHRENS, T. E., DYRBY, T. B., COALSON, T., KENNEDY, H., KNOBLAUCH, K., VAN ESSEN, D. C. & GLASSER, M. F. 2016. Using Diffusion Tractography to Predict Cortical Connection Strength and Distance: A Quantitative Comparison with Tracers in the Monkey. *The Journal of Neuroscience,* 36**,** 6758.

DOSTROVSKY, J. O. 1984. Brainstem influences on transmission of somatosensory information in the spinocervicothalamic pathway. *Brain Research,* 292**,** 229-38.

DOW, R. S. 1988. Contribution of electrophysiological studies to cerebellar physiology. *Journal of Clinical Neurophysiology,* 5**,** 307-23.

DREW, T. & ROSSIGNOL, S. 1990. Functional organization within the medullary reticular formation of intact unanesthetized cat. II. Electromyographic activity evoked by microstimulation. *Journal of Neurophysiology,* 64**,** 782-95.

DUBIN, A. E. & PATAPOUTIAN, A. 2010. Nociceptors: the sensors of the pain pathway. *The Journal of clinical investigation,* 120**,** 3760-3772.

DUM, R. P., LEVINTHAL, D. J. & STRICK, P. L. 2009. The spinothalamic system targets motor and sensory areas in the cerebral cortex of monkeys. *Journal of Neuroscience,* 29**,** 14223-35.

DUM, R. P. & STRICK, P. L. 2003. An unfolded map of the cerebellar dentate nucleus and its projections to the cerebral cortex. *Journal of Neurophysiology,* 89**,** 634-9.

DURET, H. 1873. Sur la distribution des arteres nourricieres du bulbe rachidien. *Arc Physiol Norm Pathol***,** 97-114.

EASSON, K., ROHLICEK, C. V., HOUDE, J. C., GILBERT, G., SAINT-MARTIN, C., FONTES, K., MAJNEMER, A., MARELLI, A., WINTERMARK, P., DESCOTEAUX, M. & BROSSARD-RACINE, M. 2020. Quantification of apparent axon density and orientation dispersion in the white matter of youth born with congenital heart disease. *Neuroimage,* 205**,** 116255.

EDGLEY, S. A. & GALLIMORE, C. M. 1988. The morphology and projections of dorsal horn spinocerebellar tract neurones in the cat. *Journal of Physiology,* 397**,** 99-111.

ELLINGSON, B. M., KURPAD, S. N. & SCHMIT, B. D. 2008. Ex vivo diffusion tensor imaging and quantitative tractography of the rat spinal cord during long-term recovery from moderate spinal contusion. *Journal of Magnetic Resonance Imaging,* 28**,** 1068-79.

ENNIS, D. B. & KINDLMANN, G. 2006. Orthogonal tensor invariants and the analysis of diffusion tensor magnetic resonance images. *Magnetic Resonance in Medicine,* 55**,** 136-46.

ESSAYED, W. I., ZHANG, F., UNADKAT, P., COSGROVE, G. R., GOLBY, A. J. & O'DONNELL, L. J. 2017. White matter tractography for neurosurgical planning: A topography-based review of the current state of the art. *NeuroImage: Clinical,* 15**,** 659-672.

EYRE, J. A. 2007. Corticospinal tract development and its plasticity after perinatal injury. *Neuroscience & Biobehavioral Reviews,* 31**,** 1136-49.

EYRE, J. A., MILLER, S., CLOWRY, G. J., CONWAY, E. A. & WATTS, C. 2000. Functional corticospinal projections are established prenatally in the human foetus permitting involvement in the development of spinal motor centres. *Brain,* 123 (Pt 1)**,** 51-64.

FAN, Q., WITZEL, T., NUMMENMAA, A., VAN DIJK, K. R. A., VAN HORN, J. D., DREWS, M. K., SOMERVILLE, L. H., SHERIDAN, M. A., SANTILLANA, R. M., SNYDER, J., HEDDEN, T., SHAW, E. E., HOLLINSHEAD, M. O., RENVALL, V., ZANZONICO, R., KEIL, B., CAULEY, S., POLIMENI, J. R., TISDALL, D., BUCKNER, R. L., WEDEEN, V. J., WALD, L. L., TOGA, A. W. & ROSEN, B. R. 2016. MGH-USC Human Connectome Project datasets with ultra-high b-value diffusion MRI. *NeuroImage,* 124**,** 1108-1114.

FARQUHARSON, S. & TOURNIER, J.-D. 2016. High Angular Resolution Diffusion Imaging. *Diffusion Tensor Imaging: A Practical Handbook.* New York, NY: Springer New York.

FEDOROV, A., BEICHEL, R., KALPATHY-CRAMER, J., FINET, J., FILLION-ROBIN, J.-C., PUJOL, S., BAUER, C., JENNINGS, D., FENNESSY, F., SONKA, M., BUATTI, J., AYLWARD, S., MILLER, J. V., PIEPER, S. &

KIKINIS, R. 2012. 3D Slicer as an image computing platform for the Quantitative Imaging Network. *Magnetic resonance imaging,* 30**,** 1323-1341.
FELLEMAN, D. & VAN ESSEN, D. 1991. Distributed hierarchical processing in the primate cerebral cortex, *Cerebral Cortex*, 1(1), 1-47.
FENG, C., XU, Y., BAI, X., HUA, T., LI, Q., TANG, G. Y., CHEN, Y. J., LIU, X. Y. & HUANG, J. 2013. Basilar artery atherosclerosis and hypertensive small vessel disease in isolated pontine infarctions: a study based on high-resolution MRI. *European Neurology,* 70**,** 16-21.
FENOY, A. J. & SCHIESS, M. C. 2017. Deep Brain Stimulation of the Dentato-Rubro-Thalamic Tract: Outcomes of Direct Targeting for Tremor. *Neuromodulation: Technology at the Neural Interface,* 20**,** 429-436.
FERNANDEZ-MIRANDA, J. C., PATHAK, S., ENGH, J., JARBO, K., VERSTYNEN, T., YEH, F.-C., WANG, Y., MINTZ, A., BOADA, F., SCHNEIDER, W. & FRIEDLANDER, R. 2012. High-Definition Fiber Tractography of the Human Brain: Neuroanatomical Validation and Neurosurgical Applications. *Neurosurgery,* 71**,** 430-453.
FISHER, B., BOYD, L. & WINSTEIN, C. 2006. Contralateral cerebellar damage impairs imperative planning but not updating of aimed arm movements in humans. *Experimental Brain Research,* 174**,** 453-466.
FLOOD, S. & JANSEN, J. 1966. The efferent fibres of the cerebellar nuclei and their distribution on the cerebellar peduncles in the cat. *Cells Tissues Organs,* 63**,** 137-166.
FOIX, C. & NICULESCU, I. T. 1925. *Anatomie Cerebrale; Les Noyaux Grs Centraux et la Region Mesencephalo-Sous-Optique,*, Masson et cie.
FORD, A., COLON-PEREZ, L., TRIPLETT, W., GULLETT, J., MARECI, T. & FITZGERALD, D. 2013. Imaging White Matter in Human Brainstem. *Frontiers in Human Neuroscience,*7.
FOX, C. H., JOHNSON, F. B., WHITING, J. & ROLLER, P. P. 1985. Formaldehyde fixation. *Journal of Histochemistry & Cytochemistry,* 33**,** 845-853.
FRAZIER, J. L., LEE, J., THOMALE, U. W., NOGGLE, J. C., COHEN, K. J. & JALLO, G. I. 2009. Treatment of diffuse intrinsic brainstem gliomas: failed approaches and future strategies. *Journal of Neurosurgery: Pediatrics,* 3**,** 259-69.
FRIEDBERG, M. H., LEE, S. M. & EBNER, F. F. 2004. The contribution of the principal and spinal trigeminal nuclei to the receptive field properties of thalamic VPM neurons in the rat. *Journal of Neurocytology,* 33**,** 75-85.
FRIEHS, G. M., SCHROTTNER, O. & PENDL, G. 1995. Evidence for segregated pain and temperature conduction within the spinothalamic tract. *Journal of Neurosurgery,* 83**,** 8-12.
FUKUSHIMA, K., PETERSON, B. W., UCHINO, Y., COULTER, J. D. & WILSON, V. J. 1977. Direct fastigiospinal fibers in the cat. *Brain Research,* 126**,** 538-42.
GALEA, M. P. & DARIAN-SMITH, I. 1994. Multiple corticospinal neuron populations in the macaque monkey are specified by their unique cortical origins, spinal terminations, and connections. *Cerebral Cortex,* 4**,** 166-94.
GARCÍA-GUILLÉN, I. M., MARTÍNEZ-DE-LA-TORRE, M., PUELLES, L., AROCA, P. & MARÍN, F. 2021. Molecular Segmentation of the Spinal Trigeminal Nucleus in the Adult Mouse Brain, *Frontiers in Neuroanatomy,* 15.

GEORGE, M. S., NAHAS, Z., LISANBY, S. H., SCHLAEPFER, T., KOZEL, F. A. & GREENBERG, B. D. 2003. Transcranial magnetic stimulation. *Neurosurgery Clinics of North America,* 14**,** 283-301.

GILDENBERG, P. L. 2009. Ablative Spinal Cord Procedures for Cancer Pain. *Textbook of Stereotactic and Functional Neurosurgery.* Berlin, Heidelberg: Springer Berlin Heidelberg.

GILIBERTO, G., LANZINO, D. J., DIEHN, F. E., FACTOR, D., FLEMMING, K. D. & LANZINO, G. 2010. Brainstem cavernous malformations: anatomical, clinical, and surgical considerations. *Neurosurgery Focus,* 29**,** E9.

GINGER, M., BONY, G., HABERL, M. & FRICK, A. 2015. USE OF RHABDOVIRUSES TO STUDY NEURAL CIRCUITRY. *Biology and Pathogenesis of Rhabdo- and Filoviruses.*

GLENDINNING, D. S., COOPER, B. Y., VIERCK, C. J., JR. & LEONARD, C. M. 1992. Altered precision grasping in stumptail macaques after fasciculus cuneatus lesions. *Somatosensory & Motor Research,* 9**,** 61-73.

GLICKSTEIN, M., BUCHBINDER, S. & III, J. L. M. 1998. Visual control of the arm, the wrist and the fingers: pathways through the brain. *Neuropsychologia,* 36**,** 981-1001.

GO, J. L., KIM, P. E. & ZEE, C. S. 2001. The trigeminal nerve. *Seminars in Ultrasound, CT & MRI,* 22**,** 502-20.

GOLBY, A. J., KINDLMANN, G., NORTON, I., YARMARKOVICH, A., PIEPER, S. & KIKINIS, R. 2011. Interactive diffusion tensor tractography visualization for neurosurgical planning. *Neurosurgery,* 68**,** 496-505.

GRAF, D. & SCHRAMM, U. 1984. Diameter of axons and thickness of myelin sheaths of the pyramidal tract fibres in the adult human medullary pyramid. *Anatomischer Anzeiger,* 157**,** 97-111.

GRANUM, S. L. 1986. The spinothalamic system of the rat. I. Locations of cells of origin. *Journal of Comparative Neurology,* 247**,** 159-80.

GRANZIERA, C., SCHMAHMANN, J. D., HADJIKHANI, N., MEYER, H., MEULI, R., WEDEEN, V. & KRUEGER, G. 2009. Diffusion Spectrum Imaging Shows the Structural Basis of Functional Cerebellar Circuits in the Human Cerebellum In Vivo. *PLOS ONE,* 4**,** e5101.

GRAY, H., WILLIAMS, P. L. & BANNISTER, L. H. 1999. *Gray's anatomy : the anatomical basis of medicine and surgery,* New York, Churchill Livingstone.

GREEN, A. M. & ANGELAKI, D. E. 2010. Internal models and neural computation in the vestibular system. *Experimental brain research,* 200**,** 197-222.

GRILLNER, S., HONGO, T. & LUND, S. 1970. The vestibulospinal tract. Effects on alpha-motoneurones in the lumbosacral spinal cord in the cat. *Experimental Brain Research,* 10**,** 94-120.

GUBERINIC, A., SOUVEREIN, V., VOLKERS, R., VAN CAPPELLEN VAN WALSUM, A. M., VISSERS, K. C., MOLLINK, J. & HENSSEN, D. J. 2020. Mapping the trigeminal root entry zone and its pontine fibre distribution patterns. *Cephalalgia,* 40**,** 1645-1656.

HABAS, C., GUILLEVIN, R. & ABANOU, A. 2010. In vivo structural and functional imaging of the human rubral and inferior olivary nuclei: a mini-review. *The Cerebellum,* 9**,** 167-173.

HAGMANN, P., THIRAN, J. P., JONASSON, L., VANDERGHEYNST, P., CLARKE, S., MAEDER, P. & MEULI, R. 2003. DTI mapping of human brain

connectivity: statistical fibre tracking and virtual dissection. *Neuroimage,* 19**,** 545-54.
HAINES, D. 1987. *Neuroanatomy: An Atlas of Structures, Sections and Systems*, Urban & Schwarzenberg.
HALL, W. A. 1993. Infectious lesions of the brain stem. *Neurosurgery Clinics of North America,* 4**,** 543-51.
HAMANI, C., FLORENCE, G., HEINSEN, H., PLANTINGA, B. R., TEMEL, Y., ULUDAG, K., ALHO, E., TEIXEIRA, M. J., AMARO, E. & FONOFF, E. T. 2017. Subthalamic Nucleus Deep Brain Stimulation: Basic Concepts and Novel Perspectives. 4**,** *eNEURO*, 0140-17.2017.
HAMANN, W. C., HONG, S. K., KNIFFKI, K. D. & SCHMIDT, R. F. 1978. Projections of primary afferent fibres from muscle to neurones of the spinocervical tract of the cat. *Journal of Physiology,* 283**,** 369-78.
HARTMANN-VON MONAKOW, K., AKERT, K. & KÜNZLE, H. 1981. Projection of precentral, premotor and prefrontal cortex to the basilar pontine grey and to nucleus reticularis tegmenti pontis in the monkey (Macaca fascicularis). *Schweizer Archiv fur Neurologie, Neurochirurgie und Psychiatrie = Archives suisses de neurologie, neurochirurgie et de psychiatrie,* 129**,** 189-208.
HARTMANN, P., RAMSEIER, A., GUDAT, F., MIHATSCH, M. J. & POLASEK, W. 1994. Normal weight of the brain in adults in relation to age, sex, body height and weight. *Pathologe,* 15**,** 165-70.
HAYEM, G. 1868. Sur la thrombose par arterite du tronc basilaire comme cause de mort rapide. *Arc Physiol Norm Pathol***,** 270-89.
HE, X., LIU, W., LI, X., LI, Q., LIU, F., RAUH, V. A., YIN, D., BANSAL, R., DUAN, Y., KANGARLU, A., PETERSON, B. S. & XU, D. 2014. Automated assessment of the quality of diffusion tensor imaging data using color cast of color-encoded fractional anisotropy images. *Magnetic resonance imaging,* 32**,** 446-456.
HÉBERT, J. M. & FISHELL, G. 2008. The genetics of early telencephalon patterning: some assembly required. *Nature reviews. Neuroscience,* 9**,** 678-685.
HEFFNER, R. S. & MASTERTON, R. B. 1983. The Role of the Corticospinal Tract in the Evolution of Human Digital Dexterity. *Brain, Behavior and Evolution,* 23**,** 165-183.
HENDELMAN, W. 2000. *Atlas of Functional Neuroanatomy*, CRC Press.
HENDERSON, F., ABDULLAH, K. G., VERMA, R. & BREM, S. 2020. Tractography and the connectome in neurosurgical treatment of gliomas: the premise, the progress, and the potential. *Neurosurgical Focus FOC,* 48**,** E6.
HENDERSON, J. 2012. "Connectomic surgery": diffusion tensor imaging (DTI) tractography as a targeting modality for surgical modulation of neural networks. *Frontiers in Integrative Neuroscience,* 6.
HENSSEN, D. J. H. A., MOLLINK, J., KURT, E., VAN DONGEN, R., BARTELS, R. H. M. A., GRÄBEL, D., KOZICZ, T., AXER, M. & VAN CAPPELLEN VAN WALSUM, A.-M. 2019. Ex vivo visualization of the trigeminal pathways in the human brainstem using 11.7T diffusion MRI combined with microscopy polarized light imaging. *Brain Structure and Function,* 224**,** 159-170.

HEPP-REYMOND, M.-C. & WIESENDANGER, M. 1972. Unilateral pyramidotomy in monkeys: Effect on force and speed of a conditioned precision grip. *Brain Research,* 36**,** 117-131.

HIRSHBERG, R. M., AL-CHAER, E. D., LAWAND, N. B., WESTLUND, K. N. & WILLIS, W. D. 1996. Is there a pathway in the posterior funiculus that signals visceral pain? *Pain,* 67**,** 291-305.

HODGE, C. J., JR. & APKARIAN, A. V. 1990. The spinothalamic tract. *Critical Reviews in Neurobiology,* 5**,** 363-97.

HOLCK, P. 2001. Alf Brodal--the great brain scientist. *Tidsskr Nor Laegeforen,* 121**,** 3408-9.

HOLSTEGE, G. 1987. Some anatomical observations on the projections from the hypothalamus to brainstem and spinal cord: an HRP and autoradiographic tracing study in the cat. *Journal of Comparative Neurology,* 260**,** 98-126.

HOLSTEGE, G. & TAN, J. 1988. Projections from the red nucleus and surrounding areas to the brainstem and spinal cord in the cat. An HRP and autoradiographical tracing study. *Behavioural brain research,* 28**,** 33-57.

HONG, J. H., BAI, D. S., JEONG, J. Y., CHOI, B. Y., CHANG, C. H., KIM, S. H., AHN, S. H. & JANG, S. H. 2010a. Injury of the spino-thalamo-cortical pathway is necessary for central post-stroke pain. *European Neurology,* 64**,** 163-8.

HONG, J. H., SON, S. M. & JANG, S. H. 2010b. Identification of spinothalamic tract and its related thalamocortical fibers in human brain. *Neuroscience Letters,* 468**,** 102-5.

HONG, J. H., SON, S. M. & JANG, S. H. 2010c. Somatotopic location of corticospinal tract at pons in human brain: A diffusion tensor tractography study. *NeuroImage,* 51**,** 952-955.

HONGO, T., KUDO, N. & TANAKA, R. 1975. The vestibulospinal tract: crossed and uncrossed effects on hindlimb motoneurones in the cat. *Experimental Brain Research,* 24**,** 37-55.

HOUGHTON, A. K., KADURA, S. & WESTLUND, K. N. 1997. Dorsal column lesions reverse the reduction of homecage activity in rats with pancreatitis. *Neuroreport,* 8**,** 3795-800.

HOUK, J. & MUGNAINI, E. 2003. *Fundamental neuroscience,* Amsterdam, The Netherlands: Academic Press.

HUERTA, M. F. & KAAS, J. H. 1990. Supplementary eye field as defined by intracortical microstimulation: connections in macaques. *Journal of Comparative Neurology,* 293**,** 299-330.

HUERTA, M. F., KRUBITZER, L. A. & KAAS, J. H. 1986. Frontal eye field as defined by intracortical microstimulation in squirrel monkeys, owl monkeys, and macaque monkeys: I. Subcortical connections. *Journal of Comparative Neurology,* 253**,** 415-39.

HUGHES, A. 1976. The development of the dorsal funiculus in the human spinal cord. *Journal of Anatomy,* 122**,** 169-75.

HUGHES, M. A., FREDERICKSON, A. M., BRANSTETTER, B. F., ZHU, X. & SEKULA, R. F. 2016. MRI of the Trigeminal Nerve in Patients With Trigeminal Neuralgia Secondary to Vascular Compression. *American Journal of Roentgenology,* 206**,** 595-600.

HURLEY, R. A., FLASHMAN, L. A., CHOW, T. W. & TABER, K. H. 2010. The brainstem: anatomy, assessment, and clinical syndromes. *Journal of Neuropsychiatry & Clinical Neuroscience,* 22**,** iv, 1-7.

HYLDEN, J. L., ANTON, F. & NAHIN, R. L. 1989. Spinal lamina I projection neurons in the rat: collateral innervation of parabrachial area and thalamus. *Neuroscience,* 28**,** 27-37.

IGGO, A. 1985. Sensory receptors in the skin of mammals and their sensory functions. *Revue Neurologique,* 141**,** 599-613.

INGLESE, M. & BESTER, M. 2010. Diffusion imaging in multiple sclerosis: research and clinical implications. *NMR in Biomedicine,* 23**,** 865-72.

JACKOWSKI, M., KAO, C. Y., QIU, M., CONSTABLE, R. T. & STAIB, L. H. 2005. White matter tractography by anisotropic wavefront evolution and diffusion tensor imaging. *Medical Image Analysis,* 9**,** 427-40.

JANG, S. & KWAK, S. 2017. Aberrant Pyramidal Tract in Comparison with Pyramidal Tract on Diffusion Tensor Tractography: A Mini-Review. *Frontiers in Neurology,* 8.

JANG, S. H., KIM, S. H. & SEO, J. P. 2016. Spinothalamic Tract Injury Due to Primary Brainstem Injury: A Case Report. *American Journal of Physical Medicine & Rehabilitation,* 95**,** e42-e43.

JANG, S. H. & KWON, H. G. 2015. Injury of the dentato-rubro-thalamic tract in a patient with mild traumatic brain injury. *Brain Injury,* 29**,** 1725-8.

JANG, S. H., KWON, J. W. & YEO, S. S. 2018. Three Dimensional Identification of Medial and Lateral Vestibulospinal Tract in the Human Brain: A Diffusion Tensor Imaging Study. *Frontiers in Human Neuroscience,* 12**,** 229.

JANG, S. H. & SEO, J. P. 2015. Differences of the medial lemniscus and spinothalamic tract according to the cortical termination areas: A diffusion tensor tractography study. *Somatosensory & Motor Research,* 32**,** 67-71.

JANJUA, M. B., BAN, V. S., EL AHMADIEH, T. Y., HWANG, S. W., SAMDANI, A. F., PRICE, A. V., WEPRIN, B. E. & BATJER, H. 2020. Diffuse intrinsic pontine gliomas: Diagnostic approach and treatment strategies. *Journal of Clinical Neuroscience,* 72**,** 15-19.

JANKOWSKA, E. & EDGLEY, S. A. 2006. How Can Corticospinal Tract Neurons Contribute to Ipsilateral Movements? A Question With Implications for Recovery of Motor Functions. *The Neuroscientist,* 12**,** 67-79.

JBABDI, S. & JOHANSEN-BERG, H. 2011. Tractography: Where Do We Go from Here? *Brain Connectivity,* 1**,** 169-183.

JELLISON, B. J., FIELD, A. S., MEDOW, J., LAZAR, M., SALAMAT, M. S. & ALEXANDER, A. L. 2004. Diffusion tensor imaging of cerebral white matter: a pictorial review of physics, fiber tract anatomy, and tumor imaging patterns. *AJNR American Journal of Neuroradiology,* 25**,** 356-69.

JOHNSON, G. A., BENVENISTE, H., BLACK, R. D., HEDLUND, L. W., MARONPOT, R. R. & SMITH, B. R. 1993. Histology by magnetic resonance microscopy. *Magnetic Resonance Quarterly,* 9**,** 1-30.

JONES, D. K. 2004. The effect of gradient sampling schemes on measures derived from diffusion tensor MRI: A Monte Carlo study†. *Magnetic Resonance in Medicine,* 51**,** 807-815.

JONES, D. K. 2008. Studying connections in the living human brain with diffusion MRI. *Cortex,* 44**,** 936-52.

JONES, D. K., SIMMONS, A., WILLIAMS, S. C. & HORSFIELD, M. A. 1999. Non-invasive assessment of axonal fiber connectivity in the human brain via diffusion tensor MRI. *Magnetic Resonance in Medicine,* 42**,** 37-41.

JONES, E. G., WISE, S. P. & COULTER, J. D. 1979. Differential thalamic relationships of sensory-motor and parietal cortical fields in monkeys. *Journal of Comparative Neurology,* 183**,** 833-881.

JÜRGENS, U. 1984. The efferent and afferent connections of the supplementary motor area. *Brain Research,* 300**,** 63-81.

KÁDÁR, A., WITTMANN, G., LIPOSITS, Z. & FEKETE, C. 2009. Improved method for combination of immunocytochemistry and Nissl staining. *Journal of neuroscience methods,* 184**,** 115-118.

KAMALI, A., KRAMER, L. A., BUTLER, I. J. & HASAN, K. M. 2009. Diffusion tensor tractography of the somatosensory system in the human brainstem: initial findings using high isotropic spatial resolution at 3.0 T. *European Radiology,* 19**,** 1480-1488.

KAMALI, A., KRAMER, L. A., FRYE, R. E., BUTLER, I. J. & HASAN, K. M. 2010. Diffusion tensor tractography of the human brain cortico-ponto-cerebellar pathways: a quantitative preliminary study. *Journal of Magnetic Resonance Imaging,* 32**,** 809-17.

KANDEL, E. R., SCHWARTZ, J. H., JESSELL, T. M., SIEGELBAUM, S., HUDSPETH, A. J. & MACK, S. 2000. *Principles of neural science*, McGraw-hill New York.

KARAMPINOS, D. C., VAN, A. T., OLIVERO, W. C., GEORGIADIS, J. G. & SUTTON, B. P. 2009. High-resolution diffusion tensor imaging of the human pons with a reduced field-of-view, multishot, variable-density, spiral acquisition at 3 T. *Magnetic Resonance in Medicine,* 62**,** 1007-16.

KAWAI, Y., DEMONBRUN, A. G., CHAMBERS, R. S., NOLAN, D. A., DOLCOURT, B. A., MALAS, N. M. & QUASNEY, M. W. 2017. A Previously Healthy Adolescent With Acute Encephalopathy and Decorticate Posturing. *Pediatrics,* 139.

KAYALIOGLU, G. 2009. Chapter 10 - Projections from the Spinal Cord to the Brain. *The Spinal Cord.* San Diego: Academic Press.

KEIZER, K. & KUYPERS, H. G. 1984. Distribution of corticospinal neurons with collaterals to lower brain stem reticular formation in cat. *Experimental Brain Research,* 54**,** 107-20.

KERR, F. W. 1975. The ventral spinothalamic tract and other ascending systems of the ventral funiculus of the spinal cord. *Journal of Comparative Neurology,* 159**,** 335-56.

KEVETTER, G. A. & WILLIS, W. D. 1983. Collaterals of spinothalamic cells in the rat. *Journal of Comparative Neurology,* 215**,** 453-64.

KEVETTER, G. A. & WILLIS, W. D. 1984. Collateralization in the spinothalamic tract: new methodology to support or deny phylogenetic theories. *Brain Research,* 319**,** 1-14.

KHALID, S. & TUBBS, R. S. 2017. Neuroanatomy and Neuropsychology of Pain. *Cureus,* 9**,** e1754-e1754.

KIEVIT, J. & KUYPERS, H. G. J. M. 1977. Organization of the thalamo-cortical connexions to the frontal lobe in the rhesus monkey. *Experimental Brain Research,* 29**,** 299-322.

KIM, J. H., EBNER, T. J. & BLOEDEL, J. R. 1986. Comparison of response properties of dorsal and ventral spinocerebellar tract neurons to a physiological stimulus. *Brain Research,* 369**,** 125-35.

KINDLMANN, G. 2004. Superquadric tensor glyphs. *Proceedings of the Sixth Joint Eurographics - IEEE TCVG conference on Visualization.* Konstanz, Germany: Eurographics Association.

KINDLMANN, G. & WESTIN, C. F. 2006. Diffusion tensor visualization with glyph packing. *IEEE Transactions on Visualization and Computer Graphics,* 12**,** 1329-35.

KINGSLEY, P. B. 2006. Introduction to diffusion tensor imaging mathematics: Part I. Tensors, rotations, and eigenvectors. *Concepts in Magnetic Resonance Part A,* 28A**,** 101-122.

KITAHATA, L. M. 1993. Pain pathways and transmission. *Yale Journal of Biology and Medicine,* 66**,** 437-42.

KLOP, E. M., MOUTON, L. J. & HOLSTEGE, G. 2005. Segmental and laminar organization of the spinothalamic neurons in cat: evidence for at least five separate clusters. *Journal of Comparative Neurology,* 493**,** 580-95.

KREHER, B. W., MADER, I. & KISELEV, V. G. 2008. Gibbs tracking: a novel approach for the reconstruction of neuronal pathways. *Magnetic Resonanc in Medicine,* 60**,** 953-63.

KUBICKI, M., MCCARLEY, R., WESTIN, C. F., PARK, H. J., MAIER, S., KIKINIS, R., JOLESZ, F. A. & SHENTON, M. E. 2007. A review of diffusion tensor imaging studies in schizophrenia. *Journal of Psychiatric Research,* 41**,** 15-30.

KUCHLER, M., FOUAD, K., WEINMANN, O., SCHWAB, M. E. & RAINETEAU, O. 2002. Red nucleus projections to distinct motor neuron pools in the rat spinal cord. *Journal of Comparative Neurology,* 448**,** 349-59.

KUHNT, D., BAUER, M. H., SOMMER, J., MERHOF, D. & NIMSKY, C. 2013. Optic radiation fiber tractography in glioma patients based on high angular resolution diffusion imaging with compressed sensing compared with diffusion tensor imaging - initial experience. *PLoS One,* 8**,** e70973.

KUMAR, V., MANG, S., GRODD, W. & FUNCTION 2015. Direct diffusion-based parcellation of the human thalamus. *Brain Structure and Function,* 220**,** 1619-1635.

KUYPERS, G. A. 1981. Anatomy of the Descending Pathways. *Comprehensive Physiology.*

KWON, H. G., HONG, J. H., HONG, C. P., LEE, D. H., AHN, S. H. & JANG, S. H. 2011a. Dentatorubrothalamic tract in human brain: diffusion tensor tractography study. *Neuroradiology,* 53**,** 787-791.

KWON, H. G., HONG, J. H., LEE, M. Y., KWON, Y. H. & JANG, S. H. 2011b. Somatotopic Arrangement of the Corticospinal Tract at the Medullary Pyramid in the Human Brain. *European Neurology,* 65**,** 46-49.

LANGE, N., DUBRAY, M. B., LEE, J. E., FROIMOWITZ, M. P., FROEHLICH, A., ADLURU, N., WRIGHT, B., RAVICHANDRAN, C., FLETCHER, P. T., BIGLER, E. D., ALEXANDER, A. L. & LAINHART, J. E. 2010. Atypical diffusion tensor hemispheric asymmetry in autism. *Autism Research,* 3**,** 350-8.

LARSEN, K. D. & YUMIYA, H. 1980. The red nucleus of the monkey. Topographic localization of somatosensory input and motor output. *Experimental Brain Research,* 40**,** 393-404.

LASSEK, A. M. 1940. The pyramidal tract. II. A numerical investigation of the Betz cells of the motor area. *Archives of Neurology and Psychiatry,* 44**,** 718-724.

LASSEK, A. M. & EVANS, J. P. 1946. The human pyramidal tract; a study of the representation of the cortico-spinal components in the spinal cord. *Journal of Comparative Neurology,* 84**,** 11-6.

LAVOIE, S. & DREW, T. 2002. Discharge characteristics of neurons in the red nucleus during voluntary gait modifications: a comparison with the motor cortex. *Journal of Neurophysiology,* 88**,** 1791-814.

LAZAR, M., WEINSTEIN, D. M., TSURUDA, J. S., HASAN, K. M., ARFANAKIS, K., MEYERAND, M. E., BADIE, B., ROWLEY, H. A., HAUGHTON, V., FIELD, A. & ALEXANDER, A. L. 2003. White matter tractography using diffusion tensor deflection. *Human Brain Mapping,* 18**,** 306-21.

LE BIHAN, D. 2003. Looking into the functional architecture of the brain with diffusion MRI. *Nature Reviews Neuroscience,* 4**,** 469-80.

LE BIHAN, D., BRETON, E., LALLEMAND, D., GRENIER, P., CABANIS, E. & LAVAL-JEANTET, M. 1986. MR imaging of intravoxel incoherent motions: application to diffusion and perfusion in neurologic disorders. *Radiology,* 161**,** 401-7.

LE BIHAN, D., MANGIN, J. F., POUPON, C., CLARK, C. A., PAPPATA, S., MOLKO, N. & CHABRIAT, H. 2001. Diffusion tensor imaging: concepts and applications. *Journal of Magnetic Resonance Imaging,* 13**,** 534-46.

LEENEN, L., MEEK, J. & NIEUWENHUYS, R. 1982. Unmyelinated fibers in the pyramidal tract of the rat: a new view. *Brain Research,* 246**,** 297-301.

LEICHNETZ, G. 1981. The median subcallosal fasciculus in the monkey: A unique prefrontal corticostriate and corticocortical pathway revealed by anterogradely transported horseradish peroxidase. *Neuroscience letters,* 21**,** 137-142.

LEICHNETZ, G. R. & GONZALO-RUIZ, A. 1996. Prearcuate cortex in the Cebus monkey has cortical and subcortical connections like the macaque frontal eye field and projects to fastigial-recipient oculomotor-related brainstem nuclei. *Brain Research Bulletin,* 41**,** 1-29.

LEONARD, C. M., GLENDINNING, D. S., WILFONG, T., COOPER, B. Y. & VIERCK, C. J., JR. 1992. Alterations of natural hand movements after interruption of fasciculus cuneatus in the macaque. *Somatosensory & Motor Research,* 9**,** 75-89.

LEONG, S. K., SHIEH, J. Y. & WONG, W. C. 1984. Localizing spinal-cord-projecting neurons in adult albino rats. *Journal of Comparative Neurology,* 228**,** 1-17.

LI, Q. & MARTIN, J. H. J. E. B. R. 2000. Postnatal development of differential projections from the caudal and rostral motor cortex subregions. *Experimental Brain Research,* 134**,** 187-198.

LOEWY, A. D. & BURTON, H. 1978. Nuclei of the solitary tract: Efferent projections to the lower brain stem and spinal cord of the cat. *Journal of Comparative Neurology,* 181**,** 421-449.

LOPE-PIEDRAFITA, S. 2018. Diffusion Tensor Imaging (DTI). *Methods in Molecular Biology,* 1718**,** 103-116.
LUCIANI, L. 1893. Il Cervelletto. Nuovi Studi di Fisiologia Normale e Patologica. *Philosophical Review*. 2**,** 475-477.
LURIA, V. & LAUFER, E. 2007. Lateral motor column axons execute a ternary trajectory choice between limb and body tissues. *Neural development,* 2**,** 13-13.
MAARBJERG, S., DI STEFANO, G., BENDTSEN, L. & CRUCCU, G. 2017. Trigeminal neuralgia - diagnosis and treatment. *Cephalalgia,* 37**,** 648-657.
MACEFIELD, V. G. & KNELLWOLF, T. P. 2018. Functional properties of human muscle spindles. *Journal of Neurophysiology,* 120**,** 452-467.
MACMORE, J., SCHMAHMANN, J. D. & KO, R. 2004. The human basis pontis: motor syndromes and topographic organization. *Brain,* 127**,** 1269-1291.
MAI, J. K. & PAXINOS, G. 2012. *The Human Nervous System*. Elsevier.
MAIER-HEIN, K. H., NEHER, P. F., HOUDE, J.-C., CÔTÉ, M.-A., GARYFALLIDIS, E., ZHONG, J., CHAMBERLAND, M., YEH, F.-C., LIN, Y.-C. & JI, Q. J. N. C. 2017. The challenge of mapping the human connectome based on diffusion tractography. *Nature, Communications,* 8**,** 1-13.
MALLER, J. J., THOMSON, R. H., LEWIS, P. M., ROSE, S. E., PANNEK, K. & FITZGERALD, P. B. 2010. Traumatic brain injury, major depression, and diffusion tensor imaging: making connections. *Brain Research Reviews,* 64**,** 213-40.
MARFEO, A. 2010. Neuroanatomy Through Clinical Cases. *The Yale Journal of Biology and Medicine,* 83**,** 165-166.
MARKOV, N. T., ERCSEY-RAVASZ, M. M., RIBEIRO GOMES, A. R., LAMY, C., MAGROU, L., VEZOLI, J., MISERY, P., FALCHIER, A., QUILODRAN, R., GARIEL, M. A., SALLET, J., GAMANUT, R., HUISSOUD, C., CLAVAGNIER, S., GIROUD, P., SAPPEY-MARINIER, D., BARONE, P., DEHAY, C., TOROCZKAI, Z., KNOBLAUCH, K., VAN ESSEN, D. C. & KENNEDY, H. 2014. A weighted and directed interareal connectivity matrix for macaque cerebral cortex. *Cerebral Cortex,* 24**,** 17-36.
MARMAROU, C. R. 2011. Pyramidal System. *In:* KREUTZER, J. S., DELUCA, J. & CAPLAN, B. (eds.) *Encyclopedia of Clinical Neuropsychology.* New York, NY: Springer New York.
MARTIN, J. H. 2016. Myelin-Stained Sections Through the Central Nervous System. *Neuroanatomy Text and Atlas, 4e.* New York, NY: McGraw-Hill Medical.
MARTIN, R. J. 2004. Central pontine and extrapontine myelinolysis: the osmotic demyelination syndromes. *Journal of Neurology, Neurosurgery & Psychiatry,* 75**,** iii22-iii28.
MARTIN, R. J., APKARIAN, A. V. & HODGE, C. J., JR. 1990. Ventrolateral and dorsolateral ascending spinal cord pathway influence on thalamic nociception in cat. *Journal of Neurophysiology,* 64**,** 1400-12.
MARTINEZ-DE-LA-TORRE, M., LAMBERTOS, A., PENAFIEL, R. & PUELLES, L. 2018. An exercise in brain genoarchitectonics: Analysis of AZIN2-Lacz expressing neuronal populations in the mouse hindbrain. *Journal of Neuroscience Research,* 96**,** 1490-1517.
MARTINI, F. H. & NATH, J. L. 2009. *Anatomy and Physiology with IP-10*, Benjamin-Cummings Publishing Company.

MARVEL, C. L. & DESMOND, J. E. 2010. The contributions of cerebro-cerebellar circuitry to executive verbal working memory. *Cortex,* 46**,** 880-95.
MASON, P. 1999. Central mechanisms of pain modulation. *Current Opinion in Neurobiology,* 9**,** 436-41.
MASSION, J. 1967. The mammalian red nucleus. *Physiological Reviews,* 47**,** 383-436.
MATLAB 2018. The MathWorks. Massachusetts, United states: Inc, Natick.
MATSUSHITA, M., HOSOYA, Y. & IKEDA, M. 1979. Anatomical organization of the spinocerebellar system in the cat, as studied by retrograde transport of horseradish peroxidase. *Journal of Comparativ Neurology,* 184**,** 81-106.
MATSUSHITA, M. & YAGINUMA, H. 1995. Projections from the central cervical nucleus to the cerebellar nuclei in the rat, studied by anterograde axonal tracing. *Journal of Comparative Neurology,* 353**,** 234-46.
MAYERHOEFER, M. E., SZOMOLANYI, P., JIRAK, D., MATERKA, A. & TRATTNIG, S. 2009. Effects of MRI acquisition parameter variations and protocol heterogeneity on the results of texture analysis and pattern discrimination: an application-oriented study. *Medical Physics,* 36**,** 1236-43.
MCCALL, A. A., MILLER, D. M. & YATES, B. J. 2017. Descending Influences on Vestibulospinal and Vestibulosympathetic Reflexes. *Frontiers in Neurology,* 8.
MCGOVERN, A. E., DRIESSEN, A. K., SIMMONS, D. G., POWELL, J., DAVIS-POYNTER, N., FARRELL, M. J. & MAZZONE, S. B. 2015. Distinct brainstem and forebrain circuits receiving tracheal sensory neuron inputs revealed using a novel conditional anterograde transsynaptic viral tracing system. *The Journal of neuroscience : the official journal of the Society for Neuroscience,* 35**,** 7041-7055.
MCNAB, J. A., EDLOW, B. L., WITZEL, T., HUANG, S. Y., BHAT, H., HEBERLEIN, K., FEIWEIER, T., LIU, K., KEIL, B., COHEN-ADAD, J., TISDALL, M. D., FOLKERTH, R. D., KINNEY, H. C. & WALD, L. L. 2013. The Human Connectome Project and beyond: initial applications of 300 mT/m gradients. *Neuroimage,* 80**,** 234-45.
MEHLER, W. R., FEFERMAN, M. E. & NAUTA, W. J. 1960. Ascending axon degeneration following anterolateral cordotomy. An experimental study in the monkey. *Brain,* 83**,** 718-50.
MELONAKOS, J., MOHAN, V., NIETHAMMER, M., SMITH, K., KUBICKI, M. & TANNENBAUM, A. 2007. Finsler tractography for white matter connectivity analysis of the cingulum bundle. *Medical Image and Computer Assisted Intervention,* 10**,** 36-43.
MENDOZA, J. E. & FOUNDAS, A. L. 2008. The somatosensory systems. *Clinical Neuroanatomy: A Neurobehavioral Approach.* Springer.
MENETREY, D., CHAOUCH, A. & BESSON, J. M. 1980. Location and properties of dorsal horn neurons at origin of spinoreticular tract in lumbar enlargement of the rat. *Journal of Neurophysiology,* 44**,** 862-77.
MENÉTREY, D. & DE POMMERY, J. 1991. Origins of Spinal Ascending Pathways that Reach Central Areas Involved in Visceroception and Visceronociception in the Rat. *European Journal of Neuroscience,* 3**,** 249-259.
MENSE, S. S. 2004. Functional neuroanatomy for pain stimuli. Reception, transmission, and processing. *Schmerz,* 18**,** 225-37.

MEOLA, A., COMERT, A., YEH, F.-C., SIVAKANTHAN, S. & FERNANDEZ-MIRANDA, J.-C. 2016a. The nondecussating pathway of the dentatorubrothalamic tract in humans: human connectome-based tractographic study and microdissection validation. *Journal of Neurosurgery JNS,* 124**,** 1406-1412.

MEOLA, A., YEH, F.-C., FELLOWS-MAYLE, W., WEED, J. & FERNANDEZ-MIRANDA, J. C. 2016b. Human Connectome-Based Tractographic Atlas of the Brainstem Connections and Surgical Approaches. *Neurosurgery,* 79.

MIHAILOFF, G. A., MCARDLE, C. B. & ADAMS, C. E. 1981. The cytoarchitecture, cytology, and synaptic organization of the basilar pontine nuclei in the rat. I. Nissl and Golgi studies. *Journal of Comparative Neurology,* 195**,** 181-201.

MIKULA, S., TROTTS, I., STONE, J. M. & JONES, E. G. 2007. Internet-enabled high-resolution brain mapping and virtual microscopy. *NeuroImage,* 35**,** 9-15.

MILLAN, M. J. 1999. The induction of pain: an integrative review. *Progress in Neurobiology,* 57**,** 1-164.

MILLER, K. L., STAGG, C. J., DOUAUD, G., JBABDI, S., SMITH, S. M., BEHRENS, T. E., JENKINSON, M., CHANCE, S. A., ESIRI, M. M. & VOETS, N. L. 2011. Diffusion imaging of whole, post-mortem human brains on a clinical MRI scanner. *Neuroimage,* 57**,** 167-181.

MOFFIE, D. 1975. Spinothalamic fibres, pain conduction and cordotomy. *Clinical Neurology and Neurosurgery,* 78**,** 261-8.

MOLINARI, M. 2002. Cerebellum. *Encyclopedia of the Human Brain.* New York: Academic Press.

MOLLET, G. A. 2008. Fundamentals of Human Neuropsychology, 6(th) Edition. *Journal of Undergraduate Neuroscience Education,* 6**,** R3-R4.

MOLLINK, J., KLEINNIJENHUIS, M., CAPPELLEN VAN WALSUM, A. V., SOTIROPOULOS, S. N., COTTAAR, M., MIRFIN, C., HEINRICH, M. P., JENKINSON, M., PALLEBAGE-GAMARALLAGE, M., ANSORGE, O., JBABDI, S. & MILLER, K. L. 2017. Evaluating fibre orientation dispersion in white matter: Comparison of diffusion MRI, histology and polarized light imaging. *Neuroimage,* 157**,** 561-574.

MOLLINK, J., VAN BAARSEN, K. M., DEDEREN, P. J. W. C., FOXLEY, S., MILLER, K. L., JBABDI, S., SLUMP, C. H., GROTENHUIS, J. A., KLEINNIJENHUIS, M. & VAN CAPPELLEN VAN WALSUM, A. M. 2016. Dentatorubrothalamic tract localization with postmortem MR diffusion tractography compared to histological 3D reconstruction. *Brain Structure and Function,* 221**,** 3487-3501.

MORECRAFT, R. J., GE, J., STILWELL-MORECRAFT, K. S., ROTELLA, D. L., PIZZIMENTI, M. A. & DARLING, W. G. 2018. New Corticopontine Connections in the Primate Brain: Contralateral Projections From the Arm/Hand Area of the Precentral Motor Region. *Frontiers in Neuroanatomy,* 12.

MORI, S. 2002. Principle and Applications of Diffusion Tensor Imaging. *Computational Neuroanatomy: Principles and Methods.* Totowa, NJ: Humana Press.

MORI, S. 2007. *Introduction to Diffusion Tensor Imaging*, Elsevier Science.

MORI, S., CRAIN, B. J., CHACKO, V. P. & VAN ZIJL, P. C. 1999. Three-dimensional tracking of axonal projections in the brain by magnetic resonance imaging. *Annals of Neurology,* 45**,** 265-9.

MORI, S., FREDERIKSEN, K., VAN ZIJL, P. C. M., STIELTJES, B., KRAUT, M. A., SOLAIYAPPAN, M. & POMPER, M. G. 2002. Brain white matter anatomy of tumor patients evaluated with diffusion tensor imaging. *Annals of Neurology,* 51**,** 377-380.

MORITA, T., ASADA, M. & NAITO, E. 2016. Contribution of Neuroimaging Studies to Understanding Development of Human Cognitive Brain Functions. *Frontiers in human neuroscience,* 10**,** 464-464.

MULDER, M. J., KEUKEN, M. C., BAZIN, P.-L., ALKEMADE, A. & FORSTMANN, B. U. 2019. Size and shape matter: The impact of voxel geometry on the identification of small nuclei. *PLOS ONE,* 14**,** e0215382.

MURRAY, H. M. & GURULE, M. E. 1979. Origin of the rubrospinal tract of the rat. *Neurosci Letters,* 14**,** 19-23.

NAGAE-POETSCHER, L. M., JIANG, H., WAKANA, S., GOLAY, X., VAN ZIJL, P. C. M. & MORI, S. 2004. High-Resolution Diffusion Tensor Imaging of the Brain Stem at 3 T. *American Journal of Neuroradiology,* 25**,** 1325-1330.

NAIDICH, T. P., DUVERNOY, H. M. & DELMAN, B. N. 2009. Duvernoy's Atlas of the Human Brain Stem and Cerebellum. *AJNR: American Journal of Neuroradiology,* 30**,** e75-e75.

NAITO, A. & KITA, H. 1994. The cortico-nigral projection in the rat: an anterograde tracing study with biotinylated dextran amine. *Brain Research,* 637**,** 317-322.

NAKANISHI, R., GOTO, J., EZURE, H., MOTOURA, H., AYABE, S. & ATSUMI, T. 2004. Morphometric analyses of axons in the human lateral corticospinal tract: cervical/lumbar level comparison and relation to the ageing process. *Okajimas Folia Anatomica Japonica,* 81**,** 1-4.

NAMAVAR, Y., BARTH, P. G. & BAAS, F. 2011. Classification, diagnosis and potential mechanisms in pontocerebellar hypoplasia. *Orphanet journal of rare diseases,* 6**,** 1-14.

NANDA, A., KHAN, I. S. & APUZZO, M. L. 2016. Renaissance Neurosurgery: Italy's Iconic Contributions. *World Neurosurgery,* 87**,** 647-55.

NASH, P. G., MACEFIELD, V. G., KLINEBERG, I. J., GUSTIN, S. M., MURRAY, G. M. & HENDERSON, L. A. 2010. Bilateral activation of the trigeminothalamic tract by acute orofacial cutaneous and muscle pain in humans. *Pain,* 151**,** 384-393.

NASH, P. G., MACEFIELD, V. G., KLINEBERG, I. J., MURRAY, G. M. & HENDERSON, L. A. 2009. Differential activation of the human trigeminal nuclear complex by noxious and non-noxious orofacial stimulation. *Human Brain Mapping*, 30**,** 3772-3782.

NATHAN, P. W., SMITH, M. & DEACON, P. 1996. Vestibulospinal, reticulospinal and descending propriospinal nerve fibres in man. *Brain,* 119 (Pt 6)**,** 1809-33.

NATHAN, P. W., SMITH, M. & DEACON, P. 2001. The crossing of the spinothalamic tract. *Brain,* 124**,** 793-803.

NATHAN, P. W. & SMITH, M. C. 1955. Long descending tracts in man. I. Review of present knowledge. *Brain,* 78**,** 248-303.

NATHAN, P. W. & SMITH, M. C. 1982. The rubrospinal and central tegmental tracts in man. *Brain,* 105**,** 223-69.
NATHAN, P. W., SMITH, M. C. & DEACON, P. 1990. The corticospinal tracts in man. Course and location of fibres at different segmental levels. *Brain,* 113 (Pt 2)**,** 303-24.
NAUTA, H. J., HEWITT, E., WESTLUND, K. N. & WILLIS, W. D., JR. 1997. Surgical interruption of a midline dorsal column visceral pain pathway. Case report and review of the literature. *Journal of Neurosurgery,* 86**,** 538-42.
NECTOW, A. R. & NESTLER, E. J. 2020. Viral tools for neuroscience. *Nature Reviews Neuroscience,* 21**,** 669-681.
NILSSON, M., SZCZEPANKIEWICZ, F., VAN WESTEN, D. & HANSSON, O. 2015. Extrapolation-Based References Improve Motion and Eddy-Current Correction of High B-Value DWI Data: Application in Parkinson's Disease Dementia. *PloS one,* 10**,** e0141825-e0141825.
NIOCHE, C., CABANIS, E. & HABAS, C. 2009. Functional connectivity of the human red nucleus in the brain resting state at 3T. *American Journal of Neuroradiology,* 30**,** 396-403.
NOBACK, C. R., STROMINGER, N. L., DEMAREST, R. J. & RUGGIERO, D. A. 2005. Lesions of the Brainstem. *The Human Nervous System: Structure and Function.* Totowa, NJ: Humana Press.
NOSEK, T. M. 1998. *Essentials of Human Physiology*, Gold Standard Multimedia Incorporated.
NYBERG-HANSEN, R. 1964. The Location and Termination of Tectospinal Fibers in the Cat. *Experimental Neurology,* 9**,** 212-27.
NYBERG-HANSEN, R. 1965. Sites and Mode of Termination of Reticulo-Spinal Fibers in the Cat. An Experimental Study with Silver Impregnation Methods. *J Comparative Neurology,* 124**,** 71-99.
NYBERG-HANSEN, R. 1966. Functional organization of descending supraspinal fibre systems to the spinalcord. Anatomical observations and physiological correlations. *Ergebnisse der Anatomie und Entwicklungsgeschichte,* 39**,** 3-48.
NYBY, O. & JANSEN, J. 1951. *An experimental investigation of the corticopontine projection in Macaca mulatta,* Oslo, I Kommisjon hos J. Dybwad.
O'DONNELL, L. J., WESTIN, C. F. & GOLBY, A. J. 2009. Tract-based morphometry for white matter group analysis. *Neuroimage,* 45**,** 832-44.
OBERMANN, M. 2010. Treatment options in trigeminal neuralgia. *Therapeutic advances in neurological disorders,* 3**,** 107-115.
OLDENBOURG, R. 2013. Polarized light microscopy: principles and practice. *Cold Spring Harbor Protocols,* 2013.
OLSZEWSKI, J. & BAXTER, D. 1954. Cytoarchitecture of the human brainstem. *Journal of Comparative Neurology,* 101**,** 825-825.
ONODERA, S. & HICKS, T. P. 2009. A comparative neuroanatomical study of the red nucleus of the cat, macaque and human. *PLoS One,* 4**,** e6623.
PADEL, Y., ANGAUT, P., MASSION, J. & SEDAN, R. 1981. Comparative study of the posterior red nucleus in baboons and gibbons. *Journal of Comparative Neurology,* 202**,** 421-38.
PAJEVIC, S. & PIERPAOLI, C. 1999. Color schemes to represent the orientation of anisotropic tissues from diffusion tensor data: application to white matter fiber

tract mapping in the human brain. *Magnetic Resonance in Medicine,* 42**,** 526-40.

PALECEK, J., PALECKOVA, V. & WILLIS, W. D. 2002. The roles of pathways in the spinal cord lateral and dorsal funiculi in signaling nociceptive somatic and visceral stimuli in rats. *Pain,* 96**,** 297-307.

PALESI, F., DE RINALDIS, A., CASTELLAZZI, G., CALAMANTE, F., MUHLERT, N., CHARD, D., TOURNIER, J. D., MAGENES, G., D'ANGELO, E. & GANDINI WHEELER-KINGSHOTT, C. A. M. 2017. Contralateral cortico-ponto-cerebellar pathways reconstruction in humans in vivo: implications for reciprocal cerebro-cerebellar structural connectivity in motor and non-motor areas. *Scientific Reports,* 7**,** 12841.

PALESI, F., TOURNIER, J.-D., CALAMANTE, F., MUHLERT, N., CASTELLAZZI, G., CHARD, D., D'ANGELO, E. & WHEELER-KINGSHOTT, C. A. 2015. Contralateral cerebello-thalamo-cortical pathways with prominent involvement of associative areas in humans in vivo. *Brain Structure and Function,* 220**,** 3369-3384.

PALKOVITS, M., MAGYAR, P. & SZENTAĪGOTHAI, J. J. B. R. 1972. Quantitative histological analysis of the cerebellar cortex in the cat. IV. Mossy fiber-Purkinje cell numerical transfer. *Brain Research,* 45**,** 15-29.

PANESAR, S. S., ABHINAV, K., YEH, F. C., JACQUESSON, T., COLLINS, M. & FERNANDEZ-MIRANDA, J. 2019. Tractography for Surgical Neuro-Oncology Planning: Towards a Gold Standard. *Neurotherapeutics,* 16**,** 36-51.

PARÉ, M., BEHETS, C. & CORNU, O. 2003. Paucity of presumptive ruffini corpuscles in the index finger pad of humans. *Journal of Comparative Neurology,* 456**,** 260-6.

PARÉ, M., ELDE, R., MAZURKIEWICZ, J. E., SMITH, A. M. & RICE, F. L. 2001. The Meissner Corpuscle Revised: A Multiafferented Mechanoreceptor with Nociceptor Immunochemical Properties. *Journal of Neuroscience,* 21**,** 7236-7246.

PÁRRAGA, R. G., POSSATTI, L. L., ALVES, R. V., RIBAS, G. C., TÜRE, U. & DE OLIVEIRA, E. 2016. Microsurgical anatomy and internal architecture of the brainstem in 3D images: surgical considerations. *Journal of Neurosurgery JNS,* 124**,** 1377-1395.

PAXINOS, G. 2015. *The rat nervous system,* Amsterdam, Elsevier.

PAXINOS, G., FURLONG, T. & WATSON, C. 2020. *Human Brainstem: Cytoarchitecture, Chemoarchitecture, Myeloarchitecture*, Elsevier Science Publishing Co Inc.

PAXINOS, G., WATSON, C., CALABRESE, E., BADEA, A. & JOHNSON, G. A. 2015. *MRI/DTI Atlas of the Rat Brain*, Academic Press.

PAXINOS, G., WATSON, C., PETRIDES, M., MARCELLO, R. & HIRONOBU, T. 2012. *The Marmoset Brain In Stereotaxic Coordinates,* San Diego, United States, Elsevier Science Publishing Co Inc.

PEARCE, J. M. S. 2000. Wallerian degeneration. *Journal of Neurology, Neurosurgery and Psychiatry,* 69**,** 791-791.

PETERSEN, K. J., REID, J. A., CHAKRAVORTI, S., JUTTUKONDA, M. R., FRANCO, G., TRUJILLO, P., STARK, A. J., DAWANT, B. M., DONAHUE,

M. J. & CLAASSEN, D. O. 2018. Structural and functional connectivity of the nondecussating dentato-rubro-thalamic tract. *Neuroimage,* 176**,** 364-371.
PETERSON, B. & BARNES, C. 1984. Brain stem control of spinal cord function, Academic Press.
PETERSON, B. W., MAUNZ, R. A., PITTS, N. G. & MACKEL, R. G. 1975. Patterns of projection and braching of reticulospinal neurons. *Experimental Brain Research,* 23**,** 333-51.
PFEFFERBAUM, A., SULLIVAN, E. V., ADALSTEINSSON, E., GARRICK, T. & HARPER, C. 2004. Postmortem MR imaging of formalin-fixed human brain. *Neuroimage,* 21**,** 1585-1595.
PIERPAOLI, C., JEZZARD, P., BASSER, P. J., BARNETT, A. & DI CHIRO, G. 1996. Diffusion tensor MR imaging of the human brain. *Radiology,* 201**,** 637-48.
PLATT, T., LADD, M. E. & PAECH, D. 2021. 7 Tesla and Beyond: Advanced Methods and Clinical Applications in Magnetic Resonance Imaging. *Investigative radiology,* 56**,** 705-725.
PLUM, F. & POSNER, J. B. 1972. The diagnosis of stupor and coma. *Contemporary Neurology Series,* 10**,** 1-286.
PRESS, W. H., VETTERLING, W. T., TEUKOLSKY, S. A. & FLANNERY, B. P. 1986. *Numerical recipes*, Cambridge university press Cambridge.
PUELLES, L., MARTINEZ, M., MARTINEZ, S., WATSON, C. & PAXINOS, G. 2018. *The Chick Brain in Stereotaxic Coordinates and Alternative Stains,* London, United Kingdom, Academic Press.
PURVES, D., AUGUSTINE, G., FITZPATRICK, D., KATZ, L., LAMANTIA, A., MCNAMARA, J. & WILLIAMS, S. 2001. *Neuroscience, Central Pain Pathways: The Spinothalamic tract*.
PURVES, D., AUGUSTINE, G. J., FITZPATRICK, D., HALL, W. C., LAMANTIA, A. S., MOONEY, R. D., PLATT, M. L. & WHITE, L. E. 2018. *Neuroscience,* Oxford University Press, United Kingdom.
QIU, M.-G., ZHANG, J.-N., ZHANG, Y., LI, Q.-Y., XIE, B. & WANG, J. 2012. Diffusion Tensor Imaging-Based Research on Human White Matter Anatomy. *The Scientific World Journal,* 2012**,** 530432.
RALSTON, D. D. & MILROY, A. M. 1989. Red nucleus of Macaca fascicularis: an electron microscopic study of its synaptic organization. *Journal of Comparative Neurology,* 284**,** 602-620.
RALSTON, H. J., 3RD 2005. Pain and the primate thalamus. *Progress in Brain Research,* 149**,** 1-10.
RALSTON, H. J., 3RD & RALSTON, D. D. 1992. The primate dorsal spinothalamic tract: evidence for a specific termination in the posterior nuclei (Po/SG) of the thalamus. *Pain,* 48**,** 107-18.
RAMNANI, N. 2006. The primate cortico-cerebellar system: anatomy and function. *Nature Reviews in Neuroscience,* 7**,** 511-22.
RAUSELL, E. & JONES, E. 1991. Chemically distinct compartments of the thalamic VPM nucleus in monkeys relay principal and spinal trigeminal pathways to different layers of the somatosensory cortex. *The Journal of Neuroscience,* 11**,** 226-237.

RAZEK, A. A. K. A., ALVAREZ, H., BAGG, S., REFAAT, S. & CASTILLO, M. 2014. Imaging Spectrum of CNS Vasculitis. *RadioGraphics,* 34**,** 873-894.

RECALDE, R. J., FIGUEIREDO, E. G. & DE OLIVEIRA, E. 2008. Microsurgical anatomy of the safe entry zones on the anterolateral brainstem related to surgical approaches to cavernous malformations. *Neurosurgery,* 62**,** 9-15; discussion 15-7.

REED, W. R., SHUM-SIU, A., ONIFER, S. M. & MAGNUSON, D. S. K. 2006. Inter-enlargement pathways in the ventrolateral funiculus of the adult rat spinal cord. *Neuroscience,* 142**,** 1195-1207.

RIDDLE, C. N., EDGLEY, S. A. & BAKER, S. N. 2009. Direct and indirect connections with upper limb motoneurons from the primate reticulospinal tract. *The Journal of neuroscience : the official journal of the Society for Neuroscience,* 29**,** 4993-4999.

RINVIK, E. 1966. The cortico-nigral projection in the cat an experimental study with silver impregnation methods. *Jornal of Comparative Neurology,* 126**,** 241-254.

ROBAK, A., SZTEYN, S., BOGUS-NOWAKOWSKA, K., DOBOSZYŃSKA, T. & RÓWNIAK, M. 2000. The cytoarchitectonic and neuronal structure of the red nucleus in guinea pig: Nissl and Golgi studies. *Folia morphologica,* 59**,** 333-342.

RODRÍGUEZ-MENA, R. & TÜRE, U. 2017. The Medial and Lateral Lemnisci: Anatomically Adjoined But Functionally Distinct Fiber Tracts. *World Neurosurgery,* 99**,** 241-250.

ROMANOWSKI, C. A. J., HUTTON, M., ROWE, J., YIANNI, J., WARREN, D., BIGLEY, J. & WILKINSON, I. D. 2011. The Anatomy of the Medial Lemniscus within the Brainstem Demonstrated at 3 Tesla with High Resolution Fat Suppressed T1-Weighted Images and Diffusion Tensor Imaging. *The Neuroradiology Journal,* 24**,** 171-176.

ROOSTAEI, T., NAZERI, A., SAHRAIAN, M. A. & MINAGAR, A. 2014. The human cerebellum: a review of physiologic neuroanatomy. *Neurologic Clinics,* 32**,** 859-69.

ROSE, F. C. 2009. Cerebral localization in antiquity. *Jornal of the History of Neurosciences,* 18**,** 239-47.

ROSE, P. K. & ABRAHAMS, V. C. 1978. Tectospinal and tectoreticular cells: their distribution and afferent connections. *Canadian Journal of Physiology and Pharmacology,* 56**,** 650-8.

ROSENBAUM, D. A. 2009. *Human Motor Control*, Elsevier Science.

ROSENBERG, G. 2012. Brain edema and disorders of cerebrospinal fluid circulation, *Bradley's Neurology in Clinical Practice,* 1377-1395.

ROYCE, G. J. & LAINE, E. J. 1984. Efferent connections of the caudate nucleus, including cortical projections of the striatum and other basal ganglia: An autoradiographic and horseradish peroxidase investigation in the cat. *Journal of Comparative Neurology,* 226**,** 28-49.

RUSTIONI, A., HAYES, N. L. & O'NEILL, S. 1979. Dorsal column nuclei and ascending spinal afferents in macaques. *Brain,* 102**,** 95-125.

SAKAI, S. T., INASE, M. & TANJI, J. 1996. Comparison of cerebellothalamic and pallidothalamic projections in the monkey (Macaca fuscata): A double anterograde labeling study. *Journal of Comparative Neurology,* 368**,** 215-228.

SALADIN, K. S. G. C. A. C. H. N. 2018. *Anatomy & physiology : the unity of form and function*. New York, McGraw-Hill Education.
SANTOS, M. J., KANEKAR, N. & ARUIN, A. S. 2010. The role of anticipatory postural adjustments in compensatory control of posture: 2. Biomechanical analysis. *Journal of electromyography and kinesiology : official journal of the International Society of Electrophysiological Kinesiology,* 20**,** 398-405.
SAPER, C. B., LOEWY, A. D., SWANSON, L. W. & COWAN, W. M. 1976. Direct hypothalamo-autonomic connections. *Brain Research,* 117**,** 305-12.
SARWAR, T., RAMAMOHANARAO, K. & ZALESKY, A. 2019. Mapping connectomes with diffusion MRI: deterministic or probabilistic tractography? *Magnetic Resonance in Medicine,* 81**,** 1368-1384.
SATHYANESAN, A., OGURA, T. & LIN, W. 2012. Automated measurement of nerve fiber density using line intensity scan analysis. *Journal of neuroscience methods,* 206**,** 165-175.
SAVITZ, S. I., RONTHAL, M. & CAPLAN, L. R. 2006. Vertebral Artery Compression of the Medulla. *Archives of Neurology,* 63**,** 234-241.
SCHALTENBRAND, G. W. W. H. R. G. 1977. *Atlas for stereotaxy of the human brain,* Stuttgart, Thieme.
SCHILLING, K. G., DADUCCI, A., MAIER-HEIN, K., POUPON, C., HOUDE, J.-C., NATH, V., ANDERSON, A. W., LANDMAN, B. A. & DESCOTEAUX, M. J. M. R. I. 2019. Challenges in diffusion MRI tractography–Lessons learned from international benchmark competitions. Magnetic Resonance Imaging, 57**,** 194-209.
SCHLAIER, J., ANTHOFER, J., STEIB, K., FELLNER, C., ROTHENFUSSER, E., BRAWANSKI, A. & LANGE, M. 2015. Deep brain stimulation for essential tremor: targeting the dentato-rubro-thalamic tract? *Neuromodulation,* 18**,** 105-12.
SCHMAHMANN, J. & PANDYA, D. 1997. Anatomic Organization of the Basilar Pontine Projections from Prefrontal Cortices in Rhesus Monkey. *The Journal of neuroscience : the official journal of the Society for Neuroscience,* 17**,** 438-58.
SCHMAHMANN, J. D. & PANDYA, D. N. 1989. Anatomical investigation of projections to the basis pontis from posterior parietal association cortices in rhesus monkey. *Journal of Comparative Neurology,* 289**,** 53-73.
SCHMAHMANN, J. D., ROSENE, D. L. & PANDYA, D. N. 2004. Motor projections to the basis pontis in rhesus monkey. *Journal of Comparative Neurology,* 478**,** 248-268.
SCHNEIDER, R. & GAUTIER, J. C. 1994. Leg weakness due to stroke. Site of lesions, weakness patterns and causes. *Brain,* 117 (Pt 2)**,** 347-54.
SCHREIBER, J., RIFFERT, T., ANWANDER, A. & KNÖSCHE, T. R. 2014. Plausibility Tracking: A method to evaluate anatomical connectivity and microstructural properties along fiber pathways. *NeuroImage,* 90**,** 163-178.
SCLAR, G., BOARDMAN, P. & PRESTIGIACOMO, C. J. 2007. Solitary brainstem abscess. *Neurology,* 68**,** 1231-1231.
SEDRAK, M., GORGULHO, A., BARI, A., BEHNKE, E., FREW, A., GEVORKYAN, I., POURATIAN, N. & DESALLES, A. 2010. Diffusion tensor imaging (DTI) and colored fractional anisotropy (FA) mapping of the

subthalamic nucleus (STN) and the globus pallidus interna (GPi). *Acta neurochirurgica,* 152**,** 2079-2084.
SEDRAK, M., GORGULHO, A., FREW, A., BEHNKE, E., DESALLES, A. & POURATIAN, N. 2011. Diffusion tensor imaging and colored fractional anisotropy mapping of the ventralis intermedius nucleus of the thalamus. *Neurosurgery,* 69**,** 1124-9; discussion 1129-30.
SENGUL, G. & WATSON, C. 2012. Chapter 7 - Spinal Cord: Connections. *The Human Nervous System (Third Edition).* San Diego: Academic Press.
SEO, J. P., JANG, S. H., JEONG, D. & CHANG, M. C. 2019. Injury of the Medial Lemniscus Due to Compression of the Medulla Oblongata by Tortuous Vertebral Artery. *American Journal of Physical Medicine & Rehabilitation,* 98**,** e90-e91.
SERAPIDE, M. F., PANTÓ, M. R., PARENTI, R., ZAPPALÁ, A. & CICIRATA, F. J. J. O. C. N. 2001. Multiple zonal projections of the basilar pontine nuclei to the cerebellar cortex of the rat. *Journal of Comparative Neurology,* 430**,** 471-484.
SESSLE, B. J. 2000. Acute and chronic craniofacial pain: brainstem mechanisms of nociceptive transmission and neuroplasticity, and their clinical correlates. *Critical Reviews in Oral Biology & Medicine,* 11**,** 57-91.
SHATIL, A. S., MATSUDA, K. M. & FIGLEY, C. R. 2016. A Method for Whole Brain Ex Vivo Magnetic Resonance Imaging with Minimal Susceptibility Artifacts. *Frontiers in neurology,* 7**,** 208-208.
SHCHERBENKO, O. I. 2015. Diffusely growing brainstem tumors in children and adolescents: has alternating treatment policy changed results?. *Vestn Rentgenol Radiol***,** 43-51.
SHEPHERD, T. M., HOCH, M. J., COHEN, B. A., BRUNO, M. T., FIEREMANS, E., ROSEN, G., PACIONE, D. & MOGILNER, A. Y. 2017. Palliative CT-Guided Cordotomy for Medically Intractable Pain in Patients with Cancer. *American Journal of Neuroradiology,* 38**,** 387-390.
SHERRINGTON, C. S. 1898. Decerebrate Rigidity, and Reflex Coordination of Movements. *Journal of Physiology,* 22**,** 319-32.
SHOOK, B. L., SCHLAG-REY, M. & SCHLAG, J. 1990. Primate supplementary eye field: I. Comparative aspects of mesencephalic and pontine connections. *Journal of Comparative Neurology,* 301**,** 618-42.
SHUKLA, G., ALEXANDER, G. S., BAKAS, S., NIKAM, R., TALEKAR, K., PALMER, J. D. & SHI, W. 2017. Advanced magnetic resonance imaging in glioblastoma: a review. *Chinese Clinical Oncology,* 6**,** 40.
SKAGERBERG, G. & BJORKLUND, A. 1985. Topographic principles in the spinal projections of serotonergic and non-serotonergic brainstem neurons in the rat. *Neuroscience,* 15**,** 445-80.
SKORIĆ, M. K., ADAMEC, I., MAĐARIĆ, V. N. & HABEK, M. 2014. Evaluation of brainstem involvement in multiple sclerosis. *Canadian Journal of Neurological Sciences,* 41**,** 346-9.
SMITH, M. C. 1976. Retrograde cell changes in human spinal cord after anterolateral cordotomies. Location and identification after different periods of survival. *Advances in Pain Research and Therapy,* 1, 91-98.

SMITH, M. C. & DEACON, P. 1984. Topographical anatomy of the posterior columns of the spinal cord in man. The long ascending fibres. *Brain,* 107 (Pt 3)**,** 671-98.

SMITH, Y. & WICHMANN, T. 2015. The cortico-pallidal projection: An additional route for cortical regulation of the basal ganglia circuitry. *Movement Disorders,* 30**,** 293-295.

SOARES, J. M., MARQUES, P., ALVES, V. & SOUSA, N. 2013. A hitchhiker's guide to diffusion tensor imaging. *Frontiers in neuroscience,* 7**,** 31-31.

SOFRONIEW, M. V. 1985. Vasopressin- and neurophysin-immunoreactive neurons in the septal region, medial amygdala and locus coeruleus in colchicine-treated rats. *Neuroscience,* 15**,** 347-58.

SOTIROPOULOS, S. N., JBABDI, S., XU, J., ANDERSSON, J. L., MOELLER, S., AUERBACH, E. J., GLASSER, M. F., HERNANDEZ, M., SAPIRO, G., JENKINSON, M., FEINBERG, D. A., YACOUB, E., LENGLET, C., VAN ESSEN, D. C., UGURBIL, K. & BEHRENS, T. E. J. 2013. Advances in diffusion MRI acquisition and processing in the Human Connectome Project. *NeuroImage,* 80**,** 125-143.

SOUMA, Y., GOTO, N., GOTO, J., FUJIMOTO, T. & FUJIWARA, T. 2009. Morphological evaluation of the human pyramidal tract: tapering of axons. *Okajimas Folia Anatomica Japonica,* 85**,** 111-3.

SPILLER, W. G. & MARTIN, E. 1912. The treatment of persistent pain of organic origin in the lower part of the body by division of the anterolateral column of the spinal cord. *Journal of the American Medical Association,* LVIII**,** 1489-1490.

STANTON, G. B. 1980. Topographical organization of ascending cerebellar projections from the dentate and interposed nuclei in Macaca mulatta: An anterograde degeneration study. *Journal of Comparative Neurology,* 190**,** 699-731.

STANTON, G. B., GOLDBERG, M. E. & BRUCE, C. J. 1988. Frontal eye field efferents in the macaque monkey: I. Subcortical pathways and topography of striatal and thalamic terminal fields. *Journal of Comparative Neurology,* 271**,** 473-92.

STECINA, K., FEDIRCHUK, B. & HULTBORN, H. 2013. Information to cerebellum on spinal motor networks mediated by the dorsal spinocerebellar tract. *The Journal of physiology,* 591**,** 5433-5443.

STEJSKAL, E. O. & TANNER, J. E. 1965. Spin Diffusion Measurements: Spin Echoes in the Presence of a Time-Dependent Field Gradient. *The Journal of Chemical Physics,* 42**,** 288-292.

STEVENS, R. T., APKARIAN, A. V. & HODGE, C. J., JR. 1991. The location of spinothalamic axons within spinal cord white matter in cat and squirrel monkey. *Somatosensory and Motor Research,* 8**,** 97-102.

STIELTJES, B., KAUFMANN, W. E., VAN ZIJL, P. C. M., FREDERICKSEN, K., PEARLSON, G. D., SOLAIYAPPAN, M. & MORI, S. 2001. Diffusion Tensor Imaging and Axonal Tracking in the Human Brainstem. *NeuroImage,* 14**,** 723-735.

STILES, J. & JERNIGAN, T. L. 2010. The basics of brain development. *Neuropsychology review,* 20**,** 327-348.

STOODLEY, C. J. & SCHMAHMANN, J. D. 2018. Chapter 4 - Functional topography of the human cerebellum. *Handbook of Clinical Neurology.* Elsevier.

STRICK, P. L., DUM, R. P. & FIEZ, J. A. 2009. Cerebellum and nonmotor function. *Annual review of neuroscience,* 32**,** 413-434.

STROMINGER, R. N., MCGIFFEN, J. E. & STROMINGER, N. L. 1987. Morphometric and experimental studies of the red nucleus in the albino rat. *Anatomical Record,* 219**,** 420-8.

SUDHEIMER, K. D., WINN, B. M., KERNDT, G. M., SHOAPS, J. M., DAVIS, K. K., FOBBS JR., A. J. & JOHNSON, J. I. 2013. *The Human Brain Atlas* [Online]. Available: https://brains.anatomy.msu.edu/brains/human/brainstem/2000_fiber_labelled.html [Accessed 20 September 2019].

SUN, S. W., NEIL, J. J. & SONG, S. K. 2003. Relative indices of water diffusion anisotropy are equivalent in live and formalin-fixed mouse brains. *Magnetic Resonance in Medicine,* 50**,** 743-8.

SZCZEPANKIEWICZ, F., WESTIN, C.-F. & NILSSON, M. 2021. Gradient waveform design for tensor-valued encoding in diffusion MRI. *Journal of neuroscience methods,* 348**,** 109007-109007.

SZYMANSKI, L. J., HAWES, D. & GILLES, F. 2020. Corticospinal Wallerian Degeneration Before Myelination: A Case Report. *Pediatric and Developmental Pathology,* 23**,** 399-403.

TALOS, I.-F., O'DONNELL, L., WESTIN, C.-F., WARFIELD, S. K., WELLS, W., YOO, S.-S., PANYCH, L. P., GOLBY, A., MAMATA, H., MAIER, S. S., RATIU, P., GUTTMANN, C. R. G., BLACK, P. M., JOLESZ, F. A. & KIKINIS, R. Diffusion Tensor and Functional MRI Fusion with Anatomical MRI for Image-Guided Neurosurgery. *In:* ELLIS, R. E. & PETERS, T. M., eds. Medical Image Computing and Computer-Assisted Intervention - MICCAI 2003, 2003// 2003 Berlin, Heidelberg. Springer Berlin Heidelberg, 407-415.

TAN, W.-Q., YEOH, C.-S., RUMPEL, H., NADKARNI, N., LYE, W.-K., TAN, E.-K. & CHAN, L.-L. 2015. Deterministic Tractography of the Nigrostriatal-Nigropallidal Pathway in Parkinson's Disease. *Scientific Reports,* 5**,** 17283.

TANAKA, S., MITO, T. & TAKASHIMA, S. 1995. Progress of myelination in the human fetal spinal nerve roots, spinal cord and brainstem with myelin basic protein immunohistochemistry. *Early Human Development,* 41**,** 49-59.

TEKA, W. W., HAMADE, K. C., BARNETT, W. H., KIM, T., MARKIN, S. N., RYBAK, I. A. & MOLKOV, Y. I. 2017. From the motor cortex to the movement and back again. *PloS one,* 12**,** e0179288-e0179288.

TEN DONKELAAR, H. J. 1988. Evolution of the red nucleus and rubrospinal tract. *Behavioural Brain Research,* 28**,** 9-20.

TEN DONKELAAR, H. J., KUSUMA, A. & DE BOER-VAN HUIZEN, R. 1980. Cells of origin of pathways descending to the spinal cord in some quadrupedal reptiles. *Journal of Comparative Neurology,* 192**,** 827-51.

TEN DONKELAAR, H. J., LAMMENS, M., WESSELING, P., HORI, A., KEYSER, A. & ROTTEVEEL, J. 2004. Development and malformations of the human pyramidal tract. *Journal of Neurology,* 251**,** 1429-42.

TENCH, C. R., MORGAN, P. S., WILSON, M. & BLUMHARDT, L. D. 2002. White matter mapping using diffusion tensor MRI. *Magnetic Resonance in Medicine,* 47**,** 967-72.
THE HUMAN PROTEIN ATLAS. 2019a. *Brain tissue expression of GFAP* [Online]. Available: https://www.proteinatlas.org/ENSG00000131095-GFAP/brain [Accessed 23 September 2019].
THE HUMAN PROTEIN ATLAS. 2019b. *Tissue expression of MBP - Staining in Pons and Medulla* [Online]. Available: https://www.proteinatlas.org/ENSG00000197971-MBP/tissue/Pons+and+medulla#rnaseq [Accessed 23 september 2019].
TO, W. T., DE RIDDER, D., HART JR., J. & VANNESTE, S. 2018. Changing Brain Networks Through Non-invasive Neuromodulation. *Frontiers in Human Neuroscience,* 12.
TODD, A. J. 2010. Neuronal circuitry for pain processing in the dorsal horn. *Nature reviews. Neuroscience,* 11**,** 823-836.
TOHYAMA, S., HUNG, P. S.-P., CHENG, J. C., ZHANG, J. Y., HALAWANI, A., MIKULIS, D. J., OH, J. & HODAIE, M. 2020. Trigeminal neuralgia associated with a solitary pontine lesion: clinical and neuroimaging definition of a new syndrome. *Pain,* 161.
TORRES, C. V., MORO, E., LOPEZ-RIOS, A. L., HODAIE, M., CHEN, R., LAXTON, A. W., HUTCHISON, W. D., DOSTROVSKY, J. O. & LOZANO, A. M. 2010. Deep brain stimulation of the ventral intermediate nucleus of the thalamus for tremor in patients with multiple sclerosis. *Neurosurgery,* 67**,** 646-51; discussion 651.
TORVIK, A. 1957. The ascending fibers from the main trigeminal sensory nucleus. An experimental study in the cat. *American Journal of Anatomy,* 100**,** 1-15.
TOVI, M. & ERICSSON, A. 1992. Measurements of T1 and T2 over time in formalin-fixed human whole-brain specimens. *Acta Radiologica,* 33**,** 400-4.
TRACEY, D. 2004. CHAPTER 7 - Ascending and Descending Pathways in the Spinal Cord. *The Rat Nervous System (Third Edition).* Burlington: Academic Press.
TREVINO, D. L. & CARSTENS, E. 1975. Confirmation of the location of spinothalamic neurons in the cat and monkey by the retrograde transport of horseradish peroxidase. *Brain Research,* 98**,** 177-82.
TRUEX, R. C., TAYLOR, M. J., SMYTHE, M. Q. & GILDENBERG, P. L. 1970. The lateral cervical nucleus of cat, dog and man. *Journal of Comparative Neurology,* 139**,** 93-104.
TSURUOKA, M., TAMAKI, J., MAEDA, M., HAYASHI, B. & INOUE, T. 2012. Biological implications of coeruleospinal inhibition of nociceptive processing in the spinal cord. *Frontiers in Integrative Neuroscience,* 6**,** 87.
TUCH, D. S. 2004. Q-ball imaging. *Magnetic Resonance in Medicine,* 52**,** 1358-72.
TUCH, D. S., REESE, T. G., WIEGELL, M. R., MAKRIS, N., BELLIVEAU, J. W. & WEDEEN, V. J. 2002. High angular resolution diffusion imaging reveals intravoxel white matter fiber heterogeneity. *Magnetic Resonance in Medicine,* 48**,** 577-82.
TURNER, R., LE BIHAN, D. & CHESNICK, A. S. 1991. Echo-planar imaging of diffusion and perfusion. *Magnetic Resonance in Medicine,* 19**,** 247-53.
UHLÉN, M., FAGERBERG, L., HALLSTRÖM, B. M., LINDSKOG, C., OKSVOLD, P., MARDINOGLU, A., SIVERTSSON, Å., KAMPF, C., SJÖSTEDT, E.,

ASPLUND, A., OLSSON, I., EDLUND, K., LUNDBERG, E., NAVANI, S., SZIGYARTO, C. A.-K., ODEBERG, J., DJUREINOVIC, D., TAKANEN, J. O., HOBER, S., ALM, T., EDQVIST, P.-H., BERLING, H., TEGEL, H., MULDER, J., ROCKBERG, J., NILSSON, P., SCHWENK, J. M., HAMSTEN, M., VON FEILITZEN, K., FORSBERG, M., PERSSON, L., JOHANSSON, F., ZWAHLEN, M., VON HEIJNE, G., NIELSEN, J. & PONTÉN, F. 2015. Tissue-based map of the human proteome. *Science,* 347**,** 1260419.

VALVERDE, F. 1998. *Golgi Atlas of the Postnatal mouse Brain,* New York, Springer.

VAN ESSEN, D. C., SMITH, S. M., BARCH, D. M., BEHRENS, T. E., YACOUB, E. & UGURBIL, K. 2013. The WU-Minn Human Connectome Project: an overview. *Neuroimage,* 80**,** 62-79.

VAN ESSEN, D. C., UGURBIL, K., AUERBACH, E., BARCH, D., BEHRENS, T. E., BUCHOLZ, R., CHANG, A., CHEN, L., CORBETTA, M., CURTISS, S. W., DELLA PENNA, S., FEINBERG, D., GLASSER, M. F., HAREL, N., HEATH, A. C., LARSON-PRIOR, L., MARCUS, D., MICHALAREAS, G., MOELLER, S., OOSTENVELD, R., PETERSEN, S. E., PRIOR, F., SCHLAGGAR, B. L., SMITH, S. M., SNYDER, A. Z., XU, J. & YACOUB, E. 2012. The Human Connectome Project: a data acquisition perspective. *Neuroimage,* 62**,** 2222-31.

VANDERHORST, V. G., TERASAWA, E. & RALSTON, H. J., 3RD 2001. Monosynaptic projections from the nucleus retroambiguus region to laryngeal motoneurons in the rhesus monkey. *Neuroscience,* 107**,** 117-25.

VERHAART, W. J. C. 1947. ON THICK AND THIN FIBERS IN THE PYRAMIDAL TRACT. 22**,** 271-281, *Acta Psychiatrica Scandinavica*.

VILLANUEVA, L. & LE BARS, D. 1995. The activation of bulbo-spinal controls by peripheral nociceptive inputs: diffuse noxious inhibitory controls. *Biology Research,* 28**,** 113-25.

VISSER, M. M., YASSI, N., CAMPBELL, B. C. V., DESMOND, P. M., DAVIS, S. M., SPRATT, N., PARSONS, M. & BIVARD, A. 2019. White Matter Degeneration after Ischemic Stroke: A Longitudinal Diffusion Tensor Imaging Study, *Journal of Neuroimaging*. 29**,** 111-118.

VON MONAKOW, K. H., AKERT, K. & KÜNZLE, H. 1979. Projections of precentral and premotor cortex to the red nucleus and other midbrain areas in Macaca fascicularis. *Experimental brain research,* 34**,** 91-105.

VOOGD, J. 1967. Comparative aspects of the structure and fibre connexions of the mammalian cerebellum. *Progress in brain research,* 25**,** 94-134.

VOOGD, J. 1969. The importance of fiber connections in the comparative anatomy of the mammalian cerebellum. *Neurology of Cerebellar Evolution and Development***,** 493-514.

WANG, J. Y., ABDI, H., BAKHADIROV, K., DIAZ-ARRASTIA, R. & DEVOUS, M. D., SR. 2012. A comprehensive reliability assessment of quantitative diffusion tensor tractography. *NeuroImage,* 60**,** 1127-1138.

WANG, T., MANOHAR, N., LEI, Y., DHABAAN, A., SHU, H. K., LIU, T., CURRAN, W. J. & YANG, X. 2019. MRI-based treatment planning for brain

stereotactic radiosurgery: Dosimetric validation of a learning-based pseudo-CT generation method. *Medical Dosimetry,* 44**,** 199-204.
WARREN, S. & MAY, P. J. 2013. Morphology and connections of intratrigeminal cells and axons in the macaque monkey. *Frontiers in Neuroanatomy,* 7.
WASSERMANN, E. M., FUHR, P., COHEN, L. G. & HALLETT, M. 1991. Effects of transcranial magnetic stimulation on ipsilateral muscles. *Neurology,* 41**,** 1795-9.
WATSON, C., PAXINOS, G. & KAYALIOGLU, G. 2008. *The Spinal Cord A Christopher and Dana Reeve Foundation Text and Atlas*, ELSEVIER.
WEDEEN, V. J., HAGMANN, P., TSENG, W. Y., REESE, T. G. & WEISSKOFF, R. M. 2005. Mapping complex tissue architecture with diffusion spectrum magnetic resonance imaging. *Magnetic Resonance in Medicine,* 54**,** 1377-86.
WEINSTEIN, D., KINDLMANN, G. & LUNDBERG, E. 1999. Tensorlines: Advection-diffusion based propagation through diffusion tensor fields. *IEEE Computer Society*, 249-530.
WESTIN, C. F., MAIER, S. E., MAMATA, H., NABAVI, A., JOLESZ, F. A. & KIKINIS, R. 2002. Processing and visualization for diffusion tensor MRI. *Medical Image Analysis,* 6**,** 93-108.
WESTLYE, L. T., WALHOVD, K. B., DALE, A. M., BJØRNERUD, A., DUE-TØNNESSEN, P., ENGVIG, A., GRYDELAND, H., TAMNES, C. K., OSTBY, Y. & FJELL, A. M. 2010. Life-span changes of the human brain white matter: diffusion tensor imaging (DTI) and volumetry. *Cerebral Cortex,* 20**,** 2055-68.
WICK, W. & KÜKER, W. 2004. Brain Edema in Neurooncology: Radiological Assessment and Management. *Oncology Research and Treatment,* 27**,** 261-266.
WICKERSHAM, I. R., FINKE, S., CONZELMANN, K. K. & CALLAWAY, E. M. 2007. Retrograde neuronal tracing with a deletion-mutant rabies virus. *Nature Methods,* 4**,** 47-9.
WIESENDANGER, R. & WIESENDANGER, M. 1985. Cerebello-cortical linkage in the monkey as revealed by transcellular labeling with the lectin wheat germ agglutinin conjugated to the marker horseradish peroxidase. *Experimental Brain Research,* 59**,** 105-117.
WILLIAMS, P. T., KIM, S. & MARTIN, J. H. 2014. Postnatal maturation of the red nucleus motor map depends on rubrospinal connections with forelimb motor pools. *Journal of Neuroscience,* 34**,** 4432-41.
WILLIS, W. D. 1985. Nociceptive pathways: anatomy and physiology of nociceptive ascending pathways. *Philosophical Transactions of the Royal Society B Biological Sciences,* 308**,** 253-70.
WILLIS, W. D., AL-CHAER, E. D., QUAST, M. J. & WESTLUND, K. N. 1999. A visceral pain pathway in the dorsal column of the spinal cord. *Proceedings of the National Academy of Sciences,* 96**,** 7675-7679.
WILLIS, W. D. & WESTLUND, K. N. 1997. Neuroanatomy of the pain system and of the pathways that modulate pain. *Journal of Clinical Neurophysiology,* 14**,** 2-31.
WINSTON, G. P. 2012. The physical and biological basis of quantitative parameters derived from diffusion MRI. *Quantitative Imaging in Medicine and Surgery* 2**,** 254-265.

WOOLRICH, M. W., JBABDI, S., PATENAUDE, B., CHAPPELL, M., MAKNI, S., BEHRENS, T., BECKMANN, C., JENKINSON, M. & SMITH, S. M. 2009. Bayesian analysis of neuroimaging data in FSL. *NeuroImage,* 45**,** S173-S186.

WU, J. S., ZHOU, L. F., TANG, W. J., MAO, Y., HU, J., SONG, Y. Y., HONG, X. N. & DU, G. H. 2007. Clinical evaluation and follow-up outcome of diffusion tensor imaging-based functional neuronavigation: a prospective, controlled study in patients with gliomas involving pyramidal tracts. *Neurosurgery,* 61**,** 935-48; discussion 948-9.

XIAO, Y., ZITELLA, L. M., DUCHIN, Y., TEPLITZKY, B. A., KASTL, D., ADRIANY, G., YACOUB, E., HAREL, N. & JOHNSON, M. D. 2016. Multimodal 7T Imaging of Thalamic Nuclei for Preclinical Deep Brain Stimulation Applications. *Frontiers in Neuroscience,* 10.

XIE, S., ZUO, N., SHANG, L., SONG, M., FAN, L. & JIANG, T. 2015. How does B-value affect HARDI reconstruction using clinical diffusion MRI data? *PloS one,* 10**,** e0120773-e0120773.

XU, Q. & GRANT, G. 2005. Course of spinocerebellar axons in the ventral and lateral funiculi of the spinal cord with projections to the posterior cerebellar termination area: an experimental anatomical study in the cat, using a retrograde tracing technique. *Experimental Brain Research,* 162**,** 250-6.

YAGINUMA, H. & MATSUSHITA, M. 1989. Spinocerebellar projections from the upper lumbar segments in the cat, as studied by anterograde transport of wheat germ agglutinin-horseradish peroxidase. *Journal of Comparative Neurology,* 281**,** 298-319.

YAKOVLEV, P. I. & RAKIC, P. 1966. Patterns of decussation of bulbar pyramids and distribution of pyramidal tracts on two sides of the spinal cord. *Transactions of the American Neurological Association,* 91, 366-367

YANG, D. S., HONG, J. H., BYUN, W. M., KWAK, S. Y., AHN, S. H., LEE, H., HWANG, C. H. & JANG, S. H. 2009. Identification of the medial lemniscus in the human brain: Combined study of functional MRI and diffusion tensor tractography. *Neuroscience Letters,* 459**,** 19-24.

YEH, F.-C. 2021. *DSI Studio (Version 2021 May)* [Online]. [Accessed 20/09/2018].

YEH, F.-C., PANESAR, S., BARRIOS, J., FERNANDES, D., ABHINAV, K., MEOLA, A. & FERNANDEZ-MIRANDA, J. C. 2019. Automatic Removal of False Connections in Diffusion MRI Tractography Using Topology-Informed Pruning (TIP). *Neurotherapeutics,* 16**,** 52-58.

YEH, F.-C., VERSTYNEN, T. D., WANG, Y., FERNÁNDEZ-MIRANDA, J. C. & TSENG, W.-Y. I. 2013. Deterministic Diffusion Fiber Tracking Improved by Quantitative Anisotropy. *PLOS ONE,* 8**,** e80713.

YEN, C. T., HONDA, C. N. & JONES, E. G. 1991. Electrophysiological study of spinothalamic inputs to ventrolateral and adjacent thalamic nuclei of the cat. *Journal of Neurophysiology,* 66**,** 1033-47.

YILMAZER-HANKE, D., MAYER, T., MÜLLER, H.-P., NEUGEBAUER, H., ABAEI, A., SCHEUERLE, A., WEIS, J., FORSBERG, K. M. E., ALTHAUS, K., MEIER, J., LUDOLPH, A. C., DEL TREDICI, K., BRAAK, H., KASSUBEK, J. & RASCHE, V. 2020. Histological correlates of postmortem ultra-high-resolution single-section MRI in cortical cerebral microinfarcts. *Acta Neuropathologica Communications,* 8**,** 33.

YOUNG, I. R., SZEVERENYI, N. M., DU, J. & BYDDER, G. M. 2020. Pulse sequences as tissue property filters (TP-filters): a way of understanding the signal, contrast and weighting of magnetic resonance images. *Quantitative imaging in medicine and surgery,* 10**,** 1080-1120.

YOUNG, P. A. 2007. *Basic clinical neuroscience,* Philadelphia, Lippincott Williams & Wilkins.

YUSHKEVICH, P. A., ZHANG, H., SIMON, T. J. & GEE, J. C. 2008. Structure-specific statistical mapping of white matter tracts. *Neuroimage,* 41**,** 448-61.

ZARETSKY, S. 1982. The extrapyramidal nervous system. *Journal of Neuroscience Nursing,* 14**,** 295-8.

ZHAN, L., ZHOU, J., WANG, Y., JIN, Y., JAHANSHAD, N., PRASAD, G., NIR, T. M., LEONARDO, C. D., YE, J., THOMPSON, P. M. 2015. Comparison of nine tractography algorithms for detecting abnormal structural brain networks in Alzheimer's disease. *Frontiers in Aging Neuroscience,* 7.

ZHANG, C., SCHULTZ, T., LAWONN, K., EISEMANN, E. & VILANOVA, A. 2016. Glyph-Based Comparative Visualization for Diffusion Tensor Fields. *IEEE Transactions on Visualization and Computer Graphics,* 22**,** 797-806.

ZHANG, H., SCHNEIDER, T., WHEELER-KINGSHOTT, C. A. & ALEXANDER, D. C. 2012. NODDI: practical in vivo neurite orientation dispersion and density imaging of the human brain. *Neuroimage,* 61**,** 1000-16.

ZHANG, L.-Y., LIN, P., PAN, J., MA, Y., WEI, Z., JIANG, L., WANG, L., SONG, Y., WANG, Y., ZHANG, Z., JIN, K., WANG, Q. & YANG, G.-Y. 2018a. CLARITY for High-resolution Imaging and Quantification of Vasculature in the Whole Mouse Brain. *Aging and disease,* 9**,** 262-272.

ZHANG, T., KONG, J., JING, K., CHEN, H., JIANG, X., LI, L., GUO, L., LU, J., HU, X., LIU, T. 2018b. Optimization of macaque brain DMRI connectome by neuron tracing and myelin stain data. *Computerized Medical Imaging and Graphics: the official journal of the Computerized Medical Imaging Society,* 69**,** 9-20.

ZHANG, X., WENK, H. N., HONDA, C. N. & GIESLER, G. J., JR. 2000. Locations of spinothalamic tract axons in cervical and thoracic spinal cord white matter in monkeys. *Journal of Neurophysiology,* 83**,** 2869-80.

ZINGG, B., HINTIRYAN, H., GOU, L., SONG, M. Y., BAY, M., BIENKOWSKI, M. S., FOSTER, N. N., YAMASHITA, S., BOWMAN, I., TOGA, A., DONG H.W. 2014. Neural networks of the mouse neocortex. *Cell,* 156**,** 1096-1111.

ZIYAL, I. M., SEKHAR, L. N., OZGEN, T., SÖYLEMEZOĞLU, F., ALPER, M. & BEŞER, M. 2004. The trigeminal nerve and ganglion: an anatomical, histological, and radiological study addressing the transtrigeminal approach. *Surgical Neurology,* 61**,** 564-73; discussion 573-4.

ZOLI, M., TALOZZI, L., MARTINONI, M., MANNERS, D. N., BADALONI, F., TESTA, C., ASIOLI, S., MITOLO, M., BARTIROMO, F., ROCHAT, M. J., FABBRI, V. P., STURIALE, C., CONTI, A., LODI, R., MAZZATENTA, D. & TONON, C. 2021. From Neurosurgical Planning to Histopathological Brain Tumor Characterization: Potentialities of Arcuate Fasciculus Along-Tract Diffusion Tensor Imaging Tractography Measures. *Frontiers in Neurology,* 12.

ZORNOW, M. H. & PROUGH, D. S. 1995. Fluid management in patients with traumatic brain injury. *New Horizons,* 3**,** 488-98.

Appendix

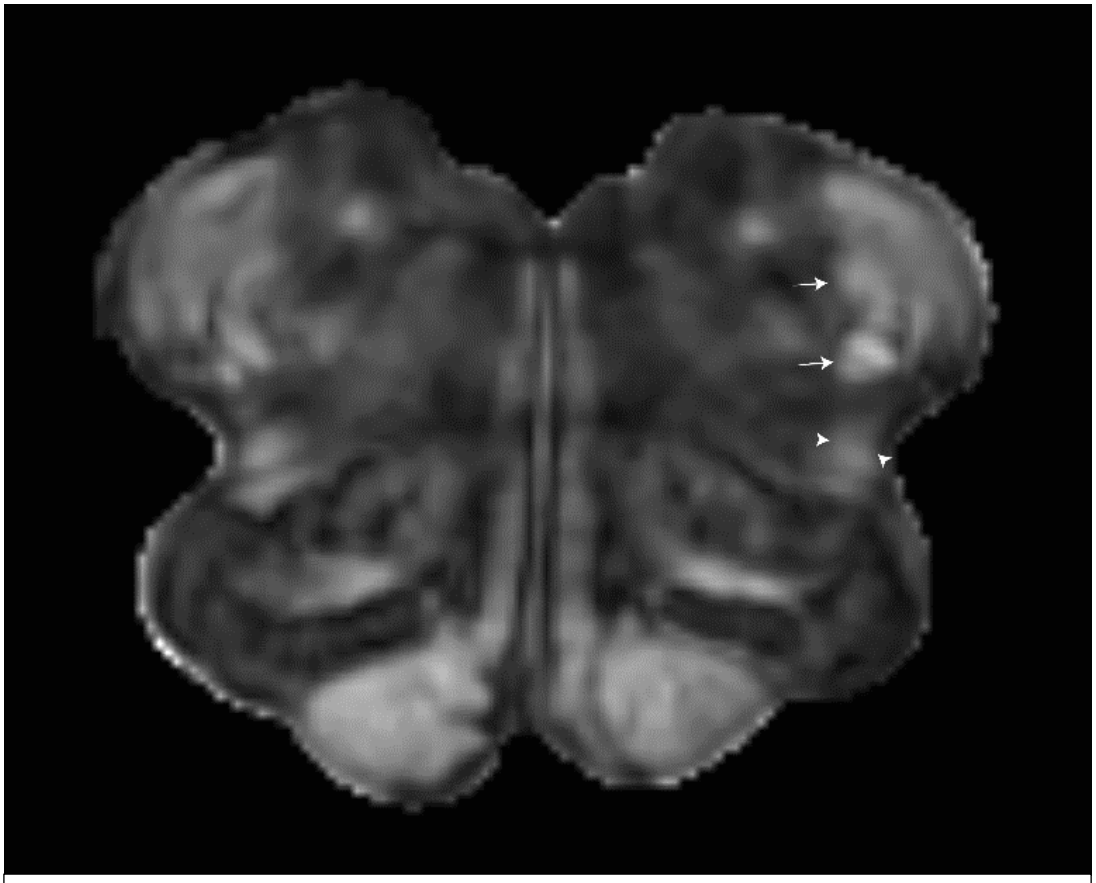

Fig. 1. Fractional Anisotropy (FA) - Transverse section, human specimen 1*. DTI contrast at 200 µm resolution, showing the medulla at the same level as the GRE in Fig. 2.1. Arrows: sp5, Arrowheads: spth*

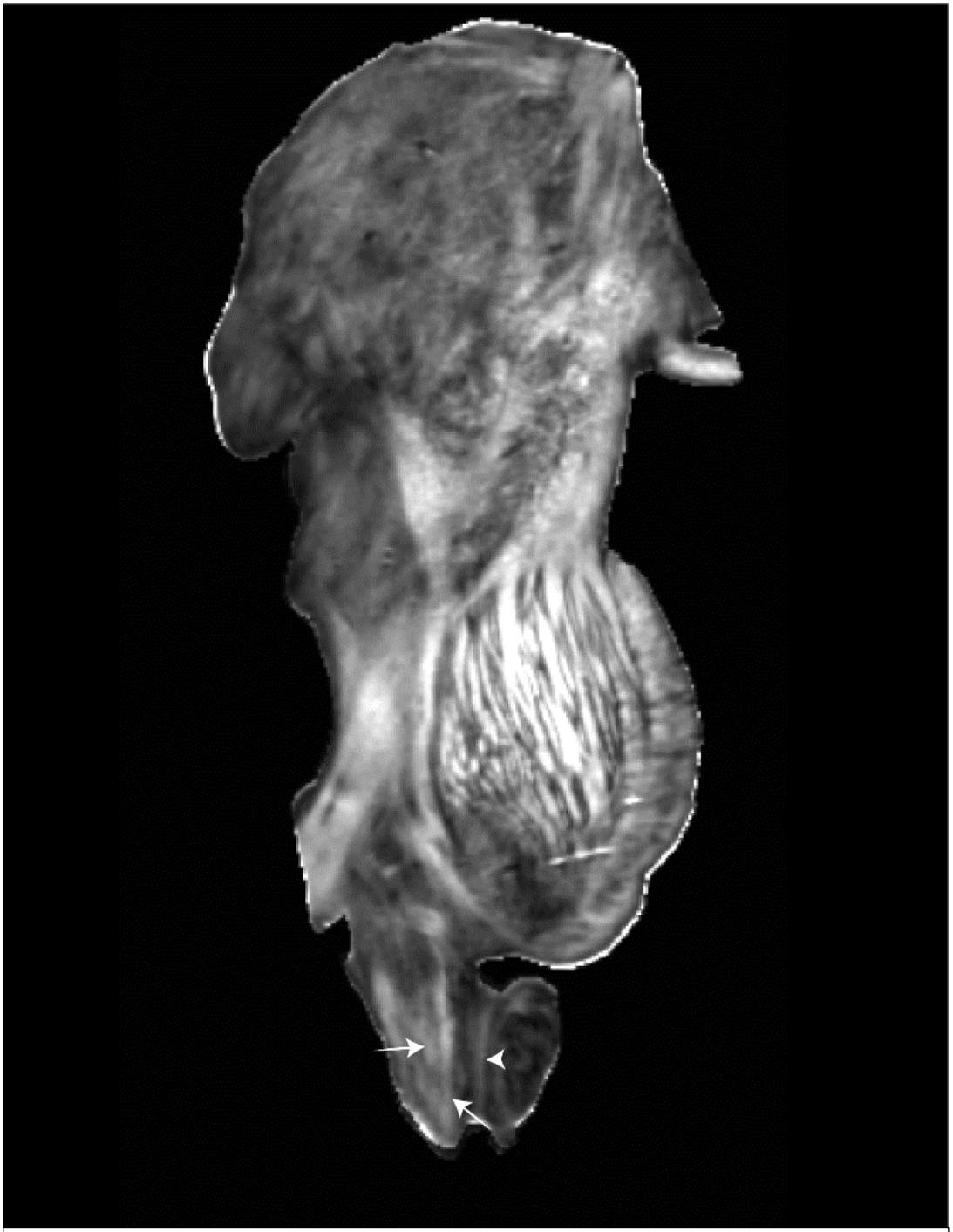

Fig. 2. Fractional Anisotropy (FA) – Sagittal section, human specimen 1, at the level of the brainstem and thalamus*. Arrow: sp5, Arrowheads: spth*

Fig. 3. Fractional Anisotropy (FA) - Coronal section, human specimen 1, at the level of the brainstem and thalamus*. Arrows: sp5, Arrowhead: spth.*

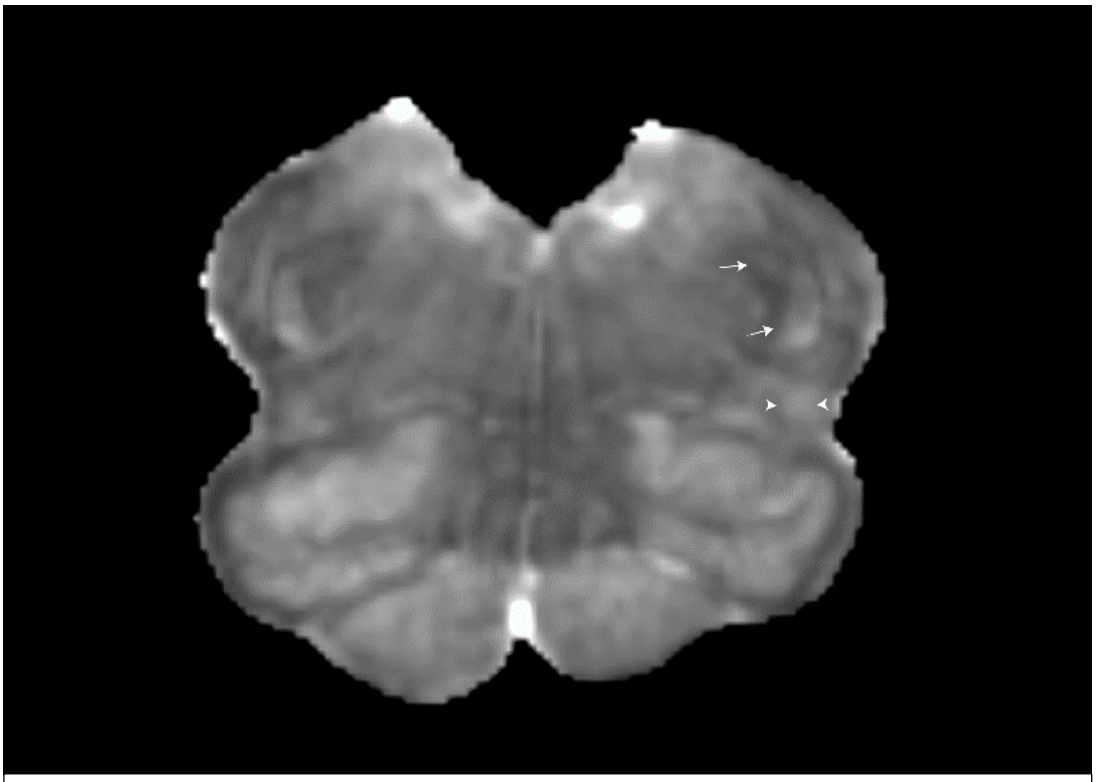

Fig. 4. Axial Diffusivity (AD) - Transverse section, human specimen 1. *DTI contrast at 200 μm resolution of the medulla at the same level as the above DTI contrasts (e.i., compare with FA in Fig. 1). Arrows: sp5, Arrowheads: spth.*

Fig. 5. Axial Diffusivity (AD) - Coronal section, human specimen 1, at the level of the brainstem and thalamus*. Arrow: sp5*

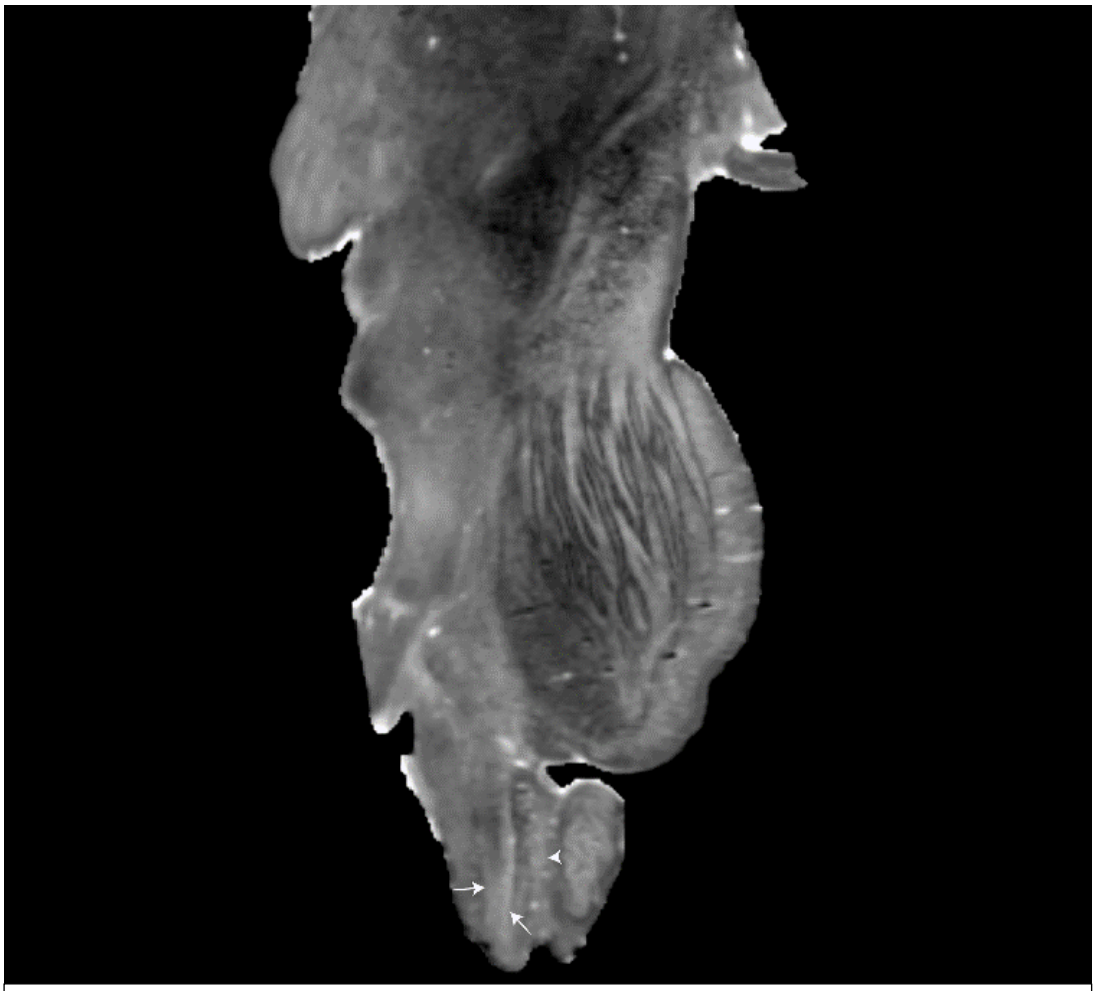

Fig. 6. Axial diffusivity (AD) - Sagittal section, human specimen 1, at the level of the brainstem and thalamus*. Arrows: sp5, Arrowhead: spth.*

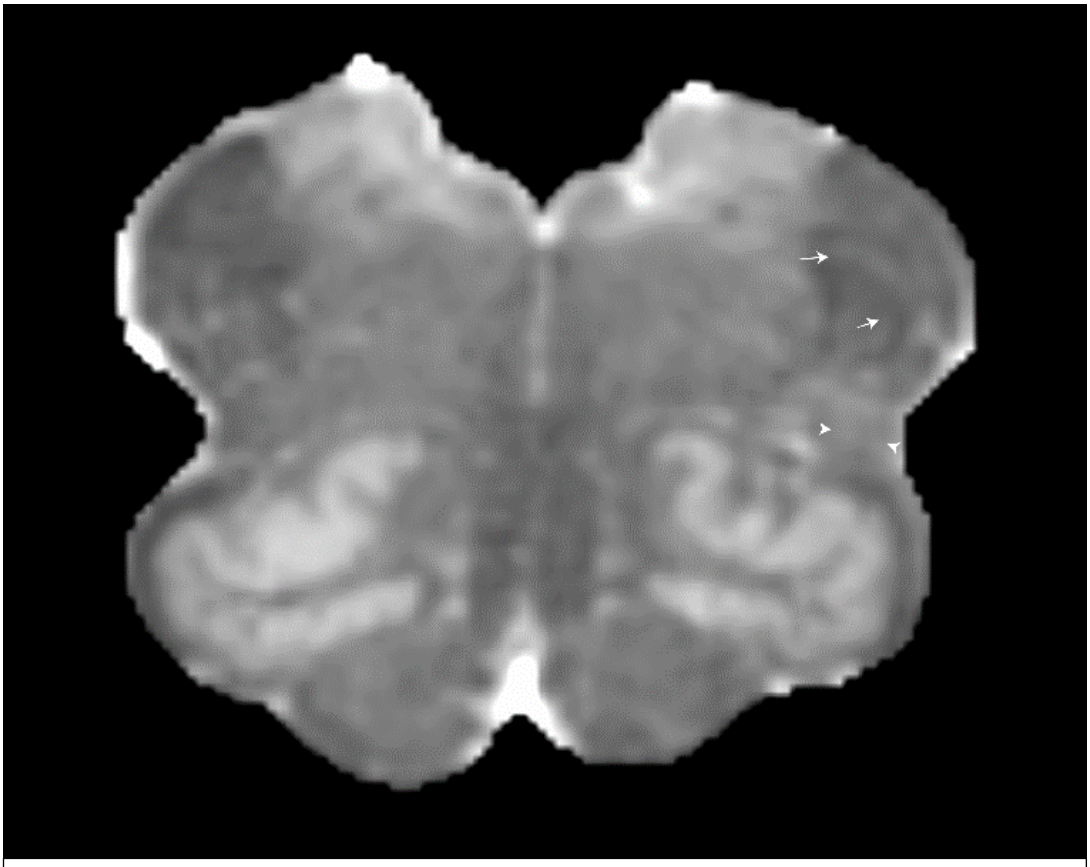

Fig. 7. Mean Diffusivity (MD) - Transverse section, human specimen 1*. DTI contrast at 200 µm resolution, showing the medulla at the same level as the other DTI contrasts (i.e., compare Figs 1 and 4). Arrows: sp5, Arrowheads: spth*

Fig. 8. Mean diffusivity (MD) - Coronal section, human specimen 1 showing the brainstem and thalamus*. Arrow: sp5*

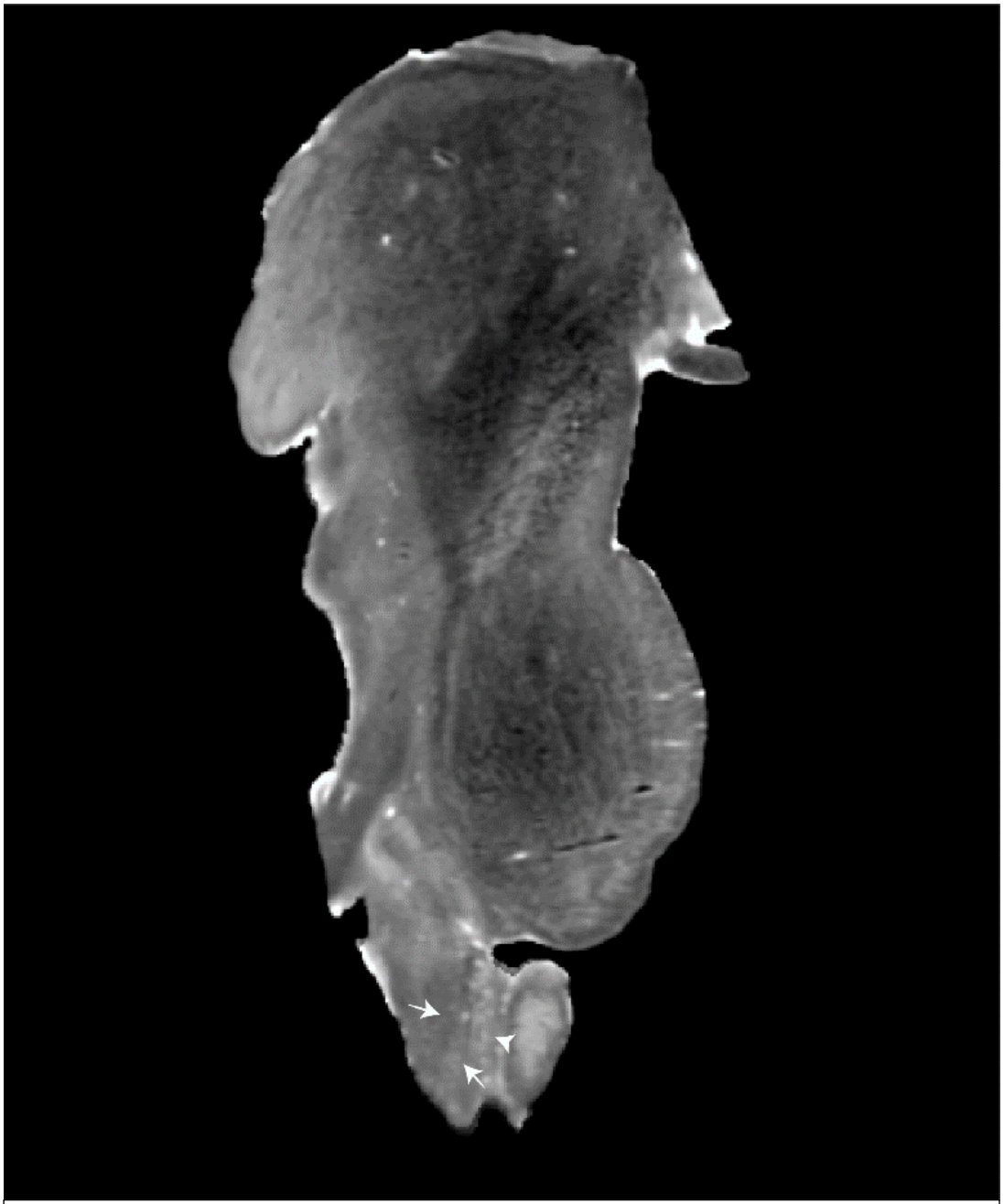

Fig. 9. Mean Diffusivity (MD) - Sagittal section, human specimen 1 of the brainstem and thalamus*. Arrows: sp5, Arrowhead: spth.*

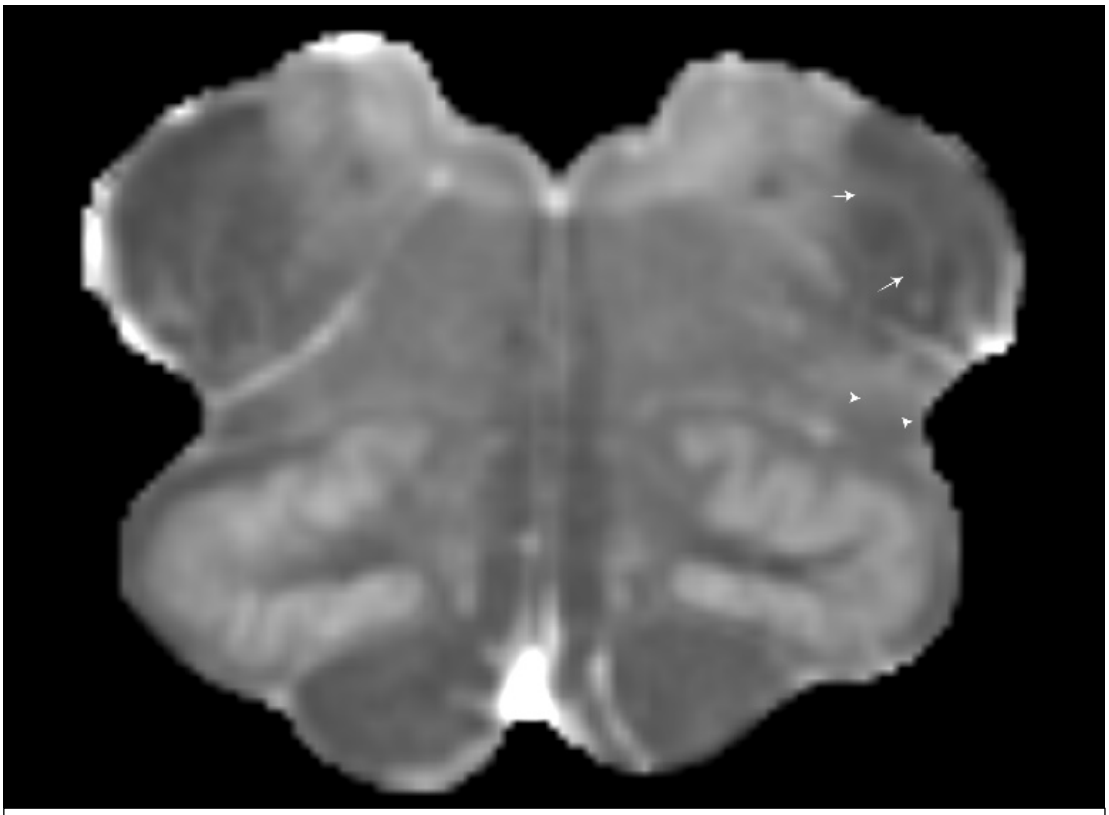

Fig. 10. Radial Diffusivity (RD) - Transverse section, human specimen 1. *DTI contrast at 200 μm resolution, showing the medulla at the same level as the other DTI contrasts (i.e., compare Figs. 1, 4, 7). Arrows: sp5, Arrowheads: spth*

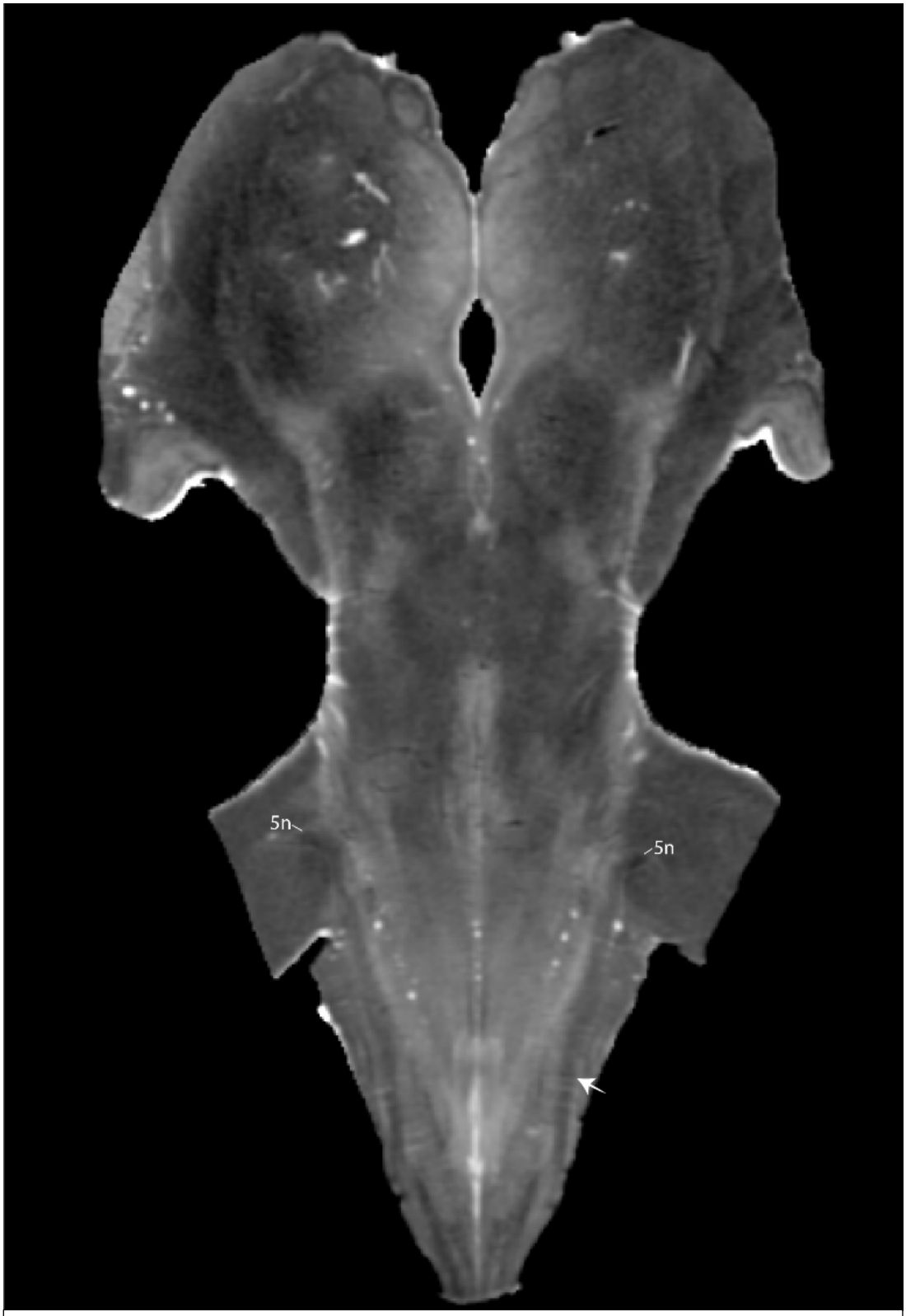

Fig. 11. Radial Diffusivity (RD) - Coronal section, human specimen 1 of the brainstem and thalamus*. Arrow: sp5*

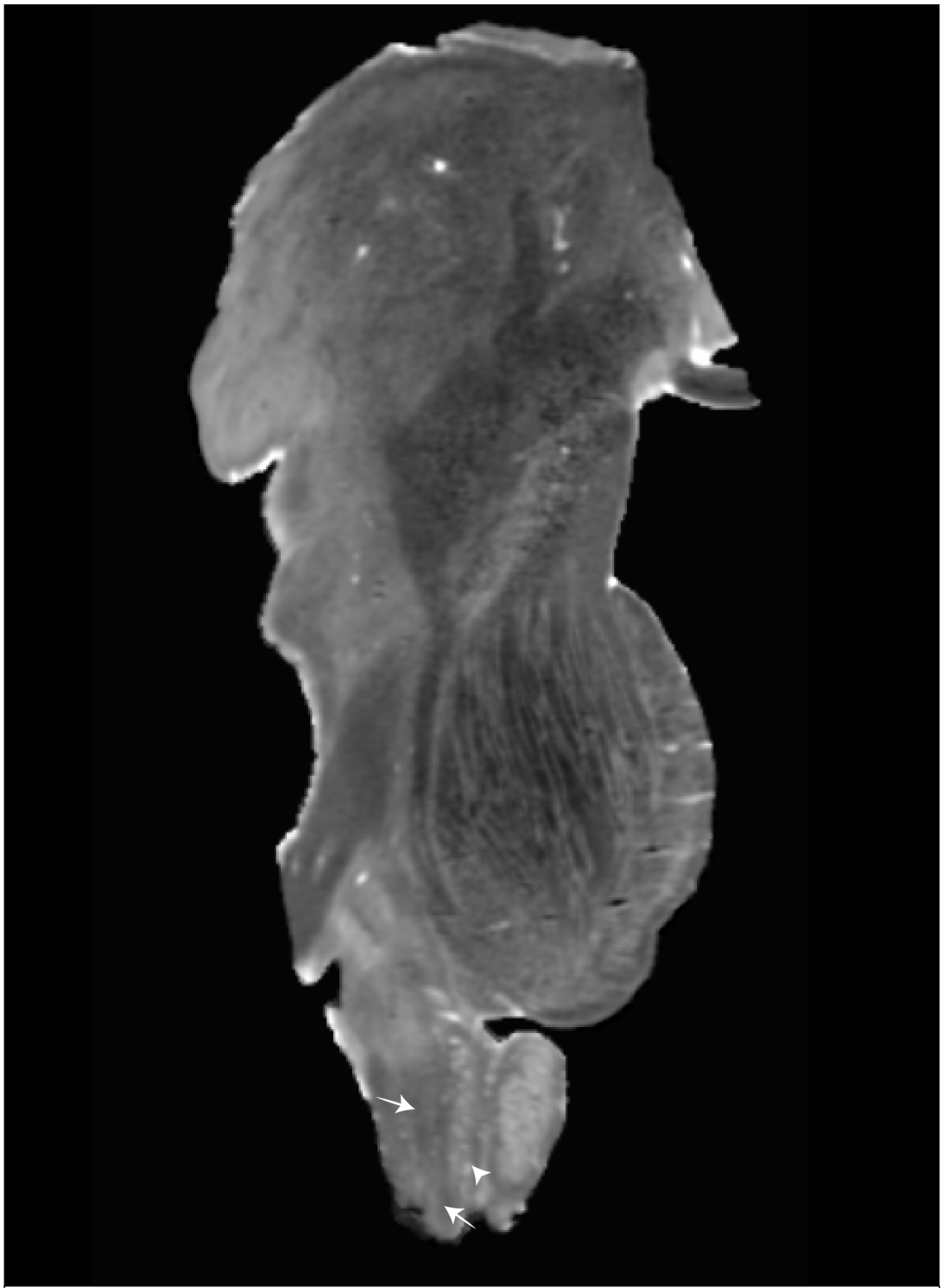

Fig. 12. Radial Diffusivity (RD) - Sagittal section, human specimen 1 of the brainstem and thalamus*. Arrows: sp5, Arrowhead: spth*

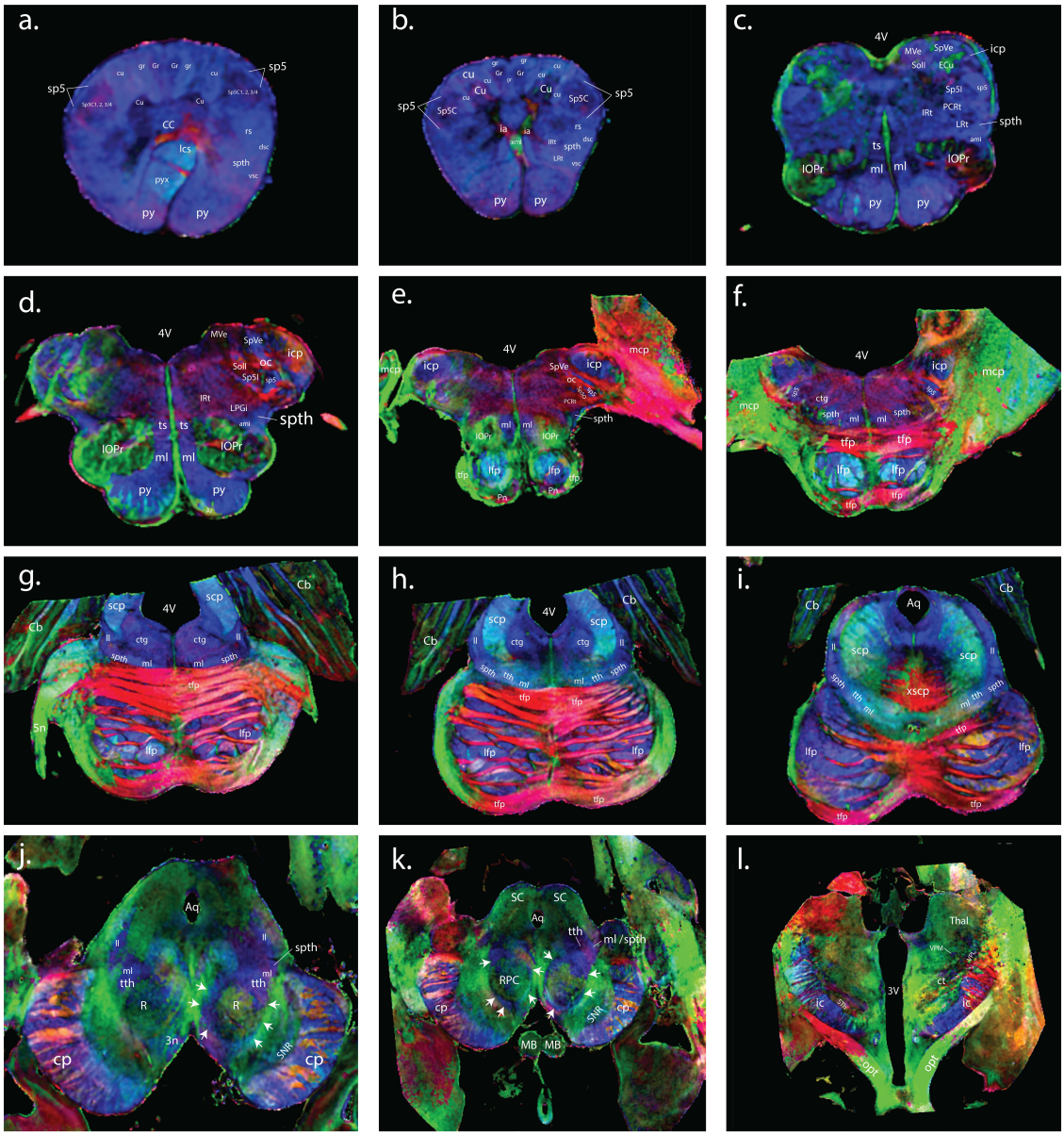

Human specimen 2

Fig. 13. Transverse FAC sections from the level of the pyramidal decussation in the medulla oblongata (panel a) until the ventral tier of the thalamus (panel l). *Each section is derived from the same specimen (human specimen 2). Compare with the higher quality GRE and FAC images from human specimen 1 (Figs in Ch 4 and 5), used as background for 3D tractography throughout the brainstem and thalamus. The location of the gr, cu, spth and their relationship with adjacent structures are indicated. The sp5, and the components of its nucleus (oralis, interpolaris, and caudalis) can be followed through their course, and the tth can be traced from mid pontine levels until the VPM. In addition, the FAC shows the course and configuration of the scp, xscp, and the ct that surrounds the red nucleus like a "penumbra" (arrows in j and k; blue signature on the FAC) to project within the ventral thalamus. Red, blue, and green represent anisotropy along medial-lateral, rostral-caudal, and ventral-dorsal orientation, respectively. Abbreviations: tth: trigeminothalamic tract, spth: spinothalamic tract, 5n: trigeminal nerve, sp5: spinal trigeminal tract, ml: medial lemniscus, xml: sensory decussation, ia: internal arcuate fibres, pyx: pyramidal decussation, CC: central canal, Sp5C,1,2,3/4: spinal trigeminal nucleus, caudal part, laminae one to four, Cu: cuneate nucleus, cu: cuneate fasciculus, Gr: gracile nucleus, py: pyramidal tract, lcs: lateral corticospinal tract, Sp5C: spinal trigeminal nucleus, caudal part, icp: inferior cerebellar peduncle, vsc: ventral spinocerebellar tract, dsc: dorsal spinocerebellar tract, rs: rubrospinal tract, scp: superior cerebellar peduncle, xscp: decussation of the superior cerebellar peduncle, mcp: middle cerebellar peduncle, Cb: cerebellum, ct: cerebellothalamic tract,*

MVe: medial vestibular nucleus, SpVe: spinal vestibular nucleus, ECu: external cuneate nucleus, SolI: solitary nucleus, interstitial part, Sp5I: spinal trigeminal nucleus, interpolar part, ts: tectospinal tract, IOPr: inferior olive, principal nucleus, 3V: third ventricle, 4V: fourth ventricle, oc: olivocerebellar tract, Sp5O: spinal trigeminal nucleus, oral part, lfp: longitudinal fibres of the pons, tfp: transverse fibres of the pons, Pn: pontine nuclei, PCRt: parvicellular reticular nucleus, IRt: intermediate reticular nucleus, LRt: lateral reticular nucleus, LPGi: lateral paragigantocellular nucleus, ami: amiculum, ctg: central tegmental tract, Ar: arcuate nucleus, SNR: substantia nigra, pars reticulata, ll: lateral lemniscus, SC: superior colliculus, Aq: cerebral aqueduct, R: red nucleus, RPC: red nucleus, parvicellular part, STh: subthalamic nucleus of Luys, MB: mammillary bodies, 3n: third nerve, f: fornix.

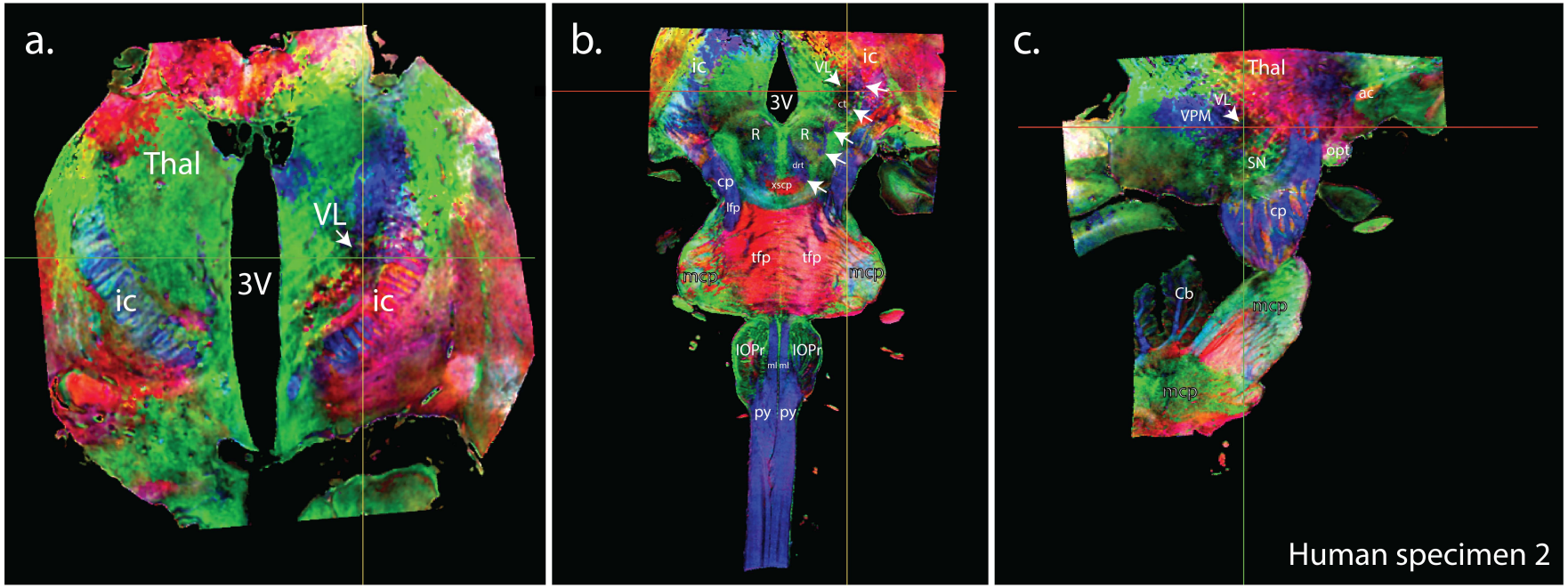
a.
Thal
VL
3V
ic
ic
b.
ic
VL
ic
3V
ct
R
R
drt
cp
xscp
lfp
tfp
tfp
mcp
mcp
lOPr
lOPr
ml ml
py
py
c.
Thal
VL
VPM
ac
opt
SN
cp
Cb
mcp
mcp
Human specimen 2

Fig. 14. Transverse and the corresponding intersecting coronal and sagittal planes in the 2nd human specimen, displayed with FAC. *The point at which the line intersections are visualised, the FAC reveals the VL located medial to the ic. In a (transverse), b (coronal) and c (sagittal) planes. Note in (b) the course of the drt from the xscp through the red nucleus and its ascent antidromically (compared to the bundles that form the ic) to the thalamus (see arrows in b). In (c) the FAC shows a sagittal section of the thalamus and the corresponding location of the VL at the point where the intersecting lines can be seen. Red, blue, and green on the FAC maps represent anisotropy along medial-lateral, rostral-caudal, and ventral-dorsal orientations, respectively. Abbreviations: 3V: third ventricle, Thal: thalamus, ct: cerebellothalamic tract, opt: optic tract, ac: anterior commissure, cp: cerebral peduncle, VL: ventral lateral nucleus of the thalamus, VPM: ventral posteromedial nucleus of the thalamus, SN: substantia nigra, ic: internal capsule, R: red nucleus, drt: dentato-rubro-thalamic tract, xscp: decussation of the superior cerebellar peduncle, mcp: middle cerebellar peduncle, Cb: cerebellum, pyx: decussation of the pyramidal tract, SC: superior colliculus, IC: inferior colliculus, ml: medial lemniscus, lfp: longitudinal fibres of the pons, tfp: transverse fibres of the pons, IOPr: inferior olive, principal nucleus, ac: anterior commissure.*

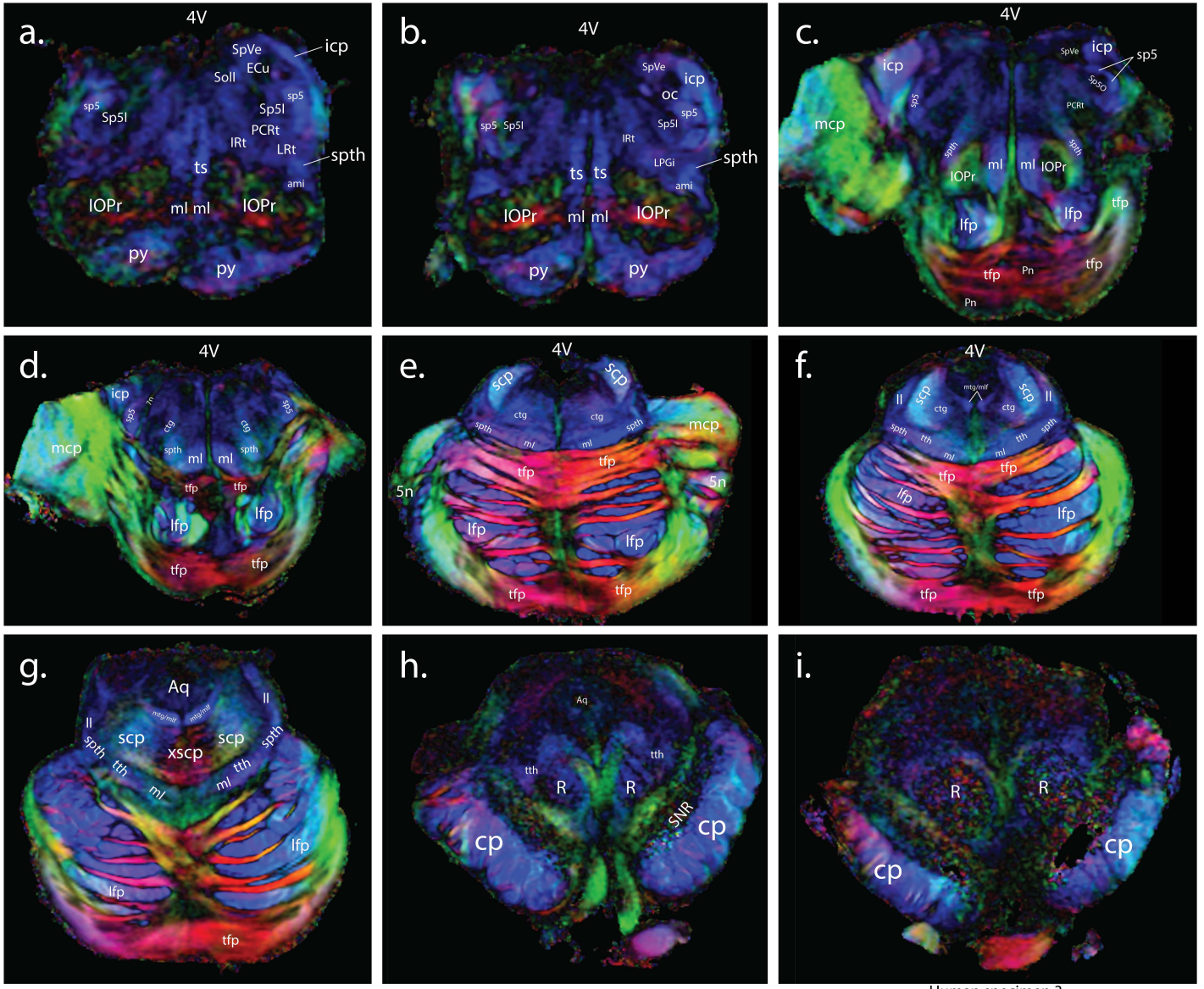

Human specimen 3

Fig. 15. Transverse sections from the level of the IOPr in the medulla oblongata (panel a) until the midbrain (panel i). *Each section is derived from the same specimen (human specimen 3). Compare with the high quality GRE and FAC images from human specimen 1 (Figs in Ch 4 and 5). The precise location of the spth and its relationship with adjacent structures can be visualised on the FAC. In addition, the sp5, and the two components of its nucleus (Sp5 oralis, and interpolaris) can be followed throughout their course. Moreover, the tth can be traced from mid pontine levels until the midbrain behind the red nucleus. The caudal medulla and midbrain can be clearly seen on the images are damaged, limiting the ability to follow fibre tracts with tractography. However, this FAC is still informative enough to broadly confirm the gross anatomical findings from human specimen 1. On the FAC maps red, blue, and green represent anisotropy along medial-lateral, rostral-caudal, and ventral-dorsal orientations, respectively. Abbreviations: tth: trigeminothalamic tract, spth: spinothalamic tract, 5n: trigeminal nerve, sp5: spinal trigeminal tract, ml: medial lemniscus, xml: sensory decussation, ia: internal arcuate fibres, pyx: pyramidal decussation, Cu: cuneate nucleus, cu: cuneate fasciculus, Gr: gracile nucleus, py: pyramidal tract, icp: inferior cerebellar peduncle, scp: superior cerebellar peduncle, mtg: mammillotegmental tract, mlf: medial longitudinal fasciculus, xscp: decussation of the superior cerebellar peduncle, mcp: middle cerebellar peduncle, MVe: medial vestibular nucleus, SpVe: spinal vestibular nucleus, ECu: external cuneate nucleus, SolI: solitary nucleus, interstitial part, Sp5I: spinal trigeminal nucleus, interpolar part, ts: tectospinal tract, IOPr: inferior olive, principal nucleus, 4V: fourth ventricle, oc: olivocerebellar tract, Sp5O: spinal trigeminal nucleus, oral part, lfp: longitudinal fibres of the pons, tfp: transverse fibres of the pons, Pn: pontine nuclei, PCRt: parvicellular reticular nucleus, IRt: intermediate reticular nucleus, LRt: lateral reticular nucleus, LPGi: lateral paragigantocellular nucleus, ami: amiculum, ctg: central tegmental tract, SNR: substantia nigra, pars reticulata, ll: lateral lemniscus, Aq: cerebral aqueduct, R: red nucleus.*

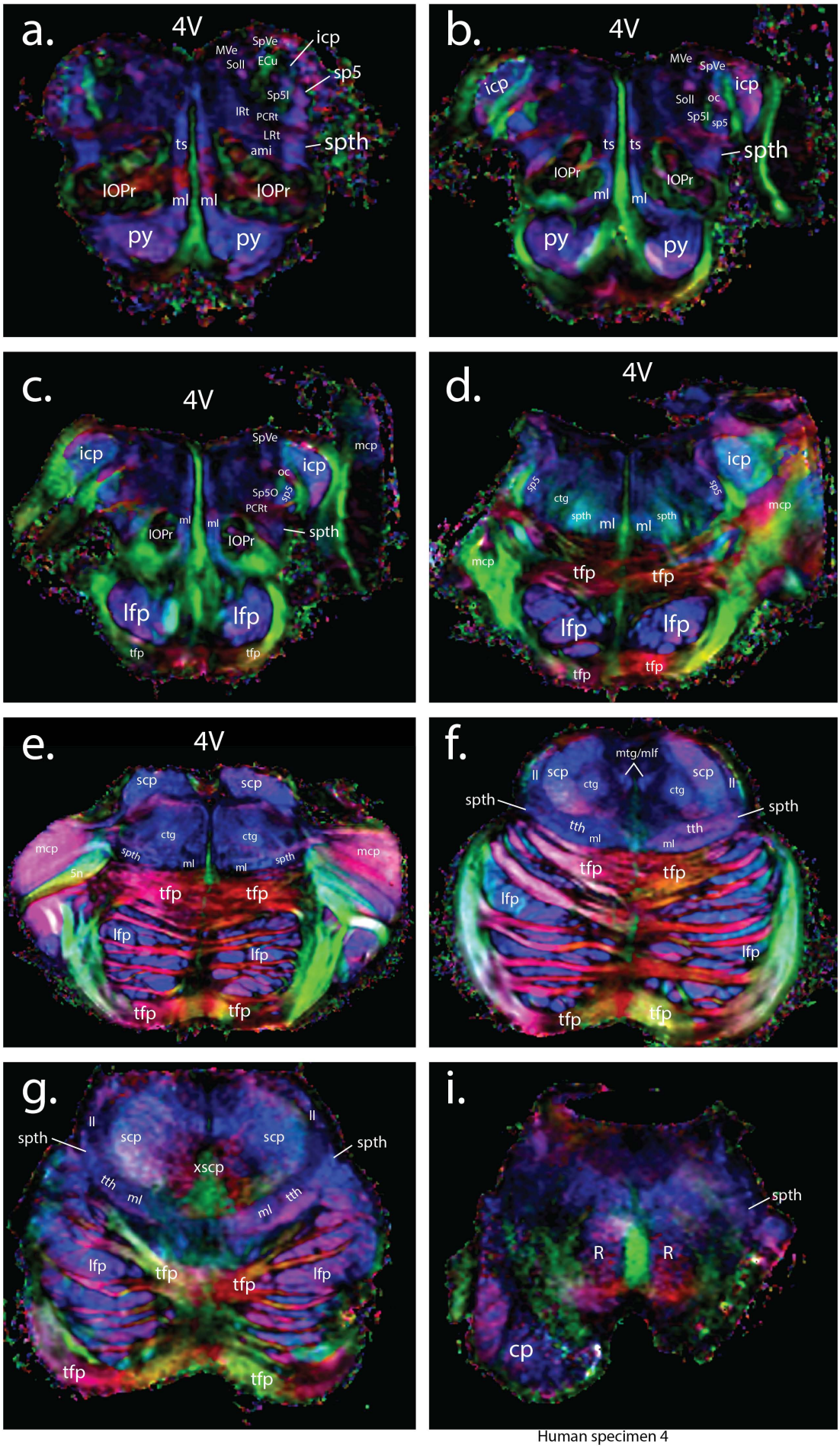

Human specimen 4

Fig. 16. Transverse sections from the level of the IOPr in the medulla oblongata (panel a) until the midbrain (panel i). *This FAC dataset from human specimen 4 is also not of sufficient quality to allow fibre tracking with tractography, but the FAC from the rostral medulla until the rostral pons does support the gross anatomical conclusions from human specimen 1 reported in Chapters 4 and 5. The location of the spth and its relationship with adjacent structures can be visualised of the FAC. The ml can be followed from the rostral medulla behind the pyramid, until the midbrain where it twists to further ascend. In addition, the sp5, and the two components of its nucleus (Sp5 oralis, and interpolaris) can be followed throughout their course. Moreover, the tth can be followed from mid pontine levels until the midbrain. The poor quality of the caudal medulla and midbrain may result from blood clots. On the FAC maps red, blue, and green represent anisotropy along medial-lateral, rostral-caudal, and ventral-dorsal orientations, respectively. Abbreviations: tth: trigeminothalamic tract, spth: spinothalamic tract, 5n: trigeminal nerve, sp5: spinal trigeminal tract, ml: medial lemniscus, Cu: cuneate nucleus, cu: cuneate fasciculus, Gr: gracile nucleus, py: pyramidal tract, icp: inferior cerebellar peduncle, scp: superior cerebellar peduncle, xscp: decussation of the superior cerebellar peduncle, mcp: middle cerebellar peduncle, mtg: mammillotegmental tract, mlf: medial longitudinal fasciculus, MVe: medial vestibular nucleus, SpVe: spinal vestibular nucleus, ECu: external cuneate nucleus, SolI: solitary nucleus, interstitial part, Sp5I: spinal trigeminal nucleus, interpolar part, ts: tectospinal tract, IOPr: inferior olive, principal nucleus, 4V: fourth ventricle, oc: olivocerebellar tract, Sp5O: spinal trigeminal nucleus, oral part, lfp: longitudinal fibres of the pons, tfp: transverse fibres of the pons, PCRt: parvicellular reticular nucleus, IRt: intermediate reticular nucleus, LRt: lateral reticular nucleus, ctg: central tegmental tract, ll: lateral lemniscus, R: red nucleus.*

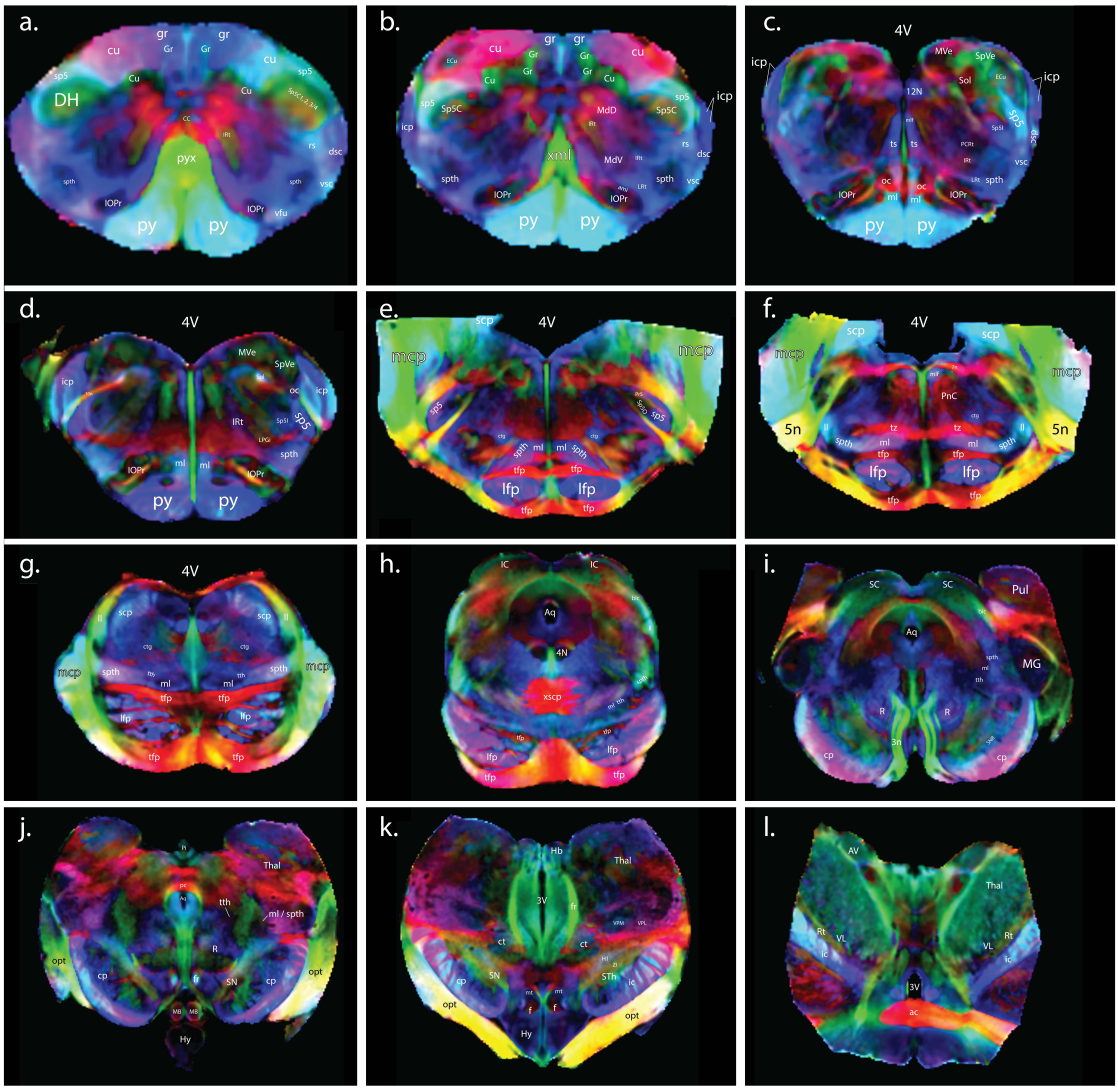
a.
b.
c.
d.
e.
f.
g.
h.
i.
j.
k.
l.
4V
DH
pyx
py
xml
mcp
scp
icp
lfp
tfp
5n
Pul
MG
Thal
Macaca mulatta

Fig. 17. Transverse sections at 100 µm isotropic resolution from the level of the pyramidal decussation (panel a) until the ventral tier of the thalamus (panel l). *Sections derive from the same primate (macaque) specimen and displayed as FAC with red, blue, and green representing anisotropy along medial-lateral, rostral-caudal, and ventral-dorsal orientations, respectively. The FAC shows and confirms the relationship between the ascending sensory tracts such as the gr, cu, and the spth (panels a, b), as well as the descending sp5 (panels e - a) and its configuration that surrounds the Sp5 nucleus like a crescent (blue in FAC, see panels b, a). Finally, the ml, tth, scp, xscp and the course of the drt from the midbrain through the red nucleus until the thalamus are highlighted on the FAC maps. Abbreviations: tth: trigeminothalamic tract, spth: spinothalamic tract, 5n: trigeminal nerve, sp5: spinal trigeminal tract, ml: medial lemniscus, xml: sensory decussation, pyx: pyramidal decussation, CC: central canal, Sp5C,1,2,3/4: spinal trigeminal nucleus, caudal part, laminae one to four, Cu: cuneate nucleus, cu: cuneate fasciculus, Gr: gracile nucleus, py: pyramidal tract, vfu: ventral funiculus, MdD: medullary reticular nucleus, dorsal part, MdV: medullary reticular nucleus, ventral part, Sp5C: spinal trigeminal nucleus, caudal part, icp: inferior cerebellar peduncle, scp: superior cerebellar peduncle, xscp: decussation of the superior cerebellar peduncle, mcp: middle cerebellar peduncle, ct: cerebellothalamic tract, MVe: medial vestibular nucleus, SpVe: spinal vestibular nucleus, ECu: external cuneate nucleus, Sol: solitary nucleus, Sp5I: spinal trigeminal nucleus, interpolar part, ts: tectospinal tract, IOPr: inferior olive, principal nucleus, 3V: third ventricle, 4V: fourth ventricle, oc: olivocerebellar tract, Sp5O: spinal trigeminal nucleus, oral part, lfp: longitudinal fibres of the pons, tfp: transverse fibres of the pons, PCRt: parvicellular reticular nucleus, IRt: intermediate reticular nucleus, LRt: lateral reticular nucleus, LPGi: lateral paragigantocellular nucleus, ami: amiculum, ctg: central tegmental tract, SNR: substantia nigra, pars reticulata, ll: lateral lemniscus, SC: superior colliculus, Aq: cerebral aqueduct, R: red nucleus, STh: subthalamic nucleus of Luys,*

MB: mammillary bodies, 3n: third nerve, f: fornix, Hy: hypothalamus, opt: optic tract, ct: cerebellothalamic tract, ac: anterior commissure, VPM: ventral posteromedial nucleus of the thalamus, VPL: ventral posterolateral nucleus of the thalamus, VL: ventral lateral nucleus of the thalamus, ic: internal capsule, bic: brachium of the inferior colliculus, DH: dorsal horn of the spinal cord, 12N: hypoglossal nucleus, 10n: vagus nerve, Pr5: principal sensory trigeminal nucleus, 7n: facial nerve, 4N: trochlear nucleus, Pul: pulvinar, MG: medial geniculate nucleus, Thal: thalamus, fr: fasciculus retroflexus, Hb: habenula, AV: anteroventral nucleus of the thalamus, Rt: reticular nucleus, mlf: medial longitudinal fasciculus, tz: trapezoid body, PnC: pontine reticular nucleus, caudal part, H1: field H1 of Forel, ZI: zona incerta.

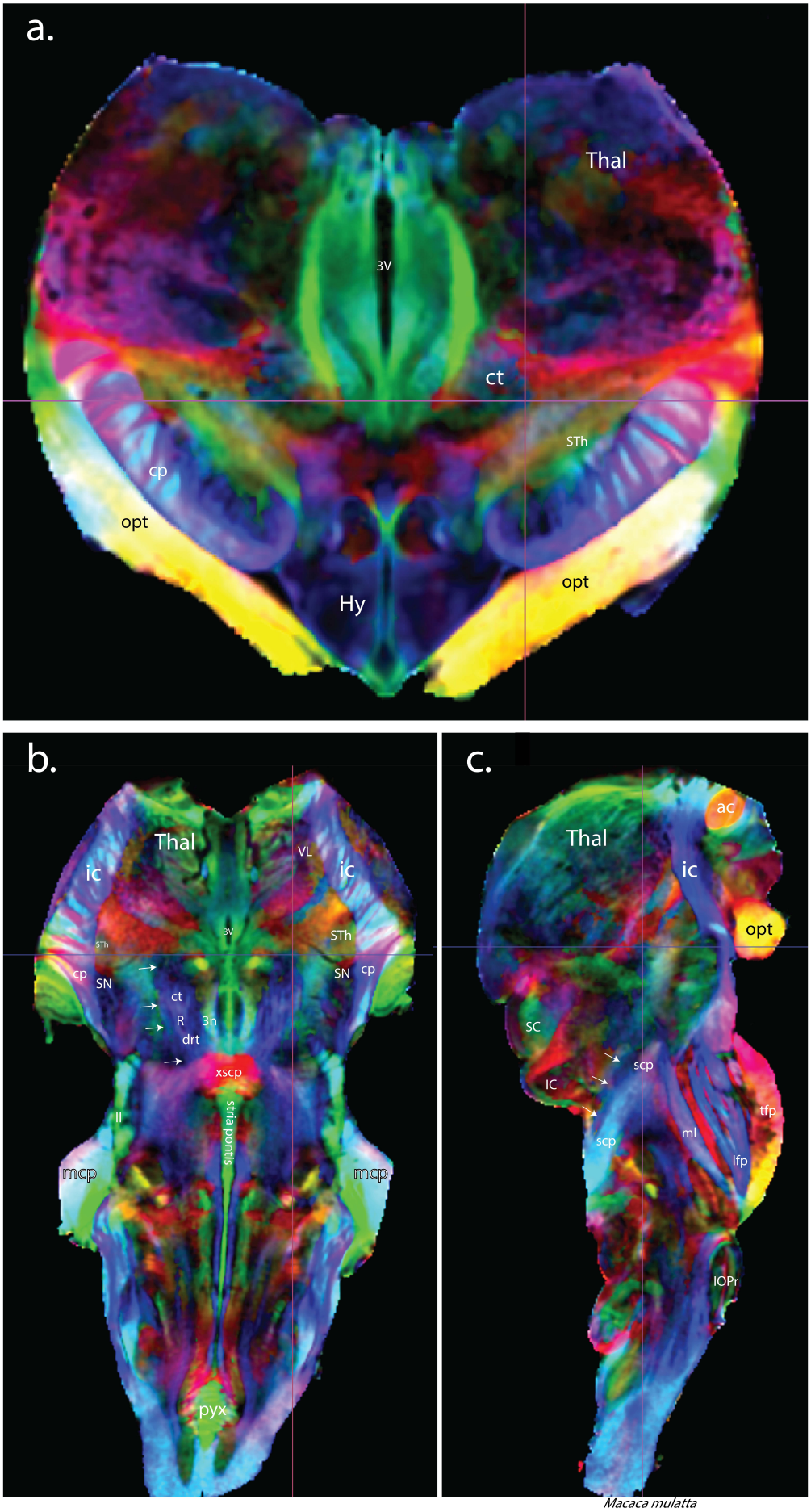

Macaca mulatta

Fig. 18. Transverse and the corresponding intersecting coronal and sagittal planes in the macaque. *Sections all derive from the same macaque as in Fig. 17 and displayed as FAC, with red, blue, and green representing anisotropy along medial-lateral, rostral-caudal, and ventral-dorsal orientations, respectively. The point at which the line intersections are visualised, the FAC reveals the rostral part of the ct through the ventral thalamus in a (transverse), b (coronal), and c (sagittal) planes. Note in (b) the course of the drt from the xscp through the red nucleus and how it ascends laterally (see arrows in b) to reach the thalamus. In (c) the FAC shows the course of the scp from caudal pontine levels until the rostral pons. Abbreviations: 3V: third ventricle, Thal: thalamus, ct: cerebellothalamic tract, STh: subthalamic nucleus of Luys, opt: optic tract, cp: cerebral peduncle, Hy: hypothalamus, VL: ventral lateral nucleus of the thalamus, SN: substantia nigra, ic: internal capsule, R: red nucleus, drt: dentato-rubro-thalamic tract, xscp: decussation of the superior cerebellar peduncle, 3n: third nerve, mcp: middle cerebellar peduncle, pyx: decussation of the pyramidal tract, SC: superior colliculus, IC: inferior colliculus, ml: medial lemniscus, lfp: longitudinal fibres of the pons, tfp: transverse fibres of the pons, IOPr: inferior olive, principal nucleus, ac: anterior commissure.*

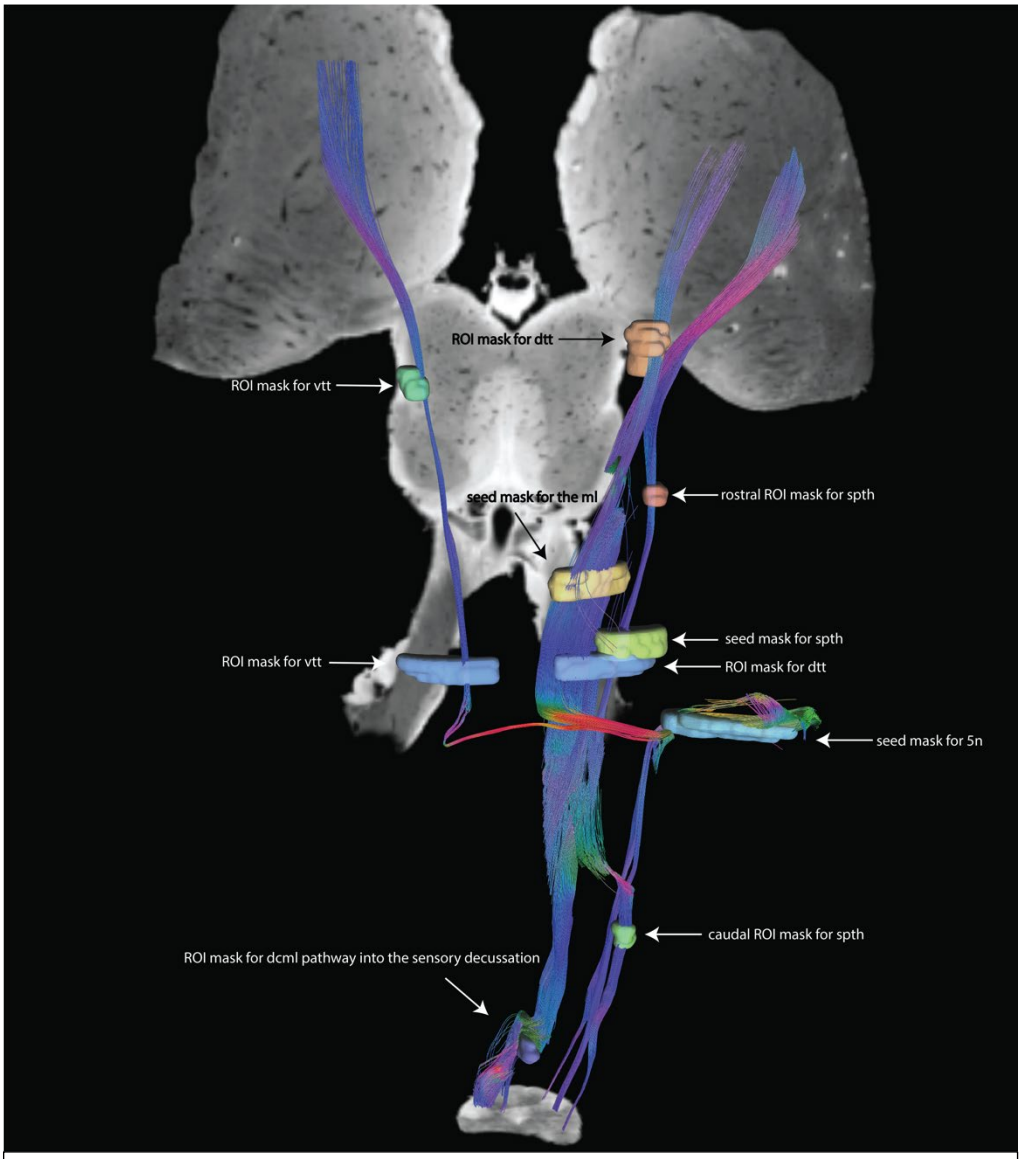

Fig. 19. Masks used for fibre tracking of the Pain pathways*. See tractography in Ch 4, the seed masks here represent the point from which tractography commences to calculate the trajectory of a pathway under investigation towards the corresponding region of interest (ROI). The program uses an algorithm (Euler method) to produce fibre tracts after a number of iterations. I report an example of how the seed and ROI masks could be used for this novel way of fibre tracking. Abbreviations: vtt: ventral trigeminothalamic tract, dtt: dorsal trigeminothalamic tract, ml: medial lemniscus, spth: spinothalamic tract, 5n: trigeminal nerve, dcml: dorsal column – medial lemniscus pathway, ROI: region of interest.*

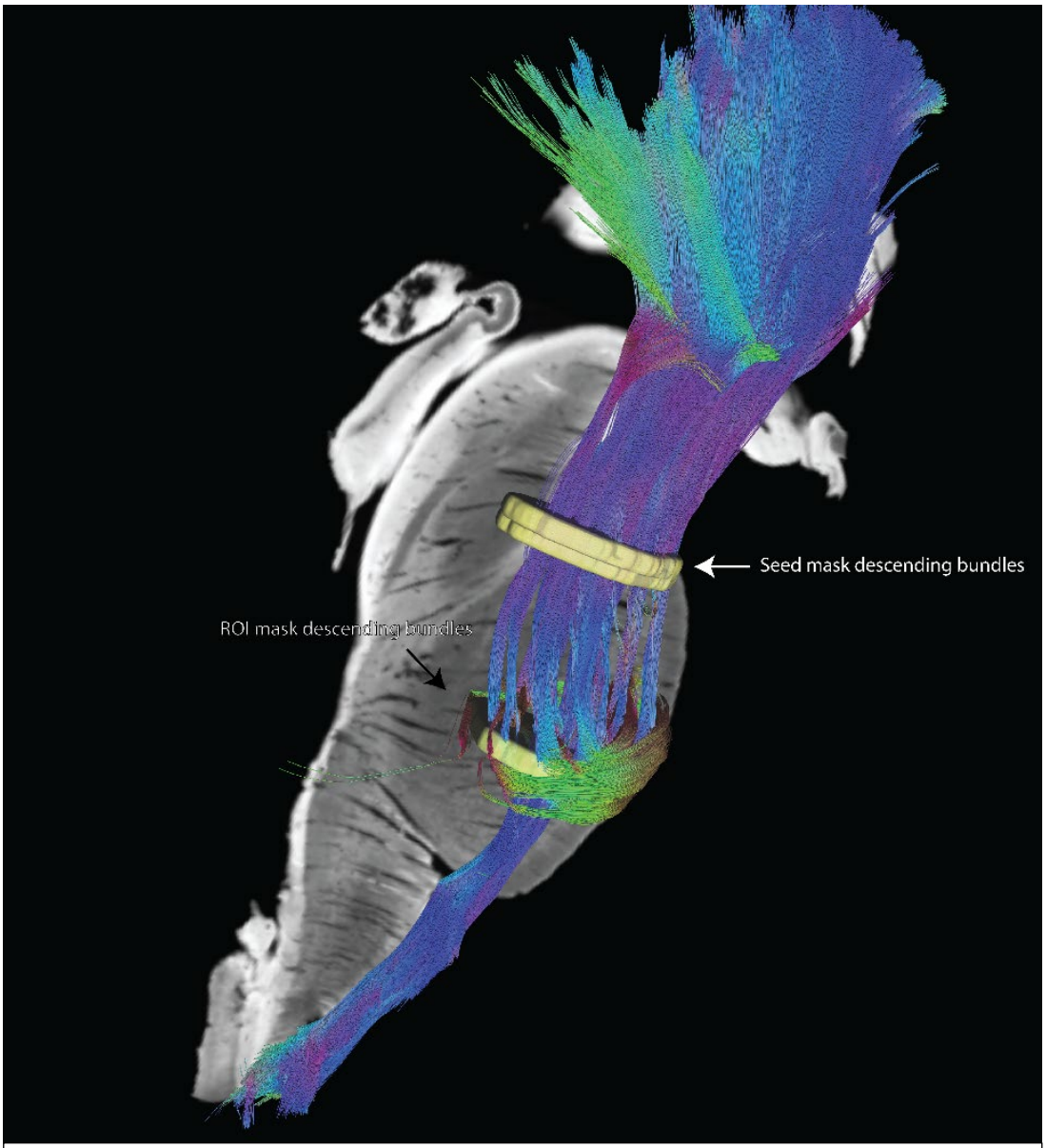

Fig. 20. Descending fibre bundles masks*. I report herein the seed mask at the level of the crus cerebri and the ROI mask at midpons. Both were used for the identification of the nine descending bundles.*

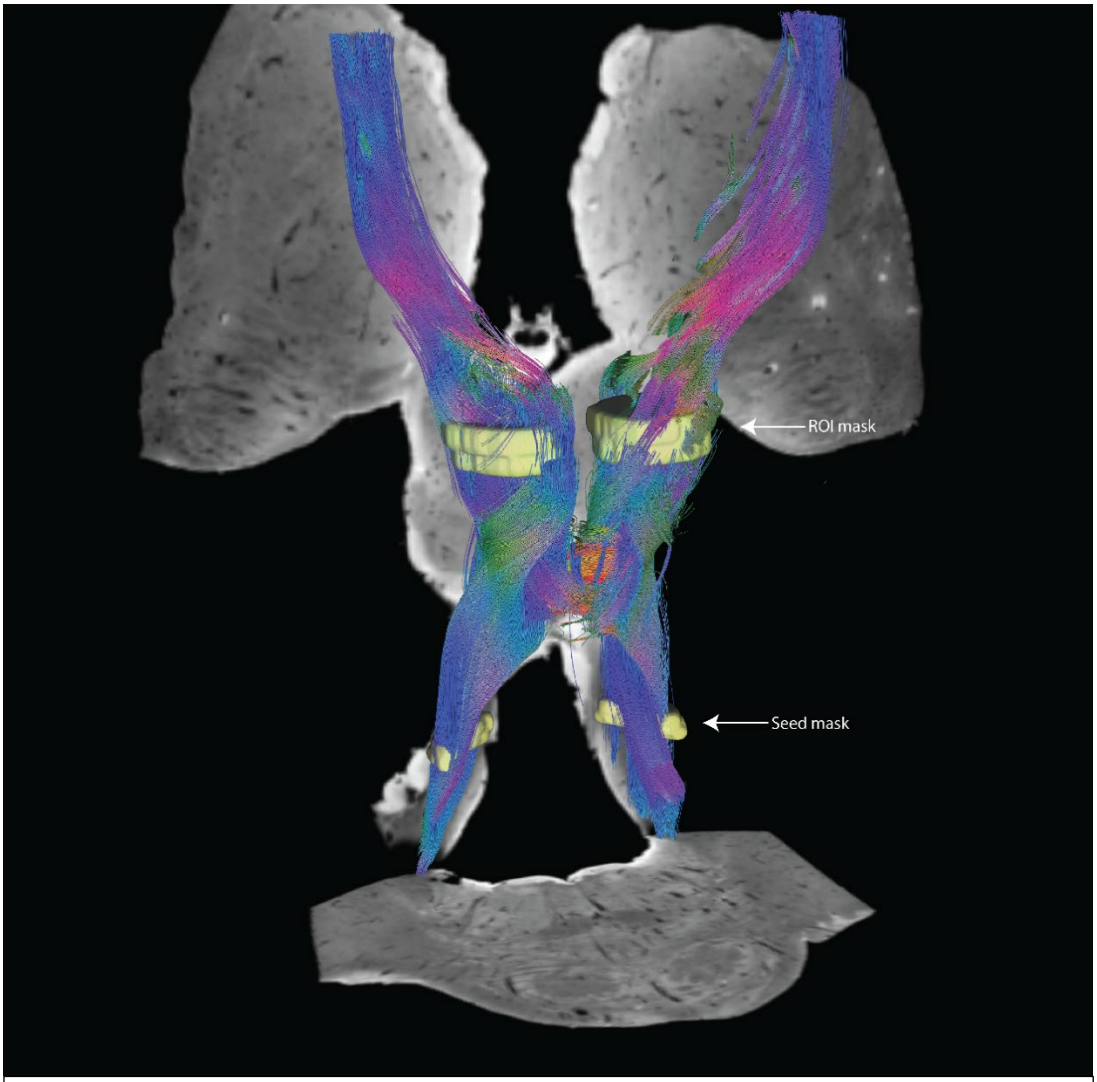

Fig. 21. Seed and region of interest (ROI) masks for the identification of the dentato-rubro-thalamic tract (drt)*. I show the bilateral seed masks at the level of the scp and the ROI masks within the red nucleus.*

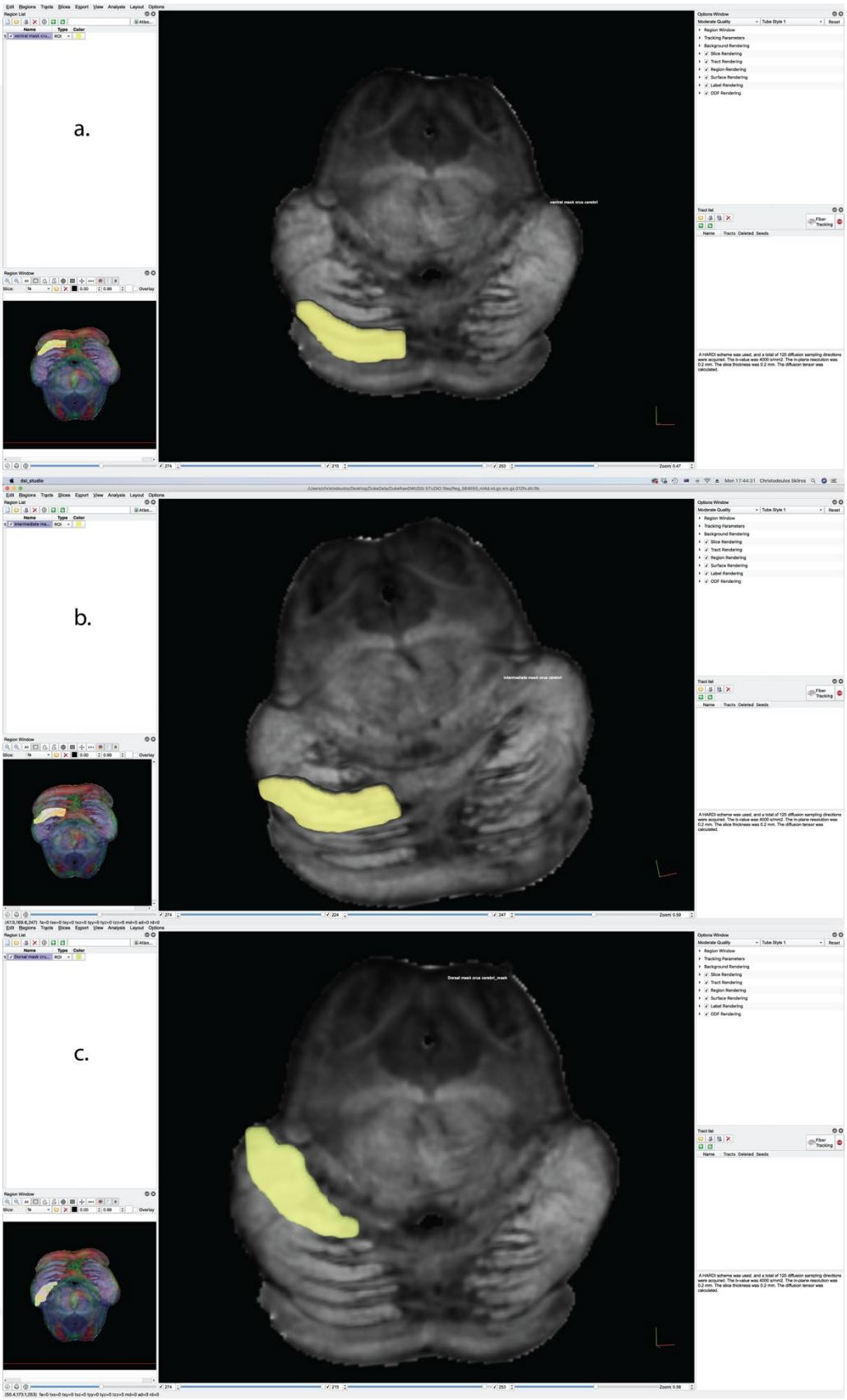
a.
b.
c.

Fig. 22. Graphical user interface of DSI Studio as seen in pane a, b, and c. *Each panel represents a screen shot from the tractography software tool for diffusion MRI analysis, showing how the seed masks were set for human specimen 1. The main figure inset shows the diffusion images from which the fibre tracts are calculated. With the inset to the left showing the corresponding eigenvectors which overlap the FAC contrast. The insets to the right show the tractography parameters. The three panels (a – c) show the seed masks at the level of the crus cerebri. Note the ventral, intermediate, and dorsal lamellae-like manually drawn seed masks that highlight the organisation of the descending bundles.*

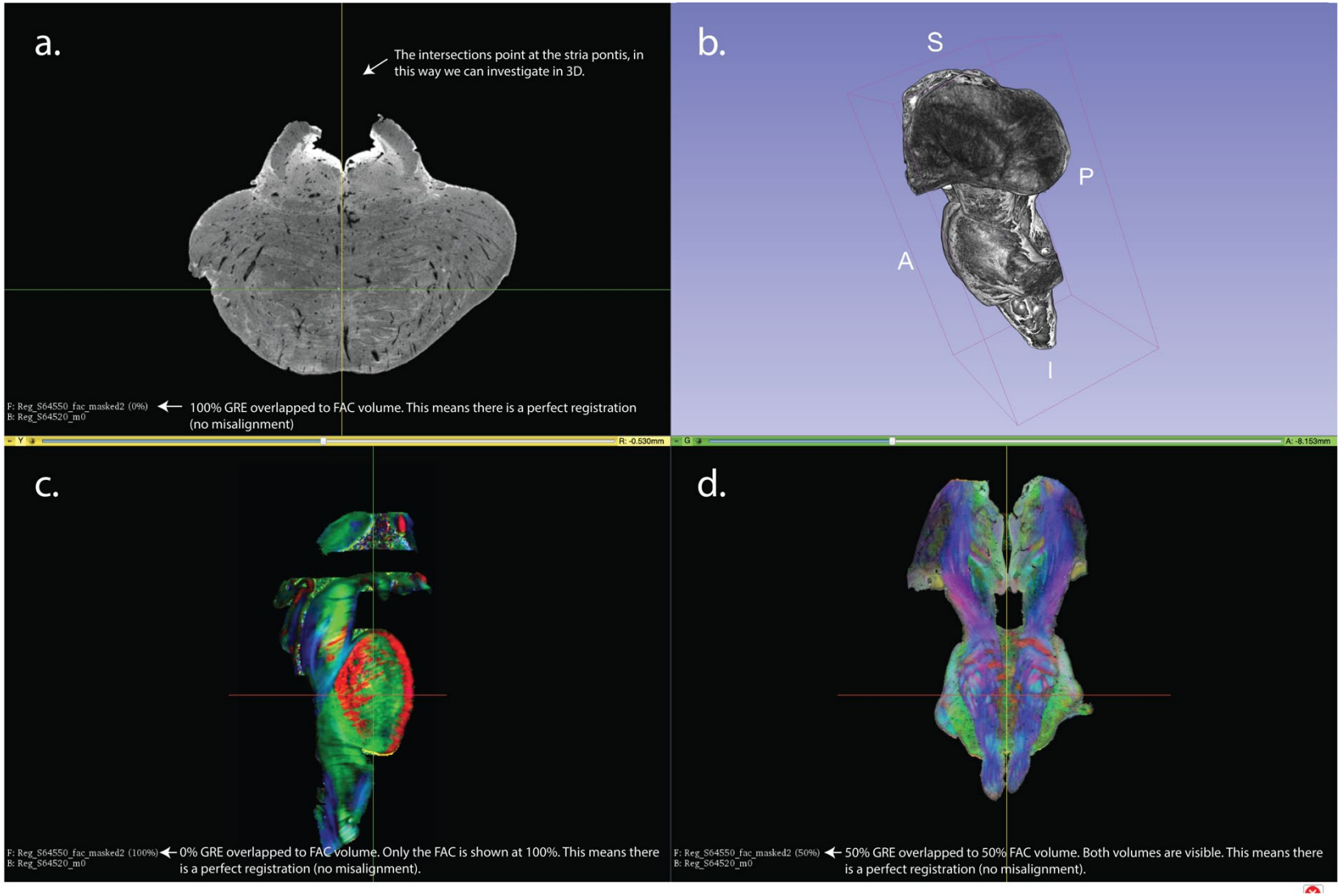
a.
The intersections point at the stria pontis, in this way we can investigate in 3D.
F: Reg_S64550_fac_masked2 (0%)
B: Reg_S64520_m0
100% GRE overlapped to FAC volume. This means there is a perfect registration (no misalignment)
b.
S
P
A
I
c.
F: Reg_S64550_fac_masked2 (100%)
B: Reg_S64520_m0
0% GRE overlapped to FAC volume. Only the FAC is shown at 100%. This means there is a perfect registration (no misalignment).
d.
F: Reg_S64550_fac_masked2 (50%)
B: Reg_S64520_m0
50% GRE overlapped to 50% FAC volume. Both volumes are visible. This means there is a perfect registration (no misalignment).

Fig. 23. Overlap of different contrasts to achieve an accurate 3D visualisation of brain structures in 3D Slicer. *Two different contrasts such as the GRE and FAC of human specimen 1 are shown. In panel a, the GRE is overlapped to the FAC. However, the FAC is not visualised. Panel b shows the 3D view of the brainstem and thalamus as computationally reconstructed by the transverse, sagittal, and coronal planes. In panel c the sagittal view of the FAC on the GRE is also shown, however, the GRE is not visualised. Finally, panel d shows the coronal view of the brainstem and thalamus at 50 % visualisation for both the GRE and FAC. As an example, I have set an intersection point at the Stria Pontis at the level of the midpons, and this intersect can be seen in each contrast in transverse, sagittal, and coronal sections to enable the investigator to anatomically describe the landmarks of the pathway. Note the high level of alignment between the GRE and FAC.*

Figure 1. (**A**) Brain magnetic resonance imaging(MRI) images at 14 months after onset show no abnormal lesions. (**B**) Results of diffusion tensor tractography (DTT) for the corticospinal tract (CST) and corticofugal tract (CFT). On a 14-month DTT configuration, the left CST, CFT from supplementary motor area, and CFT from dorsal premotor cortex show similar configuration with a normal subject (24-year old female). (**C**) Results of transcranial magnetic stimulation (TMS). On a 14-month TMS study, motor evoked potential (MEP) is obtained at the right abductor pollicis brevis muscle during stimulation of the left hemisphere with 60% of maximal output (the MEP of shortest latency; 21.0 msec, amplitude: 5.1 mV).

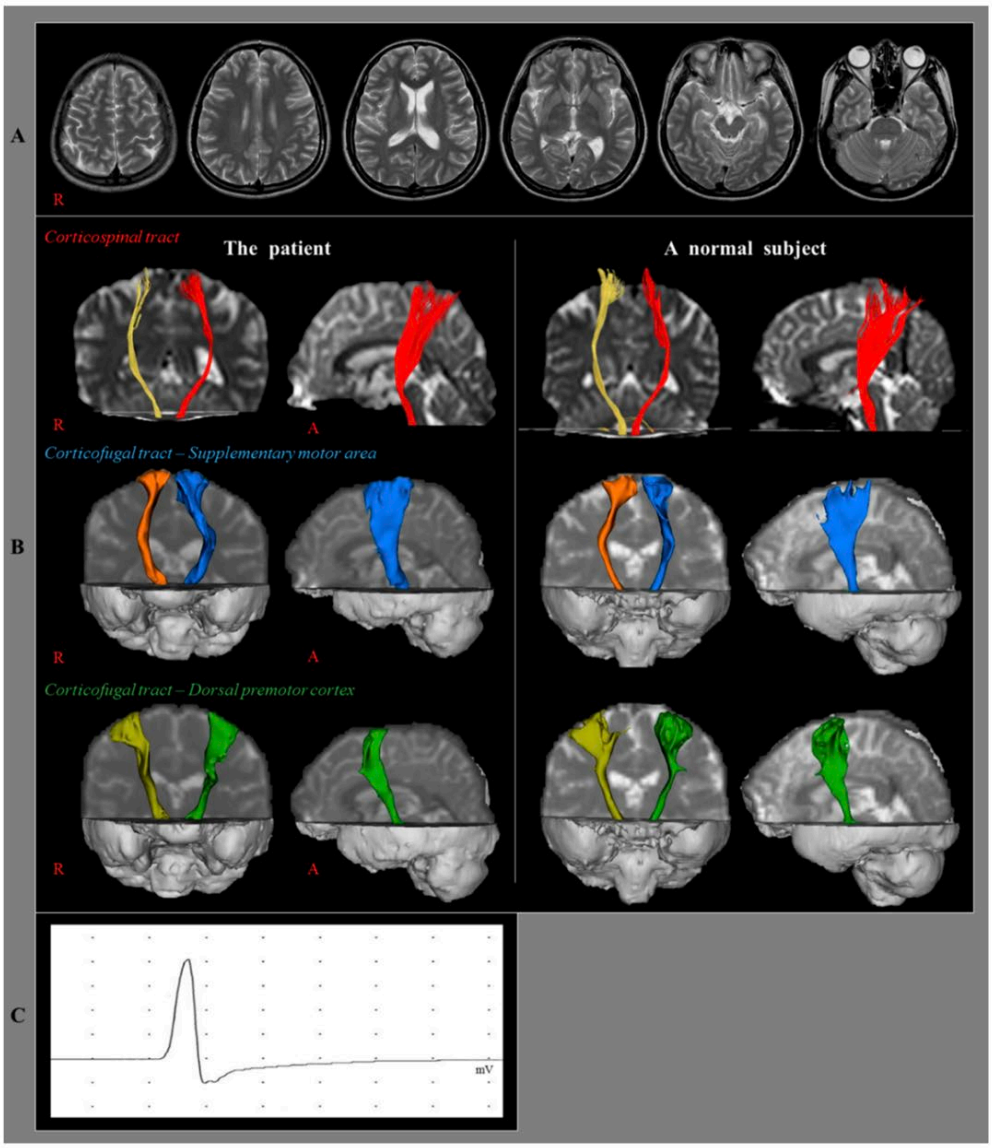

Fig. 24. Corticofugal pathways as reported by DTI and tractography at 1.25 x 1.25 x 1.25 mm^3 voxel size*. I report, herein, an example of tractography to be compared with the tractography in my current research. Note the corticospinal and corticofugal projections as revealed in the latest diffusion tensor tractography (published in late 2019). Also note the omission of anatomical information nor any subdivisions throughout the brainstem. Image taken from: https://doi.org/10.3390/diagnostics9040155*

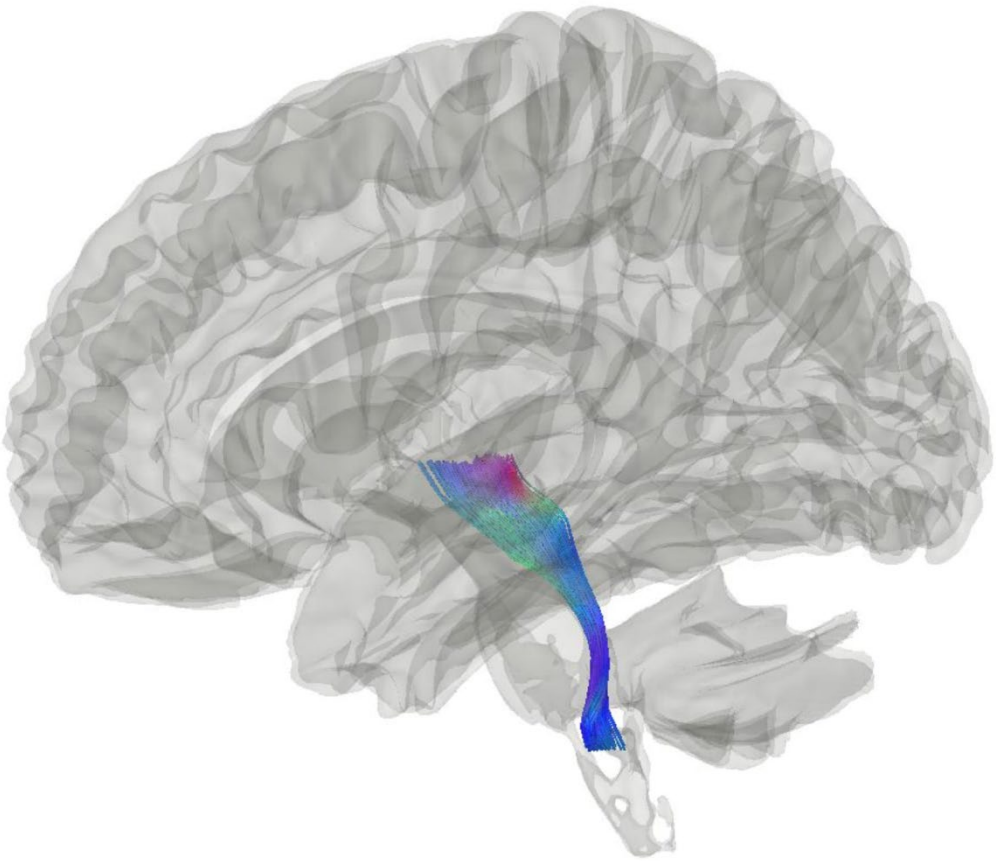

Fig. 25. The medial lemniscus as reported by scanning multiple subjects at 1.25 mm isotropic spatial resolution. *By comparison with the medial lemniscus (ml) in Figs 4.1 – 4.7 in Ch 4 (200 μm isotropic resolution for the diffusion data – 50 μm isotropic resolution for the GRE background). The image above is from the Human Brain MRI Data and Connectome Atlas (published in 2018). Image taken from: http://brain.labsolver.org/*

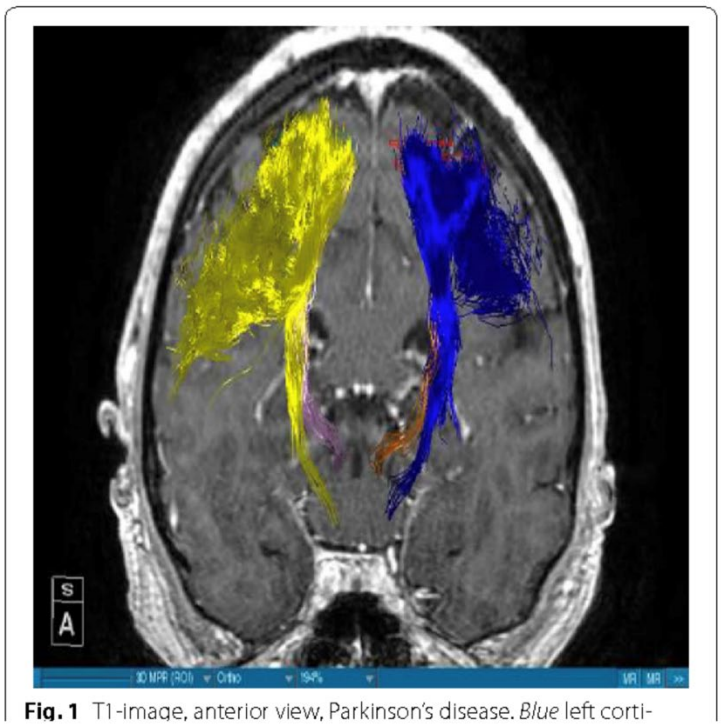

Fig. 1 T1-image, anterior view, Parkinson's disease. *Blue* left corti-

Fig. 1 T1-image, anterior view, Parkinson's disease. Blue left corti- cospinal tract, Yellow right corticospinal tract, Gold left dentatoru- brothalamic tract, Bright purple right dentatorubrothalamic tract

Fig. 26. The drt and corticospinal tracts as reported by tractography at 2 X 2 X 2 mm isotropic*. In comparison to my tractography, I report an image regarding the dentato-rubro-thalamic (drt) and corticospinal tracts as depicted by an article published in 2016 whereby the authors tried to shed light on these complex tracts due to their clinical significance. Image taken from:* https://doi.org/10.1186/s13104-016-2162-8

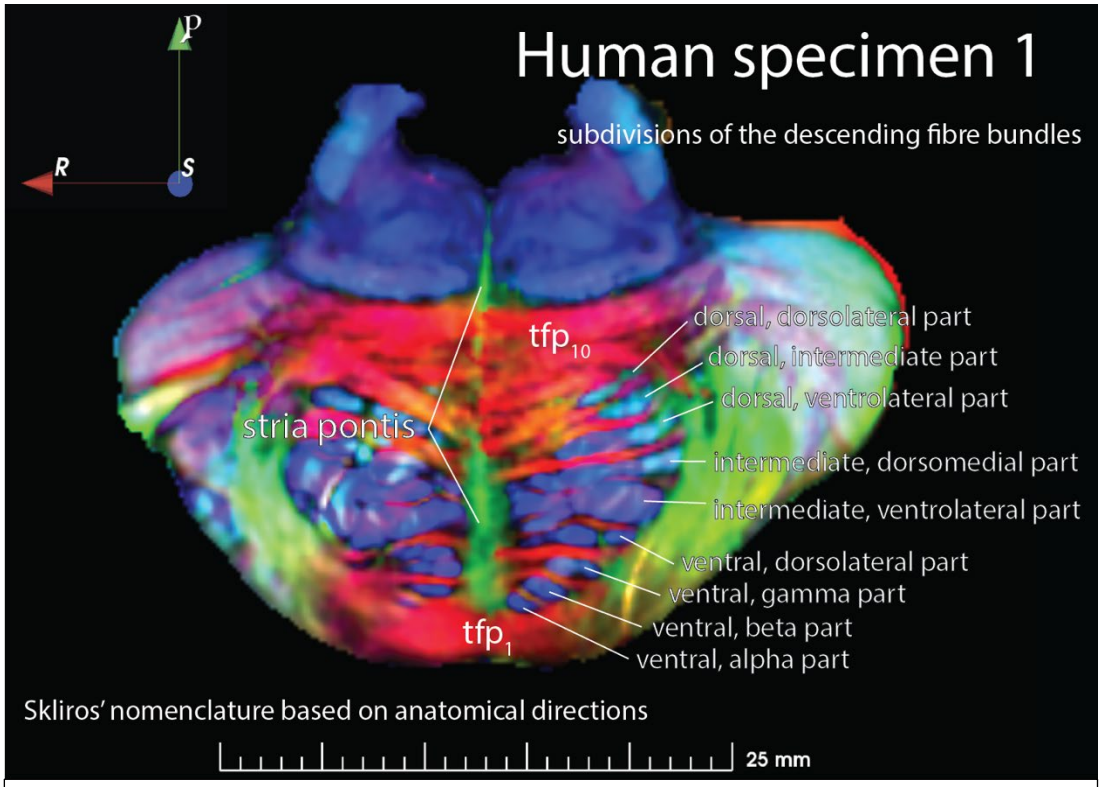

Fig. 27. Subdivisions of the descending fibre bundles*. In this figure, I report the subdivisions of the descending fibre bundles according to cardinal anatomical directions. Therefore, the descending bundles within the basilar pons (longitudinal fibres of the pons) are subdivided into three main groups of bundles; ventral, intermediate and dorsal (primary subdivisions; which are always stable). These bundles can be further subdivided into a total of nine bundles (four ventral, two intermediate, and three dorsal). This nomenclature reflects their lamellar shape and position from the crus cerebri and throughout the basilar pons. For example, the three most ventral descending bundles (v_1 or ventral, alpha part; v_2 or ventral, beta part; v_3 or ventral, gamma part) are united in the crus cerebri and they divide as they descend caudalwards at the level of the midpons to reunite again medially including the forth bundle (v_4 or ventral, dorsolateral part) as cervical pyramidal tract. Similarly, the two bundles that form the intermediate group (thoracic component of the pyramidal tract) are united in the crus cerebri and split in the rostral pons forming a ventrolateral (i_1 or intermediate, ventrolateral part) and a dorsomedial (i_2 or intermediate, dorsomedial part) lamellae, and so on.*

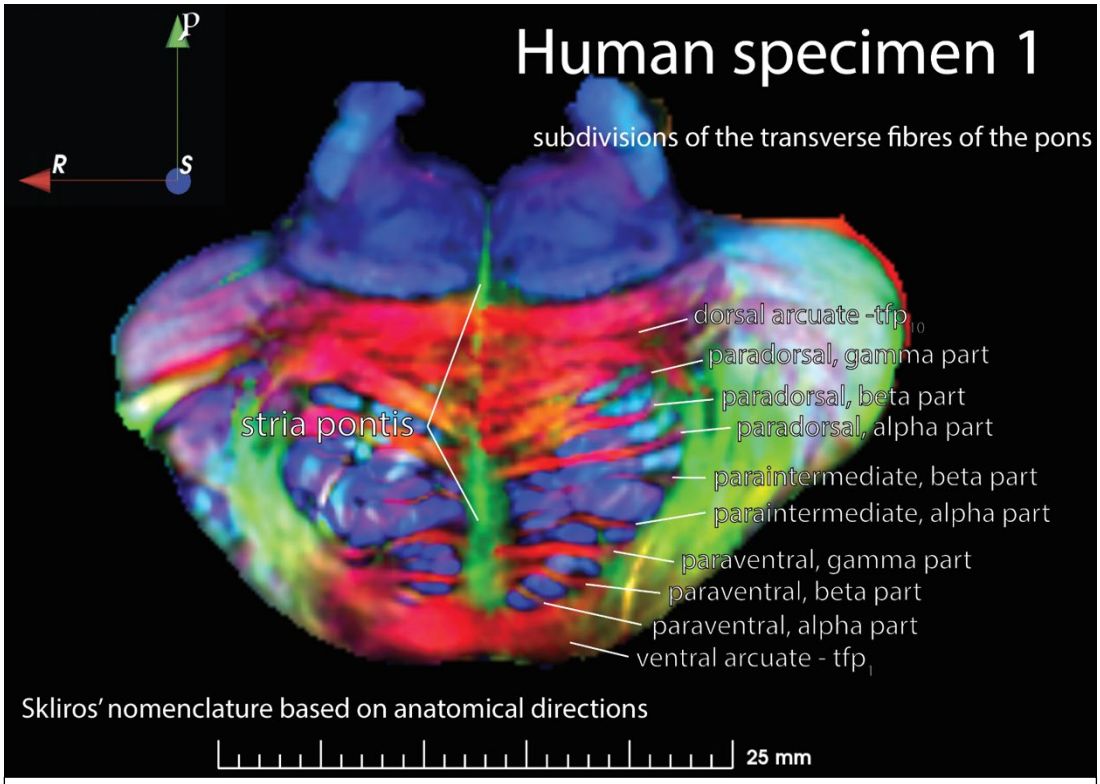

Fig. 28. Subdivisions of the transverse fibres of the pons*. I report herein, the subdivisions of the transverse fibres of the pons as I named them in relation to the nine descending fibre bundles. Thus, the transverse fibres of the pons are subdivided in three primary groups which are anatomically and functionally related to the primary subdivisions of the descending bundles (ventral, intermediate, dorsal). The two transverse fibres located at the extremities of the basilar pons are always stable between the two sides of the brainstem and between the various specimens, therefore, I named them as ventral and dorsal arcuate respectively, which reflects the shape that these two bundles assume and resembles to an arch. Similarly, I inserted the prefix "para" to the rest of the bundles due to the fact that the transverse fibres are adjacent to the descending bundles. For example, the most ventral descending bundle v1 (in blue) sheds corticopontine fibres which innervate adjacent pontine grey matter, which in turn forms the ventral arcuate (tfp1) and the paraventral, alpha part, and so on. Therefore, the cortical information from one descending bundle courses through two transverse fibres of the pons.*

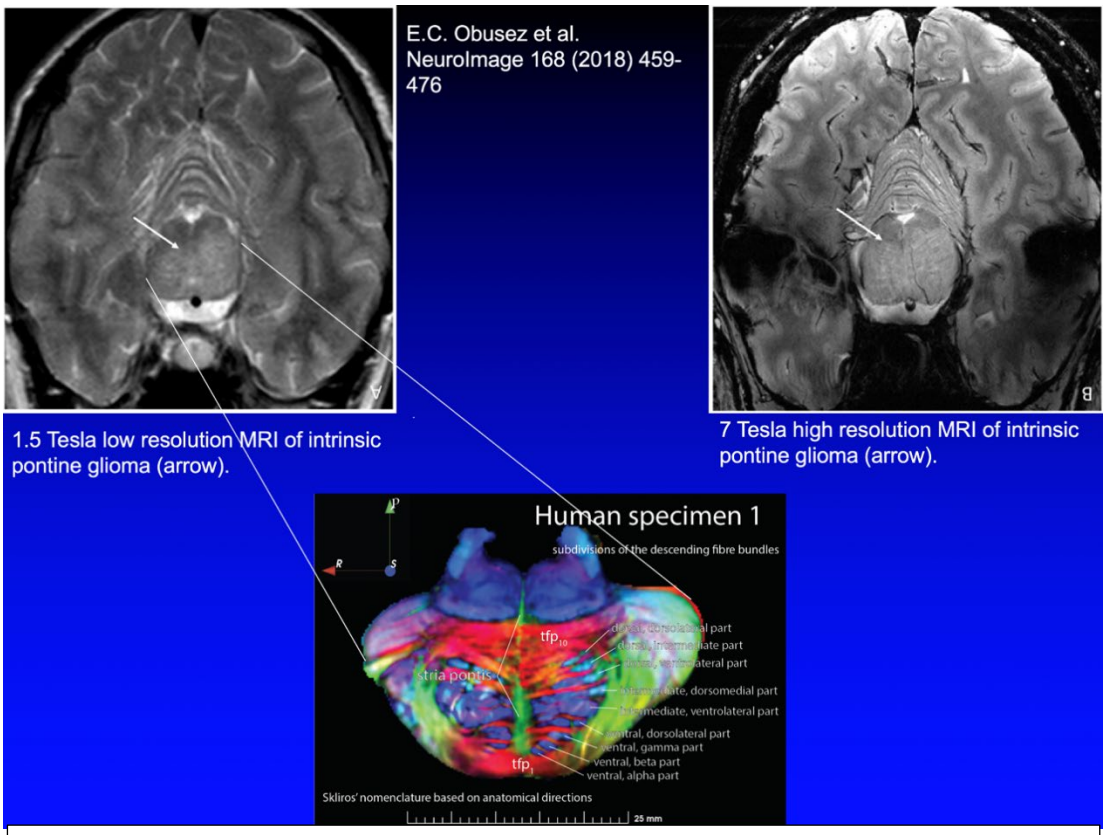

Fig. 29. An example of how my subdivisions could be used in clinical practice*. I report an example of how the map of the bundles through the pons (which constituted an uncharted territory) can be used for therapeutic purposes and most particularly for radiation therapy such as Gamma knife and minimally invasive approaches such as keyhole neurosurgery. For example, the above patient who presents a right pontine glioma (arrows) will gradually lose the function of the left lower limb. Only now will we be able to precisely treat through my subdivisions and maps, with minimal damage to adjacent bundles, this kind of cerebral lesions, so that the tumour and edema do not further spread onto the intermediate group of bundles with thoracic deterioration.*

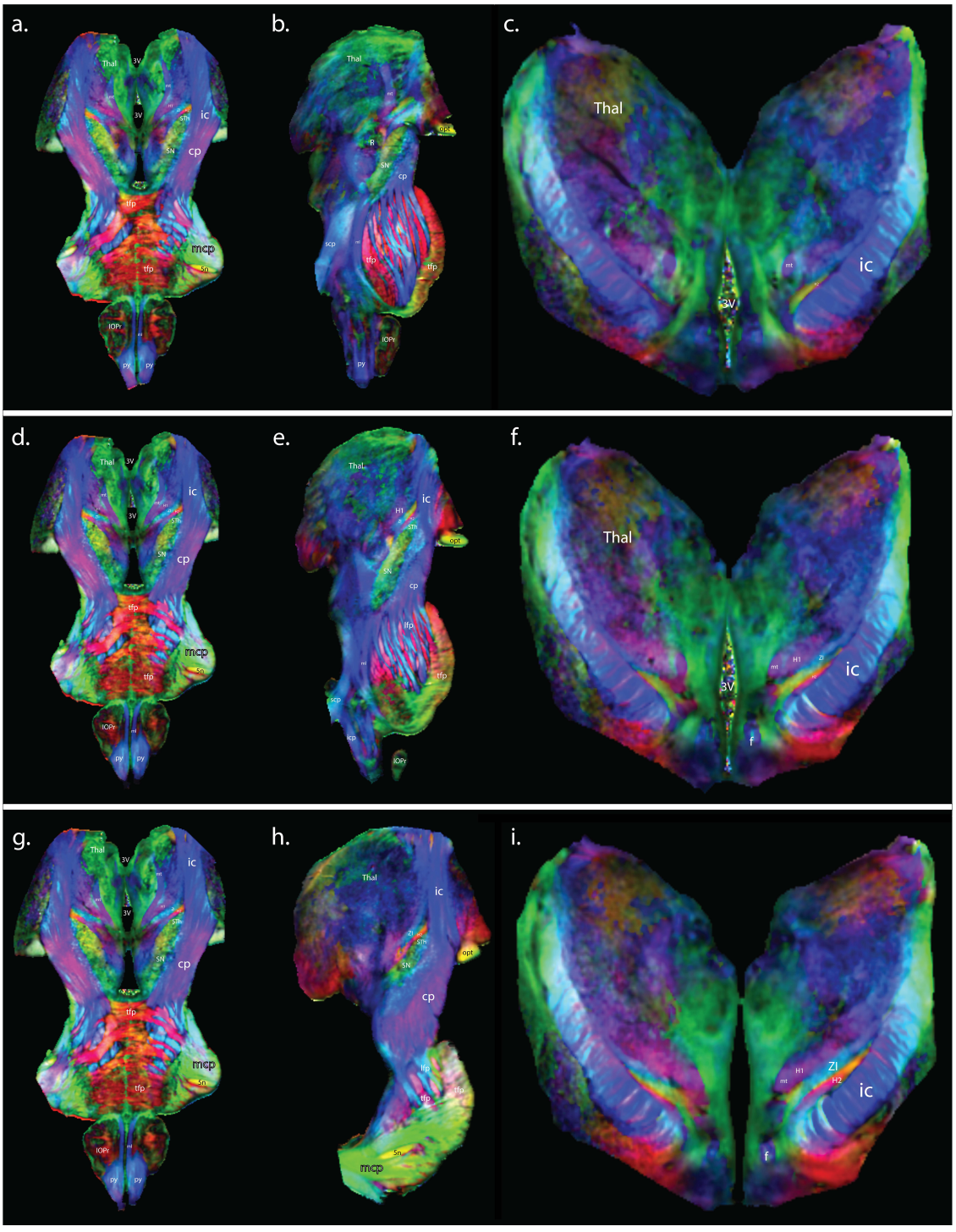
a.
b.
c.
d.
e.
f.
g.
h.
i.
Thal
3V
ic
cp
tfp
mcp
IOPr
py
SN
STh
opt
scp
H1
H2
ZI
mt
f

Fig. 30. Fractional coloured anisotropy (FAC) maps of the human brainstem and thalamus in coronal (a), (d), (g), sagittal (b), (e), (h), and transverse (c), (f), (i) sections. *The 3D maps show the relationship between the fields H2 and H1 of Forel, the zona incerta, the subthalamic nucleus of Luys, and the mammillothalamic tract which could highlight the topography and guide more efficiently deep brain stimulation of structures such as the subthalamic nucleus and zona incerta for Parkinson's disease (see anatomical descriptions on page 144). This topography was particularly evident on human specimen 1 as shown bilaterally in (a), (d), and (g). On the FAC maps red, blue, and green represent anisotropy along medial-lateral, rostral-caudal, and ventral-dorsal orientations, respectively. Abbreviations: Thal: thalamus, 3V: third ventricle, mt: mammillothalamic tract, H1: Field H1 of Forel, ZI: zona incerta, H2: Field H2 of Forel, STh: subthalamic nucleus of Luys, ic: internal capsule, cp: cerebral peduncle, tfp: transverse fibres of the pons, mcp: middle cerebellar peduncle, 5n: trigeminal nerve, IOPr: inferior olive, principal nucleus, ml: medial lemniscus, py: pyramidal tract, opt: optic tract, R: red nucleus, SN: substantia nigra, scp: superior cerebellar peduncle, lfp: longitudinal fibres of the pons, f: fornix.*

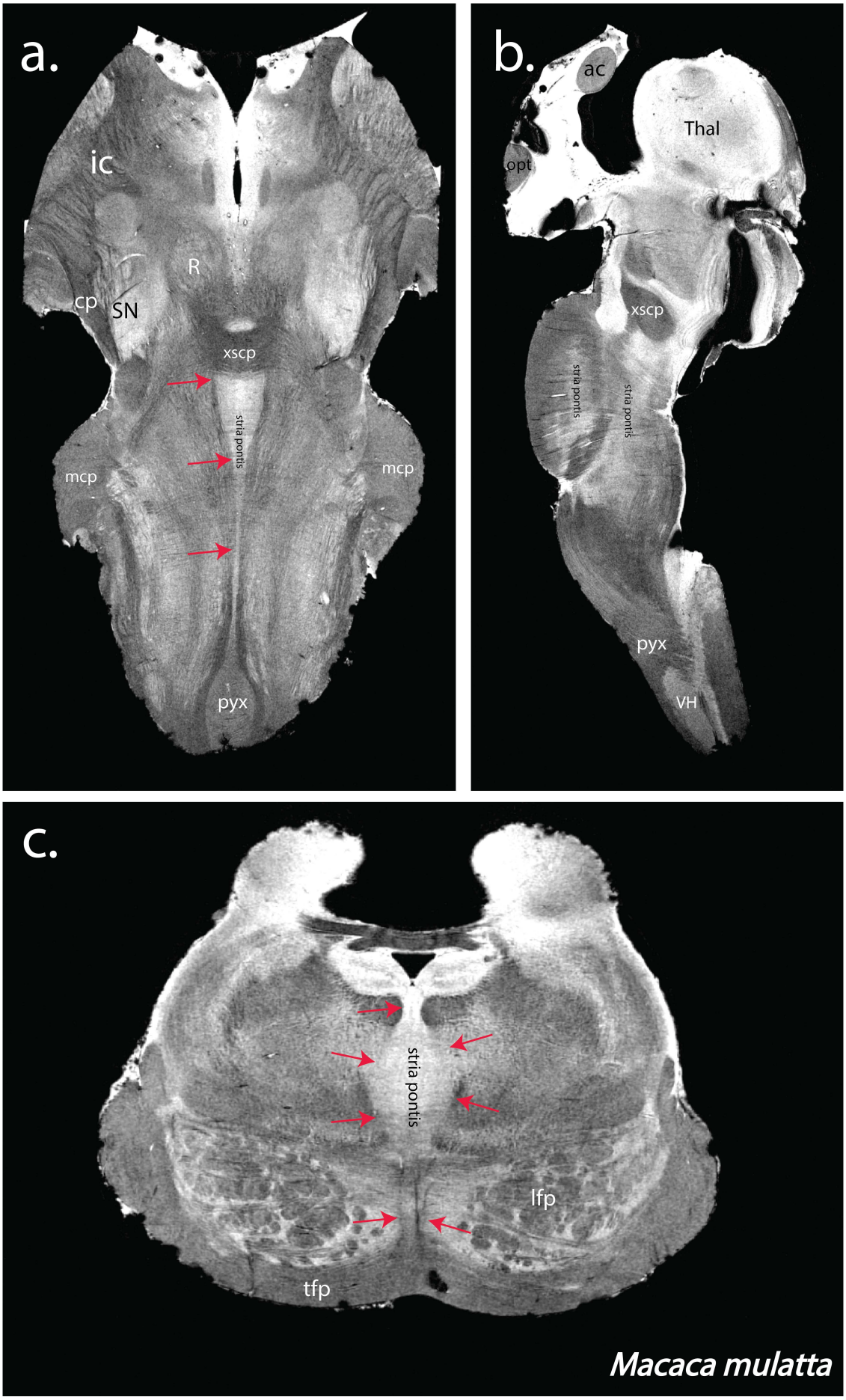
a.
ic
R
cp
SN
xscp
stria pontis
mcp
mcp
pyx
b.
ac
Thal
opt
xscp
stria pontis
stria pontis
pyx
VH
c.
stria pontis
lfp
tfp
Macaca mulatta

Fig. 31. GRE (gradient recalled echo) sequence at 25 µm of isotropic resolution showing the coronal (a), sagittal (b), and transverse (c) sections of the brainstem and thalamus in the macaque. *Brain mapping at its natural 3D space enables the investigator to identify and anatomically describe brain structures. The GRE at this microscopic resolution shows a clear distinction between fibre tracts such as the Stria Pontis (arrow heads) and other rostrocaudally and lateromedially oriented fibres (e.g. the fibres decussating within the xscp in panels a and b). The signal of the Stria Pontis in the GRE images appears as a continuous linear structure which expands like a wedge, at rostral pontine levels (this expansion seems peculiar to the macaque and was not seen in the four human specimens). Note that the boundaries of the Stria extend from rhombomere 2 to rhombomere 4 as highlighted by red arrows in (a). Abbreviations: ic: internal capsule, cp: cerebral peduncle, SN: substantia nigra, R: red nucleus, xscp: decussation of the superior cerebellar peduncle, mcp: middle cerebellar peduncle, pyx: decussation of the pyramidal tract, lfp: longitudinal fibres of the pons, tfp: transverse fibres of the pons, ac: anterior commissure, opt: optic tract, Thal: thalamus, VH: ventral horn of the spinal cord.*

UNSW SYDNEY

Faculty of Medicine

Christodoulos Skliros

Principles of organisation within the pathways in the brainstem and thalamus

The author's final considerations:
The ambition of this study is to advance brain mapping and fibre tracing towards a new generation of sophisticated methods and techniques, which will facilitate the study of brain pathways in their natural 3D space. Combining DTI contrasts of 3D volumetric set of brainstem data brought about the identification in 3D of white matter tracts, as well as the fibre patterning within the brainstem pathways under investigation. Pioneers in biomedical engineering such as Professor G. Allan Johnson led the way towards the development of innovative magnetic resonance imaging technologies, which laid the foundation that enabled me to discover a novel pathway at the midline of the pons, which I named and anatomically described in this research.

This is a highly detailed 3D study in descriptive anatomy of the human and macaque brainstems, at resolutions that approach that of histology. As a result, we successfully characterised 117 known parts, areas and structures within the brainstem and thalamus. In addition, this study is the first to successfully map the pathways in the basilar pons, so that my subdivisions may be used by the physicians for therapeutic invasive and non invasive procedures. Finally, i succeeded in establishing standard anatomical landmarks between the white matter tracts under investigation for the current comprehension of brainstem anatomy, as well as therapeutic advances in neurological disorders.

This multidisciplinary investigative study based on ultra-high-field magnetic resonance imaging was only feasable due to knowledge in biomedical engineering, computer science, computer programming language, neuroimaging, descriptive anatomy, comparative anatomy, histology, neuroscience, functional anatomy, biomechanics, neurophysiology, molecular basis of diseases, general physiopathology, internal medicine, neurological diseases, brain networks, brain mapping, atlas making and fibre tracing.

Paul Lauterbur and Sir Peter Mansfield were awarded the Nobel Prize in Physiology for their discoveries "concerning magnetic resonance imaging" and this reflects the fundamental importance and applications of MRI/DTI in medicine. In the future, the advent of superconducting electromagnets and the optimisation of the techniques connected to ultra-high-field diffusion MR histology will gradually effectuate images the resolution of which surpasses that of histology (1µm). Hence, brain mapping shall not be limited in the mesoscale, rather it will take on a new dimension into the microscale.

Thesis for the Degree of Philosophiae Doctorem (Ph.D.) 2022
International collaboration UNSW - Duke University - Johns Hopkins University
School of Medical Sciences - Department of Anatomy - Neuroscience Research Australia (NeuRA)

ISBN